

รายงานวิจัยฉบับสมบูรณ์

โครงการ

คุณลักษณะทางการไหลสองสถานะของสารทำความเย็น ชนิดใหม่ในท่อขนาดเล็ก

โดย

ศาสตราจารย์ ดร. สมชาย วงศ์วิเศษ

30 พฤศจิกายน 2544



รายงานวิจัยฉบับสมบูรณ์

โครงการ

คุณลักษณะทางการไหลสองสถานะของสารทำความเย็น ชนิดใหม่ในท่อขนาดเล็ก

โดย

ศาสตราจารย์ ดร. สมชาย วงศ์วิเศษ

	a.n. 2546
ำันที่	<u> </u>
เลขทะเบียน	R\$.4
เลงเรียกหนังสื	ło
	a. By

30 พฤศจิกายน 2544

สำนักงานกองทุนสนับสนุนการวิจัย (สกว.) ชั้น 14 อาคาร เอส เอ็ม ทาวเวอร์ เลขที่ 979/17-21 ถบบพกลโยธิน แขวงสามเสนใน าลหญาไท กรุงเทพฯ 10400

(113.298-0455 Înacta 298-0476 Home page: http://www.trf.or.th E-mail: trf-info(a)trf.or.th



รายงานวิจัยฉบับสมบูรณ์

โครงการ

คุณลักษณะทางการไหลสองสถานะของสารทำความเย็น ชนิดใหม่ในท่อขนาดเล็ก

โดย

ศาสตราจารย์ ดร. สมชาย วงศ์วิเศษ ภาควิชาวิศวกรรมเครื่องกล คณะวิศวกรรมศาสตร์ มหาวิทยาลัยเทคโนโลยีพระจอมเกล้าธนบุรี

สนับสนุนโดยสำนักงานกองทุนสนับสนุนการวิจัย

(ความเห็นในรายงานนี้เป็นของผู้วิจัยแต่เพียงผู้เดียว สกว.ไม่จำเป็นต้องเห็นด้วยเสมอไป)

กิติกรรมประกาศ

ผู้เขียนไม่สามารถทำงานวิจัยนี้ให้สำเร็จลงได้ ถ้าผู้เขียนไม่ได้รับทุนพัฒนานักวิจัย (ทุนเมธี วิจัย) รุ่นที่ 5 จากสำนักงานกองทุนสนับสนุนการวิจัย (สกว) ผู้เขียนขอกราบขอบพระคุณผู้บริหาร สกว. อาทิ ศ.นพ. วิจารณ์ พานิช ศ. ดร. วิชัย บุญแสง ศ.ดร. ปิยะวัติ บุญ-หลง ผศ. วุฒิพงศ์ เตชะดำรงสิน ตลอดจนผู้บริหารและเจ้าหน้าที่ ของ สกว. ทุกระดับชั้น ความกรุณาจากสกว. ใน ครั้งนี้ทำให้ผู้เขียนมีกำลังใจในการทำวิจัย และได้สร้างผลงานวิจัย สร้างนักวิจัย จนประสบความ สำเร็จในวิชาชีพในระดับหนึ่ง และยังช่วยให้ สกว. บรรลุถึงเป้าหมายที่ได้ตั้งปณิธาณไว้

ผู้เขียนขอกราบขอบพระคุณ ดร. กฤษณพงศ์ กีรติกร (อธิการบดีมหาวิทยาลัยเทคโนโลยี พระจอมเกล้าธนบุรี) รศ. ดร. มานิจ ทองประเสริฐ (อาจารย์ประจำ ภาควิชาวิศวกรรมเครื่องกล จุฬาลงกรณ์มหาวิทยาลัย) ที่ได้ออกใบรับรอง เมื่อครั้งผู้เขียนสมัครขอรับทุนนี้

ผู้เขียนขอกราบขอบพระคุณผู้ทรงคุณวุฒิทุกท่านที่ประเมินผลงานของผู้เขียน และให้ข้อคิด เห็นที่เป็นประโยชน์ จนทำให้งานสำเร็จลุล่วงไปด้วยดี

ท้ายที่สุดงานนี้จะไม่สำเร็จลุล่วงไปได้เลย ถ้าปราศจากความร่วมมือร่วมใจของนักศึกษาทุก คนในห้องปฏิบัติการ กลศาสตร์ของไหล วิศวกรรมอุณหภาพและ การไหลหลายสถานะ (<u>Flu</u>id Mechanics, <u>T</u>hermal Engineering and Multiphase Flow <u>Re</u>search Laboratory, FUTURE) ผู้ เขียนขอขอบคุณทุกท่านไว้ณ.ที่นี้

บทคัดย่อ

การใหลสองสถานะเป็นปรากฏการณ์จริงที่เกิดขึ้นในกระบวนการต่างๆทั้งในธรรมชาติและ ในอุตสาหกรรมโดยเฉพาะอย่างยิ่ง การไหลร่วมกันของก๊าซและของเหลวซึ่งถือว่าเป็นการไหลสอง สถานะที่มีปรากฏการณ์ซับซ้อนที่สุดในจำนวนการไหลสองสถานะประเภทต่างๆ (ของเหลว-ก๊าซ ของแข็ง-ก๊าซ, ของเหลว-ของเหลว, ของเหลว-ของแข็ง) ทั้งนี้เนื่องจากก๊าซเป็นของไหลที่อัดตัวได้ ทำให้เกิดความซับซ้อนที่ผิวที่สัมผัสกันระหว่างของไหลทั้งสองสถานะ อันเป็นผลทำให้เกิดรูปแบบ การไหลต่างๆ ได้มีการศึกษาเกี่ยวกับการไหลสองสถานะกันอย่างกว้างขวางทั้งจากการทดลองและ การคำนวณ อย่างไรก็ตามยังคงมีแง่มุมที่ได้รับความสนใจน้อยหรือบางอย่างก็ยังไม่เคยมีใครทำมาก่อน และเป็นประเด็นที่ สังคมวิจัยยังคงต้องการคำตอบโดยจะมุ่งเน้นศึกษาทั้งในเชิงทฤษฎีและการทดลอง

ในเชิงทฤษฏีได้สร้างแบบจำลองทางคณิตศาสตร์โดยอาศัยหลักการพื้นฐานทางการอนุรักษ์ มวล พลังงาน และ โมเมนตัม เพื่อศึกษาการใหลของสารทำความเย็นที่ใหลในท่อคาปิลลารีซึ่งเป็น อุปกรณ์สำคัญในระบบปรับอากาศและอุปกรณ์ทางความเย็น แบบจำลองที่ได้สามารถนำไปใช้ใน การออกแบบหาขนาดที่เหมาะสมของท่อคาปิลลารี ได้อย่างไม่มีขีดจำกัด โดยเฉพาะอย่างยิ่งกับการ ออกแบบระบบที่ใช้สารทำความเย็นชนิดใหม่ที่ไม่ทำลายสิ่งแวดล้อมเพียงแต่ป้อนค่าคุณสมบัติทาง กายภาพและทางเทอร์โมไดนามิกส์ที่ถูกต้องเท่านั้น ในเชิงการทดลองได้สร้างอุปกรณ์การทดลองที่ ทันสมัยมาก เพื่อใช้ในการศึกษารูปแบบการไหล สัมประสิทธิ์การถ่ายเทความร้อน และการลดลง ของความดัน ขณะที่สารทำความเย็นไหลและเปลี่ยนสถานะ ข้อมูลการถ่ายเทความร้อนและความ ดันที่ลดลงขณะสารทำความเย็นไหลจำนวนมากได้ถูกนำมาสร้างสหสัมพันธ์เพื่อสะดวกในการนำไป ใช้ในการออกแบบระบบท่อที่ใช้ในระบบปรับอากาศและระบบทำความเย็น อุปกรณ์ทดลองที่พัฒนา ขึ้นนี้ยังสามารถนำไปใช้ทดลองเพื่อศึกษาถึงลักษณะการถ่ายเทความร้อน และลักษณะการไหลภาย ในท่อประเภทอื่น ๆและสารทำความเย็นชนิดต่าง ๆได้อีกมากมาย ผลงานบางส่วนจากงานวิจัยนี้ได้ ถูกตีพิมพ์ลงในวารสารวิชาการระดับนานาชาติที่มีการตรวจทานเต็มรูปแบบ อันเป็นหลักประกันว่า สิ่งที่ได้ทำมีคุณค่าทางวิชาการและเป็นสิ่งที่สัมคมวิจัยในสาขานี้ยอมรับ

Abstract

Two-phase gas-liquid flow in horizontal pipe lines has become of greater concern in a wide variety of engineering equipments and processes. This type of flow has been encountered extensively in an increasing number of important situations for example in gas-oil pipelines, flow of steam in boilers, chemical and nuclear reactors, flow of refrigerant during phase change etc. Among four types of two-phase flow (gas-liquid, gas-solid, liquid-liquid and liquid-solid) the gas-liquid flows are the most complex one. Because the gas-liquid interface is deformable, a infinite number of flow patterns may be encountered. Many studies have been carried out both experimentally and analytically on two-phase flow. However, there are still some topics which has received comparatively little attention in literature.

This research provides the results of simulations using an adiabatic capillary tube model which is developed to study the flow characteristics in adiabatic capillary tubes used as a refrigerant control device in refrigerating systems. The developed model can be considered as an effective tool of capillary tubes' design and optimization for systems using newer alternative refrigerants. Moreover, in the present study, a modern experimental apparatus was designed and constructed to study the two-phase flow pattern, the two-phase heat transfer coefficient characteristics and pressure drop of an alternative refrigerant evaporating under forced flow conditions inside a smooth horizontal tube. New correlations for the convection heat transfer coefficient and pressure drop are proposed for practical applications. The results of this study are of technological importance for the efficient design when systems are assigned to utilize various alternative refrigerants. In addition, some part of this research was published in the international journals. This shows that the results from the present study are valuable and needed for the research society in this field.

Content

		Page
	Acknowledgement	
	Abstract (Thai)	
	Abstract (English)	
1.	Project Title	1
2.	Researcher	1
3.	Field of Research	1
4.	Background and Rationale	1
5.	Objectives	4
6.	Literature Reviews	4
7.	References	11
8.	Other Related with Researchers in this Field	15
9.	Research Methodology	15
10.	Scope of Research	17
11.	Experimental Apparatus and Procedure	18
12.	Three Years Research Plan	22
13.	Practical Significance & Usefulness	22
14.	Output	23
15	Annendix	26

1. PROJECT TITLE

Two-Phase Flow Characteristics of New Refrigerants in Small Diameter Tubes

2. RESEARCHER

2.1 Name Somchai Wongwises,

2.2 **Degree** Ph.D., Dr.-lng.

2.3 **Position** Professor

2.4 Address King Mongkut's University of Technology Thonburi

91 Suksawas 48, Bangmod, Bangkok 10140

Tel: 02-470-9115; Fax: 02-470-9111,

E-mail: somchai.won@kmutt.ac.th

3. FIELD OF RESEARCH

Two-Phase Flow, Fluid Mechanics, Heat Transfer and Thermodynamics

4. BACKGROUND AND RATIONALE

Stratospheric ozone absorbs the sun's high energy ultraviolet rays and prevents them from reaching ground levels where they would interact harmfully with both animal and plant life. A growing body of evidence shows that this protective layer of ozone is being depleted. Measurement by high flying planes, balloons, and satellites have shown severe depletion in polar regions (Fig.1) and smaller reductions of stratospheric ozone levels globally. Much research has been done to determine the cause of this ozone depletion (Molina and Rowland,1974; UNEP,1994; Wuebbles,1995; Lean and Rind,1996), and the general consensus is that free chlorine radicals act as catalysts for the chemical degradation of ozone into normal oxygen molecules. Other chemicals such as bromine can also promote the degradation of ozone.

The presence of chlorine in the stratosphere is believed to be the result of migration of chlorine-containing chemicals. These chemicals have long lifetimes before being broken down into their elemental constituents. This long lifetime allows them to be carried over time into the stratosphere, where they eventually break down and release chlorine. A large class of chemicals which behaves in this manner are the chlorofluorocarbons (CFCs). These

chemicals are widely used by both consumers and industries around the world due to their nonflammability, low toxicity, and material compatibility. CFCs are commonly used as refrigerants, solvents, and blowing agents for foams.

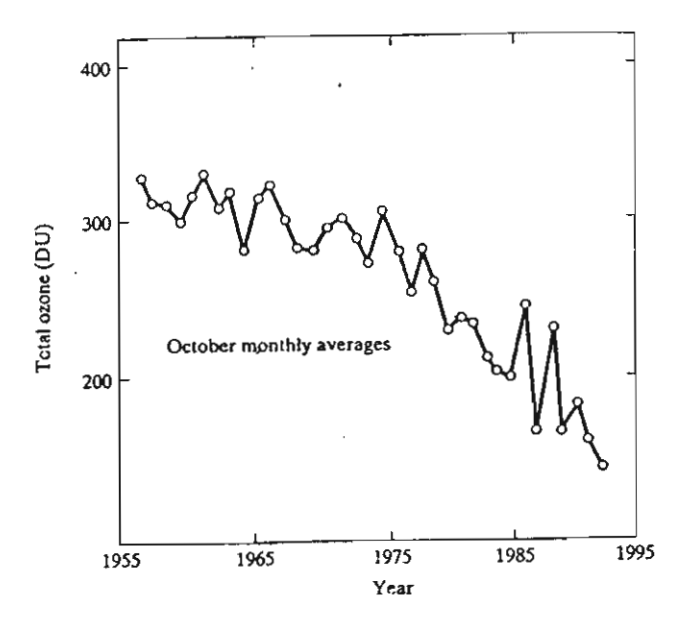


Figure 1. Historical springtime total ozone record for Halley Bay, Antarctica (76°S)

(G. M. Master, 1998)

The concept of ozone depletion potentials (ODPs) have become an integral part of the regulatory approach to controlling emissions of ozone-depleting substances (ODSs). In 1987 an international group of government officials and scientists met to formulate the Montreal Protocol. This agreement called for having the use of CFCs by 1998. A Revised Montreal Protocol was enacted in 1990, and calls for a 50 % cut by 1995, an 85 % cut in 1997, with complete phaseout of CFCs by 2000. In addition to CFCs, other chlorine containing compounds such as carbon tetrachloride and methyl chloroform are addressed in the latest protocol (Aldhous, 1990).

Since the initial discovery of ozone depletion, corporations have been looking for replacements for CFCs. Table 1 lists ODPs for a number of CFCs, halons, and possible replacements. The reference gas used for this comparison is CFC-11 (CFCl₃). By definition, CFC-11 has an ODP of 1.0 which is the highest ODP of any of the CFCs. Halons-1211 and-

1301 have much higher ODPs than CFC-11 due to the higher reactivity of bromine and the reduced effectiveness of deactivation traps compared with chlorine. Notice that the replacement HCFCs have low ODPs, typically less than 0.1, which is a reflection of their short atmospheric lifetimes.

Table 1. Steady-state ozone depletion potentials (Wuebbles,1995)

Species	Chemical formula	Ozone depletion potential relative to CFC-11
CFC-11	CFCI ₃	1.0
CFC-12	CF ₂ Cl ₂	0.9
CFC-113	C ₂ F ₃ Cl ₃	0.9
HCFC-22	CF₂HCI	0.04
HCFC-123	C₂F₃HCI	0.014
HCFC-124	C ₂ F ₄ HCI	0.03
HCFC-141b	C ₂ FH ₃ Cl ₂	0.10
HFC-134a	C₂H₂F₄	< 5 ×10 ⁻⁴
Halon-1211	CF₂CIBr	5.1
Halon-1301	CF₃Br	13
Methyl chloroform	CH ₃ CCl ₃	0.12
Methyl bromide	CH₃Br	0.6

The replacement of ODSs by ozone-safe chemicals is a daunting but challenging task, simply because of the large amounts being produced and used. Also stratospheric ozone depletion is one of the problems that cannot be reversed in a short period of time.

5. OBJECTIVES

- 5.1 To develop mathematical models for predicting the performance of refrigerant flow in capillary tubes
- 5.2 To compare the flow characteristic between various traditional with alternative refrigerants flowing in a capillary tubes.
- 5.3 To develop an experimental apparatus to obtain the flow regime maps for two-phase flow of refrigerant HFC-134a in a small diameter horizontal tube
- 5.4 To determine the two-phase evaporative heat transfer coefficients and pressure drop of refrigerant HFC-134a flowing under forced flow conditions in a small diameter horizontal tube

6. LITERATURE REVIEWS

6.1 Literature review for Objective 5.1 & 5.2

The capillary tube is one type of expansion device used in small vapour-compression refrigerating and air conditioning systems. The capillary tube is made from an extreamly small-bore hollow copper tube (in the order of 0.5×10^{-3} to 1.5×10^{-3} m. diameter) of about 2 to 5 m. in length. It is used as an automatic flow rate controller for the refrigerant when varying load conditions and varying condenser and evaporator temperatures are to be encountered. Its simplicity, low initial cost and low starting torque of compressors are compelling reasons for its use.

Since the depletion of the earth's ozone layer and global warming have been discovered, many conventional refrigerants are being phased out from the industries. As a result, many corporations have been forced to find alternative chemicals to them. To meet the demand for saving the environment and also improving the performance of any equipment, reevaluation of the individual components in particular the capillary tube by using alternative ozone-safe substance is necessary. The proper size of the capillary tube used with a new alternative refrigerant is one of the important factors for the optimum performance of refrigerating and air conditioning systems.

The capillary tube's physical configuration is very simple, the design and analysis of flow and heat transfer characteristics inside the tube, however, are complex ones. In practical consideration, the main concern is to determine the appropriate length and diameter of the tube at given refrigeration capacity and inlet and outlet conditions.

During the last 50 years, the performance of adiabatic capillary tubes has been studied extensively. In one of the first theoretical presentations, Marcy (1949) concluded that capillary tubes could be considered drawn tubing, and "the problem of variation in surface roughness is eliminated". Further, it was concluded that the two-phase Reynolds number should be calculated using the liquid-phase viscosity. Marcy used a graphical integration method to solve the governing momentum equation through the two-phase region, assuming an isenthalpic expansion process. Experimental verification of the technique was made with capillary tubes of diameter 0.58 mm and the lengths of 2,286 and 4,572 mm, with R-12 and SQ₂. Although the predicted flow rates were within 5 % of the measured data, the measured flow rates were much lower than those seen in typical applications.

Hopkins (1950) presented a graphical method to integrate flow equations used in Marcy's studies. The capillary tube rating curves for R-12 and R-22 were developed based on the solution of the momentum equation, also assuming an isenthalpic expansion. In the initial phase of the study, friction factor was calculated using the correlation f = 0.082Re^{-0.25} given by McAdams (1933). Then, based on a comparison to actual system performance data, the analytical results were calibrated through a modification to the friction factor correlation. The final flow predictions were compared to one set of measured R-12 data from Bolstad and Jordan (1948) and showed reasonable agreement. However, the accuracy of the prediction method was not estimated. Rezk and Awn (1979) improved the charts' Hopkin by using Rhomberg integration to solve flow equations. Whitesel (1957) studied adiabatic capillaries assuming constant friction factor, which was determined by averaging the liquid and vapour friction factors experimentally. Whitesel's analysis was later coupled with Hopkin's work and Rezk and Awn's work to produce the well known ASHRAE (1988) charts for capillary tube selection.

In more recent years; Rizza (1982) developed a theoretical flow model assuming that the flow regimes include subcooled, bubble, slug, and mist flow and that the transition points within the capillary tube are predictable. The friction factor equations used were developed based on measured refrigerant flow in standard tubing and then modified by a constant factor to account for the larger inner wall roughness height-to-diameter ratio (E/D) in capillary tubes. The flow model was calibrated to experimental data by adjusting relative cell length parameters. A cell was defined as an identifiable mass containing a single vapor bubble with a diameter approximately equal to the capillary tube diameter and an amount of liquid equal to the mass of liquid between equally spaced adjacent bubbles. The experimental testing was done using R-22 and included capillary tubes of diameters 0.914, 1.78, and 2.29 mm and the lengths of 0.305 and 1.52 m. Both subcooled and quality inlet conditions were included in the testing. Good agreement between the final predictions and the experimental data was shown. However, no verification of the model was made using an independent set of capillary tubes.

Wijaya (1991) presented the first experimental capillary tube study comparing the adiabatic performance of R-12 and R-134a and also presented a theoretical flow model that was also used in the performance comparison. The model employed the Niaz and de Vahl Davis (1969) single-phase friction factor in combination with the Cicchitti two-phase viscosity model (Cicchitti et al.,1960). Although the metastable flow phenomenon was observed experimentally, the model assumed thermodynamic equilibrium throughout the two-phase region and therefore did not account for the metastable liquid region. This probably explains in part why the model consistently underpredicted measured flow rates.

Kuehl and Goldschmidt (1991) presented a theoretical model developed in conjunction with an experimental evaluation of adiabatic capillary tube performance with R-22 (Kuehl and Goldschmidt,1990). R-22 is still the common refrigerant in many airconditioning units, even through it is marked for phase-out in the future. This study covered one of the wider application ranges, which was developed based on an industry survey. The theoretical model employed the Colebrook equation for friction factor using an average tube wall roughness height of 0.000457 mm in combination with the McAdams two-phase viscosity model. The metastable liquid region correction was made using an average

underpressure value of 216.4 kPa, which was based on a match between measurements and model predictions. Without the metastable correction, the flow model predicted a tube length for a specified mass flow rate that was "25 % or so" less than the actual tube length. Thus, the flow model without the metastable correction would underpredict the measured mass flow rate for a given tube length. The magnitude of the difference between measured and predicted results without the metastable correction in terms of flow rate was not specifically reported. As a point of reference, through, Kuehl and Goldschmidt did present a model sensitivity plot for a representative case for which a \pm 5% change in mass flow rate roughly corresponded to a \pm 15% change in predicted tube length.

The behavioral characteristics of the metastable flow region have been experimentally documented by several researchers since Cooper et al. (1957) first documented the phenomenon. Li et al. (1990a) probably presented the most thorough experimental evaluation of the metastable behavior to date. Based on extensive testing with R-12, Chen et al. (1990) presented a correlation among dimensionless groupings on which the metastable liquid length (referred to in terms of an underpressure) was expected to depend.

A recently capillary tube study by Dirik et al. (1994) incorporated the Chen underpressure model in aflow model that was used to predict flow rates with R-134a in capillary tubes of 0.66 and 0.80 mm diameter. Their flow model employed the Colebrook correlation for friction factor, using a roughness height of 0.000457 mm, in combination with the McAdams two-phase viscosity model (McAdams et al. 1942). For the majority of the adiabatic data reported, predictions fell well within the ±10 % of the measured data.

Wong et al. (1994) also presented a capillary tube theoretical model that was used primarily to study the effect of various design parameters on capillary tube performance. The model employed the Colebrook equations for friction, along with the Dukler two-phase viscosity model (Dukler et al.,1964). A comparison of model predictions of pressure drop within the capillary tube to experimental data from Li et al. (1990b) showed good agreement. However, the inner wall roughness height-to-diameter ratio (E/D) was apparently used in calibrating the model to measured data.

Melo et al.(1994,1995) have studied temperature and pressure distributions along the capillary tubes and developed a mathematical model by using the two-phase flow friction factor based on the correlation obtained from literature. Wong and Ooi (1996) developed a separated flow model using the frictional pressure gradient correlations of Lin et al.'s (1990). They reported that it gave a better prediction than the homogeneous flow models. Bansal and Rupasinghe (1998) presented a homogeneous two-phase flow model to study the performance and design aspects of adiabatic capillary tubes. The REFPROP data base which is based on the Carnahan-Starling-DeSantis equation of state was used to determine the thermodynamics and transport properties of the refrigerants.

6.2 Literature review for Objective 5.3 & 5.4

Stratospheric ozone absorbs the high energy ultraviolet rays from the sun and protects both humans and other living thing from the exposure to ultraviolet radiation. Results from many researches show that the ozone layer is being depleted. The general consensus for the cause of this event is that the free chlorine radicals removes ozone from the atmosphere and later the chlorine atom is continued to convert more ozone to oxygen. The presence of chlorine in the stratosphere is the result of migration of chlorine-containing chemicals. The chlorofluorocarbons (CFCs) is a large class of chemicals which behaves in this manner. These chemicals have many unusual properties for example, nonflammability, low toxicity, and material compatibility that have led to their common widespread use, both consumers and industries around the word as refrigerants, solvents, and blowing agents for foams.

As suggested by Hosler (1968), knowing the flow pattern in two-phase flow is analogous to the differences of laminar or turbulent flow in single-phase flow. It is not possible to understand the two-phase flow phenomena without a clear understanding of the flow patterns encountered. It is to be expected that two-phase pressure drop, holdup, system stability, exchange rates of momentum, heat and mass will be influenced by the flow pattern which exists. Therefore, it is important to understand the in-tube two-phase flow pattern to correctly model the heat transfer and friction characteristics of the two-phase system. There have been numerous studies on this project. Many studies have been carried out to perform the flow regime maps (also called "flow pattern map") which is a two dimensional graph separated into area corresponding to various flow patterns, mostly for air-water system (Alves,1954; Baker, 1954; Barnea,1987; Chisholm, 1973; Collier et al. 1994; Hoogendoorn, 1959; Lin and Hanratty,1987; Mandhane et al. 1974; Spedding and Spence,1993; Taitel and Dukler,1976; Wong and Yau, 1997; Wongwises, 1997; Wongwises et al.,1998.).

Refrigerant flow regime maps have received comparatively very little attention in the literature. Moreover, the majority of previous two-phase refrigerant flow pattern studies were associated with diameters on the order of 10 to 75 mm, tested at mass velocities greater than 300 kg/m²s, (Kuo et al., 1996a; Kuo et al., 1996b; NIST, 1996; VDI, 1993; Wambsganss et al., 1991; Yang, 1996). Unfortunately, in HVAC&R applications, tubes having a diameter

less than 10 mm and mass velocities less than 300 kg/m²s are often encountered. Furthermore, Kattan et al. (1995) found that the existing flow pattern maps may poorly represent the experimental data of new refrigerants R-123, R-134a, R-502, R-402A, and R-404A. Therefore, it is of value to quantify the phenomena for better understanding of the intube two-phase system.

Accordingly, the purpose of this study is to observe all flow patterns (as depicted by Wongwises (1997), Wongwises et al. (1998) for air-water system) and present new experimental data, and also search a suitable existing flow pattern map that can describe the present experimental data.

Since the depletion of the earth's ozone layer has been discovered, many corrporations have been forced to find alternative chemicals to CFCs.Because the thermophysical properties of HFC-134a are very similar to those of CFC-12. Refrigerant HFC-134a is receiving the supporting from the refrigerant and air-conditioning industry as a potential replacement for CFC-12. However, even the difference in properties between both refrigerants is small but it may result in significant differences in the overall system performance. Therefore, the properties of HFC-134a should be studied in detail before it is applied.

Evaporation of refrigerants has been studied by a large number of researchers, both experimentally and analytically, mostly for pure refrigerants. However, most of the data reported in previous literature has not been obtained from the high flow rate and high near flux conditions. In the present study, the main concern is to obtain and analyze the heat transfer coefficient and pressure drop of the pure HFC-134a during forced convection in a horizontal tube under high flow rate and high heat flux conditions. The data obtained from the present study are also compared with the correlations reported in the literature. In addition, suitable correlations are proposed to predict the evaporative heat transfer coefficient and pressure drop of the refrigerant HFC-134a.

7. REFERENCES

7.1 References for Introduction

- [1] P. Aldhous, Warming to global agreement, Nature, July 5, 1990,6-8.
- [2] J. Lean, and D. Rind, The sun and climate, Consequences, 1996;.2(1), 27-36.
- [3] G.M. Masters, Introduction to engineering and science, Prentice-Hall, 1998.
- [4] M.J, Molina and F.S. Rowland, Stratospheric sink for chlorofluormethanes:Chlorine atom catalyzed destruction of ozone, *Nature*, 1974; 249, 810-812.
- [5] United Nations Environment Programme (UNEP), Montreal Protocal on Substances that Deplete the Ozone Layer, Scientific Assessment of Ozone Depletion, World Meteorological Organization Global Ozone Research and Monitoring Project-Report No. 37, Geneva, Switzerland, 1994.
- [6] D.J. Wuebbles, Weighing functions for ozone depletion and greenhouse gas effects on climate, *Annual Review of Energy and Environment*, 1995; 20, 45-70

7.2 References for Literature Review 6.1

- [7] ASHRAE, 1988 ASHRAE Handbook-Equipment, Chap. 19, American society of Heating, Refrigerating and Air-Conditioning Engineers, Inc., Atlanta, 1988.
- [8] P.K. Bansal and A.S. Rupasinghe, A homogeneous model for adiabatic capillary tubes, *Applied Thermal Engineering*, 1998; 207-219.
- [9] M.M Bolstad and R.C. Jordan, Theory and use of the capillary tube expansion device, Refrigerating Engineering, 1949; 57, 572-583.
- [10] Z.H. Chen, R.Y. Li, S. Lin and A.Y. Chen, A correlation for metastable flow of R-12 through capillary tubes, *ASHRAE Transactions*,1990; 96(1): 550-554.
- [11] A. Cicchitti, C. Lombardi, M. Silvestri, G. Soldaini, and R. Zavattarelli, Two-phase cooling experiments-Pressure drop, heat transfer and burnout measurements, *Energia Nucleare*, 1960; 7(6), 407-425.
- [12] L. Cooper, C.K. Chu and W.R. Brisken, Simple selection method for capillaries derived from physical flow conditions, *RefrigeratingEngineering*,1957; 65(7), 37-46.
- [13] E. Dirik, C. Inan and M.Y. Tanes, Numerical and experimental studies on adiabatic and nonadiabatic capillary tubes with HFC-134a, In *proceedings of the International Refrigeration Conference*, Purdue University, Vol. 1, 365-370, 1994.

- [14] A.E. Dukler, M. Wicks and R.G. Cleveland, Frictional pressure drop in two-phase flow-Parts A and B, *AlChE Journal*, 1964; 10(1): 38-51.
- [15] N.E Hopkins, Rating the restrictor tube, Refrigerating Engineering, 1950;58 (11),1087 -1095.
- [16] S.J. Kuehl and V.W. Goldschmidt, Steady flows of R-22 through capillary tubes: Test data, *ASHRAE Transactions*, 1990; 96(1): 719-728.
- [17] S. Lin, C.C.K. Kwok, R.Y. Li, Z.H. Chen and Z.Y. Chen, Local frictional pressure drop during during vaporization of R-12 through capillary tubes, *Int.J. Multiphase Flow*, 1991; 17 (1), 95-102.
- [18] R.Y. Li, S. Lin and Z.H. Chen, Numerical modeling of thermodynamic nonequilibrium flow of refrigerant through capillary tubes, *ASHRAE Transactions*, 1990b; 96(1): 542-549.
- [19] R.Y. Li, S. Lin, Z.Y. Chen and Z.H. Chen, Metastable flow of R-12 through capillary tubes, *Int. J. Refrigeration*, 1990a; 13(3): 181-186.
- [20] G.P. Marcy, Pressure drop with change of phase in a capillary tube, *Refrigerating Engineering*,1949; 57(1), 53-57.
- [21] W.H. McAdams, Heat transmission, McGraw-Hill, New York, 1933.
- [22] M.O. McLinden, J.G. Gallagher, M.L. Huber and G. Morrison, REFPROP refrigerant properties database: capabilities, limitations and future directions, ASHRAE NIST refrigerants Conference, Gaitherburg, 1998.
- [23] C. Melo, R.T.S. Ferreira, C. B. Neto, J.M. Goncalves, R.H. Pereira and M.R. Thiessen, Evaluation of HC-600a, HFC-134a and CFC-12 mass flow rates through capillary tubes, In *Proceedings of the IIR Conference*, Hannover, Germany, 621-630,1994.
- [24] C. Melo, R.T.S. Ferreira, C. B. Neto and J.M. Goncalves, Experimentation and analysis of refrigerant flow through adiabatic capillary tubes, In *Proceedings ASME Int. Mech. Engrs. Congress and Exposition*, AES, Vol.34, 19-30, 1995.
- [25] B.D. Purvis and W.E. Dunn, Development of a computer model for refrigerant flow in small diameter tubes, ACRC TR-27-Air Conditioning and Refrigeration Center, November.
- [26] J.J. Rizza, Numerical solutions to transonic two-phase capillary tube flow, Journal of Energy, 1982; 6(4): 285-288. -

- [27] A. Rezk and A. Awn, Investigation on flow of R12 through capillary tubes, In *Proceedings of the 15 th International Congress of Refrigeration*, Commission, B2, Vol. 2, 443-452, 1979.
- [28] H.A. Whitesel, Capillary two-phase flow, part II, Refrigerating Engieering, 1957; 65(9), 35-47.
- [29] H. Wijaya, Adiabatic capillary tube test data for HFC-134a, In *Proceedings of the International Refrigeration Conference on Energy Efficient and New Refrigerants*, Purdue University, West Lafayette, USA,Vol.1, 63-71, 1992.
- [30] T.N. Wong, K.T. Ooi and C.T. Khoo, A study on capillary tube flow, in Proceedings of the IIR-Purdue Conference, West Lafayette, USA, 371-376,1992.
- [31] T.N. Wong and K.T. Ooi, Adiabatic capillary tube expansion devices: a comparison of the homogeneous flow and the separated flow models, *Applied Thermal Engineering*.,1996;16(7), 625-634.

7.3 References for Literature Review 6.2

- [32] G.E. Alves, Cocurrent liquid gas flow in a pipeline contactor, *Chem. Eng. Prog.*, 1954; 50 (9), 449-456.
- [33] O. Baker, Design of pipe lines for simultaneous flow of oil and gas, *Oil andGas J.*, 1954; 53, 185-195.
- [34] D. Barnea, A unified model for prediction of flow pattern transitions in the whole range of pipe inclination, *Int. J. Multiphase Flow*, 1987; 13, 1-12.
- [35] D.Chisholm, Pressure gradient due to friction during the flow of evaporating twophase mixtures in smooth tube and channels, *Int. J. Heat Mass Transfer*, 1973; 16, 347-348.
- [36] J.G. Collier and J.R. Thome, Convective boiling and condensation,1994; 3d ed. Oxford University Press.
- [37] C.J. Hoogendoorn, Gas liquid flow in horizontal pipes, Chem. Eng. Sci.,1959;9(4),205-217.
- [38] E.R. Hosler, Flow patterns in high pressure two-phase (steam-water) flow with heat addition, AIChE Symp., 1968; Ser. 64,54-66.

- [39] N. Kattan, J.R. Thome, and D. Favrat, Measurement and prediction of two-phase flow patterns for new refrigerants inside horizontal tubes, *ASHRAE Transactions*, 1995; 101(2): 1251-1257.
- [40] C.S. Kuo and C.C. Wang, Horizontal flow boiling of R22 and R407C in a 9.52 mm micro-fin tube, *Applied Thermal Engng.*, 1996a; 16(8/9):719-731.
- [41] C.S. Kuo and C.C. Wang, In tube evaporation of HCFC-22 in a 9.52 mm micro-fin/smooth tube; horizontal flow boiling of R22 and R407C in a 9.52 mm micro-fin tube, *Int.J. Heat Mass Transfer*, 1996b; 39(12):2559-2569.
- [42] P.Y. Lin and T.J. Hanratty, Effect of pipe diameter on flow patterns for air-water flow in horizontal pipes, *Int. J. Multiphase Flow*, 1987; 13, 549-563.
- [43] J.M. Mandhane, G.A. Gregory and K.Aziz, A flow pattern map for gas liquid flow in horizontal pipes, Int. J. Multiphase Flow, 1974;1,534-553.
- [44] NIST, REFPROP, thermodynamic properties of refrigerants and refrigerant mixtures, version 5.0. Gaithersburg, Md.: National Institute of Standards and Technology, 1996..
- [45] P.L. Spedding and D.R. Spence, Flow regimes in two-phase gas-liquid flow, *Int. J. Multiphase Flow*, 1993;19, 245-280.
- [46] Y. Taitel and A.E. Dukler, A model for prediction of flow regimes in horizontal and near horizontal gas-liquid flow, *AIChE J.*, 1976;22(1),47-55.
- [47] M.W.Wambsganss, J.A., Jendrzejczyk, and D.M. France, Two-phase flow pattern and transition in a small horizontal rectangular channel, *Int. J. Multiphase Flow*, 1991;17(3): 327-342.
- [48] VDI-warmeatlas, Heat transfer to boiling saturated liquids VDI Heat Atlas, chap. Hbb1, Germany: VDI-Verlag GmbH, 1993.
- [49] T.N. Wong and Y.K. Yau, Flow patterns in two phase air-water flow, *Int. Comm. Heat and Mass Transfer*, 1997; 24(1), 111-117.
- [50] S. Wongwises, Method for prediction of pressure drop and liquid hold-up in horizontal stratified two-phase flow in pipes, *Proceedings of the 1997 ASME Symposium on Gas Liquid Two-Phase Flows*, June 22-26, 1997, Vancouver, Canada, pp.1-7.
- [51] S. Wongwises and W. Wimonkaew, Flow regime maps for the developing steady gasliquid two-phase flow in a horizontal pipe, *ASEAN Journal on Science and Technology for Development*, 1998 (in press).

[52] C.Y.Yang and R.L.Webb, Friction pressure drop of R-12 in small hydraulic diameter extruded aluminium tubes with and without micro-fin, *Int.J.Heat Mass Transfer*,1996,39(4): 801-809.

8. OTHER RELATED WITH RESEARCHERS IN THIS FIELD

Professor Dr.-Ing. D. Mewes
Institut fuer Verfahrenstechnik
Universitaet Hannover, Callin Str. 36
Hannover, Germany

9. RESEARCH METHODOLOGY

9.1 A mathematical model is developed to study the flow characteristics of refrigerants in adiabatic capillary tubes. The basic physical equations governing the flow are established from the conservation of mass, energy and momentum. The obtained differential equations are solved simultaneously by the Runge-Kutta method. The model input parameters are pressure and temperature at capillary tube inlet, mass flow rate of refrigerant, roughness and diameter of the capillary. The simulation can be used to determine the appropriate size of the capillary tubes used in household air conditioners and refrigerators, especially to select the capillary tube length for given operating conditions.

The capillary tube between points 3 and 4 can be divided into numerous sections as shown in Figure 2. Since P₃ is known (saturated liquid), the pressure at any section 'i' can be calculated from

$$P_i = P_3 - i\Delta P$$

With the known pressure (P_i) , and the quality (x_i) , the entropy of the section can be calculated from

$$s_i = s_{if}(1-x) + s_{ig}x$$

The two-phase friction factor (f_{tp}) can be calculated from Colebrook's equation where the Reynolds number is defined by

Re =
$$\frac{VD}{\mu_{tp} \nu_{tp}}$$

V = $G\nu_{tp}$ = $G(x\nu_{g} + (1-x) \nu_{t})$

where

The different viscosity models are used to calculate μ_{tp} .

All refrigerant thermodynamic and thermophysical properties are taken from the REFPROP computer program, Version 6.01 and are developed in the function of pressure.

By using a particular $\mu_{\rm tp}$ to determine the Reynolds number, the friction factor can then be calculated by the Colebrook formula.

The calculation is done section by section along the capillary tube. For each section P_i , T_i , x_i , s_i and f_i are calculated. The gradual increasing of the entropy is obtained in the direction to the capillary exit. Eventually, a point which the entropy is maximum is reached. At this point, the fluid velocity is equal to the local speed of sound and the flow is choked. With further calculation over this point, the entopy decreases. This violates the second law of thermodynamics. Therefore the calculation must be terminated at this point.

The pressure of the element where entropy is maximum $(P_i)_{smax}$ is then compared to the evaporator pressure (P_{evap}) .

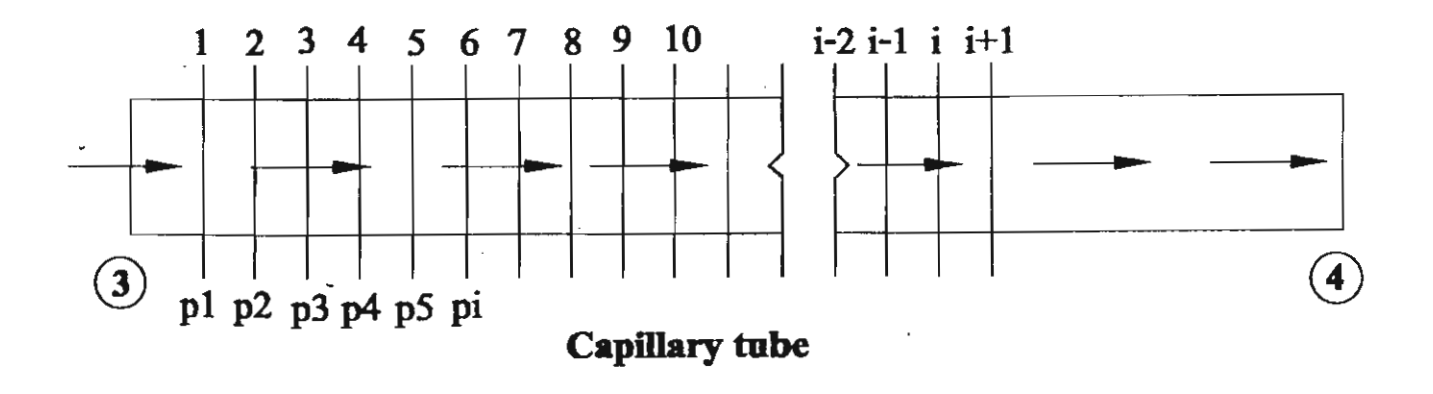


Figure 2. Simplified diagram of the adiabatic capillary tube

The calculation is done section by section along the capillary tube. For each section the pressure, temperature, dryness fraction, entropy and friction factor are calculated.

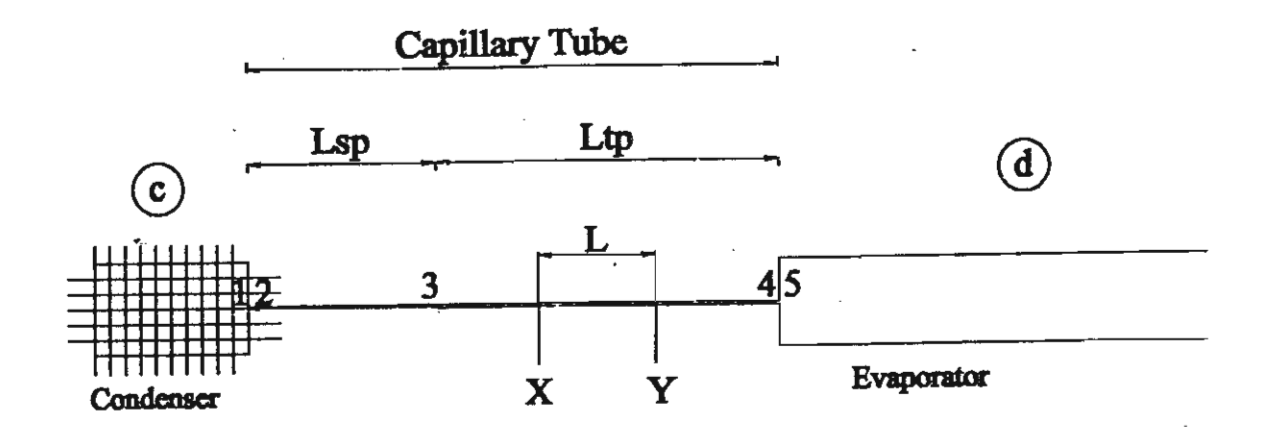


Figure 3. Grid system for the numerical simulation

- 9.2 The results calculated by the present model is compared with those of other researchers and with the experimental data.
 - 9.3 The separated flow model is developed.
- 9.4 The results calculated by the present model is compared with those of other researchers and with the experimental data.
- 9.5 An experimental apparatus is developed to determine the heat transfer coefficient and pressure drop in a small horizontal tube.
- 9.6 The experimental apparatus is used to determine the flow patterns in small horizontal pipes.
- 9.7 Two-phase flow patterns is observed. A set of standardised terminology for the two-phase flow patterns through experimental observation by Wongwises (1997) and Wongwises et al. (1998) is used. The flow regime maps are developed and then compared to several flow regime maps to determine the applicability of these maps to new refrigerants.

10. SCOPE OF RESEARCH

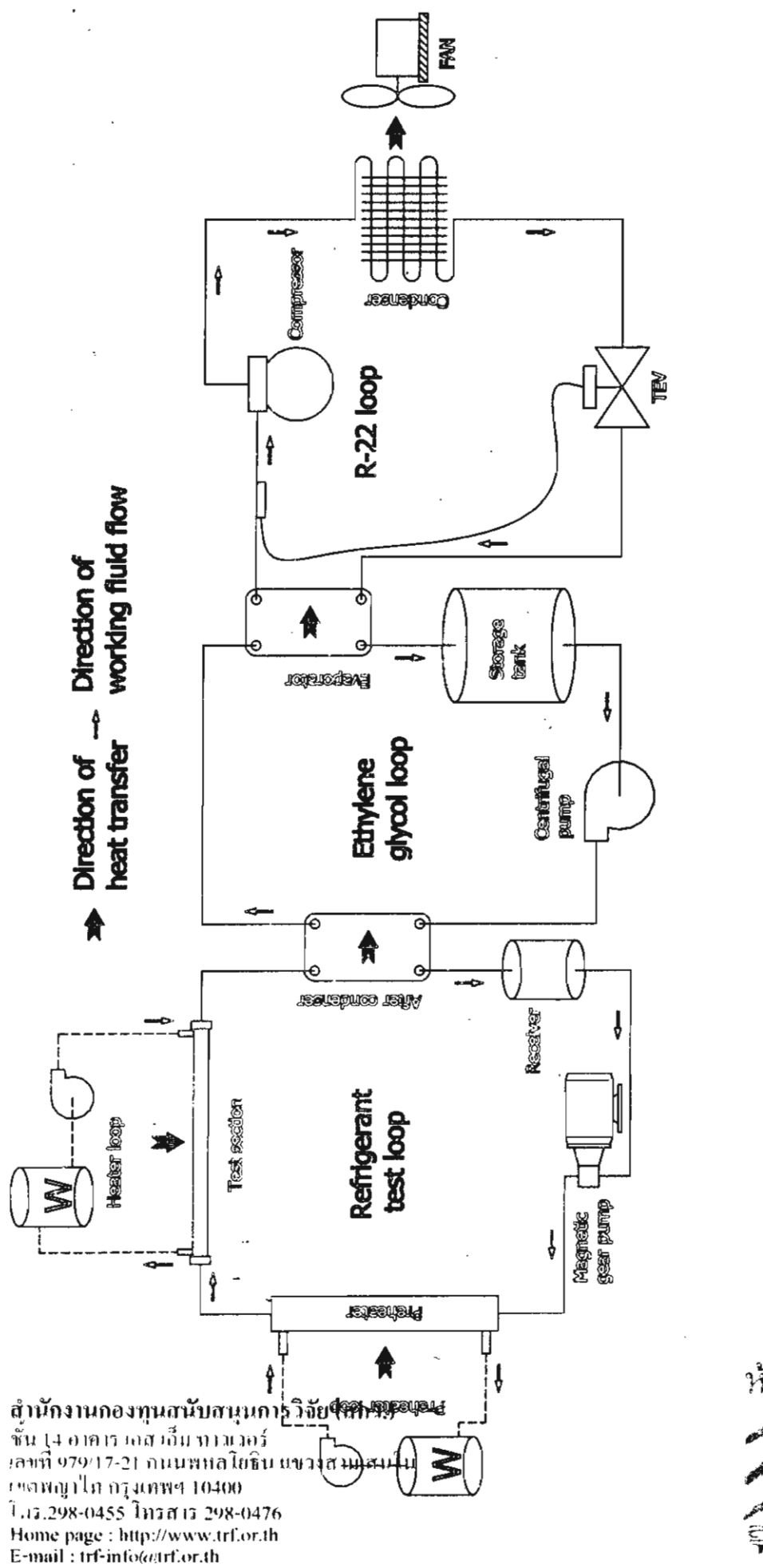
- 10.1 Both theoretical and experimental studies will be done.
- 10.2 R134a is a refrigerant used in the experimental work.
- 10.3 The experimental studies will be associated with less than 10 mm. diameters.
- 10.4 The results of each step will be used to achieve the objective in the next step.

11, EXPERIMENTAL APPARATUS AND PROCEDURE

A schematic diagram of a test apparatus is shown in Fig. 4. The main components of the system are a test section, refrigerant loop, heating water flow loops, subcooling loop and instrumentation. A commercial HFC-134a is used as the working fluid. A refrigerant loop capable of investigating HFC-134a flowing in horizontal tubes is the main feature. Two city water loops are connected to the refrigerant loop to provide heating the refrigerant. The purpose of the subcooling loop is to absorb heat from the main refrigerant loop. The test section and the connections of the piping system are designed such that parts can be changed or repaired very easily. In addition to the loop components, a full set of instruments for measuring and control of temperature and pressure of all fluids, refrigerant pump speeds and electrical power, is installed at all important points in the circuit.

The refrigeration flow loop is set up with the desired test section. Liquid refrigerant is discharged by a gear pump which its speed is controlled by an inverter, and is passed through a filter/dryer, a sight glass, a refrigerant flow meter, preheater, sightglass tube and test section. Since heat from heating water is added in the test section, the refrigerant partially evaporates in the test section and flows to subcooler, receiver and then returns to the refrigerant pump. The cycle is then repeated. Instrumentation is located at various positions to give information on the state of the flowing fluid at each respective point. All sensors are wired directly to terminal control panels mounted on the bench. The inside diameter of each piece of additional equipment is_adjusted to be equal to the diameter of the refrigerant line, so perturbations in the flow pattern are minimized.

A double tube heat exchanger is used to preheat the liquid refrigerant flowing to the test section. The heat exchanger is connected to the heating water loop which consists of a storage tank an electric heater controlled by adjusting the voltage, a thermostat and a stirrer. After the water is heated to the required temperature, the hot water is pumped out of the storage tank, delivered to the inner tube and then returned to the storage tank. With this, more heat is added to the refrigerant through heating water and the quality of the two-phase refrigerant flowing into the test section can be varied.



Schematic diagram of experimental apparatus

Figure 4



The test section is a horizontal counterflow heat exchanger. It consists of a tube within a tube.. Such an arrangement operates in counterflow with the refrigerant passing through the inside of the inner tube and the hot water passing through the annular space to add heat to vaporize the refrigerant flowing in the inner tube. Both outer and inner tubes are made from smooth copper tubes. This inner tube is located concentrically within an outer tube which serves as a water jacket. The heating water flow loop also consists of the same components as the first one. In order to decrease the watyer temperature, a R-22 chiller loop is used to absorb heat from the heating water loop and reject it to the atmosphere. At the ends of the test section, pressure transducers and thermocouples are also installed to measure the refrigerant pressures and temperatures inside the test section. The ends of the inner tube of the test section are connected to the refrigerant loop by special fittings with an inside diameter identical to that of the test section. These fittings allow removal of the test section without disturbing either side of the test section. The experimental set-up is equipped with three basic instrumentation systems; temperature, pressure and flow rate.

In order to subcool the two-phase refrigerant flowing out from the test section, a R-22 chiller loop and an antifreezer loop are used to transfer heat from the main loop to the atmosphere through two plate heat exchangers. Refrigerant temperature and inner tube wall temperature in the test section are measured by type-T copper-constantan thermocouples. Refrigerant bulk temperature is measured in several positions with 1 mm. diameter probes extending inside the tube in which the refrigerant flows. The entering and exiting fluid temperatures of all heat exchangers are also measured by the same type of thermocouple, each with two-thermocouples. All temperature measuring devices are well calibrated in a controlled temperature bath using standard precision mercury glass thermometers. Uncertainty of temperature measurements after considering the data acquisition system is \pm 0.1°C.

An internal platinum resistance temperature detector is used together with a heater to control the temperature of fluid in each storage tanks. Thermocouples are mounted at many longitudinal positions on the inner tube wall surface, each with four thermocouples equally spaced around the tube circumference. The thermocouples are soldered into a small hole drilled 0.5 mm. deep into the tube wall surface. Besides the inlet and outlet of the test

section which pressure is measured by the pressure transducers, refrigerant pressures are measured by precision Bourdon tube pressure gauges. The pressure is measured through a tap with a 1.5 mm hole drilled into the tube in which the refrigerant flows. All static pressure taps are mounted flush in the tube wall. The pressure transducers and pressure gauges are calibrated against a primary standard, the dead weight tester.

Three sets of precision flow meters are used to measure the volumetric flow rate of the refrigerant. These flow meters are armored, of a variable area type and have a float that moves vertically in a tapered metering tube. The flow meters are specially calibrated for R-134a from the manufacturer.

Experiments were conducted with various flow rates of refrigerants, various quality of refrigerant entering and exiting the test section and various temperatures and pressures of refrigerant evaporating in the test section. In the experiments, the refrigerant flow rate was controlled by adjusting the speed of the gear pump. The inverter was used to control the speed of the motor for driving the pump. To vary the refrigerant quality at the inlet of the test section, the heating water flow rates and/or the water temperature at the preheater were varied by small increments while the refrigerant flow rate was kept constant. The electric power going into the water heater was measured by Watt transducers and controlled by a thermostat. The refrigerant temperature was controlled by adjusting the flow rate and/or the temperature of the Ethylene glycol-water solution. The system was allowed to approach the steady state before any data was recorded. The steady state condition was reached when the pressure, temperature and flow rate at the measuring points were not fluctuating. After stabilization, temperatures on the tube wall, temperature and pressure of refrigerant at the locations mentioned above, inlet and outlet temperature of heating water and the flow rates of heating water and refrigerant were recorded.

12. THREE YEARS RESEARCH PLAN

Activity		Time (year)			
	0	1	2		
9.1-9.2		****			
9.3-9.4	,	******	**		
9.5		****	******	*	
9.6	*****	*****	*****	*****	
9.7		*****	*****	*****	

13. PRACTICAL SIGNIFICANCE & USEFULNESS

- The mathematical model developed will help designers to understand the thermophysical behaviour of refrigerant flow in capillary tube and design better capillaries.
- The test apparatus developed can provide the large data base needed for efficient design of evaporators using the new refrigerants. The large amounts of data collected enables the correlation and prediction of evaporative heat transfer coefficients and pressure drops.
- The results of this research will be of technological importance in the future for reducing emissions of ozone-depleting substances and solving a part of global environmental problems.

14. OUTPUT

14.1 Publications

- [1]. Wongwises, S., Kalinitchenko, V.A., Mean Velocity Distributions in a Horizontal Air-Water Flow, Int.J. Multiphase Flow, 2002; 28(1): 167-174.
- [2]. Wongwises, S., Kongkiatwanitch, W., Interfacial Friction Factor in Vertical Upward Gas-Liquid Annular Two-Phase Flow, *Int. Com. Heat Mass Transfer*, 2001; 28(3): 323-336.
- [3]. Wongwises, S., Pirompak, W., Flow Characteristics of Pure Refrigerants and Refrigerant Mixtures in Adiabatic Capillary Tubes, *Applied Thermal Engineering*, 2001; 21(8): 845-861.
- [4] Wongwises, S., Songnetichavarit, T., Lokathada, N., Kritsadathikarn, A Comparison of the Flow Characteristics of Refrigerants Flowing Through Adiabatic Capillary Tubes, Int. Com. Heat Mass Transfer, 2000; 27(5): 611-621.
- [5]. Wongwises, S., Napon, P., Heat Transfer and Flow Characteristics in Vertical Annular Two-Phase Two-Component Flow, *TIJSAT*, 2000; 5(1): 16-27.
- [6]. Wongwises, S., Chan, P., Luesuwanatat, N., Purattanarak, T., Two-Phase Separated Flow Model of Refrigerants Flowing Through Capillary Tubes, Int. Com. Heat Mass Transfer, 2000; 27(3): 343-356.
- [7]. Wongwises, S., Disawas, S., Kaeon J., Onurai C., Two-Phase Evaporative Heat Transfer Coefficients of Refrigerant HFC-134a Under Forced Flow Conditions in a Smooth Horizontal Tube, *Int. Com. Heat Mass Transfer*, 2000; 27(1): 35-48.
- [8]. Kalinitchenko, V., Sekerj-Zenkovitch, S., Wongwises, S., Mijangos, R., The Generation of Sand Waves by Oscillating Flows, Proceedings of the International Conference on Modern Approaches to Flows in Porous Media, Moscow, September 6-8, 1999.
- [9]. Wongwises, S., Pornsee, A., Siroratsakul, E., Gas-Wall Shear Stress Distribution in Horizontal Stratified Two-Phase Flow, Int. Com. Heat Mass Transfer, 1999; 26(6): 849-860.

- [10]. Wongwises, S., Kritsadathikarn, P., Songnetichavarit, T., Lokathada, N., Pressure Distribution of Refrigerant Flow in an Adiabatic Capillary Tube, *Science Asia*, (in press)
- [11] Bazitevsky, A.V., Wongwises, S., Kalinitchenko, V.A., Sekerj-Zenkovitch S.Ya., Experimental Study on the Effect of Bottom Structures on Damping of Standing Surface Waves in Rectangular Tank, *Journal of Fluid Dynamics* (in press).
- [12] Wongwises, S., Lokathada, N., Kritsadathikarn, P., Songnetichavarit, T., A Simulation of Refrigerant Flow Through Capillary Tube Expansion Device, Asian J. of Energy and Environment, 2001; 2 (1): 69-88.
- [13]. Wongwises, S., Songnetichavarit, T., Lokathada, N., Kritsadathikarn, P., Investigation on Adiabatic Flows of Traditional and Alternative Refrigerants Through Capillary Tubes, *J. of Energy Heat and Mass Transfer* (in press).
- [14]. Wongwises, S., Kaewon, J., Wongchang, T., Wang, C.C., A Visual Study of Two Phase Flow Patterns of HFC-134a and Lubricating Oil Mixtures, *Heat Transfer Engineering* (revised).
- [15]. Wongwises, S., Sripattarapan, W., A Theoretical Investigation on Evaporation of Refrigerants Under Forced Flow Conditions in a Horizontal Tube, Applied Thermal Engineering (submitted).
- [16]. Wongwises, S., Duangthongsuk, W., Tube-Side Two-Phase Heat Transfer Coefficients of Refrigerant HFC-134a Flowing Through A Fin-And-Tube Evaporator, Int. Com. Heat Mass Transfer (submitted).
- [17]. Wongwises, S., Naphon, P., Investigation on the Performance of Spiral Coil Fin and Tube Heat Exchangers under Dehumidifying Conditions, *Applied Thermal Engineering* (submitted).
- [18]. Wongwises, S., Sinpiboon, J., A Homogeneous Flow Model for Non-Adiabatic Capillary Tubes, *Int. J. Refrigeration* (submitted).

14.2 Patent

ระบบการออกแบบขนาดของท่อคาปิลลารีที่ใช้ในระบบปรับอากาศและระบบทำความเย็น (อยู่ระหว่างการรอผลพิจารณาจาก กรมทรัพย์สินทางปัญญา)

14.3 External committee for Ph.D. thesis examination

- School of Energy and Material, King Mongkut's University of Technology Thonburi
- Department of Mechanical Engineering, Chulalongkorn University

14.4 Reviewer for National Innovation Competition

- Thailand Innovation Awards 2001 (Science Association of Thailand and The German Technical Cooperation)
- Agricultural Machinery and Environment 2001 (Ministry of Science, Technology and Environment)

14.5 Reviewer for Research Fund

- The Thailand Research Fund
- Kasetsart University
- King Mongkut's University of Technology Thonburi

14.6 Reviewer for National Journals and National Conference

- Journal of Engineering Institute of Thailand
- Thammasart International Journal on Science and Technology
- Songklanakarin Journal of Science and Technology
- National Conference in Mechanical Engineering

14.7 Reviewer for International Journals and International Conference

- International Journal of Multiphase Flow
- Applied Thermal Engineering
- The First International Conference in Heat Transfer, Fluid Mechanics and Thermodynamics (HEFAT), Skukuza, South Africa, 8-10 April 2002.

14.8 Other prizes

- Research grant prize from the Thailand Toray Science Foundation (TTSF) for year 2000 (รางวัลทุนช่วยเหลือการวิจัยทางวิทยาศาสตร์และเทคโนโลยีมูลนิธิโทเรเพื่อการพัฒนา วิทยาศาสตร์ประเทศไทย โดยุรับจาก พณ. พลเอก เปรม ติณสูลานนท์ ประชานองคมนตรี เมื่อ 31 มกราคม 2543)

Wongwises, S., Kalinitchenko, V.A., Mean Velocity Distributions in a Horizontal Air-Water Flow, Int.J. Multiphase Flow, 2002; 28(1): 167-174.



International Townal of Multiphase

International Journal of Multiphase Flow 28 (2002) 167-174

www.elsevier.com/locate/ijmulflow

Brief communication

Mean velocity distributions in a horizontal air-water flow

Somchai Wongwises a,*, Vladimir Kalinitchenko b

^a Thermal Engineering and Multiphase Flow Research Laboratory (FUTURE), Department of Mechanical Engineering, Fluid Mechanics, King Mongkut's University of Technology Thonburi, Bangmod, Bangkok 10140, Thailand b Institute for Problems in Mechanics, Russian Academy of Sciences, Vernadsky Ave. 101, Moscow 117526, Russia

Received 18 May 2001; received in revised form 15 August 2001

1. Introduction

Problems involving the interaction between an air stream and a water layer flowing parallel to it or being stagnant are commonly met in engineering and geophysical practice (see Butterworth and Hewitt, 1977; Phillips, 1977). Existing theories are unable to give detailed and quantitative explanations of the mechanism of drift current and wave generation and rely to a large extent on empirical results. Experimental investigations of flow structure therefore play a key role in the development of knowledge in this field. Data in horizontal air-water flow presented here is to gain essential information on current structure inside air and water layers. Velocity measurements of some relevance to this study have been reported in Hanratty and Engen (1957), Lin and Gad-el-Hak (1984), Caulliez (1987), Paras and Karabelas (1992), Paras et al. (1998). The determination of the velocity field has been made either in water (see Baines and Knapp, 1965; Goossens et al., 1982; Kranenburg, 1985; Caulliez, 1987; Tsanis, 1989; Paras and Karabelas, 1992) or in air (see Hanratty and Engen, 1957; Wu, 1975; Lin and Gad-el-Hak, 1984; Paras et al., 1998). In principle, the results so obtained are generally incomplete for lack of simultaneous measurements of air and water velocity profiles under the same experimental conditions. In the present work, we are mainly interested in water and air velocity fields when the interface is undisturbed and transition from stratified to wavy flow takes place. The interaction of two-phase streams is reflected in the form of the velocity profiles.

2. Experimental setup and procedure

The velocity measurements were carried out in an experimental setup developed at FUTURE, where cocurrent horizontal air-water flow was established in a 54 × 54 mm rectangular channel

Corresponding author. Tel.: +662-02470-9115; fax: +662-02470-9111. E-mail address: somchai.won@kmutt ac.th (S. Wongwises).

0301-9322/02/\$ - see front matter © 2001 Elsevier Science Ltd. All rights reserved.

PII: \$0301-9322(01)00056-8

with a 2.2 m long straight test section. The setup included the test section, air supply, water supply, instrumentation, and data acquisition system (see Wongwises et al., 1999). Water was pumped from the storage tank through the rotameter to the inlet section at the bottom of the feed pipe. A suction-type blower supplied air to the test section. It passed through a filter and then entered the mixing section through the pressure regulator. Both the air and water streams were brought together in a mixer and then passed through the test section cocurrently. The air velocity could be varied from 0.5 to 10 m/s and the water velocity from 0 to 30 cm/s. Although the water surface elevation along the downwind shore was raised to a sizable amount (~1-2 mm), producing the wind setup, the fetch length which is a length of wind action on the interface, was 10³ or more times this dimension.

Velocity distributions were measured across the channel at the distance x = 140 cm from the inlet. A He-Ne based Laser Doppler Anemometer (LDA-03, Dantec) with photomultiplier was employed in order to make measurements of local horizontal velocity within the liquid phase. The ellipsoidal measuring volume, formed by the intersection of two focused laser beams, had major and minor axes 3.5 and 0.25 mm, respectively. The photomultipliers output signal caused by forward-scattered light was fed to the flow velocity analyzer FVA58N20 which performed statistical analysis of Doppler signal. The traverse mechanism provided precise spatial movement of the measuring volume. For each run, measurements of local instantaneous horizontal velocity, u, were made along the vertical channels direction, y, starting at a distance as close as 0.5 mm from the channel bottom and ending 0.5-1.5 mm from the air-water interface to avoid light reflections.

Air velocity in a cocurrent flow was measured by using constant temperature anemometer (CTA-90CN10/C10, Dantec) with automatic probe setup and execution of experiments. The StreamWare software setup the anemometer modules, performed velocity and directional calibrations and provided an experiment platform, where automatic sequences of hardware setup, data acquisitions and data reductions could be carried out. The probe used in this experiment was the wedge-shaped, right-angled film probe 55R33 with noncylindrical sensor in 1×0.2 mm. The probe was placed on a carrier which could be positioned anywhere in a given section of the channel. The error of the velocity measurements was about 8-10%. The surface velocity of the water was estimated roughly by placing small 2 mm diameter paper pieces on the water and measuring the time required for them to move past fixed stations downstream.

3. Results and discussion

Before the main experiments, the velocity profile in single-phase air-water flow was measured to assess the overall accuracy of experimental results. The mean streamwise velocities measured in the channel for the five different cases are plotted in semi-logarithmic form in Fig. 1. Reynolds numbers of 5535, 15862, 17786, and 23670 described symmetric air flow, and the Reynolds number of 7250 depicted the asymmetric open-channel flow of water with zero shear stress at the free surface. The Reynolds number, Re, is based on the maximal velocity, flow depth and kinematic viscosity: $u_{\text{max}} = 1.64$, 4.70, 5.27, and 7.01 m/s, and $h_1 = 54$ mm, $v_1 = 0.12$ cm²/s for air, and $u_{\text{max}} = 1.64$ cm/s, $h_2 = 25$ mm, $v_2 = 0.01$ cm²/s for water, respectively. The vertical coordinate, v_1 , and the mean velocity, v_2 , were rescaled on the basis of wall-related variables, v_2 is the friction velocity defined by

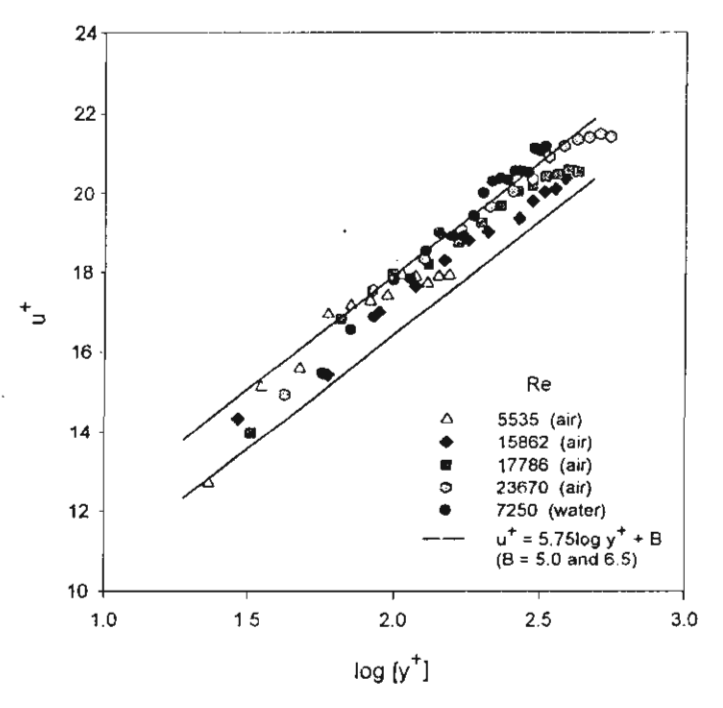


Fig. 1. Velocity distribution on the depth of the single phase flow; air: Re = 5535, 15862, 17786 and 23670; water: Re = 7250, calculation: $u^+ = 5.75 \log y^+ + B$ (B = 5.0 and 6.5)

$$u^* = 0.477 u_{\text{max}} / \ln(0.06 Re_x). \tag{1}$$

The local Reynolds number, Re_x , is defined by $Re_x = u_{\text{max}}x/v$, where v is kinematic viscosity and x is the measuring section of the channel (140 cm). Fig. 1 shows the relationship between $\log y^+$ and u^+ measured with CTA and LDA. The lines represent log-law, $u^+ = 5.75 \log y^+ + B$ (Schlichting, 1951), with B = 5.0 and 6.5, respectively. Good agreement between the measured values and those predicted by well-known universal velocity profile was obtained.

The mean streamwise air velocities measured in the channel for the different cases for a stagnant water are plotted in Fig. 2 and those for a flowing water in Fig. 3. The coordinate y in these figures was measured from the undisturbed air—water interface to the top of the channel wall. In all cases, the plane of maximum air velocity was located closer to the air—water interface. In the former case, the plane of maximum velocity was determined by $y/h_1 \approx 0.40$; in the latter case, $y/h_1 \approx 0.45$. Up to maximal air velocity, u_{max} , of about 4.6 m/s, no waves appeared on the water surface. When u_{max} exceeded 4.6 m/s, the small three-dimensional disturbances had wavelengths of 1-2 cm and amplitudes of 0.1-0.2 mm. For the air velocities in the range of $u_{\text{max}} = 6-8$ m/s, significant two-dimensional waves developed from the initial ripples, and traveled with crests approximately normal to the air direction. Under the action of steady air motion, the waves traveled downstream at an increasing celerity ($\sim 30-40$ cm/s), while growing both in amplitude and in length. In the measurements section, x = 140 cm, typical magnitudes of the observed amplitudes and wavelengths were of order of 0.5-1.0 mm and 2.5 cm, correspondingly. These factors allowed the water surface not to be smooth and the shear stress to be larger at the interface than at the top of an enclosed air space. Similar to Parthasaraty and Muste (1994), we can assume

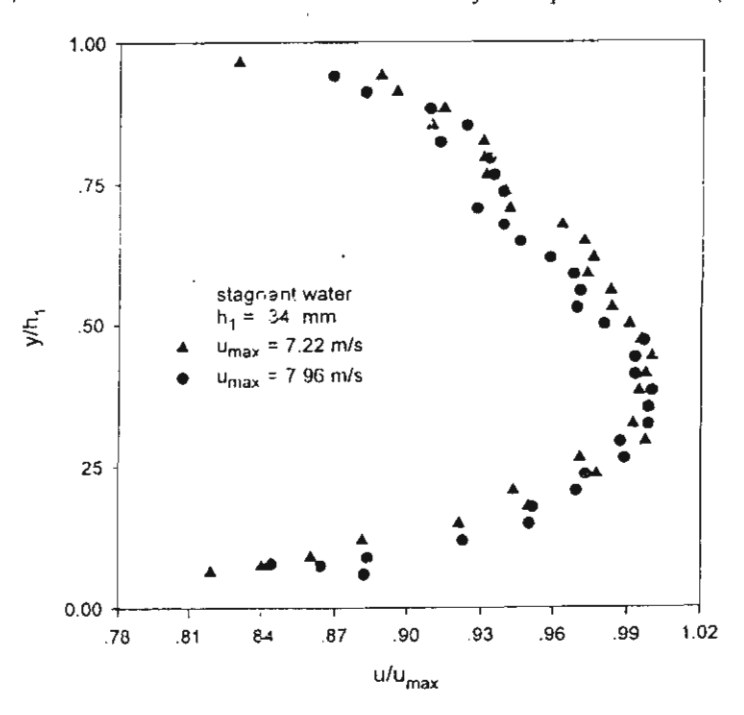


Fig. 2. Typical horizontal air velocity profile along the vertical for a stagnant water. The coordinate y is measured from the undisturbed air-water interface to the top of the channel wall; $h_1 = 34$ mm, $u_{\text{max}} = 7.22$ and 7.96 m/s.

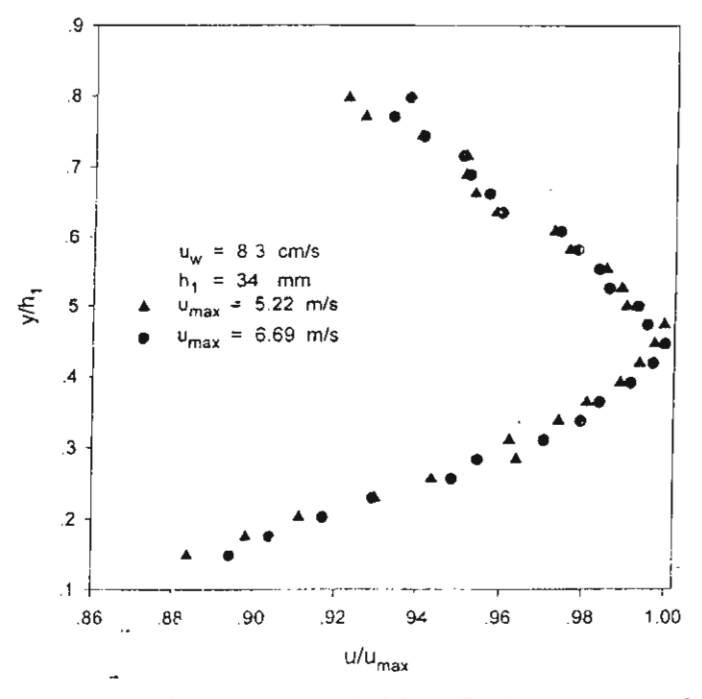


Fig. 3. Typical horizontal air velocity profile along the vertical for a flowing water, $u_w = 8.3$ cm/s. The coordinate y is measured from the undisturbed air-water interface to the top of the channel wall; $h_1 = 34$ mm, $u_{\text{max}} = 5.22$ and 6.69 m/s.

the noncoincidence of the plane of maximum air velocity and zero shear stress – it means that the plane of zero shear stress lies closer to the smooth surface, the upper wall. These trends are in agreement with those observed by Paras et al. (1998). However the measured air velocity profiles obtained by Hanratty and Engen (1957) and Dykhno et al. (1994) display a significantly different behavior having their maximal velocity above the center of the air flow space. Their mean shifts are about 10–12% towards the top of the channel wall.

The air flow had a strong influence on the water layer. Since the air was forced by the fan through the channels part of approximately constant cross-section, a pressure gradient was developed in the downstream direction. This pressure gradient increased with air velocity and the water depth. In the closed channel (initially stagnant water) the air flow resulted in a drift current in the upper layer just below the interface and a reverse flow near the bottom. In the case of a flowing water, effect of air was seen in a dramatic distortion of water velocity profiles.

The water surface velocity, u_s , against the maximal air velocity, u_{max} , is shown in Fig. 4. Measurements were conducted in the range of $u_{max} = 3-8$ m/s, thus far, no consideration has been given to the role of breaking waves. The surface velocity ranged from 2 to 18 cm/s and varied nearly quadratically with the air velocity. A curve in Fig. 4 was fitted to the data, with result that $u_s = 0.003 \ u_{max}^2$.

Air-driven water currents were investigated in the present experiments for the wide range of maximal air velocity, $u_{\text{max}} = 1.0-8.0 \text{ m/s}$, and two depths of initially stagnant water layer, $h_2 = 12$ and 20 mm. At $u_{\text{max}} < 3.5 \text{ m/s}$, the main water currents followed the air direction, and the return flow near the bottom was small. If u_{max} exceeded 3.5 m/s, a strong return flow was extended to 70% of the water layer except near the surface. Typical distributions of mean water velocity normalized by the surface velocity, u_{s} , are presented in Fig. 5. Notice that a distinct peak near the

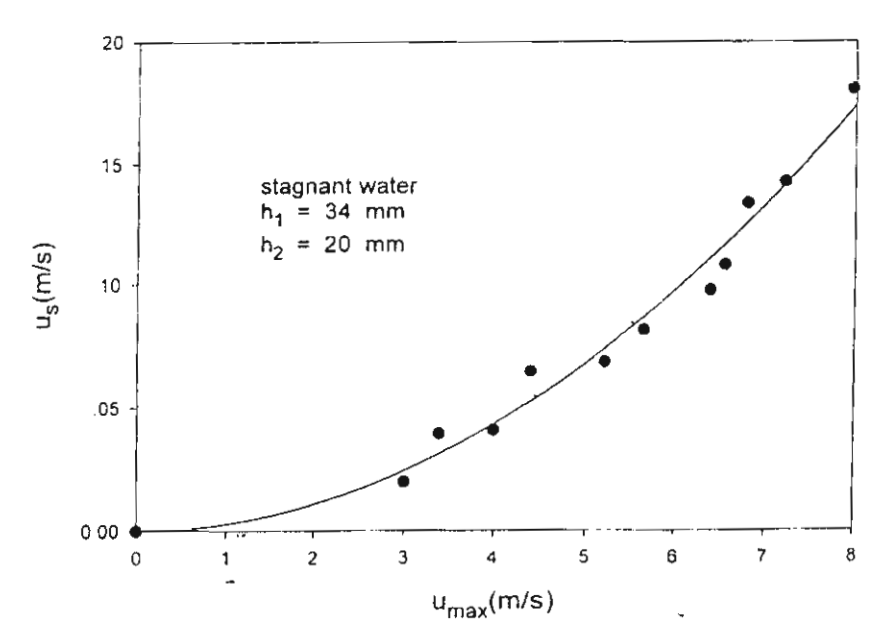


Fig. 4. Water surface velocity, u_s as a function of maximal air velocity, u_{max} (stagnant water, $h_1 = 34$ mm, $h_2 = 20$ mm).

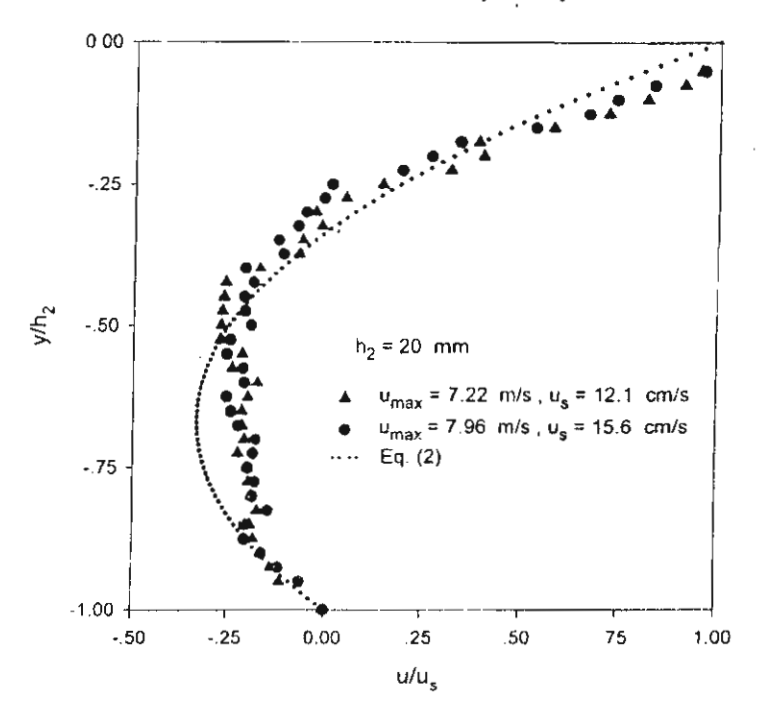


Fig. 5. Distribution of mean velocity in air-driven water currents, $h_2 = 20$ mm: $u_{\text{max}} = 7.22$ m/s, $u_s = 12.1$ cm/s and $u_{\text{max}} = 7.96$ m/s, $u_s = 15.6$ cm/s.

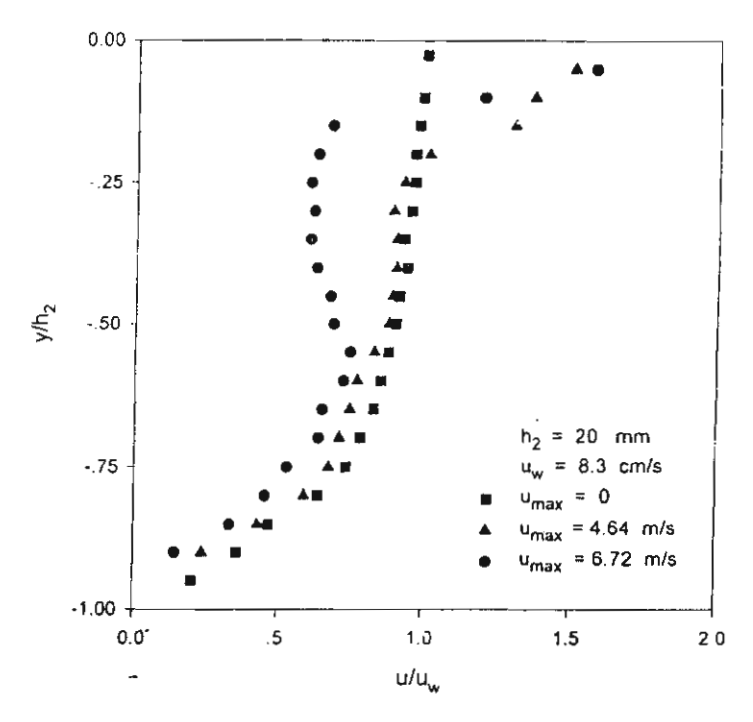


Fig. 6. Distribution of mean velocity in cocurrent air-water flow, $h_2 = 20$ mm, $u_w = 8.3$ cm/s: $u_{max} = 0$, 4.64 and 6.72 m/s.

bottom described by Baines and Knapp (1965) was missed. The curve shown in Fig. 5 corresponds to the well-known parabolic velocity distribution of steady-laminar shear induced flow

$$u/u_{s} = 1 + 4(y/h_{2}) + 3(y/h_{2})^{2}.$$
 (2)

For a cocurrent air-water flow, the distributions of mean water velocity are shown in Fig. 6. The velocity profile for the water flow, $u_{\rm w}=8.3$ cm/s, with zero air flow rate was smooth and completely described by the laminar open-channel model. As the air velocity increased and got to $u_{\rm max}=4.64$ m/s, the jet-like current near the interface was developed. The surface velocity, $u_{\rm s}$, was order of 1.5 $u_{\rm w}$, and the air-driven current was extended to $0 < y/h_2 < 0.2$. For the air velocity in the range of $u_{\rm max}=5-8$ m/s, the surface velocity increased, $u_{\rm s}\approx 2u_{\rm w}$, the current at all layers followed the air direction, and the typical velocity profile had a distinct local minimum $u/u_{\rm w}\sim 0.6$ at $y/h_2\approx 0.25$ and a local maximum $u/u_{\rm w}\sim 0.75$ at $y/h_2\approx 0.75$. These features of velocity distributions were common for the present experimental conditions, $u_{\rm w}=8-22$ cm/s and $h_2=12-20$ mm.

4. Conclusion

This paper presents new experimental data on the simultaneous measurement of the velocity profile in the air and underlying water layer. In conclusion, our results show that the interaction between air and water flows produces the displacement of the maximum air velocity plane toward the interphase. This behavior should be taken into account in phenomenological models trying to reproduce the shear stress distribution. We have found that in cocurrent two-phase flow air effect is seen in a dramatic distortion of water velocity profiles.

Acknowledgements

The present work was supported financially by the Thailand Research Fund (TRF) whose guidance and assistance are gratefully acknowledged.

References

Baines, W.D., Knapp, D.J., 1965. Wind driven water currents. J. Hydraul. Div. ASCE 91, 205-221.

Butterworth, D., Hewitt, G.F., 1977. Two-Phase Flow and Heat Transfer. Oxford University Press, Oxford.

Caulliez, G., 1987. Measuring the wind-induced water surface flow by laser Doppler velocimetry. Exp. Fluids 5, 145-153.

Dykhno, L.A., Williams, L.R., Hanratty, T.J., 1994. Maps of mean gas velocity for stratified flows with and without atomization. Int. J. Multiphase Flow 20, 691-702.

Goossens, L.H.J., van Pagee, H.J.A., Tessel, P., 1982. Vertical turbulent diffusion in air-driven water flows. J. Hydraul. Div. ASCE 108, 995-1009.

Hanratty, T.J., Engen, J.M., 1957. Interaction between a turbulent air stream and a moving water surface. AIChE 3, 299-304

Kranenburg, C., 1985. Mixed-layer deepening in lakes after wind setup. J. Hydraul. Eng. ASCE 111, 1279-1297.

Lin, J.T., Gad-el-Hak, M., 1984. Turbulent current measurements in a wind-wave tank. J. Geophys. Res. 89, 627-636. Paras, S.V., Karabelas, A.J., 1992. Measurements of local velocities inside thin liquid films in horizontal two-phase flow. Exp. Fluids 13, 190-198.

Paras, S.V., Vlachos, N.A., Karabelas, A.J., 1998. LDA measurements of local velocities inside the gas phase in horizontal stratified atomization two-phase flow. Int. J. Multiphase Flow 24, 651-661.

Parthasaraty, R.M., Muste, M., 1994. Velocity measurements in asymmetric turbulent channel flows, J. Hydraul. Eng. ASCE 120, 1000–1020.

Phillips, O.M., 1977. The Dynamics of the Upper Ocean. Cambridge University Press, London.

Schlichting, H., 1951. Grenzschicht-Theorie. Braun GmbH, Karlsruhe.

Tsanis, I.K., 1989. Simulation of wind-induced water currents. J. Hydraul. Eng. ASCE 115, 1113-1134.

Wongwises, S., Pornsee, A., Siroratsakul, E., 1999. Gas-wall shear stress distribution in horizontal stratified two-phase flow. Int. Comm. Heat Mass Transfer 26, 849–860.

Wu, J., 1975. Wind-induced drift currents. J. Fluid Mech. 58, 49-70.

Wongwises, S., Kongkiatwanitch, W., Interfacial Friction Factor in Vertical Upward Gas-Liquid Annular Two-Phase Flow, *Int. Com. Heat Mass Transfer*, 2001; 28(3): 323-336.



PII: S0735-1933(01)00238-X

INTERFACIAL FRICTION FACTOR IN VERTICAL UPWARD GAS-LIQUID ANNULAR TWO-PHASE FLOW

Somehai Wongwises and Wittaya Kongkiatwanitch
Fluid Mechanics and Turbomachinery Research Laboratory (FUTURE)
Department of Mechanical Engineering,
King Mongkut's University of Technology Thonburi,
Bangmod, Bangkok 10140, Thailand

(Communicated by J.P. Hartnett and W.J. Minkowycz)

ABSTRACT

This paper presents new data on the gas-liquid interfacial friction factor in annular two-phase upward co-current flow in a vertical circular pipe. Different from most previous work, the present studies have been performed at relatively high film thickness, taking into consideration the effect of the entrained droplets which occur from the breakup of the disturbance waves. The test section has an inner diameter of 29 mm and the length of 3 m. The porous wall injector is used to introduce the liquid into the test section. The two phase pressure drop is measured by two static pressure tubes connected with a manometer. The film thickness is measured by calibrated stainless ring electrodes mounted flush in the tube wall. The electrode operates on the principle of the variation of electrical resistance with changes in the liquid film thickness between two parallel electrode rings. The entrained liquid flow rate is measured by using a sampling probe connected with a cyclone separator. The entrainment flow rate in the gas core is calculated from an assumption that the sampling is carried out in an isokinetic manner. The results from the experiments are compared with those calculated from correlations reported in the literature. A new empirical correlation for predicting the interfacial friction factors for practical applications is proposed. © 2001 Elsevier Science Ltd

Introduction

Vertical upward gas-liquid two-phase annular flow is encountered in several industrial applications including the flow of refrigerants in air conditioning and refrigerating systems, the flow of oil and gas in petroleum industries and the flow of steam in power plants e.g. in emergency core cooling (ECC) systems of a nuclear reactor during the postulated loss of coolant accidents (LOCA). Annular two-phase flow is one of the most important flow regimes and is characterized by a phase interface separating a thin liquid film from the gas flow in the core region. Because of its practical importance and the relative ease to which analytical treatment may be applied, this flow regime has received the most attention both analytically and experimentally. In this flow regime, it is generally true that due to the breakup of the

disturbance wave, part of liquid phase is entrained as droplets into the gas core. It is also accepted that mass, momentum and energy transfers are strongly affected by entrainment of the droplets to the gas core [1].

Interfacial shear stress in the annular two-phase flow is one of the main parameters governing transport phenomena and is required for modeling the flow. It has been intensively studied, especially for the flow assuming that all liquid travels in the liquid film. Some of earliest work was performed by Cousins [2], Wallis [3], Webb [4], Whalley [5,6], Andreussi [7], Hewitt [8], Asali [9], Azzopardi [10], Fukano [11]. Recently, Fore et al. [12] has obtained the film thickness and pressure gradient data for cocurrent upward flow of nitrogen and water under high pressure in a rectangular duct. A correlation of the interfacial friction factor obtained from their own data and those from several others mentioned in the literature was proposed.

Although some information is currently available on interfacial friction factor for annular two-phase flow, there still remains room to discuss whether it gives reliable predictions of the interfacial shear stress in two-phase annular flow. The purpose of this work is to obtain the experimental results of interfacial shear stress while considering the droplet entrainment from relatively high liquid film thickness. The results from the experiment are compared with those calculated from the correlations reported in the literature. A new empirical correlation for predicting the interfacial friction factors for vertical upward gas-liquid two-phase annular flow with droplets entrained into the gas core is proposed.

Experimental Apparatus and Method

The experimental apparatus is shown schematically in Fig. 1. Air and water are used as the working fluids. The main components of the system consist of the vertical test section, air supply, water supply, instrumentation and data acquisition system. The test section, with an inside diameter of 29 mm and the length of 3 m is made of transparent acrylic glass to permit visual observation of the flow patterns. An upper closed end condition [13] is used in the experiments. The connections of the piping system are designed such that parts can be changed very easily. Water is pumped from the storage tank through the rotameter, the air-water mixer and the test section. Air is injected from a compressor to pass through the reservoir, the regulation valve, the orifice, the mixer and the test section.

The air-water mixer is constructed from two concentric tubes, the inner tube being a part of the test section which is radially drilled with many small holes. The inner tube is also covered with a porous material. They serve to introduce water smoothly along the test section. The water from the air-water mixer flows upward together with air and then flows back to the storage tank. At a position 2.06 m from

the water inlet section, a sampling probe connected with a cyclone separator is mounted for collecting the entrained droplets. The sampling probe has an i.d. of 7 mm and o.d. of 9 mm. These diameters are considered to be small enough so that the flow in the test section can not be disturbed by the probe and the disturbance waves can not be sampled. The entrained water flows through the cyclone separator, the water is returned to a graduated beaker while the separated air is exhausted into the atmosphere. The cyclone separator is typical for normal use and designed by a technique described in Mycock et al. [14].

The inlet flow rates of air and water are measured by means of an orifice and rotameter respectively. Two static pressure tubes connected with manometer are used to measure the pressure drop. Stainless ring electrodes are mounted flush in the tube wall for measuring the film thickness. The measuring positions are located at 1.2 m from the lower end of the test section. They operate on the principle of the variation of electrical resistance with changes in the water film thickness between two parallel electrode rings. The same description of the calibration procedures for annular flow can be found in Wongwises et al. [15]. Due to the variation of conductivity with temperature and coating of the electrodes with impurities, the gauges are calibrated before and after each run. The measured electrical resistance is a function of the electrode distance, the electrode width, and the liquid film thickness between electrodes.

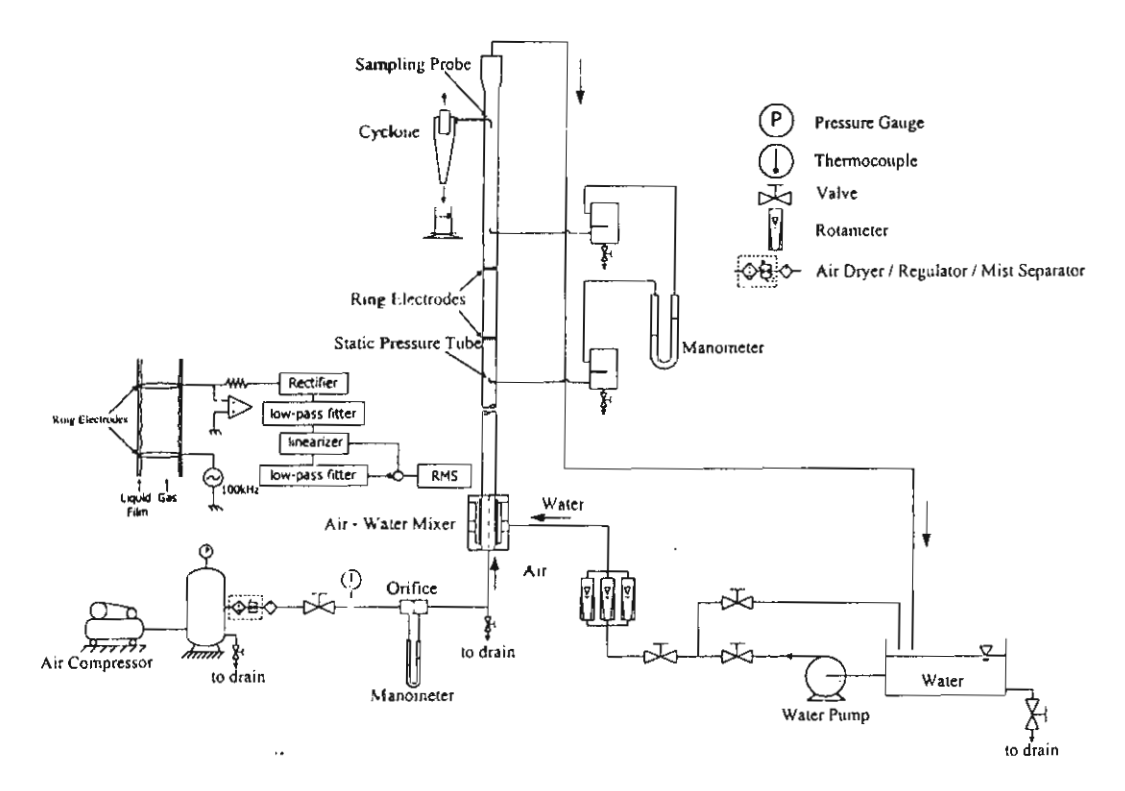


FIG. 1
Schematic diagram of experimental apparatus

Experiments are conducted at various air and water flow rates in the annular flow regime. The air flow rate is increased by small increments while the water flow rate is kept constant. The system is allowed to approach the steady condition before any data is recorded. After stabilization, the air and water flow rates are recorded. The entrained droplets are sampled at specific periods. The pressure drop across the test section is detected. The film thickness is registered through the transducers. The flow phenomena are also detected by visual observation and sometimes by a digital camera. The experiments are carried on until the annular flow pattern disappears.

Mathematical Model

The interfacial shear stress on the surface between the liquid and gas phase can be determined by using the conservation equations for an element of steady vertical upward cocurrent gas-liquid annular flow. The mathematical model is based on that of Fore et al. [12] with the following assumptions:

- The flow is fully developed and steady.
- The liquid film is thin compared to the tube diameter and the shear stress in the liquid film is assumed constant and is equal to the interfacial shear stress.
- The effect of vaporization and condensation on the gas flow field is neglected.
- Physical properties of the fluids are constant and independent of the composition.
- The concentration of the liquid droplets in the gas core is determined on a homogeneous basis.

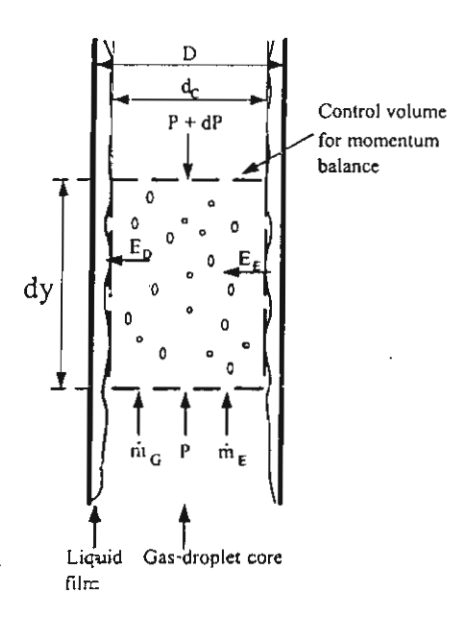


FIG. 2
Control volume for analysis of vertical upward two phase annular flow

The one-dimensional equation for momentum conservation of the gas - liquid droplets mixture yields the Newton's second law formulation for a nonaccelerating control volume (Fig. 2.), is given by

$$\iint \rho_c u_y^2 dA = -\rho_c g A_c dy - (A_c dP + \tau_i S_c dy)$$
 (1)

The left-hand side term represents the net rate of the momentum efflux through the control surface, in this case, is the momentum changes caused by the entrainment of droplets into the control volume and deposition of the droplets out of the control volume. The following equation is then obtained:

$$\iint \rho_c u_y^2 dA = S_c (E_D U_D - E_E U_E) dy + A_c d(\rho_c U_y^2)$$
CS
(2)

The two terms on the right-hand side of Eq. (1) are regarded as body and surface forces acting on this nonaccelerating control volume respectively.

where u_y is the local velocity in the axial direction, ρ_C is the density of mixture in the gas core, A_C is the cross sectional area of the gas core, S_C is the perimeter of the gas core, E_D is the rate of mass flux of depositing droplets on the liquid film, E_E is the rate of mass flux of entrained droplets from the liquid film, U_y is the mean velocity of mixture, τ_i is the interfacial shear stress, U_E and U_D are the mean axial velocities of entraining and depositing droplets, respectively.

Substituting Eq. (2) into Eq. (1) then gives

$$\tau_{i} = E_{E}U_{E} - E_{D}U_{D} - \frac{1}{S_{c}} \left[A_{c} \frac{dP}{dy} + \frac{d}{dy} \left(\rho_{c} A_{c} U_{y}^{2} \right) + \rho_{c} A_{c} g \right]$$
 (3)

where the pressure gradient, dP/dy, is the pressure drops with increasing axial vertical length and is necessarily negative.

Total mass flow rate of the mixture can be determined from

$$\dot{\mathbf{m}}_{G} + \dot{\mathbf{m}}_{E} = \rho_{c} \mathbf{U}_{y} \mathbf{A}_{c} \tag{4}$$

where \dot{m}_G and \dot{m}_E represent the mass flow rates of gas and entrainment, respectively

Further, from the continuity equation and ideal gas law (P = ρ RT; R is a gas constant, T is an absolute temperature), we have

$$-\frac{dU}{U} = \frac{d\rho}{\rho} = \frac{dP}{P} \tag{5}$$

Substituting Eq. (5) into the derivative of $U_y(\dot{m}_G + \dot{m}_E)$ and substituting the result into Eq. (3) with assuming that $U_y = U_G$, we obtain

$$\tau_i = E_E U_E - E_D U_D - \frac{1}{S_c} \left[A_c \frac{dP}{dy} + U_G \frac{d\dot{m}_E}{dy} - \left(\frac{\rho_c A_c U_G^2}{P} \right) \frac{dP}{dy} + \rho_c A_c g \right]$$
(6)

It should be noted that if all the liquid travel in the film (or without entrainment), Eq.(6) may be reduced to

$$\tau_i = -\frac{A_c}{S_c} \left[\frac{dP}{dy} + \rho_c g \right]$$
 (7)

Eq. (7) is very well known and has been commonly used to study the interfacial shear stress in annular two phase flow [6, 9, 11, 16].

Results and Discussion

By assuming that the sampling is carried out in an isokinetic manner [17], the superficial velocities of air flowing through the sampling probe are therefore equal to those in the test section. The entrainment volumetric flow rates in the gas core, $Q_{\rm F}$, can be then determined from the following equation

$$Q_E = A_P (1 - H_L) (Q'_E / A_{SP})$$
 (8)

where A_P is the cross-sectional area of pipe, H_L is the liquid hold up which is defined as the ratio of the cross-sectional area filled with liquid to the total cross-sectional area of the pipe, A_{SP} is the cross-sectional area of the sampling probe and Q_E' is the entrainment volumetric flow rate through sampling probe. This entrainment volumetric flow rate, Q_E , is further used to determine several parameters.

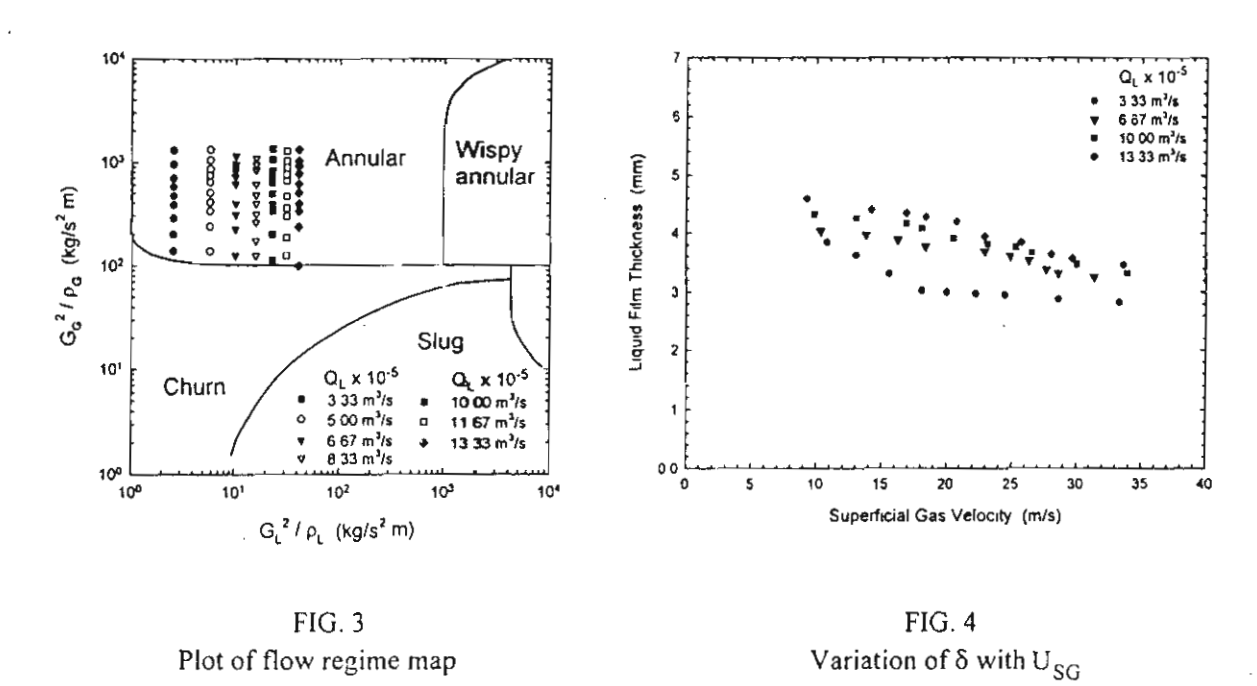
In the experiments, air flow rate was increased in small increments while the injected water flow rates were kept constant. Visual observation showed that different annular flow patterns might occur. In general, the separation of the three parts was observed; the liquid phase formed an annulus flowing partly as a thin film on tube wall, the gas phase formed the core and a part of liquid phase formed as droplets entrained in the gas core. The usual method in the presentation of flow pattern data is to classify the flow pattern by visual observation and plot the data in the flow regime map in terms of system parameters. Fig. 3 shows a comparison of the observed flow patterns with a flow regime map developed by Hewitt and Roberts [18]. The map is based on extensive data bank is given using the momentum fluxes of gas and liquid as the coordinates. Plotting the data points on this flow regime map, it is found to be in very good agreement qualitatively. It also corresponds with the criterion that when the dimensionless superficial gas velocity,

U_{SG}, where is given by

$$U_{SG}^{*} = U_{SG} \left[\rho_{G} / (\rho_{L} - \rho_{G}) gD \right]^{1/2}$$
 (9)

is greater than 1, annular flow is often said to occur [16].

In the experiment, the mean liquid film thickness was measured at y = 1.20 m from the water inlet section. Figure 4 shows the variation of the mean liquid film thickness with the superficial gas velocity obtained from the present experiment. As the superficial gas velocity increases and the liquid flow rate is held constant, the liquid film thickness decreases and asymptotically approaches a value. The mean liquid film thickness at high gas flow rates for all liquid flow rates is, however, nearly the same.



The comparison of the present experimental liquid film thickness with the calculation results from two existing correlations for annular flow of Henstock and Hanratty [19] developed on the basis that the liquid droplets are entrained in the gas core and the roll wave existed on the liquid film:

$$\delta U_{L}^{*} / V_{L} = \left(\left(0.707 \, \text{Re}_{LF}^{0.5} \right)^{2.5} + \left(0.0379 \, \text{Re}_{LF}^{0.9} \right)^{2.5} \right)^{0.4}$$
 (10)

and of Asali et al. [9]:

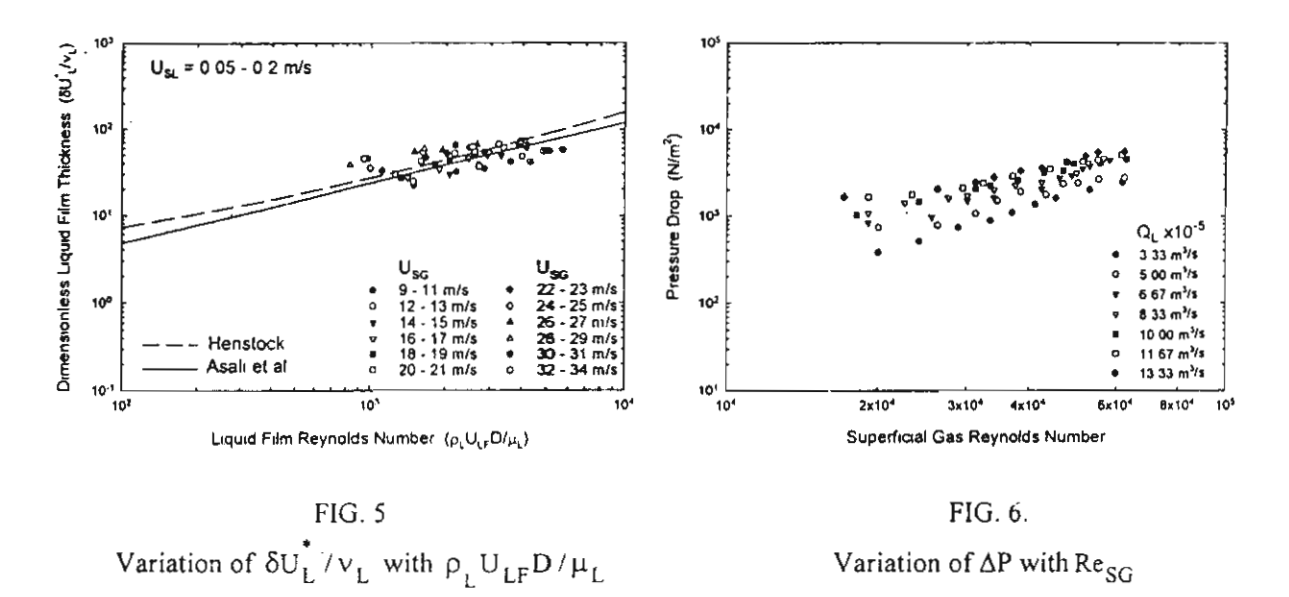
$$\delta U_L^* / V_L^{} = 0.19 \, \text{Re}_{LF}^{0.7}$$
 (11)

where Re I F is the liquid film Reynolds number determined from

$$Re_{LF} = \rho_1 U_{LF} D/\mu_L \tag{12}$$

are shown in Fig.5. The results from the correlations are in good agreement and also show similar tendencies to the present experimental data.

Figure 6 shows the variation of the measured pressure drop, ΔP , with superficial gas Reynolds number, Re_{SG} . As expected, as the superficial gas Reynolds number increases, the pressure drop also increases. At the same superficial gas Reynolds number, the pressure drop for higher liquid flow rate is higher than the pressure drop for lower liquid flow rate. However the slope of graph for higher liquid flow rate is slightly higher.



Due to annular flow in the present study is assumed to be equilibrium, therefore, the entrainment mass flow rate has no variation with axial length $(d\dot{m}/dy = 0)$ and the deposition rate, E_D , and the entrainment rate, E_E , become equal. In this study, the entrainment rate is estimated by using the correlation of Whalley and Hewitt [6] as follows

$$E_{F} = kC (13)$$

where C is the concentration of the liquid droplets in the gas core considered to be a homogeneous mixture and is given by

$$C = G_E/U_{GC}$$
 (14)

and G_E is the mass flux of the entrained droplets, based on whole cross sectional area of the tube;

$$G_E = \rho_L Q_E / A \qquad (15)$$

where QE is the entrainment flow rate through the gas core and UGC is the core velocity defined as

$$U_{GC} = G_G/\rho_G + G_F/\rho_L \tag{16}$$

and k is the mass deposition coefficient proposed by Whalley and Hewitt [6], this is

$$k = 87\sqrt{\tau_i \,\mu_L^2 / D\sigma \rho_L \,\rho_C} \tag{17}$$

where σ is the surface tension. Usually, the mean gas velocity in the gas-droplet core, U_G , in Eq. (6) is the function of y. However in this study, it is substituted by measured average gas velocity in the annular core. The entraining droplet velocity, U_E , and the depositing droplet velocity, U_D , are taken as two times the mean liquid film velocity [12] and 80 % of the mean gas velocity [12], respectively.

Using the experimental data and above calculated parameters, the interfacial shear stress can be determined. Figure 7 shows the variation of the interfacial shear stress obtained from the present study with the superficial gas Reynolds number. The interfacial shear stress tends to increase with increasing the superficial gas Reynolds number. At the same superficial gas Reynolds number, the interfacial shear stress for higher liquid flow rate is higher than the interfacial shear stress for lower one. It corresponds with the pressure drop curves shown in Fig. 6.

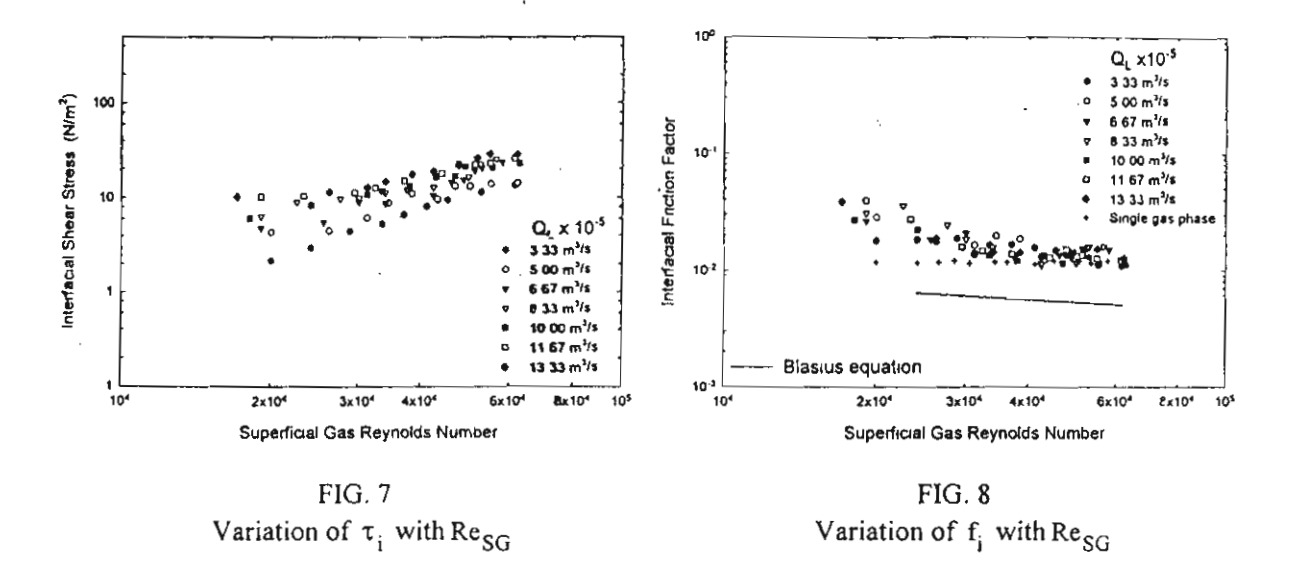
The following correlation was proposed by Wallis [20] to determine the interfacial shear stress

$$\tau_{i} = \frac{1}{2} f_{i} (\rho_{G} + C) U_{GC}^{2}$$
 (18)

Substituting τ_i calculated from Eq.(6) into Eq.(18), the interfacial friction factor, f_i , could be then determined. Figure 8 shows the variation of the interfacial friction factor with the superficial gas Reynolds number obtained from the present experiment for typical test conditions. The Blasius correlation for turbulent flow in smooth pipe is also shown in this figure. As a result of the pipe roughness, experimental friction factors for single-phase gas flow are found to be higher than those from the Blasius correlation. At lower superficial gas Reynolds number, as the liquid flow rate increases, larger disturbance waves are formed. The friction factors at higher liquid flow rates seems, therefore, a little bit higher than those at lower ones. However, for all liquid flow rates, the friction factor tends to decrease gradually. Finally, at larger superficial gas Reynolds number, the friction factor levels out at a constant value.

Figure 9 shows the relationship between the interfacial friction factor and the relative liquid film thickness, δ/D, obtained from the experiment for whole ranges of gas and liquid flow rates. For each liquid flow rate, the interfacial friction factor decreases with increasing gas flow rate. This is due to the film thickness becoming smaller as the gas flow rate increases. Because of the higher amplitude of the film thickness fluctuation at higher liquid flow rate, the interfacial friction factor increases, therefore,

sharply with increasing the film thickness. In general, the interfacial friction factor tends to increase with increasing the liquid film thickness.



Several existing correlations dealing with annular flow will be compared with the present data. Wallis [3] proposed a classical correlation for interfacial friction factor as a function of the mean liquid film thickness;

$$f_i = 0.005 (1 + 300 \delta/D)$$
 (19)

Moeck [21] also developed a similar form of interfacial friction factor correlation for the flow in the disturbance wave region;

$$f_i = 0.005 (1 + 1458 (\delta/D)^{1.42})$$
 (20)

Later, the correlation of Wallis has been modified by Fore et al. [12] for better fit to very small film thickness data obtained from several past studies;

$$f_i = 0.005 (1 + 300 (\delta / D - 0.0015))$$
 (21)

Recently, Fukano [11] suggested an empirical correlation for interfacial friction factor with the consideration of the change in the fluid viscosity.

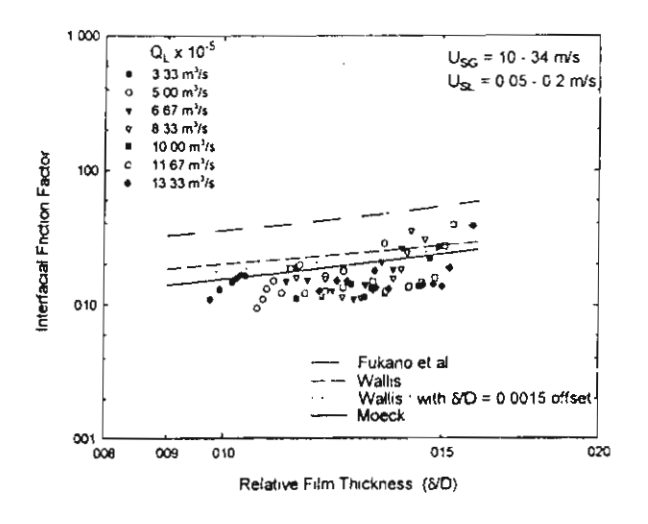
$$f_i = 0.425 (12 + v_L / v_W)^{-1.33} (1 + 12 \delta / D)^8$$
 (22)

The interfacial friction factors obtained from the present study are compared with those from the predictions by the above mentioned correlations. It should be noted that the Fukano correlation overpredicts all values of the present interfacial friction factor. Wallis, modified Wallis, and Moeck correlations are in fair agreement only with some present data. It is also clear to see that all existing correlations fail to predict the interfacial friction factor at higher mean liquid film thickness.

Figures 8 and 9 indicate that changes in the superficial gas Reynolds number and the relative film thickness have an effect on the interfacial friction factor. According to the dimensional analysis of fully developed single-phase turbulent flow in pipes, the friction factor is a function of Reynolds number and relative roughness. Also the graph shown in Fig. 8 corresponds to the transition zone in the Moody diagram. The thickness of the viscous wall layer in this transition zone decreases while the average roughness elements size begin to prod through this layer. In this zone, not only Reynolds number but also the effect of roughness becomes important. The correlation used to calculate the friction factor in this zone is that which combines the smooth and rough limit. With the afore-mentioned reasons, the significant variables for an empirical correlation obtained from the present study is considered to be the superficial gas Reynolds number and dimensionless film thickness. The empirical equation is now

$$f_i = a \operatorname{Re}_{SG}^{b} (\delta/D)^{c}$$
 (23)

Correlation of this equation with all data gives the coefficient of determination (R^2) = 0.93. The corresponding coefficients are: a = 17.172, b = -0.768 and c = -0.253.



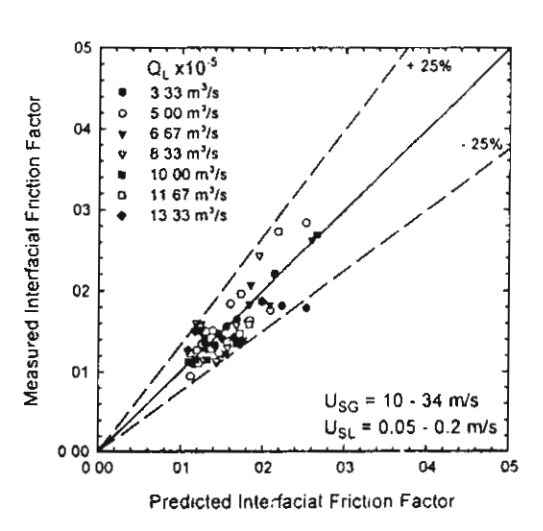


FIG. 9 Variation of f_i with δ/D

FIG. 10 Comparison of f_i

Comparison of the interfacial friction factors obtained from the experiment with those calculated by the proposed correlation is shown in Fig. 10. It is clear from this figure that the majority of the data fall within \pm 25 % of the proposed correlation.

Conclusions

Experiments in annular flow regime were performed to determine the two-phase pressure drop, interfacial shear stress and interfacial friction factor for two-phase air-water upward cocurrent flow in a 29 mm i.d., 3 m. long vertical pipe. Water was introduced through a porous wall section while air was injected at the bottom concurrently into the test section. An existing mathematical model from the literature was modified to determine the interfacial shear stress. The entrainment rate, entraining and depositing droplet velocities have been included in the model. The interfacial friction factor was further determined by using the classical relationship between the interfacial shear stress and interfacial friction factor proposed in the literature. The changes in the air flow rate and the water film thickness have been found to have an effect on the interfacial friction factor. The interfacial friction factor has then been approximated to be a function of the superficial gas Reynolds number and the dimensionless film thickness. Part of the interfacial friction factor data obtained from the present study are in reasonable agreement with some previous correlations only at low film thickness region. A new empirical correlation for predicting the interfacial friction factors in upward gas-liquid annular flow has also been developed for practical use.

Acknowledgments

The present study was supported financially by the Thailand Research Fund (TRF) whose guidance and assistance are gratefully acknowledged.

Nomenclature

Α	area, m ²	C	concentration of droplets in gas core, kg/m ³
D	pipe diameter, m	E_{D}	mass flux rate of deposition, kg/ m ² s
$E_{\mathtt{E}}$	mass flux rate of entrainment, kg/ m ² s	f	friction factor
g	gravitational acceleration, m/s2	G	mass flux, kg/ m ² s
H_L	liquid hold up	ṁ	mass flow rate, kg/s
P	pressure, N/m ²	Q	volumetric flow rate, m ³ /s
R	gas constant, kJ/kg K	Re	Reynolds number
S	perimeter, m	T	absolute temperature, K
u	local axial velocity, m/s	U	mean axial velocity, m/s
u*	friction velocity, m/s $(=(\tau_1/\rho)^{1/2})$	у	axial direction

Greek Symbols

ρ density, kg/m³ σ surface tension, N/m

τ shear stress, N/m² ν kinematic viscosity, m²/s

μ dynamic viscosity, kg/s m Δ difference

δ liquid film thickness, m

Subscripts

C gas-droplet core D deposition

E entrainment G gas

i interface L liquid

LF liquid film m mean value

out outlet p pipe

sp sampling probe SG superficial gas

w water

References

- 1. I. Kataoka, M. Ishii and A. Nakayama, Int. J. Heat Mass Transfer 43,1573 (2000).
- 2. L.B. Cousin, W.H. Denton and G.F. Hewitt, Liquid Mass Transfer in Annular Two-Phase Flow. AERE-R4926 (1965).
- 3. G.B. Wallis, One-Dimensional Two-Phase Flow, McGraw-Hill, New York (1969).
- D.Webb, Studies of the Characteristics of Downward Annular Two-Phase Flow.3. Measurements of Entrainment Rate, Pressure Gradient, Probability Distribution of Film Thickness and Disturbance Wave Inception. AERE-R6426 (1970).
- 5. P.B. Whalley, G.F. Hewitt and P. Hutchinson, Experimental Wave and Entrainment Measurements in Vertical Annular Two-Phase Flow. AERE-R7521 (1973).
- 6. P.B. Whalley and G.F. Hewitt, The Correlation of Liquid Entrainment Fraction and Entrainment Rate in Annular Two-Phase Flow. AERE-R9187 (1978).
- 7. P. Andreussi and S. Zanelli, Downward Annular-Mist Flow of Air-Water Mixtures, Int. Seminar, Dubrovrik, Yogoslavia, Sep. 4-9 (1978).
- 8. G.F. Hewitt and N.S. Hall-Taylor, Annular Two-Phase Flow, Pergamon Press, Oxford (1970).

- 9. J.C. Asali, T.J. Hanratty and P. Andreussi, AIChE Journal 31, 895 (1985).
- 10. B.J. Azzopardi and J.C.F. Teixeira, Trans. ASME: J. Fluids Eng. 116, 796 (1994).
- 11. T. Fukano and T. Furukawa, Int. J. Multiphase Flow 24, 587 (1998).
- 12. L.B. Fore, S.G. Beus and R.C. Bauer, Int. J. Multiphase Flow 26, 1755 (2000).
- 13. S. Wongwises, Int. Comm. Heat Mass Transfer 25, 117 (1998).
- 14. J.C. Mycock, J.D. McKenna and L. Theodore, Handbook of Air Pollution Control Engineering and Technology, McGraw-Hill (1995).
- 15. S. Wongwises and P. Naphon, Int. Comm. Heat Mass Transfer 25, 819 (1998).
- 16. P.B. Whalley, Boiling, Condensation and Gas-Liquid flow, Clarendon Press, Oxford (1987).
- K. Nishikawa, K.Sekoguchi, M.Nakasatomi, H.Nishi and A. Kaneuzi, Liquid Film Flow Phenomena in Upwards Two-Phase Annular Flow, Proc. JSME 1967 Semi-International Symposium, 4th-8th september, Japan, pp.65-74 (1967).
- G.F. Hewitt and D.N. Roberts, Studies of Two-Phase Flow Patterns by Simultaneous Flash and X-Ray Photography. AERE-M2159 (1969).
- 19. W.H. Henstock and T.J. Hanratty, AIChE 22, 990 (1976).
- 20. G.B. Wallis, J.Basic Eng. 92, 73 (1970).
- 21. E.O. Moeck, Annular-Dispersed Two-Phase Flow and Critical Heat Flux. AECL, 3656 (1970).

Received January 8, 2001

Wongwises, S., Pirompak, W., Flow Characteristics of Pure Refrigerants and Refrigerant Mixtures in Adiabatic Capillary Tubes, *Applied Thermal Engineering*, 2001; 21(8): 845-861.



APPLIED THERMAL ENGINEERING

Applied Thermal Engineering 21 (2001) 845-861

www.elsevier.com/locate/apthermeng

Flow characteristics of pure refrigerants and refrigerant mixtures in adiabatic capillary tubes

Somchai Wongwises *, Worachet Pirompak

Fluid Mechanics and Turbomachinery Research Laboratory (FUTURE), Department of Mechanical Engineering, King Mongkut's University of Technology Thonburi, 91 Prachautit, Bangmod, Bangkok 10140, Thailand Received 10 January 2000; accepted 15 August 2000

Abstract

This paper provides the results of simulations using an adiabatic capillary tube model which is developed to study the flow characteristics in adiabatic capillary tubes used as a refrigerant control device in refrigerating systems. The developed model can be considered as an effective tool of capillary tubes' design and optimization for systems using newer alternative refrigerants. The model is validated by comparing with the experimental data of Li et al. and Mikol for R12 and Melo et al. for R134a. In particular, it has been possible to compare various pairs of refrigerants. It is found that the conventional refrigerants consistently give longer capillary lengths than the alternative refrigerants. For all pairs, the conventional refrigerant consistently give lower pressure drops for both single-phase and two-phase flow which resulted in longer tube lengths. In addition, an example of capillary tube selection chart developed from the present numerical simulation is shown. The chart can be practically used to select the capillary tube size from the flow rate and flow condition or to determine mass flow rate directly from a given capillary tube size and flow condition. The results of this study are of technological importance for the efficient design when systems are assigned to utilize various alternative refrigerants. © 2001 Elsevier Science Ltd. All rights reserved.

Keywords: Capillary tube; Alternative refrigerant; Adiabatic; Mixture; Homogeneous flow

1. Introduction

The capillary tube is one type of expansion device used in small vapour-compression refrigerating and air conditioning systems. The capillary tube is made from an extremely small-bore hollow copper tube (in the order of 0.5– 1.5×10^{-3} m diameter) of about 2–5 m length [1]. It is

1359-4311/01/\$ - see front matter © 2001 Elsevier Science Ltd. All rights reserved. PII: \$1359-4311(00)00090-9

^{*}Corresponding author. Tel.: +662-470-9115; fax: +662-470-9111. E-mail address: somehai.won@kmuttac.th (S. Wongwises).

Nomenclature density, kg/m³ ρ dynamic viscosity, kg/m s μ e/Drelative roughness ΔT subcooling, °C capillary cross-sectional area, m² A diameter, m D f friction factor shear stress at wall, N/m2 τ... gravitational acceleration, m/s² g mass flow rate per unit area, kg/m² s Gspecific enthalpy, J/kg h total head loss, m h_1 entrance loss coefficient Llength, m P pressure, Pa Reynolds number Respecific entropy, J/kg K ς Ttemperature, °C Vvelocity, m/s specific volume, m³/kg ι quality χ height, m Subscripts cond, evap condenser and evaporator, respectively f, g liquid phase and gas phase, respectively homogeneous flow h i capillary inlet condition sp, tp single-phase and two-phase, respectively

used as an automatic flow rate controller for the refrigerant when varying load conditions and varying condenser and evaporator temperatures are to be encountered. Its simplicity, low initial cost and low starting torque of compressors are the main reasons for its use.

Since the depletion of the earth's ozone layer and global warming have been discovered, many conventional refrigerants are being phased out from the industries. As a result, many corporations have been forced to find alternative chemicals to them. To meet the demand for saving the environment and also improving the performance of any equipment, reevaluation of the individual components in particular the capillary tube by using alternative ozone-safe substance is necessary. The proper size of the capillary tube used with a new alternative refrigerant is one of the important factors for the optimum performance of refrigerating and air conditioning systems.

The capillary tube's physical configuration is very simple; however, the design and analysis of flow and heat transfer characteristics inside the tube, are complex ones. In practical consideration, the main concern is to determine the appropriate length and diameter of the tube at a given refrigeration capacity and inlet and outlet conditions.

The design and analysis of capillary tubes have been studied both analytically and experimentally, mostly for pure refrigerants [1–15]. Bansal et al. [1] presented a homogeneous two-phase flow model, CAPIL to study the performance and design aspects of adiabatic capillary tubes. The REFPROP data base which is based on the Carnahan-Starling-DeSantis equation of state was used to determine the thermodynamics and transport properties of the refrigerants. Sami et al. [12] presented a numerical model for predicting capillary tube performance using new alternative refrigerants, both pure and binary mixtures. Numerical results revealed that the proposed model fairly simulated their experimental data and those of other researchers. Wong et al. [14] compared the flow characteristics of R12 and R134a. The results showed that even with minor differences in thermophysical properties of both refrigerants, the differences in pressure, temperature, mixture velocity and dryness fraction distributions in capillary tubes may be significant.

Relatively little information on open literature, however, is currently available on flow characteristics of alternative refrigerant mixtures in a capillary tube. Therefore, this investigation was concerned about making comparisons between various alternative mixtures of refrigerant and in particular between the following pairs of CFCs and HCFCs with HFCs:

- R12 and R134a,
- R502 (R22/R115; 48.8/51.2) and R404A (R125/R143a/R134a; 44%/52%/4%),
- R502 (R22/R115; 48.8/51.2) and R507A (R125/R143a; 50%/50%),
- R22 and R407B (R32/R125/R134a; 10%/70%/20%),
- R22 and R407C (SUVA-9000; R32/R125/R134a; 23%/25%/52%),
- R22 and R410A (SUVA-9100; R32/R125; 50%/50%),
- R22 and R410B (R32/R125; 45%/55%).

Moreover, some capillary tube selection chart developed from the present numerical simulation that has never been seen before is presented. The chart is useful for selecting appropriate capillary tube for a specific application.

2. Mathematical modelling

In order to compare the flow characteristics of refrigerants, a computer program developed at FUTURE was used. This is based on the CAPIL model of Bansal et al. [1] and Stoecker et al. [13] with certain differences which are discussed below. The model includes the effect of the tube diameter, roughness, degree of subcooling, refrigerant flow rate as well as the condenser and evaporator temperature and pressure. The basic physical equations used to describe the flow characteristics are developed from the conservation equations of mass, energy and momentum. In addition, it offers a choice of five viscosity models for any given computation.

The flow of refrigerant in a capillary tube may generally be divided into two regions: single-phase subcooled liquid and two-phase liquid-vapour regions. Fig. 1 shows a schematic diagram of a typical capillary tube connecting the condenser and evaporator.

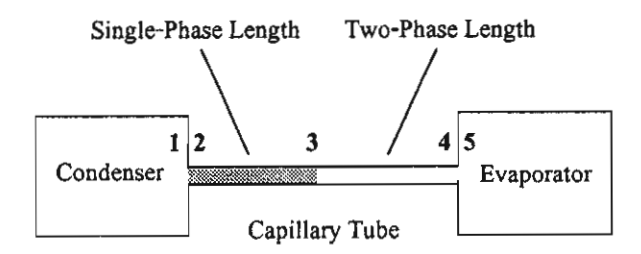


Fig. 1. Schematic diagram of an adiabatic capillary tube.

The present model for flow through the capillary uses the same assumptions as that of CAPIL, and these are as follows:

- straight horizontal and constant inner diameter and roughness capillary tube,
- one-dimensional turbulent flow,
- adiabatic and homogeneous two-phase flow,
- metastable liquid region is neglected,
- thermodynamic equilibrium through the capillary tube.

The governing equations used in describing the flow are presented below for the single-phase and two-phase flow regions, respectively.

2.1. Single-phase flow region

The steady flow energy equation between points 1 and 3 can be expressed as

$$\frac{P_1}{\rho g} + \frac{V_1^2}{2g} + z_1 = \frac{P_3}{\rho g} + \frac{V_3^2}{2g} + z_3 + h_L,\tag{1}$$

where h_L is the sum of head loss due to the sharp entrance in the capillary and head loss due to friction along the capillary tube.

For an incompressible fluid, $\rho_2 \cong \rho_3 = \rho$ and from the continuity equation

$$m = \rho_2 V_2 A = \rho_3 V_3 A = \rho V A. \tag{2}$$

Then, the total head loss can be determined from

$$h_{\rm L} = k \frac{V^2}{2g} + f_{\rm sp} \frac{L_{\rm sp}}{D} \frac{V^2}{2g},$$
 (3)

where k is the entrance loss coefficient (for square edged, k = 0.5) and $f_{\rm sp}$ is the single phase friction factor.

For $z_1 = z_3$ (horizontal tube), substituting Eq. (3) into Eq. (1) and rearranging gives

$$L_{\rm sp} = \left[(P_1 - P_3) \frac{2}{\rho V^2} - k - 1 \right] \frac{D}{f_{\rm sp}}. \tag{4}$$

The pressure at point 3 is assumed to be saturated and can be determined from the temperature at the capillary tube entrance.

Since the mass flow rate of the refrigerant per unit area (G) is ρV , the single-phase region length can be expressed as

$$L_{\rm sp} = \left[(P_1 - P_3) \frac{2\rho}{G^2} - (k+1) \right] \frac{D}{f_{\rm sp}}.$$
 (5)

The single-phase friction factor, $f_{\rm sp}$, can be calculated from the Colebrook formula as follows:

$$\frac{1}{\sqrt{f_{\rm sp}}} = 1.14 - 2\log\left[\frac{e}{D} + \frac{9.3}{Re\sqrt{f_{\rm sp}}}\right],\tag{6}$$

where
$$Re = \frac{\rho VD}{\mu}$$
. (7)

2.2. Two-phase flow region

Bansal et al. [1] and Stoecker et al. [13] presented a flow model through the two-phase region based on conservations of mass, energy and momentum. Their models will be modified for the present study. Consider a control volume in the two-phase region as shown in Fig. 1.

The conservation of mass can be expressed as follows:

$$m = \frac{AV_3}{v_3} = \frac{AV_4}{v_4} \,. \tag{8}$$

For steady-state adiabatic with no external work and neglecting the elevation difference, the conservation of energy can be expressed as follows:

$$h + \frac{V^2}{2} = \text{constant},\tag{9}$$

where h and V are the enthalpy and velocity at any point, respectively.

As the refrigerant flows along the capillary tube, its pressure gradually drops and the liquid flashes into vapour arising purely from the reduced pressure. So at any point,

$$h = h_{\rm f}(1-x) + h_{\rm g}x,$$
 (10)

$$v = v_{\rm f}(1-x) + v_{\rm g}x. \tag{11}$$

Also, $m = \rho VA = \text{constant}$

$$V = \frac{m}{\rho A} = \frac{G}{\rho} = Gv. \tag{12}$$

Considering the energy balance between point 3 and at any point along the capillary tube in two-phase flow region, substituting Eqs. (10)–(12) into Eq. (9) gives

$$h_3 + \frac{V_3^2}{2} = h_f + x(h_g - h_f) + \frac{G^2}{2}(v_f(1 - x) + v_g x)^2.$$
 (13)

Expanding the right-hand side and rearranging gives

$$\left[(v_{g} - v_{f})^{2} \frac{G^{2}}{2} \right] x^{2} + \left[G^{2} v_{f} (v_{g} - v_{f}) + (h_{g} - h_{f}) \right] x + \left[\frac{G^{2} v_{f}^{2}}{2} - h_{3} - \frac{V_{3}^{2}}{2} + h_{f} \right] = 0.$$

This is in the form of a quadratic equation in which the quality x can be expressed as

$$x = \frac{-h_{\rm fg} - G^2 v_{\rm f} v_{\rm fg} + \sqrt{\left(G^2 v_{\rm f} v_{\rm ig} + h_{\rm fg}\right)^2 - \left(2G^2 v_{\rm fg}^2\right) \left[\frac{G^2 v_{\rm f}^2}{2} - h_3 - \frac{V_3^2}{2} + h_{\rm f}\right]}}{G^2 v_{\rm fg}^2},$$
(14)

where $h_{fg} = h_g - h_f$ and $v_{fg} = v_g - v_f$.

The conservation of momentum can be expressed by again considering the element of fluid as shown in Fig. 2. The sum of the pressure forces acting on the left and right ends and the shear force acting on the inner pipe wall is equal to the time rate of change of linear momentum of the system. Therefore,

$$\left(P\frac{\pi D^2}{4}\right) - \left(P + \mathrm{d}P\right)\frac{\pi D^2}{4} - \tau_{\mathrm{w}}\pi D\,\mathrm{d}L = m\,\mathrm{d}V,$$
(15)

where τ_w is the wall shear stress and defined as

$$\tau_{\rm w} = f_{\rm tp} \rho V^2 / 8. \tag{16}$$

On rearranging, we get

$$-\frac{\pi D^2}{4} dP - \frac{f_{tp}}{8} \rho V^2 \pi D dL = m dV$$
 (17)

or

$$dL = -\frac{D}{f_{to}} \left[\frac{2dP}{\rho V^2} + \frac{2m \, dV}{A\rho V^2} \right]. \tag{18}$$

For a constant mass flow rate such that dm = 0, we have

$$\frac{-\mathrm{d}V}{V} = \frac{\mathrm{d}\rho}{\rho} \,. \tag{19}$$

Substituting Eq. (19) into Eq. (18) gives

$$dL = \frac{2D}{f_{tp}} \left[\frac{-\rho dP}{G^2} + \frac{d\rho}{\rho} \right]. \tag{20}$$

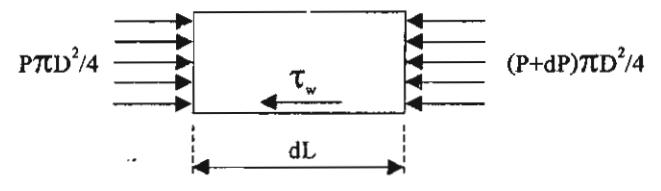


Fig. 2. Flow model incremental volume.

3. Solution method

The capillary tube between points 3 and 4 can be divided into numerous sections as shown in Fig. 3. Since P_3 is known (saturated liquid), the pressure at any section 'i' can be calculated from

$$P_i = P_3 - i\Delta P. \tag{21}$$

With the pressure P_i , and the quality, x_i , calculated from Eq. (14), the entropy of the section can be calculated from

$$s_i = s_{if}(1 - x) + s_{ig}x. (22)$$

The two-phase friction factor, f_{tp} , can be calculated from Colebrook's equation wherein the Reynolds number is defined by

$$Re = \frac{VD}{\mu_{\rm tp}v_{\rm tp}},\tag{23}$$

where

$$V = Gv_{tp} = G(xv_g + (1 - x)v_f).$$
(24)

Five different viscosity models used to calculate μ_{tp} are as follows:

(1) McAdams [16]

$$\frac{1}{\mu_{\rm tp}} = \frac{x}{\mu_{\rm g}} + \frac{1 - x}{\mu_{\rm f}},\tag{25}$$

(2) Cicchitti [17]

$$\mu_{\rm tp} = x\mu_{\rm g} + (1 - x)\mu_{\rm f},\tag{26}$$

(3) Dukler et al. [18]

$$\mu_{\rm tp} = \frac{x v_{\rm g} \mu_{\rm g} + (1 - x) v_{\rm f} \mu_{\rm f}}{x v_{\rm g} + (1 - x) v_{\rm f}},\tag{27}$$

(4) Beattie and Whalley [19]

$$\mu_{\rm tp} = \alpha_{\rm tp} \mu_{\rm g} + \mu_{\rm f} (1 - \alpha_{\rm tp}) (1 + 2.5 \alpha_{\rm tp}), \tag{28}$$

where $\alpha_{tp} = \frac{xv_g}{v_f + xv_{fg}}$,

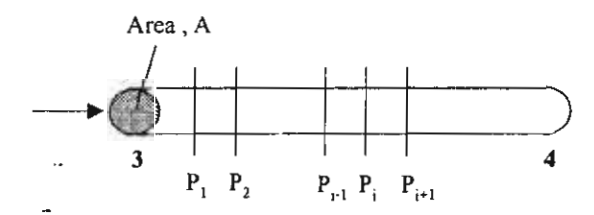


Fig. 3. Schematic diagram of simulation approach.

(5) Lin et al. [20]

$$\mu_{\rm tp} = \frac{\mu_{\rm g} \mu_{\rm f}}{\mu_{\rm g} + x^{1.4} (\mu_{\rm f} - \mu_{\rm g})}.$$
 (29)

All refrigerant thermodynamic and thermophysical properties are taken from the REFPROP computer program, version 6.01 [21] and are developed in the function of pressure.

By using a particular μ_{tp} to determine the Reynolds number, the friction factor can be calculated by the Colebrook formula.

The calculation is done section by section along the capillary tube. For each section, P_i , T_i , x_i , s_i and f_i are calculated. The gradual increase of the entropy is obtained in the direction towards the capillary exit. Eventually, a point in which the entropy is maximum is reached. At this point, the fluid velocity is equal to the local speed of sound and the flow is choked. With further calculation over this point, the entropy decreases. This violates the second law of thermodynamics. Therefore, the calculation must be terminated at this point.

The pressure of the element where entropy is maximum $(P_i)_{s \text{ max}}$ is then compared to the evaporator pressure (P_{evap}) . Therefore,

if
$$(P_i)_{s \max} = P_{\text{evap}} \Rightarrow P_4 = P_{\text{evap}}$$
,

if
$$(P_i)_{s \max} \neq P_{\text{evap}} \Rightarrow P_4 = (P_i)_{s \max}$$
.

Thus, from Eq. (20), the two-phase length can be expressed as

$$L_{\rm tp} = D \left[\frac{-2}{G^2} \int_{P_0}^{P_{\rm s, max}} \frac{\rho}{f_{\rm tp}} dP + 2 \int_{P_0}^{P_{\rm s, max}} \frac{d\rho}{\rho f_{\rm tp}} \right]$$
 (30)

in which the overall length

$$L = L_{\rm sp} + L_{\rm tp}$$
.

In order to calculate the two-phase length, Eq. (30) can be discretized for each section and expressed as follows:

$$\Delta L = D \left[\frac{-2}{G^2} \frac{\rho_i}{f_i} \Delta P + 2 \frac{\Delta \rho}{\rho_i f_i} \right]. \tag{31}$$

To calculate the friction factor for each section f_i , it is necessary to know the viscosity, μ_i , and specific volume, v_i .

The present model itself uses a WINDOWS based interface which requires the following parameters to be entered in order to calculate the length of capillary tube:

- $T_{\rm cond}$ (or $P_{\rm cond}$), $T_{\rm evap}$ (or $P_{\rm evap}$), ΔT ,
- diameter, D,
- relative roughness, e/D,
- mass flow rate, m,
- viscosity model, μ_{tp}.

4. Results and discussion

On comparing the present model with the CAPIL, on which it was based, it is found that they both use the same assumptions and compute the single-phase length in similar manner. However, there are also a number of important differences which are as follows:

- The present model uses the Colebrook friction factor model, whereas CAPIL uses the Churchill model with an additional multiplier term.
- The present model divides the two-phase region into an infinite number of sections and determines the friction factor, f_i , in each section. CAPIL instead uses an average friction factor over the entire two-phase length.
- The present model gives the option of five viscosity models which will be used together with the REFPROP database, whereas CAPIL does not give any information about determination of viscosity.
- The present model uses a discretized form for each length increment as shown in Eq. (31), whereas CAPIL uses Simpson's rule to solve the integral.
- The present model calculates the quality x based on conditions at the beginning of the twophase region, $h_3 + V_3^2/2$, whereas CAPIL uses the conditions inside the condenser.

The present model allows for a number of parameters to be included for any given computation. Mass flow rate, degree of subcooling, diameter and relative roughness were each varied in turn for different condenser pressures to investigate their effect on the total length of capillary tube. It should be noted that the model also gives the option of using condenser temperature or inlet temperature and pressure rather than condenser pressure as an input.

In order to validate the present model, comparisons were made with limited available experimental data of Li et al. [8] and Mikol [11] for R12 as well as Melo et al. [9] for R134a. Figs. 4 and 5 compare the simulation results of the present model with the R12 experimental data of Li et al. [8] for inlet temperatures of 30°C and 33.8°C, respectively. For each set of conditions, simulations were completed for all five viscosity models to show the pressure change along the capillary tube. The linear single-phase region is evident initially, before changing to non-linear two-phase flow. The model is shown to fit the data very well and in particular, the viscosity model of Dukler gives the best result which is in agreement with the results of Wong et al. [14] for R12. The viscosity model of Dukler et al. [18] gives an average underestimation of capillary length of 8.03%.

Fig. 6 compares the present model simulation results with the experimental data of Mikol [11] for R12, again for the range of viscosity models. In this case, it appears that the McAdams model gives the best fit rather than the Dukler model which gave an average error in length of 8.61%. Nonetheless this is still in agreement with Bittle et al. [2] who found that the McAdams viscosity model was the best overall predictor of refrigerant flow for a wide range of refrigerants.

Fig. 7 compares the simulation results with the experimental data of Melo et al. [9] for R134a. In this case, mass flow rate is plotted against subcooling for a fixed length of capillary tube. It is clear that as mass flow rate decreases subcooling also decreases. This is due to the fact that the pressure drop at the capillary inlet decreases as the mass flow rate decreases which results in a reduction in the level of subcooling of the refrigerant entering the tube. As shown, the model systematically overpredicts the mass flow rate for a given level of subcooling. The closest estimate is given by the Cicchitti viscosity model which gives an average error of 3.41%. This is again in

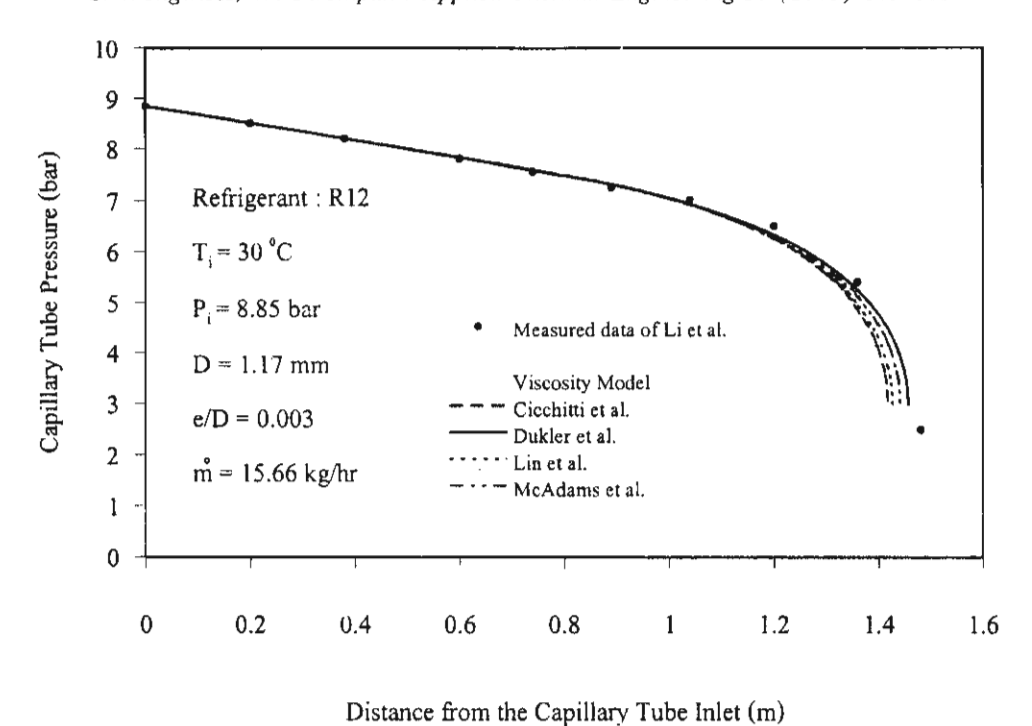


Fig. 4. Comparison of measured pressure distributions with present numerical results.

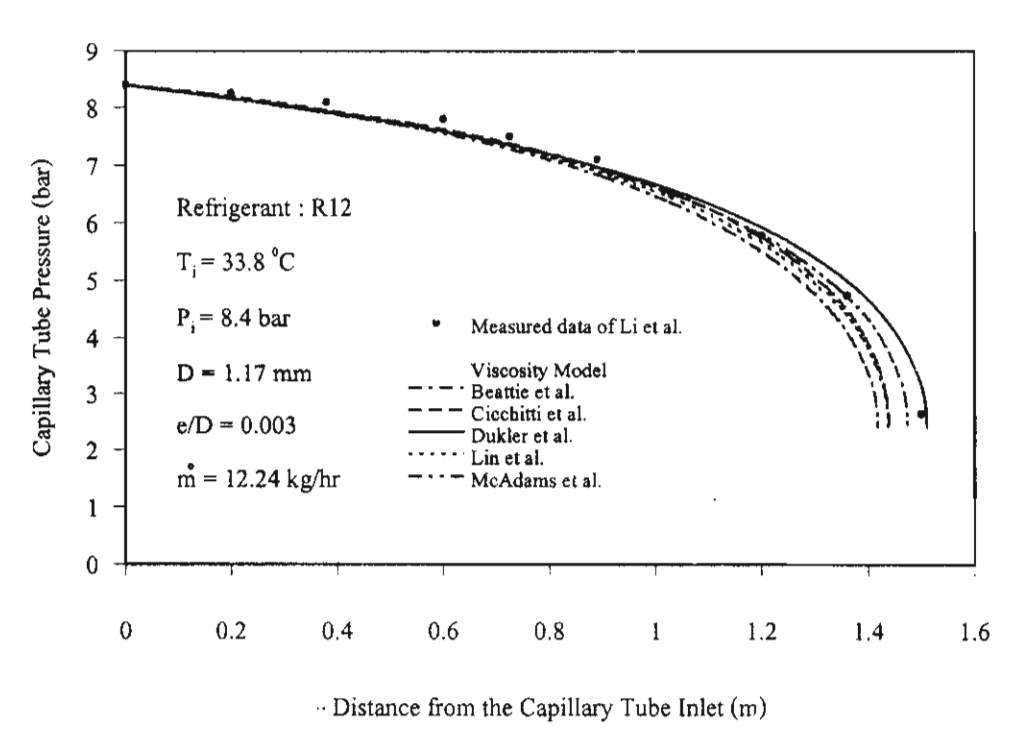


Fig. 5. Comparison of measured pressure distributions with present numerical results.

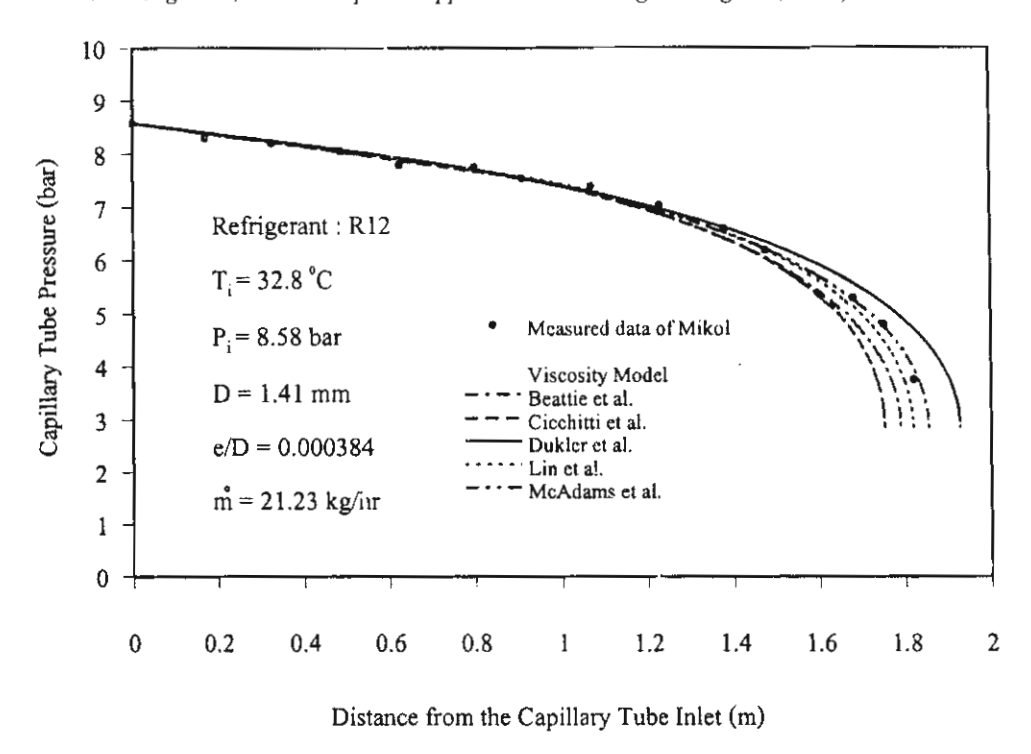


Fig. 6. Comparison of measured pressure distributions with present numerical results.

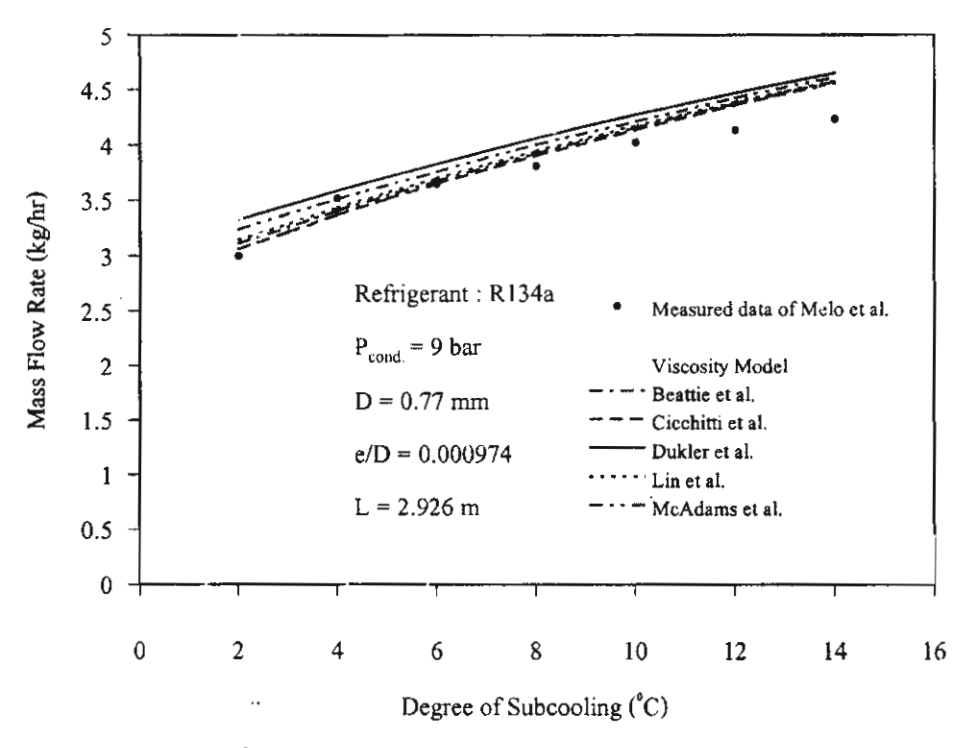


Fig. 7. Comparison of the present numerical results with experimental data.

agreement with the results of Bittle et al. [2] which found the Cicchitti model to be the best predictor of two-phase flow for R134a. It should be noted that it is not clear whether the length of capillary quoted by Melo et al. for the experimental data shown corresponds to the choked flow condition which the model computes. If Melo et al.'s measurements were in fact taken prior to the choked condition the actual length for comparison with the model should be larger which would account for the overprediction. Due to the lack of the R134a experimental data, the simulation results for R134a are compared with those from the simulations reported in the literature at the same working conditions. Fig. 8 shows the comparison of R134a simulation results of Kim [5] and Sami et al. [12] with the present model. The present model using the Cicchitti viscosity model gives a longer critical tube length.

Simulations have been performed using the present model for all of the refrigerants listed above. The viscosity models were varied depending on the refrigerant and were based on the recommendations of past research, especially those from the work of Bittle et al. [2] and Wong et al. [14]. The Dukler model was used for simulations with R12 and R22 and the Cicchitti model for R134a, while the McAdams model, as the best all-round predictor, was used for the remaining refrigerants.

By varying the model input parameters, it was possible to show that for all refrigerants, the length decreases as mass flow rate increases, increases as subcooling increases, increases as diameter increases, decreases as relative roughness increases and increases as condenser pressure increases. The model output parameters were studied to show that as position along the capillary tube increases, pressure decreases, temperature decreases, vapour fraction increases and with the

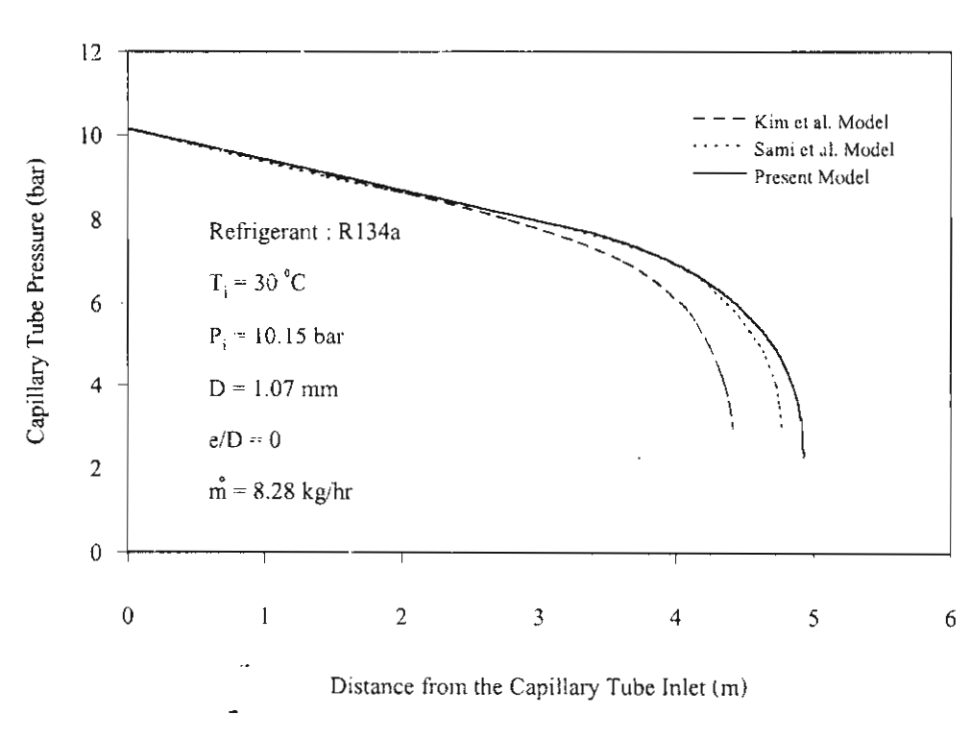


Fig. 8. Comparison of Kim et al. model and Sami et al. model with the present model.

exception of R134a, viscosity and Reynolds number increase. For the case of R134a, it was found that the physical properties of the refrigerant results in an increase in viscosity and thus a minimal increase in Reynolds number.

A large number of graphs can be drawn from the output of the simulation but because of space limitation, only typical results are shown. Figs. 9–12 show how pressure varies with position along

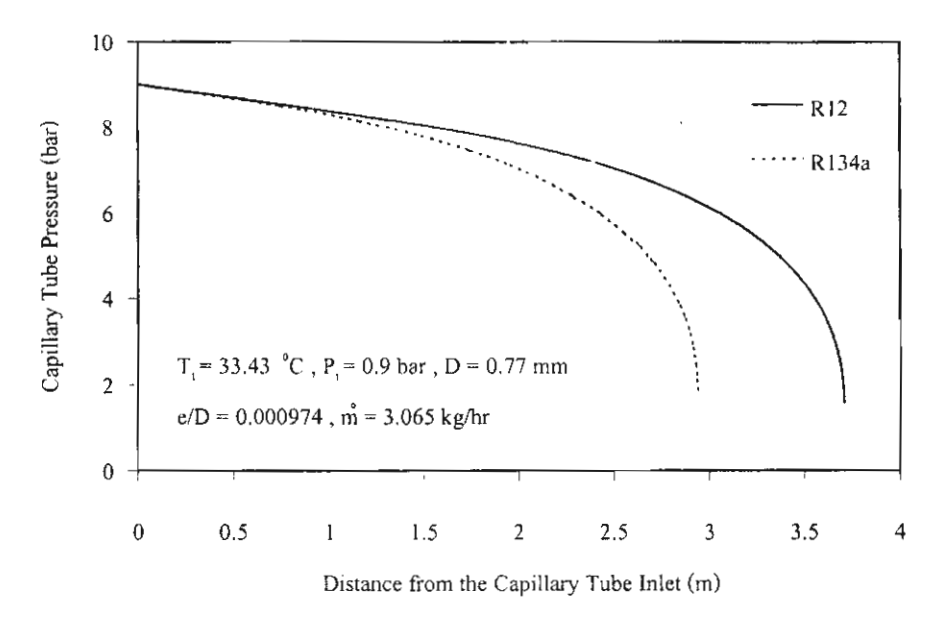


Fig. 9. Comparison of pressure distributions along the capillary tube for R12 and R134a.

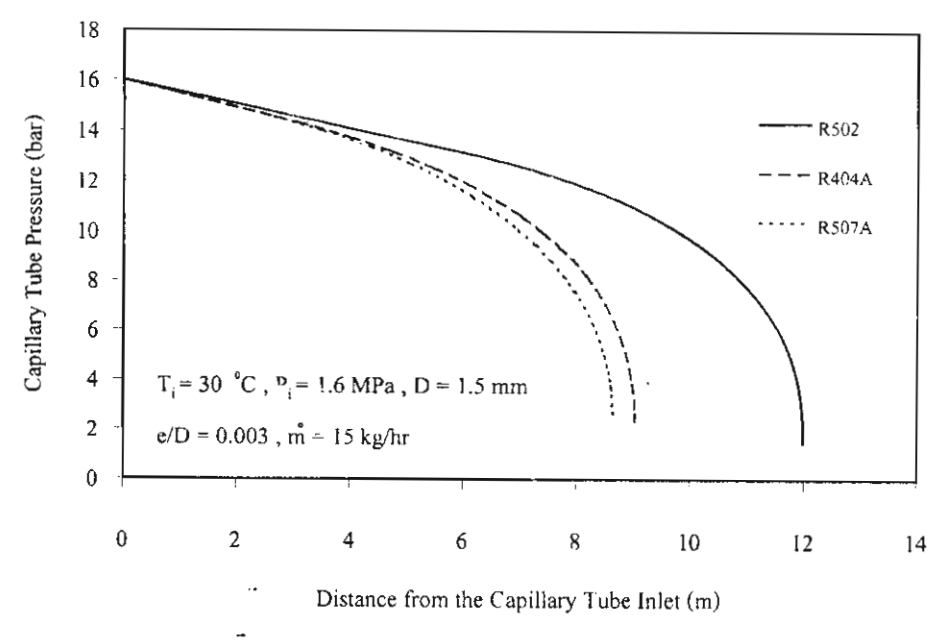


Fig. 10. Comparison of pressure distributions along the capillary tube for R502, R404A and R507A.

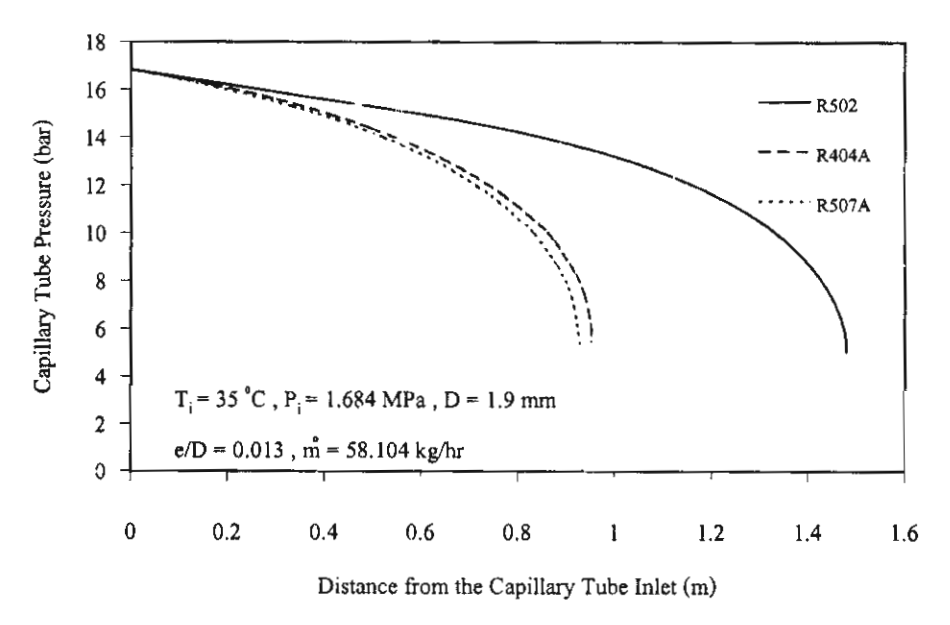


Fig. 11. Comparison of pressure distributions along the capillary tube for R502, R404A and R507A.

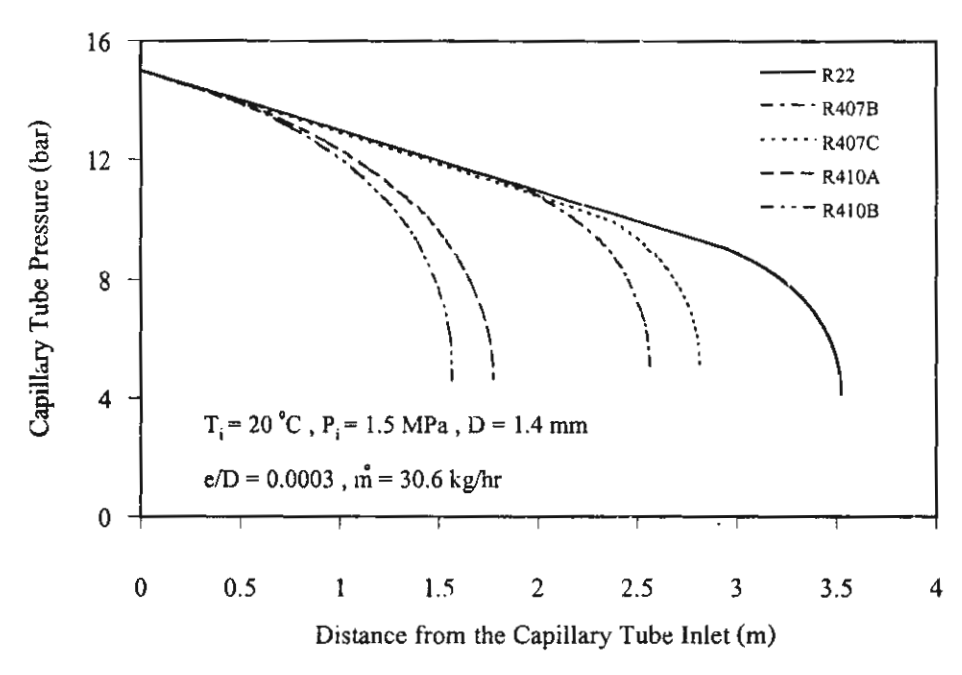


Fig. 12. Comparison of pressure distributions along the capillary tube for R22, R407B, R407C, R410A and R410B.

the capillary tube for each pair of refrigerants. In the single-phase subcooled liquid region, due to frictional effects in fully developed flow in a constant-area tube, the pressure of refrigerant drops linearly along the capillary tube. After the position of the onset of vaporization, due to frictional

and accelerational effects, the pressure of refrigerant decreases relatively fast and, more and more rapidly as the flow approaches the critical flow condition. But in fact, due to the delay of vaporization, from a single-phase subcooled liquid to a two-phase mixture, the actual starting point of vaporization may not occur at the end of the single-phase liquid region (or at the saturated liquid condition). For all cases, the quality is zero up to the flash point and then increases in a non-linear fashion, rising more rapidly as the critical length is approached. It is also shown that all alternative refrigerants vapourize earlier than their corresponding conventional refrigerants.

Comparison on the pressure drop characteristics for the rest of each pair of refrigerant shows that for all cases in the single-phase region, the conventional refrigerant flowing through capillary tubes gives a slightly lower pressure drop than the newer alternative refrigerants. This may be due to the lower viscosity of the conventional refrigerant. Nevertheless, in the two-phase flow region, the conventional refrigerant gives a meaningfully lower pressure drop than the alternative refrigerant which resulted in a longer total tube length. It is also interesting to note that the comparison between the pressure drop characteristics for 404A and 507A in Figs. 10 and 11. The result shows that although both refrigerants have a difference in composition, the pressure distributions along the capillary tube are almost the same. In all cases, in the single-phase region, the temperature of refrigerant remains constant along the capillary tube as expected. Once the inception of vaporization has taken place, the temperature drop will be accelerated as the flow approaches the choked flow condition. In general, in the two-phase region, the conventional refrigerants give a slightly lower temperature drop along the capillary tube, which agree well with the lower pressure drop as shown in Figs. 9–12.

The present mathematical model can be used to develop the charts for selecting appropriate capillary for a specific application. Fig. 13 shows an example of the preliminary selection chart for refrigerant R134a. The chart is valid only for steady adiabatic flow through capillary tubes. For a capillary tube having an internal diameter of 1.63 mm and a length of 2.03 m, the required mass flow rate can be easily determined from this chart by knowing the condenser pressure and the degree of subcooling. The chart is similar to rating charts for R12 (or R22) developed by ASHRAE [22]. It is interesting to note that ASHRAE [22] use the same chart for both R12 and R22. However, as expected, the charts for R12 and R22 developed from the present mathematical model give different values of various parameters. With the same method, the charts in the same style for the other alternative refrigerants can be also developed. However, for a capillary tube having the internal diameter, D, and length, L, other than this (D = 1.63 mm, L = 2.03 m), the correction factor (known as the flow factor) is required.

5. Conclusion

It has been possible to use the present adiabatic capillary tube model to study the flow characteristics of various refrigerants in capillary tubes. In particular, it has been possible to compare some pairs of conventional and alternative refrigerants. The present model was validated by comparing with the experimental data of Li et al. and Mikol for R12 and was found to give an average discrepancy of about 8.30%. It was also compared with the experimental data of Melo et al. for R134a and gave an average error of 3.41%. In addition, for all pairs of refrigerants, the

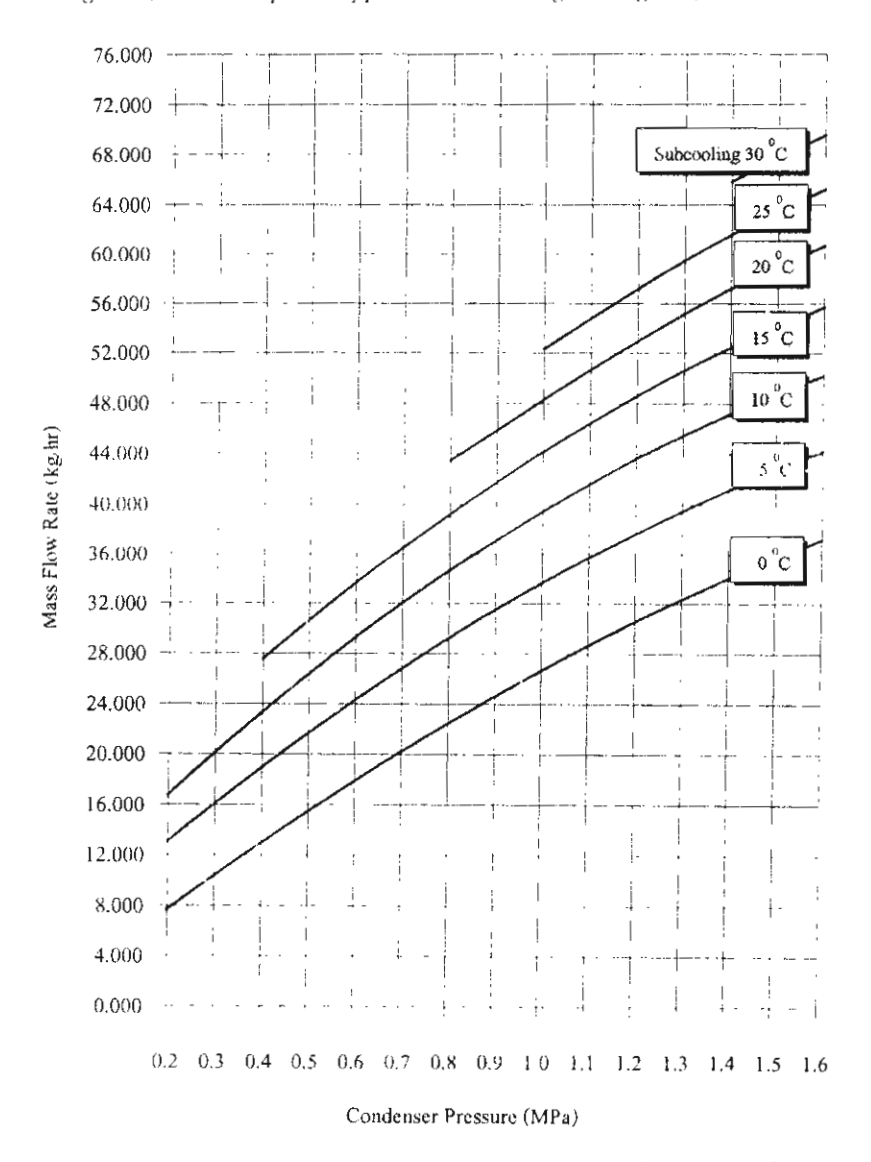


Fig. 13. Capillary tube selection chart developed from the present mathematical model for R134a (for 1.63 mm ID tube, 2030 mm long).

conventional refrigerant consistently gave lower pressure drops for both single-phase and two-phase flows, which resulted in longer capillary tube lengths.

Acknowledgements

The present study was supported financially by the Thailand Research Fund (TRF) and the National Energy Policy Office (NEPO) whose guidance and assistance are gratefully acknowledged.

References

- [1] P.K. Bansal, A.S. Rupasinghe, A homogeneous model for adiabatic capillary tubes, Applied Thermal Engineering 18 (1998) 207–219.
- [2] R.R. Bittle, A theoretical model for predicting adiabatic capillary tube performance with alternative refrigerants, ASHRAE Transaction 100 (1994) 52-64.
- [3] L. Cooper, Simple selection method for capillaries derived from physical flow conditions, Refrigerating Engineering July (1957) 37-41.
- [4] D. Jung, C. Park, B. Park, Capillary tube selection for HCFC22 alternatives, International Journal of Refrigeration 22 (1999) 604-614.
- [5] R.H. Kim, A numerical analysis of a capillary tube expansion valve in a vapour compression refrigeration system with alternative refrigerants, Heat Transfer with Alternative Refrigerants, ASME, HTD, vol. 243 (1993).
- [6] H. Koizumi, K. Yokoyama, Characteristics of refrigerant flow in a capillary tube, ASHRAE Transaction 86 (1980) 19–27.
- [7] S.J. Kuehl, V.W. Goldschmidt, Modelling of steady flows of R22 through capillary tubes, ASHRAE Transactions 97 (1991) 139-148.
- [8] R.Y. Li, S. Lin, Z.H. Chen, Numerical modelling of thermodynamic non-equilibrium flow of refrigerant through capillary tubes, ASHRAE Transaction 96 (1990) 542–549.
- [9] C. Melo, R.T.S. Ferreira, N.C. Boabaid, J.M. Goncalves, R.H. Pereira, M.R. Thiessen, Evaluation of H.C.-600a, HFC134a and CFC-12 mass flow rates through capillary tubes, Proceedings of the New Applications to Reduce Global Warming and Energy Consumption Conference, Hannover, Germany (1994) 621-630.
- [10] C. Melo, R.T.S. Ferreira, C. Boabaid Neto, J.M. Goncalves, M.M. Mezavi, An experimental analysis of adiabatic capillary tubes, Applied Thermal Engineering 19 (1999) 669-684.
- [11] E.P. Mikol, Adiabatic single- and two-phase flow in small bore tubes, ASHRAE Journal 5 (1963) 75-86.
- [12] S.M. Sami, C. Tribes, Numerical prediction of capillary tube behaviour with pure and binary alternative refrigerants, Applied Thermal Engineering 18 (1998) 491–502.
- [13] W.F. Stoecker, J.W. Jones, Refrigeration and Air Conditioning, McGraw-Hill, New York, 1982,
- [14] T.N. Wong, K.T. Ooi, Evaluation of capillary tube performance for CFC-12 and HFC-134a, International Communications in Heat and Mass Transfer 23 (1996) 993–1001.
- [15] S. Wongwises, P. Chan, N. Luesuwanatat, T. Purattanarak, Two-phase separated flow model of refrigerants flowing through capillary tubes, International Communications in Heat and Mass Transfer 27 (2000) 343-356.
- [16] W.H. McAdams, W.K. Wood, R.L. Bryan, Vaporization inside horizontal tubes. II. Benzene oil mixture, Transaction ASME 64 (1942) 193.
- [17] A.E. Cicchitti, C. Lombardi, M. Silvestri, G. Soldaini, R. Zavattarelli, Two-phase cooling experiments pressure drop, heat transfer and burnout measurements, Energia Nucleare 7 (1960) 407-425.
- [18] A.E. Dukler, M. Wicks, R.G. Cleveland, Frictional pressure drop in two-phase flow part A and B. AIChE Journal 10 (1964) 38–51.
- [19] D.R.H. Beattie, P.B. Whalley, A simple two-phase frictional pressure drop calculation method, International Journal of Multiphase Flow 8 (1981) 83-87.
- [20] S. Lin, C.C.K. Kwok, R.Y. Li, Z.H. Chen, Z.Y. Chen, Local frictional pressure drop during vaporisation of R12 through capillary tubes, International Journal of Multiphase Flow 17 (1991) 95–102.
- [21] M.O. McLinden, S.A. Klein, E.W. Lemmon, REFPROP thermodynamic and transport properties of refrigerants and refrigerant mixtures, NIST Standard Reference Database version 6.01, 1998.
- [22] ASHRAE Hand book-Equipment, American Society of Heating, Refrigerating and Air-Conditioning Engineer Inc., 1988 (Chapter 19).

Wongwises, S., Songnetichavarit, T., Lokathada, N., Kritsadathikarn, A Comparison of the Flow Characteristics of Refrigerants Flowing Through Adiabatic Capillary Tubes, Int. Com. Heat Mass Transfer, 2000; 27(5): 611-621.



è

PII: S0735-1933(00)00143-3

A COMPARISON OF THE FLOW CHARACTERISTICS OF REFRIGERANTS FLOWING THROUGH ADIABATIC CAPILLARY TUBES

S. Wongwises, T. Songnetichaovalit, N. Lokathada,
P. Kritsadathikarn, M. Suchatawat and W. Pirompak
Fluid Mechanics and Turbomachinery Research Laboratory (FUTURE)
Department of Mechanical Engineering,
King Mongkut's University of Technology Thonburi,
Bangmod, Bangkok 10140, Thailand

(Communicated by J.P. Hartnett and W.J. Minkowycz)

ABSTRACT

This paper presents theoretical comparison of the flow characteristics of many pairs of refrigerants flowing through adiabatic capillary tubes. The two-phase flow model developed was based on homogeneous flow assumption. Two-phase friction factor was determined from Colebrook correlation. The viscosity model was also based on the recommendations from the previous literature. For all pairs, numerical results showed that the traditional refrigerants consistently gave lower pressure drops for both single-phase and two-phase flow than the environmentally acceptable alternative refrigerants which resulted in longer tube lengths. © 2000 Elsevier Science Ltd

Introduction

Although the capillary tube's physical configuration is very simple, the design and analysis of flow and heat transfer characteristics inside the tube are complex issues. In practical consideration of the use of a capillary tube, the main concern is to determine the appropriate length and diameter of the tube at given refrigeration capacity and inlet and outlet conditions. The design and analysis of capillary tubes has received the most attention, both analytically and experimentally, mostly for pure refrigerants [1-15]. To date, a homogeneous two-phase flow assumption has been used extensively. Wong et al. [15] compared the flow characteristics of R12 and R134a. The results revealed that even with minor differences in refrigerant properties between both refrigerants, the differences in flow characteristics may be significant. More recently, Bansal et al. [1] presented a homogeneous two-phase flow model, CAPIL, to study the performance of adiabatic capillary tubes using R134a. The model used the REFPROP data base where the Carnahan-Starling-DeSantis equation of state was used to calculate the refrigerant properties. Sami et

al.[12] presented a numerical model for predicting capillary tube performance for some azeotropic and zeotropic binary mixtures as well as pure HFC refrigerants.

To the best of the authors' knowledge, no information exists in open literature currently available on comparisons of flow characteristics between various traditional with alternative refrigerants flowing in a capillary tube. The present investigation is concerned with making comparisons between various pairs of traditional refrigerants with new pure, binary and ternary alternative refrigerant mixtures.

Mathematical Model

The flow of refrigerant through a capillary tube can be divided into two distinct regions; a single-phase sub-cooled liquid and a two-phase region. In the present study, in the two-phase region, the model is derived from a one dimensional homogeneous two-phase flow assumption. The model is based on that of Wallis [17] and Wong [14]. In modeling, the basic physical equations governing the capillary tube flow are the continuity and conservations of energy and momentum. The model includes the various relevant parameters and is a tool to determine the size of the capillary tubes used in household refrigerators and freezers, especially to select the capillary tube length for given operating conditions.

Sub-Cooled Liquid Region

The sub-cooled liquid region is the region from the inlet of the capillary tube to the position where the saturation pressure corresponds to the inlet temperature. As the refrigerant flows along the tube in this region, the pressure decreases linearly until the refrigerant becomes a saturated liquid. For steady fullydeveloped incompressible flow, the integral form of the momentum equation at distance dz is

$$-A_0 dP - \tau_W(\pi d) dz = 0$$
 (1)

where τ_W is the wall shear stress and defined as

$$\tau_{W} = f \frac{(\rho_{L} V^{2})}{8} \tag{2}$$

where f is the Moody friction factor and can be determined from Colebrook's correlation as follows;

$$\frac{1}{f^{0.5}} = -2 \log \left(\frac{e/d}{3.7} + \frac{2.51}{\text{Re } f^{0.5}} \right)$$
 (3)

Substituting Eq. (2) into Eq. (1), the single phase sub-cooled liquid length (L_{SC}) of the capillary tube can be obtained from

$$p_i - p_{sat} = \left(f \frac{G^2}{2p_1 d}\right) L_{sc} \tag{4}$$

where the total mass flux (G) is the total mass flow rate of liquid plus vapour divided by total channel cross-sectional area (A_o) .

Two-Phase Region

The specific enthalpy of a substance at a saturation state having a given quality can be calculated by utilizing the definition of quality (x).

$$h = x h_G + (1-x)h_L$$
 (5)

where the quality is the ratio of the mass of vapour to total mass of liquid plus vapour when a substance is in a saturation state.

For homogeneous flow, the velocity of each phase can be expressed as

$$V = V_G = V_I \tag{6}$$

For homogeneous adiabatic refrigerant flow in a capillary tube with no externally applied works and neglecting the elevation changes, the following form of energy equation is obtained

$$\frac{d}{dz} \left(x h_G + (1 - x) h_L + \frac{V^2}{2} \right) = 0$$
 (7)

In the homogeneous two-phase region for a pure substance in equilibrium, the enthalpies (and also densities) are only functions of pressure.

Vapour and liquid mass fluxes (G_G and G_L) are the vapour and liquid mass flow rates divided by total channel cross-sectional area, so

$$G_G = G_{L} = \rho V \tag{8}$$

In liquid-vapour flows, void fraction (a) usually represents the time-averaged fraction of the crosssectional area or of the volume which is occupied by the vapour phase, so

$$\alpha = A_G / A_O \tag{9}$$

The homogeneous flow model takes into account the fact that the two phases physically flow with same velocities. This general correlation is then given by

$$\alpha = \frac{1}{1 + \left(\frac{1 - x}{x} \frac{\rho_G}{\rho_I}\right)} \tag{10}$$

Using the above correlations, actual average velocity of vapour and liquid phases (V_G and V_L) can be determined, so

$$V = G \upsilon = G(x \upsilon_G + (1 - x) \upsilon_L)$$
 (11)

Eventually, after rearrangement, an expression for the total pressure gradient is obtained

$$\frac{dP}{dz} = -\frac{dx}{dz} \left(\frac{A}{B} \right) \tag{12}$$

where

$$A = h_{IG} + G^2 vv_{IG}$$

$$B = x \frac{dh_G}{dP} + (1-x) \frac{dh_L}{dP} + G^2 \upsilon \left[x \frac{d\upsilon_G}{dP} + (1-x) \frac{d\upsilon_L}{dP} \right]$$

The momentum equation is often rewritten as an explicit equation for the pressure gradient. The total pressure gradient $\left(\frac{dP}{dz}\right)$ is, therefore, expressed as the sum of the three different components, so

$$\frac{dP}{dz} = \left(\frac{dP}{dz}\right)_{f} + \left(\frac{dP}{dz}\right)_{a} + \left(\frac{dP}{dz}\right)_{g}$$
 (13)

The three terms on the right hand side are regarded as frictional, accelerational, and gravitational components of the total pressure gradient. Gravitational term in Eq.(13) is negligible because the cross-sectional area of the horizontal capillary tube is constant. Accelerational pressure gradient can not be measured directly. It can be, however, calculated from measured momentum flux as follows;

$$\left(\frac{dP}{dz}\right)_{a} = -\frac{m}{A_{o}} \frac{d(V)}{dz} \tag{14}$$

and, so

$$= -G^2 \left(\frac{dP}{dz}\right) \left(x \frac{d\upsilon_G}{dP} + (1-x) \frac{d\upsilon_L}{dP} \right) - G^2 \upsilon_{LG} \frac{dx}{dz}$$

Frictional pressure gradient can be obtained from

$$\left(\frac{dP}{dz}\right)_{f} = \frac{-f_{tp} G^{2}(xv_{G} + (1-x)v_{L})}{2d}$$
(15)

Substituting Eqs. (14) and (15) into Eq. (13) then gives

$$\frac{dP}{dz} = \frac{\left(\frac{dP}{dz}\right)_{f} - C\frac{dx}{dz}}{D} \tag{16}$$

where

$$C = G^2 v_{LG}$$

$$D = 1 + G^2 \left(\frac{x dv_G}{dP} + \frac{(1-x)}{dP} \frac{dv_L}{dP} \right)$$

The homogeneous two-phase friction factor (f_{tp}) can be determined from Colebrook's equation with the Reynolds number being defined as:

$$Re = \frac{Gd}{\mu_{tp}}$$
 (17)

Three different viscosity models are used to calculate μ_{tp} and these are as follows:

- McAdams [18]:
$$\frac{1}{\mu_{tp}} = \frac{x}{\mu_{G}} + \frac{1-x}{\mu_{L}}$$
 (18)

- Cicchitti [19]:
$$\mu_{tp} = x\mu_G + (1-x)\mu_L$$
 (19)

- Dukler [20]:
$$\mu_{tp} = \frac{x \upsilon_{G} \mu_{G} + (1-x) \upsilon_{L} \mu_{L}}{x \upsilon_{G} + (1-x) \upsilon_{L}}$$
(20)

This investigation was concerned with making comparisons between various refrigerants and in particular between the following pairs of refrigerants;

- R12 vs R134a,
- R12 vs R401A (R22/R152a/R124; 53/13/34)
- R12 vs R401B (R22/R152a/R124; 61/11/28)
- R12 vs R401C (R22/R152a/R124; 33/15/52)
- R22 vs R407C (R32/R125/R134a; 23/25/52)
- R22 vs R410A (R32/R125; 50/50)
- R502 (R22/R115; 48.8/51.2) vs R404A (R125/R143a/R134a; 44/52/4)
- R502 (R22/R115; 48.8/51.2) vs R507A (R125/R143a; 50/50).

All refrigerant thermodynamic and thermophysical properties are taken from REFPROP [16] and are developed as a function of pressure. The viscosity model used in the present work varied depending on the refrigerant and was based on the recommendations of past research and in particular Bittle et al. [2] and Wong et al. [13]. The Dukler model was used for simulations with R12 and R22 and the Cicchitti model for R134a, while the McAdams model, as the best all-round predictor, was used for the remaining refrigerants. The calculation is divided into two parts; sub-cooled single-phase region and two-phase vapour liquid region. Initial conditions required in the calculation are pressure and temperature of refrigerant at capillary tube inlet, mass flow rate of refrigerant, roughness and diameter of pipe. In the single-phase flow region, after calculating the friction factor by Colebrook equation and substituting Psat with the saturation pressure of refrigerant at the inlet temperature, the single-phase region length is determined. In the two-phase flow region, a program is written to solve equations (12) and (16) by using the fourth order Runge-Kutta method. The results from the calculation are pressure, temperature and quality at each position along the capillary tubes. Initial condition of this region is the end condition of the single phase flow region. The calculation in two-phase flow region is terminated when the flow approaches the choked or critical flow condition $(dP/dz \rightarrow \infty)$. Total tube length is the sum of the single-phase region and the two-phase region lengths.

Results and Discussion

A large number of graphs were generated from the output of the simulations, however, due to space limitation, only typical results are shown. The present model allows for a number of parameters to be included for any given computation. Mass flow rate, sub-cooling, diameter and relative roughness were each varied in turn for different condenser pressures to investigate their effect on the total length of capillary tube. It should be noted that the model also gives the option of using condenser temperature or inlet temperature and pressure rather than condenser pressure as an input. However, regardness of which option is chosen the same overall trends will be shown.

Plots of variation in pressure, temperature and quality with position along the capillary tube are included in Figures 1-18. Figures 1,4,6,8,11,13,15 and 17 show how pressure varies with position along the capillary tube for all refrigerants. The results show that in the sub-cooled single-phase region, pressure decreases linearly due to tube wall friction as expected. Once the flow reaches the saturated condition flashing occurs and the pressure drop accelerates along the tube (However, due to the delay of vaporization, the actual point of inception of vaporization may not occur at the end of the sub-cooled liquid region). This effect of flashing causes the vapour and velocity in the refrigerant flow to increase further which results in rapid increases in both the frictional and acceleration pressure drops in the two-phase region.

It should be noted that comparing the pressure drop characteristics of R12 and of R134a (Figure 1), the flow through the capillary tube of R134a gives a higher pressure drop than that of R12. On the other hand, the subcooled liquid region and the critical tube lengths are shorter for the flow of R134a. Comparing the pressure drop characteristics for the rest of each pair of refrigerant type shows that for all cases in the single-phase flow region, the newer alternative refrigerant gives a slightly higher pressure drop than the traditional refrigerants because of the higher viscosity of the alternative refrigerant. Conversely, in the two-phase flow region the alternative refrigerant gives a significantly larger pressure drop than the traditional refrigerant for the same tube lengths, which resulted in a smaller total tube length. This is due to the saturated properties of alternative refrigerants compared to traditional refrigerants which results in a higher flow velocity. It is also interesting to note the comparison between the pressure drop characteristics for 404A and 507A in Figures 15 and 17. The result shows that although both refrigerants have differences in composition, the pressure distributions along the capillary tube are almost the same.

Figures 2,5,9,12 and 16 show the temperature distribution along the capillary tube for each pair of refrigerant type. In all cases there is a constant temperature distribution in the single-phase region which is followed by a sudden drop in temperature when the flash point occurs. The alternative refrigerants show a lower temperature distribution along the length of the capillary tube, which corresponds to the larger pressure drop.

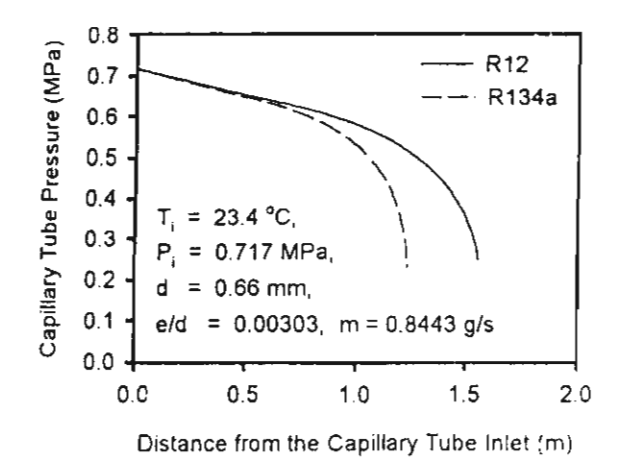


FIG. 1 Variation of P with z

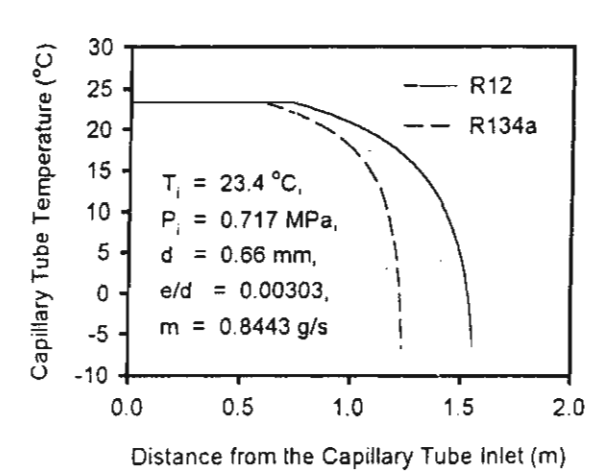


FIG. 2 Variation of T with z

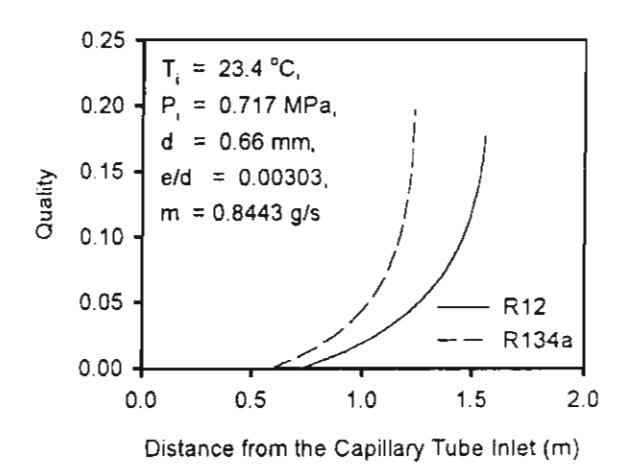


FIG. 3 Variation of x with z

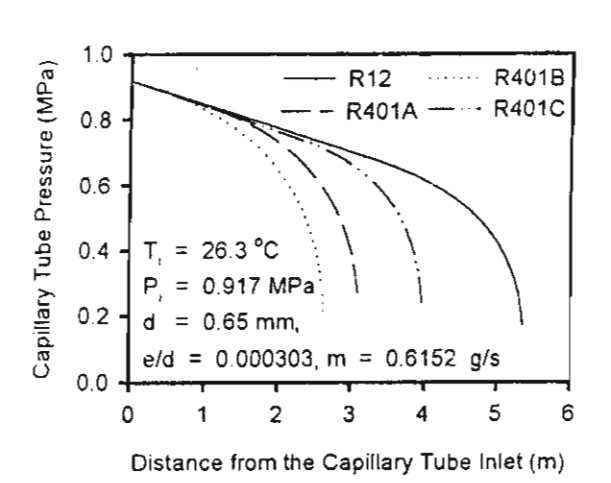


FIG. 4 Variation of P with z

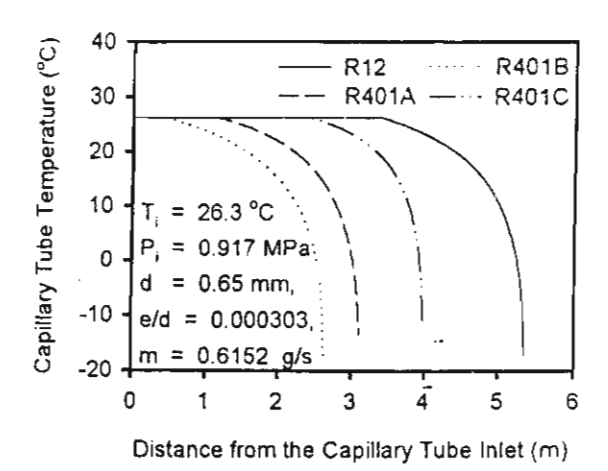
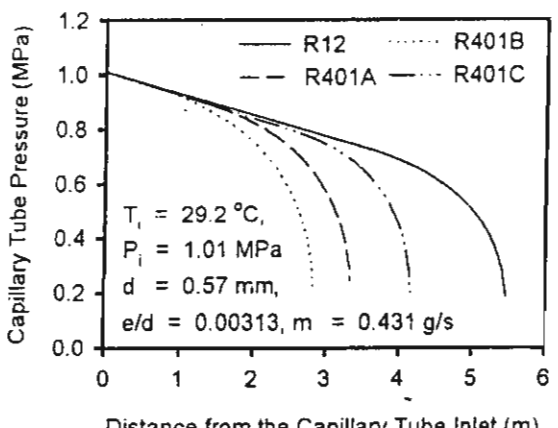


FIG. 5 Variation of T with z



Distance from the Capillary Tube Inlet (m)

FIG. 6 Variation of P with z

2.0

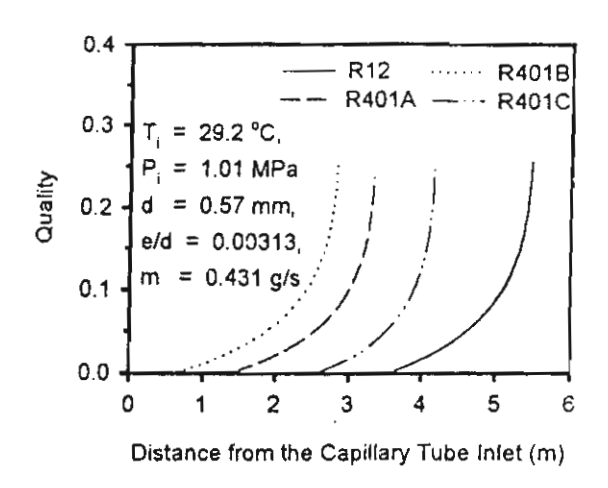
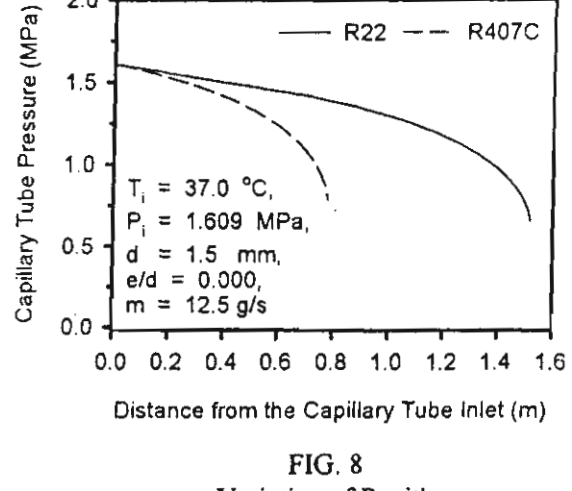


FIG. 7 Variation of x with z



Variation of P with z

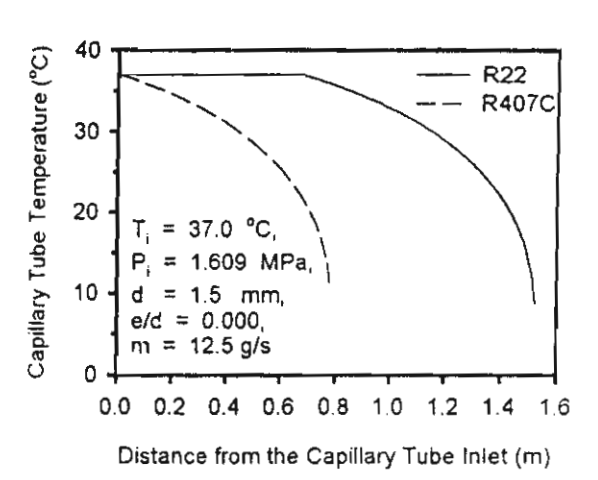


FIG. 9 Variation of T with z

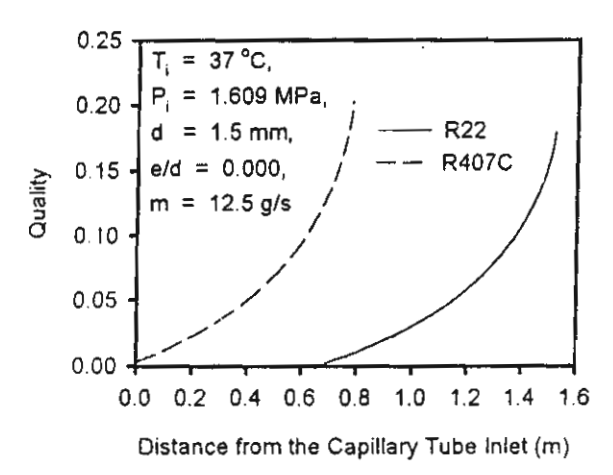


FIG. 10 Variation of x with z

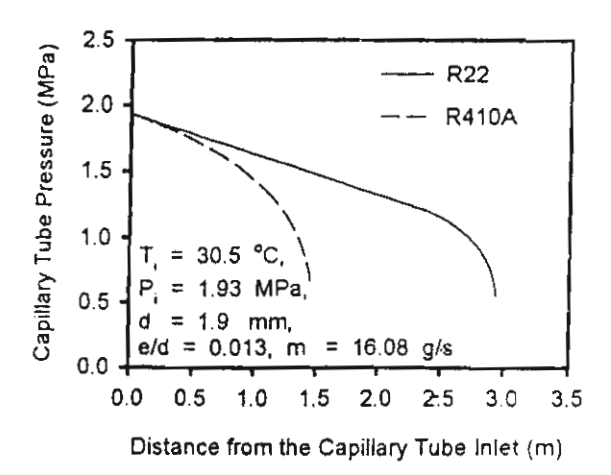


FIG. 11 Variation of P with z

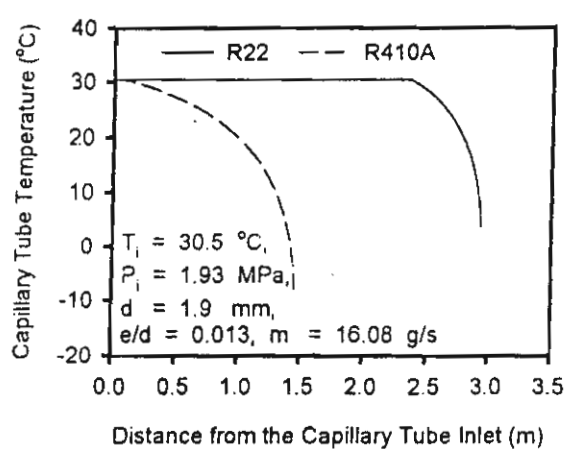


FIG. 12 Variation of T with z

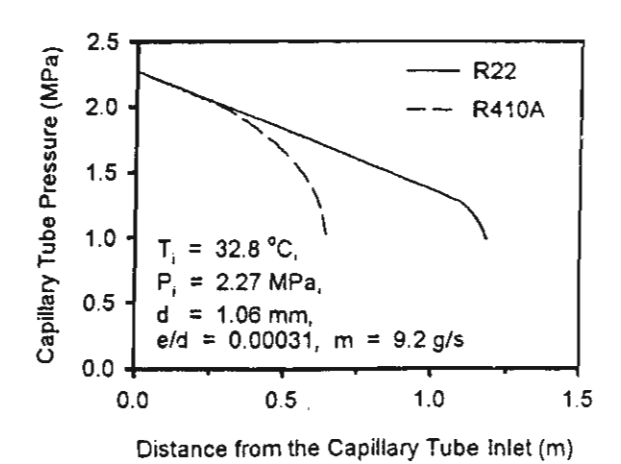


FIG. 13 Variation of P with z

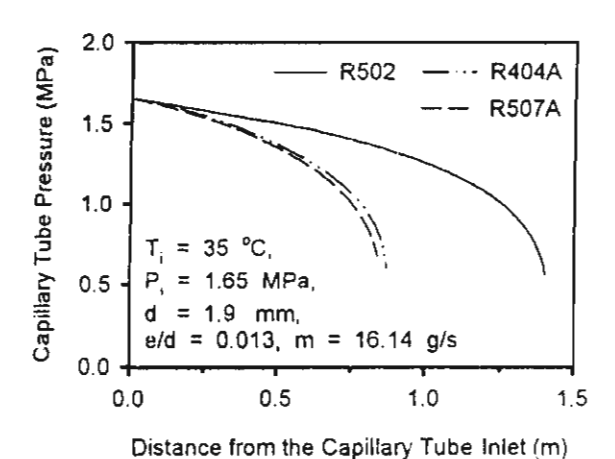


FIG. 15 Variation of P with z

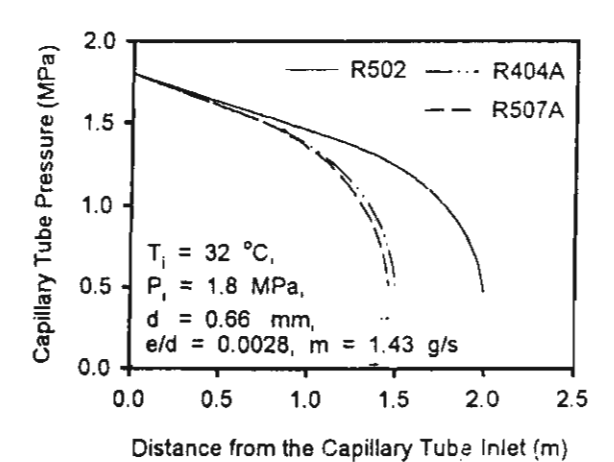


FIG. 17 Variation of P with z

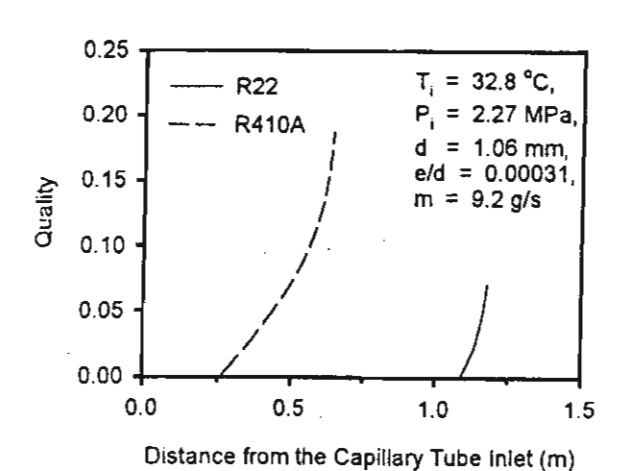
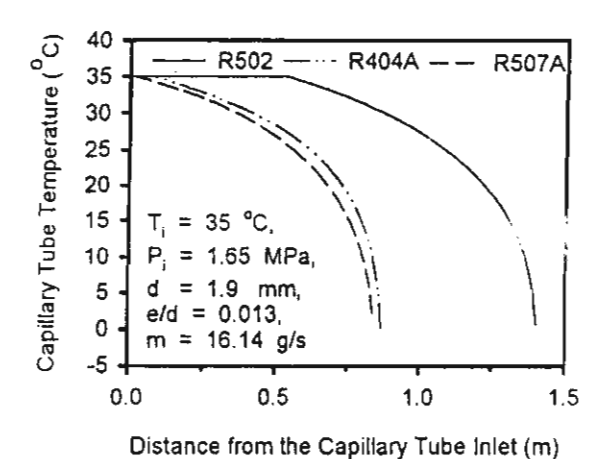


FIG. 14 Variation of x with z



. .

FIG. 16 Variation of T with z

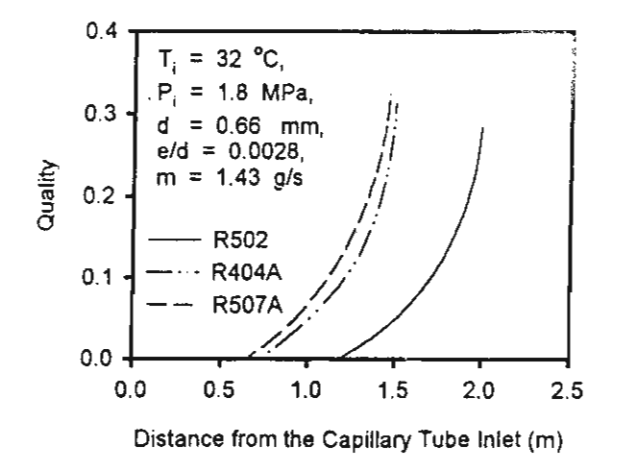


FIG. 18 Variation of x with z

Figures 3,7,10,14 and 18 show the change in quality with position along the capillary tube. As expected for all cases, the quality is zero up to the flash point and then increases in a non-linear fashion, rising more rapidly as the critical length is approached. It is also shown that all alternative refrigerants vaporize earlier than their corresponding traditional refrigerants.

Conclusions

A two-phase homogeneous flow model has been applied to determine the refrigerant flow characteristics in adiabatic capillary tubes used in vapour compression systems. The basic physical equations governing capillary tube flow are established from the conservation of mass, energy and momentum. The partial differential equations derived are solved simultaneously by using the fourth order Runge-Kutta method. Simulation was performed using the present model for all of the refrigerants listed above. The viscosity model used varied depending on the refrigerant and was based on the recommendations of past research. By varying the model input parameters for all pairs, it was found that the traditional refrigerants consistently gave lower pressure drops for both single-phase and two-phase regions which resulted in longer capillary tube lengths.

Acknowledgments

The present study was supported financially by the Thailand Research Fund (TRF) and National Energy Policy Office (NEPO) whose guidance and assistance are gratefully acknowledged.

Nomenclature

A_o cross-sectional area of tube, m² d tube diameter, m

e roughness, m f friction factor

G mass flux, kg/s m² h specific enthalpy, kJ/kg

m mass flow rate, kg/s P pressure, MPa

Re Reynolds number T Temperature, °C

V velocity, m/s x quality

z axial; direction or length, m

Greek Symbols

μ dynamic viscosity, Pa s υ specific volume, m³/kg

ρ density, kg/m³ τ shear stress, N/m²

α void fraction

Subscripts

a accelerational f frictional g gravitational G vapour i capillary tube inlet L liquid sat saturation SC sub-cooled tp two-phase w wall

References

- 1. P.K. Bansal and A.S. Rupasinghe, Applied Thermal Engineering, 18, 207 (1998).
- 2. R.R. Bittle and M.B. Pate, ASHRAE Transactions, 100, 52 (1994)
- 3. Z.H. Chen, R.Y. Li, S. Lin and Z.Y. Chen, ASHRAE Transactions, 96, 550 (1990).
- 4. L. Cooper, C.K. Chu and W.R. Brisken, Refrigerating Eng., 65, 37 (1957).
- 5. D. Jung, C. Park and B. Park, Int. J. Refrigeration, 22, 604 (1999).
- 6. H. Koizumi and K. Yokoyama, ASHRAE Transactions, 86, 19 (1980).
- 7. S.J. Kühl and V.W. Goldschmidt, ASHRAE Transactions, 97, 139 (1991).
- 8. S. Lin, C.C.K. Kwork, R.Y. Li, Z.H. Chen and Z.Y. Chen, Int.J. Multiphase Flow, 17, 95 (1991).
- 9. R.Y. Li, S. Lin and Z.H. Chen, ASHRAE Transactions, 96, 542 (1990).
- 10. C. Melo, R.T.S. Ferreira, C. B. Neto, J.M. Goncalves and M.M. Mezavila, *Applied Thermal Engineering*, 19, 669 (1998).
- 11. E.P. Mikol, ASHRAE Journal, November, 75 (1963).
- 12. S.M. Sami and C. Tribes, Applied Thermal Engineering, 18, 491 (1998)
- 13. T.N. Wong and K.T. Ooi, Int. Comm. Heat Mass Transfer, 22, 595 (1995).
- 14. T.N. Wong and K.T. Ooi, Applied Thermal Eng., 16, 625 (1996).
- 15. T.N. Wong and K.T. Ooi, Int. Comm. Heat Mass Transfer, 23, 993 (1996).
- 16. REFPROP, Thermodynamic Properties of Refrigerants and Refrigerant Mixtures, version 6.01, Gaithersburg, M.D. National Institute of Standards and Technology (1998).
- 17. G.B. Wallis, One Dimensional Two-Phase Flow, McGraw-Hill, (1969).
- 18. W.H. McAdams, W.K. Wood and R.L. Bryan, Transaction of ASME, 64, 193 (1942).
- 19. A.Cicchitti, C. Lombardi, M. Zsilvestri, G. Soldaini and R. Zavattarelli, *Energia Nucleare*, 7, 407 (1960).
- 20. A. E. Dukler, M. Wicks and R.G. Cleveland, AIChE Journal, 10, 38 (1964).

Wongwises, S., Napon, P., Heat Transfer and Flow Characteristics in Vertical Annular Two-Phase Two-Component Flow, *TIJSAT*, 2000; 5(1): 16-27.

Heat Transfer and Flow Characteristics in Vertical Annular Two-Phase Two-Component Flow

Somchai Wongwises and Paisan Naphon

Fluid Mechanics & Turbomachinery Research Laboratory (FUTURE)

Department of Mechanical Engineering,

King Mongkut's University of Technology Thonburi,

91 Suksawas 48, Bangmod, Radburana,

Bangkok 10140, Thailand

Abstract

Experimental and theoretical results on flow, heat and mass transfer characteristics for the countercurrent flow of air and water in a vertical circular pipe are compared. An experimental setup was designed and constructed. Hot water is introduced through a porous section at the upper end of a test section and flows downward as a thin liquid film on the pipe wall while the air flows countercurrently. The air and water flow rates used in this study are those before the flooding is reached. A developed mathematical model is separated into three parts: A high Reynolds number turbulence model, in which the local state of turbulence characteristics consists of the turbulent kinetic energy (k) and its dissipation rate (\varepsilon). The transport equations for both k and \varepsilon are solved simultaneously with the momentum equation to determine the kinetic turbulence viscosity, the pressure drop, interfacial shear stress and then the friction factor at the film/core interface; heat and mass transfer models are proposed in order to estimate the distribution of the temperature and the mass fraction of water vapor in gas core. The results from the model are compared with the present experimental ones. It can be shown from the present study that the influence of the interfacial wave phenomena is significant to the pressure loss, and the heat and mass transfer rates in the gas phase.

1. Introduction

Many of the two phase flow transportation processes found in industrial applications occur in the annular flow regime. Annular two-phase flow is one of the most important flow regimes and is characterized by a phase interface separating a thin liquid film from the gas flow in the core region. Two-phase annular flow occurs widely in film heating and cooling processes, particularly in power generation and especially in nuclear power reactors. This flow regime has received the most attention both analytically and experimentally [1-5] because of its practical importance and the relative ease in which analytical treatment may be applied.

Relatively little information, however, iscurrently available on the heat and mass transfer characteristics of two-phase countercurrent annular flow in a vertical pipe. Some of earliest work was performed by Suzuki et al. [6]. They proposed a theoretical method to evaluate the heat transfer and flow characteristics of a twophase, two-component annular flow with a thin film heated at low heat flux. A simple model for the wave effect employed in their study predicts the heat transfer well. Hijikata et al. [7] studied the flow characteristics and heat transfer in countercurrent water and air flows. A theoretical model based on a low Reynolds number k-& turbulence model was proposed, where an additional production term was

considered to incorporate the wave effects. In the present study, the experimental and theoretical data on flow, heat and mass transfer characteristics for the vertical countercurrent annular flow are investigated. The effects of any relevant parameter on pressure loss, and the heat and mass transfer rate are also discussed.

2. Experimental Apparatus and Method

The experimental apparatus is shown schematically in Fig.1. The test section, with an inside diameter of 24 mm and the length of 1.9 m was constructed from transparent acrylic glass to permit visual observation of the flow patterns. The water temperature was raised to the desired level by using electric heaters and was controlled by a temperature controller and then pumped through a rotameter to the water inlet section. The water inlet section was constructed from two concentric tubes, the inner tube being the test section or sinter which was radially drilled with many small holes. The inner tube of the sinter was also covered with a fine wire mesh to distribute the water smoothly along the pipe. The water in the inlet section flowed downwards as a liquid film along the test section while the air flowed countercurrently. The level of water in the water outlet section was kept constant, and the excess water was drained out.

An upper open end condition was used in the experiments. Air was supplied to the test section by a blower and the flow rate was controlled by a valve at the outlet of the blower. The inlet flow rate of air was measured by means of an orifice and micromanometer, and the inlet flow rate of water was measured by a rotameter. The relative humidities of inlet and outlet air were calculated from wet and dry bulb temperatures and were checked by digital humidity meter (electrostatic capacitance type) using a polymer film as a sensor. The water temperatures at three positions along the test section were measured by thermistors. The two phase pressure drop between the test section was measured by a digital manometer. Stainless ring electrodes were mounted flush in the tube wall for measuring the film thickness. The measuring positions were located at 30 cm and 170 cm from the lower end of the test section. They operate on the principle of the variation of

electrical resistance with changes in the water film thickness between two parallel electrode rings. The same description of the calibration procedures for annular flow can be found in Andreussi [8]. Due to the variation of conductivity with temperature and coating of the electrodes with impurities, the gauges were calibrated before and after each run.

Experiments were conducted at various air, water flow rates, and water temperatures. The air flow rate was increased by small increments while the water flow rate at a specific temperature was kept constant. After each change in the inlet air flow rate, both the air and the water flow rates, the relative humidity of air at inlet and outlet of the test section were recorded. The pressure drop across the test section and the film thickness were registered through the transducers and transferred to the data acquisition system. The flow phenomena were also detected by visual observation. The experiments were stopped before the onset of flooding was reached.

3. Mathematical model

In order to compare with the present experimental results, the theoretical model of Hijikata et al. [7] is modified for this study. In the present paper, a model based on a high Reynolds number k-ɛ turbulence model is proposed. The notation used for the calculation is shown in Fig. 2. The model is separated into three parts; flow, heat and mass transfer characteristics with the following assumptions:

- The gas flow is fully developed because of the large length-to-diameter ratio.
- The effect of vaporization on the gas flow field is neglected.
- Physical properties are constant and independent of the composition.

3.1. Turbulence flow characteristic:

In turbulent flow, velocity fluctuations exchange momentum between adjacent layers of fluid, thereby causing apparent shear stresses that must be added to the stress caused by the mean velocity gradients. For a fully developed turbulent channel flow, the total shear stress is, therefore, given by

$$\tau = \mu \frac{dU}{dv} - \rho \overline{u'v'}$$
 (1)

The term $-\rho \overline{u'v'}$ is referred to as the turbulent shear stress which is related to the mean rate of strain via a turbulent viscosity (Jones and Launder [9]).ie.

$$-\rho_{u'v'}^{\prime} = \mu_t \frac{\partial \upsilon}{\partial v} \tag{2}$$

A turbulent viscosity term therefore appears in the present model.

Momentum equation;

$$0 = -\frac{\int dP}{\rho dz} + \frac{\int \partial}{r \partial y} \left(r(\upsilon + \upsilon_t) \frac{\partial \upsilon}{\partial y} \right)$$
 (3)

Jones and Launder [9] presented turbulence models based on high and low Reynolds numbers in order to predict the laminarization. A high Reynolds number k-\varepsilon model is employed in this study.

Turbulent kinetic energy (k) equation;

$$\frac{\partial k}{\partial t} = \frac{1}{r} \frac{\partial}{\partial y} \left(r \left(\frac{\upsilon_t}{\sigma_k} \right) \frac{\partial k}{\partial y} \right) + \upsilon_t \left(\frac{\partial \upsilon}{\partial y} \right)^2 - \varepsilon \tag{4}$$

Turbulent kinetic energy dissipation (ε) equation;

$$\frac{\partial \varepsilon}{\partial t} = \frac{1}{r} \frac{\partial}{\partial y} \left(r \left(\frac{\upsilon_t}{\sigma_{\varepsilon}} \right) \frac{\partial \varepsilon}{\partial y} \right) + c_1 \frac{\varepsilon}{k} \upsilon_t \left(\frac{\partial \upsilon}{\partial y} \right)^2 - c_2 \frac{\varepsilon^2}{k}$$
(5)

Kinetic turbulent viscosity;

$$\upsilon_t = C_\mu \frac{k^2}{\varepsilon} \tag{6}$$

The equations contain five adjustable constants $C\mu$, C_1 , C_2 , σ_k , σ_{ε} . The standard k- ε model employs values for the constants that are arrived at by comprehensive data fitting for a wide

range of turbulent flows (Versteeg and Malalasekera [10]; Singhal and Spalding [11]):

$$C_{\mu} = 0.09, C_1 = 1.44, C_2 = 1.92, \sigma_k = 1.0, \sigma_{\mathcal{E}} = 1.3$$

The boundary conditions at the interface (y = 0) and the center of pipe (r = 0) are given as follows:

$$y = 0: U = -U_{lm}, k = 0, \varepsilon = 0$$
 (7)

$$r = 0: \frac{\partial U}{\partial y} = \frac{\partial k}{\partial y} = \frac{\partial \varepsilon}{\partial y} = 0$$
 (8)

where U_{lm} is the mean velocity of the liquid film obtained from the experiment.

3.2. Heat transfer characteristic:

The distributions of the temperature of the mixture between dry air and water vapor along the upward flow direction is expressed as:

$$U \frac{\partial T}{\partial z} = \frac{1}{r} \frac{\partial}{\partial y} \left(r \left(a + \frac{U_t}{Pr_t} \right) \frac{\partial T}{\partial y} \right)$$
(9)

with a boundary condition;

$$y = 0: T = T_i, \omega_v = \omega_{vs}$$
 (10)

3.3. Mass transfer characteristic:

The distributions of the mass fraction of the mixture between dry air and water vapor along the upward flow direction is also expressed as:

$$U \frac{\partial \omega_{v}}{\partial z} = \frac{1}{r} \frac{\partial}{\partial y} \left(r \left(D + \frac{U_{t}}{Sc_{t}} \right) \frac{\partial \omega_{v}}{\partial y} \right)$$
(11)

with a boundary condition;

$$r = 0: \frac{\partial T}{\partial y} = \frac{\partial \omega_{y}}{\partial y} = 0 \tag{12}$$

In turbulent flow, there is no universal relationship between the shear stress field and the mean velocity field. Thus, for turbulent flows we are forced to rely on experimental data. The velocity profile for a fully developed turbulent flow through a rough pipe from Pao

[12] is used in the calculation. The friction factor in his equation is replaced by those obtained from the present experiment. The transport equations for both k and ε are solved simultaneously with the momentum equation using the finite difference method to determine the kinetic turbulence viscosity, pressure drop, interfacial shear stress and friction factor at film/core interface.

4. Results and discussion

{

A large number of graphs can be drawn from the result of the study but because of space limitations, only typical results are shown. In the experiment, mean film thicknesses were measured at Z = 30 cm and 170 cm. Average values for both mean film thicknesses for various air and water flow rates are given in Fig. 3. The liquid film mass flow rate in this figure is on a per unit width basis in the spanwise direction. As the water flow rate is increased and the air flow rate held constant, the film thickness also increases. It can also be clearly seen that there is a great difference in the mean film thickness between experiments with and without air flow. The mean film thickness at any air flow rate for a specific water flow rate is, however, nearly the same. Figure 4 shows the relationship between the dimensionless turbulent kinetic energy $(k^+, k/(u_*)^2)$ and dimensionless distance from the interface (v^+). yu_*/v). The turbulent kinetic energy falls to zero at the interface. As a result of a wavy interface, the turbulent kinetic energy in the region close ŧo the interface, monotonically with the distance from the interface to a maximum point and then drops sharply and approaches an equilibrium value. Because the amplitude of the film thickness fluctuation increases slightly with the air flow rate, the turbulent kinetic energy near the interface for higher air flow rate is higher than for lower flow rate.

Figure 5 shows the variation of the interfacial friction factor with the air Reynolds number for typical test conditions. The friction factor for laminar flow and the Blasius correlation for turbulent flow in smooth pipe are also shown in this figure. The velocity gradient at the interface is much larger for turbulent flow

than for laminar flow. This change in velocity profile causes the interfacial shear stress to increase sharply, with the same effect on the interfacial friction factor. The friction factor decreases gradually along the smooth pipe curve. This figure shows also a comparison of friction factors obtained from the model and the experiments. The agreement of this comparison is not bad through the whole range. As a result of the pipe roughness, experimental friction factors for air single phase flow are found to be higher than those from the Blasius correlation. As the water flow rate is increased; larger disturbance waves are formed. The friction factors at higher water flow rates seem, therefore, a little bit higher than those at lower ones. It should be noted that a similar phenomenon can be found in single phase flow in rough walled pipes.

Figure 6 shows the relationship between the mass fraction of water vapor and the air temperature. The saturated line in this figure is based on the saturation vapor pressure of water. A circular point shows the inlet condition of air (dry air and water vapor), and the solid points show the outlet conditions. While the hot water flows down as a film countercurrently with air flow, vaporization occurs at the interface and water vapor from this vaporization will be added to the existing water vapor. Mass fraction of water vapor at the outlet of the test section are, therefore, higher than those of the inlet and also found to be below the saturation line. When the water temperature is higher, the points approach the saturation line. This is confirmed by visual observation that there is an absence of mist (tiny water droplets). However, if the water temperature is high enough, the water vapor from the vaporization is condensed in air stream to form a mist.

Figure 7 shows the relationship between the Nusselt (Nu) number and the value of RePr^{0.4}. A complete heat balance was used to calculate the heat transfer coefficient. The equilibrium conditions of air and water film after passing air through falling hot water film for any interval of time can be established by the following energy balance equation:

$$hA\Delta T_{ln} + \Delta GC_{p,v}T_{lm} + G_{ln}C_{p,in}T_{b,in} = G_{out}C_{p,out}T_{b,out}$$

The first, second, third and fourth term represent heat transfered from the falling water to the air stream, the enthalpy of vapor evaporated from the water film, the enthalpy of the inlet air and the enthalpy of the air leaving the test section respectively. The value of ΔT_{ln} is the log mean temperature difference between both fluids. T_{lm} is the mean water temperature at the interface. Consider the Nu number, based on a pipe diameter, rearranged in the form, Nu = hd_l/ξ and the heat transfer coefficient from the energy balance equation, the following equation is obtained;

$$Nu = \frac{d_i}{\xi} \frac{(G_{out}C_{p,out}T_{b,out} - G_{in}C_{p,in}T_{b,in} - \Delta GC_{p,v}T_{im})}{(\Delta T)_{in}\pi d_i L}$$

The latent heat of vaporization is not included because, in this paper, the Nu number is defined for a sensible heat transfer. The figure also shows the effect of the upward air flow on the heat transfer coefficient. At a specific water temperature, the Nu number (or the heat transfer coefficient) increases with increases in the air flow rate. The solid line is the Nu number calculated from Dittus-Boelter equation for fully developed turbulent flow in smooth tubes; $Nu = 0.023Re^{0.8}Pr^{0.4}$. There is a good agreement here. Any discrepancies are due to the wave formed at the interface and variation of the water temperature along the pipe. Figure 8 shows the relationship between an average temperature ratio and the dimensionless distance from the interface, at z = 1 m. At the same inlet water flow rate and temperature, an increase in air flow rate causes a higher fluctuation of the film thickness, and thus higher rate of heat transfer. It corresponds to the results in Fig. 7. The temperature profiles however, differ slightly from each other.

Mass transfer characteristics can be discussed in the same way as those of the heat transfer. Consider the Sherwood (Sh) number = $k_m d_i/D$ in which k_m is the mass transfer coefficient and D is the mass diffusivity. The mass transfer coefficient substituted in this equation is calculated from the mass balance equation and finally the following equation is obtained;

$$Sh = (1 - \omega_{vi}) \frac{d_i}{\rho D} \frac{\Delta G}{(\Delta \omega_v)_{\ln} \pi d_i L}$$

The results from Figs. 9 and 10 are closely associated with those from Figs. 7 and 8. The relationship between the Sh number and the value of Re^{0.83} Sc^{0.33} is shown in Fig. 9. The similarities between the governing equations for heat, mass, and momentum transfer suggest that the empirical correlations for the mass transfer coefficient would be similar to those for the heat transfer coefficient. This turns out to be the case, and some of the empirical relations for mass transfer from a liquid that completely wets the inside of a tube to a turbulent gas that is flowing is given by Ozisik [13]:

$$Sh = 0.023 Re^{0.83} Sc^{0.33}$$

The Sh number at any water flow rate for specific air flow rate and specific water temperature is, however, nearly the same. The solid line in Fig. 9 shows the Sh number calculated from above equation. The Sh number from the experiment is slightly higher than the theoretical value. The difference between them is considered to be a result of the wave formed at the interface. The profiles of mass fraction ratio predicted at Z= 1 m are also shown in Fig. 10. At specific water and air flows, the rate of vaporization increases with increases of the water temperature. It should be noted that in the present experiment where mist formation does occur, the temperature and concentration profiles are almost the same.

5. Conclusions

Experiments have been performed to study the flow, heat and mass transfer characteristics of air-water two-phase countercurrent annular flow in a vertical pipe. A theoretical model has been developed. The model is separated into three parts: a high Reynolds number turbulence model, in which the local state of turbulence characteristics are controlled by the turbulence kinetic energy (k) and its dissipation rate (ϵ); and the heat and mass transfer models. The transport equations for both k and ϵ are solved simultaneously with the momentum equation to

determine the kinetic turbulence viscosity, the pressure drop, interfacial shear stress and then, the friction factor at the film/core interface. The distribution of the temperature and the mass fraction of water vapor in the gas core is also estimated from the heat and mass balance equations, and the kinetic turbulence viscosity is obtained from the former step. The results from the model are in reasonable agreement with the experimental results. It was found that the interface is often wavy in nature and the influence of the interfacial wave is of significance on the momentum, heat and mass transfer characteristics.

Acknowledgments

1

The present study was supported financially by the Thailand Research Fund (TRF) whose guidance and assistance are gratefully acknowledged. The authors would like to express their appreciation to Professor Takao Nagasaki from Tokyo Institute of Technology for the valuable answers on the subject.

Nomenclature

- a thermal diffusivity, m²/s
- A heat transfer area, m²
- C_1 , C_2 and C_{μ} constant in Eqs.(5) and (6)
- Cp specific heat, J/kg °C
- Cf friction factor
- d pipe diameter, m
- d; diameter of gas core, m
- D mass diffusivity, m²/s
- G mass flow rate, kg/s
- h heat transfer coefficient, W/m² °C
- k turbulent kinetic energy, m²/s²
- k⁺ dimensionless turbulent kinetic energy
- k_m mass transfer coefficient, m/s
- L pipe length, m
- Nu Nusselt number
- P pressure, N/m²
- Pr Prandtl number
- radial distance coordinate
- Re Reynolds number
- Sc Schmidt number
- R_i distance from the pipe centerline to the interface, m
- Sh Sherwood number
- t time
- T temperature, °c

- U mean velocity, m/s
- u. friction velocity, m/s $(=(\tau_i/\rho)^{1/2})$
- u', v' fluctuating components of velocity, m/s
- $\overline{u'v'}$ time average of the product of u' and v'
- y distance from the air-water interface, m
- y^+ dimensionless distance (= yu_* / v)
- z distance from the bottom of the test section, m

Greek Symbols

- ρ density, kg/m³
- σ_k , σ_{ε} constant in Eqs. (4) and (5)
- τ shear stress, N/m²
- υ kinematic viscosity, m²/s
- μ dynamic viscosity, kg/sm
- ∆ difference
- ε turbulent kinetic energy dissipation, m²/s³
- ω mass fraction
- ξ thermal conductivity, W/mC
- δ liquid film thickness, m

Subscripts

- b bulk
- c value at the centerline of the pipe
- g air
- i interface
- in inlet
- l liquid
- In log mean difference
- m mean value
- out outlet
- t turbulent
- v water vapor
- vs saturated vapor

6. References

- [1] Azzopardi, B.J. and Williams, N.M. (1980), *Multi-Phase Transport*, McGraw-Hill, New York.
- [2] Fore, L.B. (1995), Int. J. Multiphase Flow, Vol. 21, p. 137.
- [3] Joseph, D.D. and Bannwart, A.C. (1996), Int. J. Multiphase Flow, Vol. 22, p. 1247.
- [4] Wolf, A., Jayanti, S. and Hewitt, G.F. (1996), Int. J. Multiphase Flow, Vol. 22, p. 325.

- [5] Ghiaasiaan, S.M., Wu, X., Sadowski, D.L. and Abdel-Khalik, S.I. (1997), Int. J. Multiphase Flow, Vol. 23, p. 1063.
- [6] Suzuki, K., Hagiwara, Y. and Sato, T. (1983), Int. J. Heat Mass Transfer, Vol. 26, p. 597.
- [7] Hijikata, K., Nagasaki, T., Yoshioka, J. and Mori, Y. (1988), JSME International Journal, Vol. 31, p. 429.
- [8] Andreussi, P., Di Donfrancesco, A. and Messia, M. (1988), Int. J. Multiphase Flow, Vol. 14, p. 777.
- [9] Jones, W.P. and Launder, B.E. (1972), Int.J. Heat Mass Transfer, Vol. 15, p. 301.
- [10] Versteeg, H.K. and Malalasekera, W. (1995), An Introduction to Computational Fluid Dynamics, 1st ed., Longman, London.
- [11] Singhal, A.K. and Spalding, D.B. (1981), Computer Methods in Applied Mechanics & Eng., Vol. 25, p. 365.
- [12] Pao, R.H.F. (1961), Fluid Mechanics, Wiley, New York.
- [13] Ozisik, M. (1985), Heat Transfer, McGraw-Hill, New York.

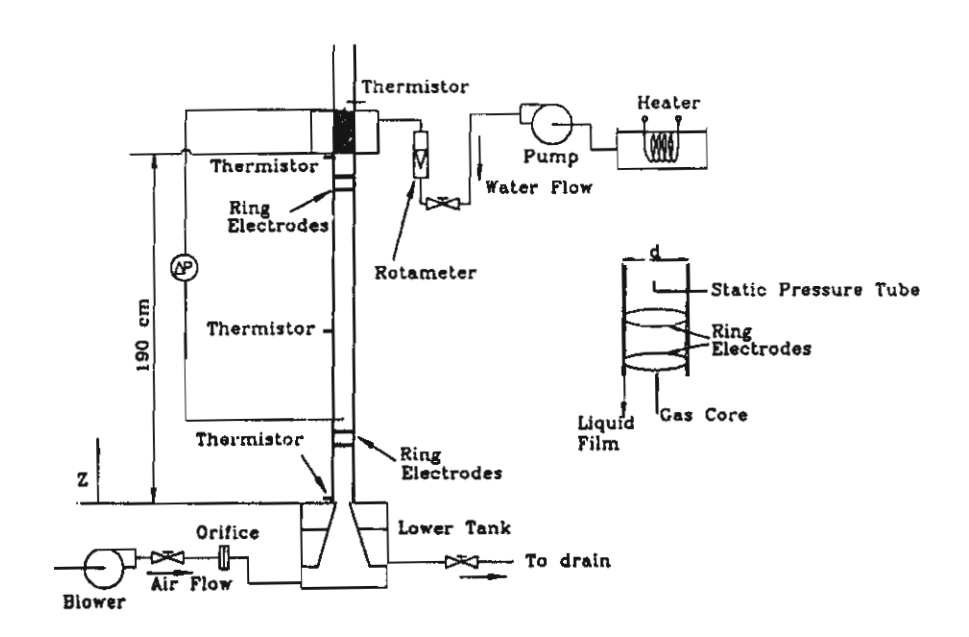


Figure 1. Schematic diagram of experimental apparatus

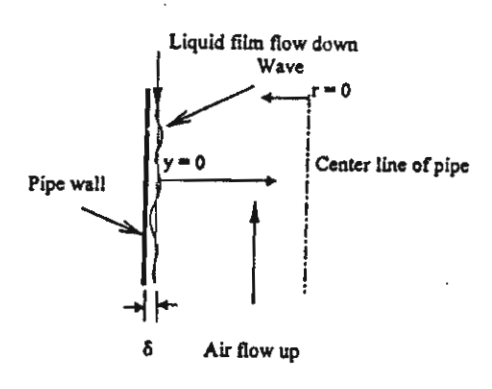


Figure 2. Geometry of annular flow

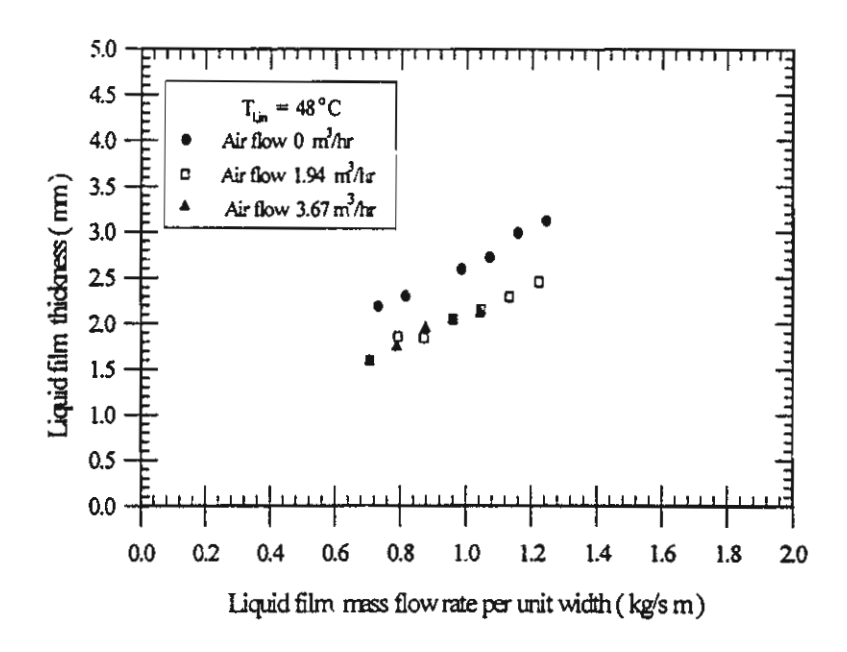


Figure 3. Plot of film thickness against mass flow rate

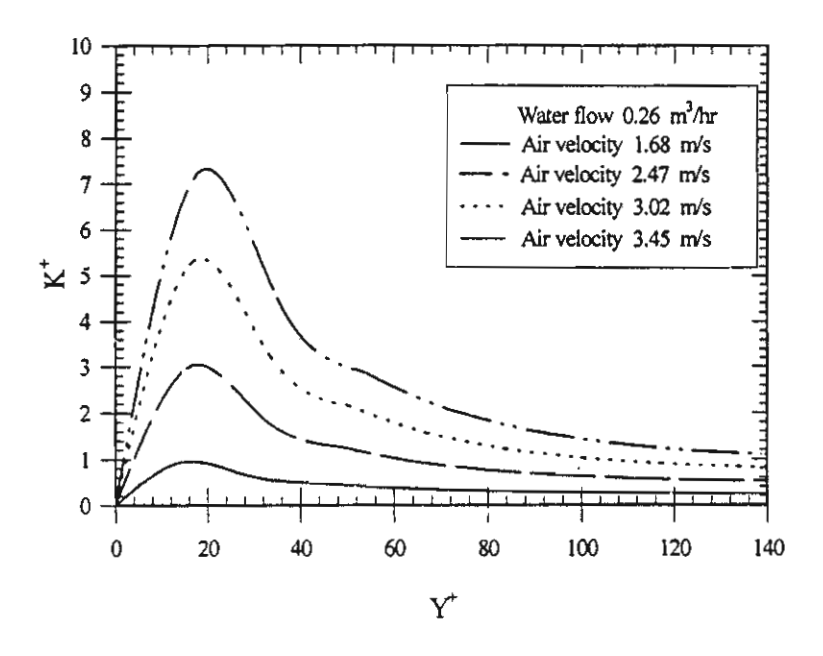


Figure 4. Fully developed kinetic energy profiles

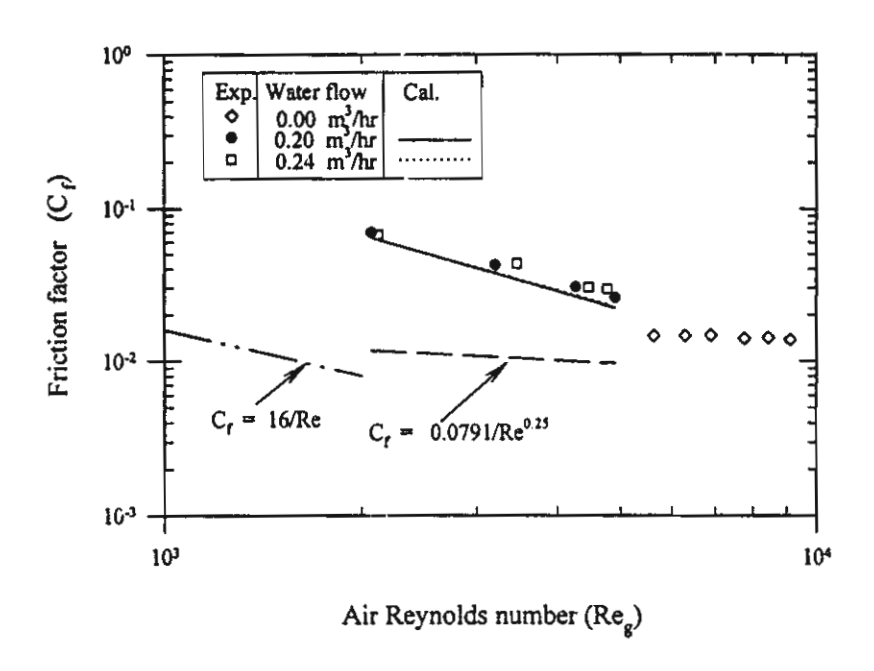


Figure 5. Plot of friction factor against Reynolds number

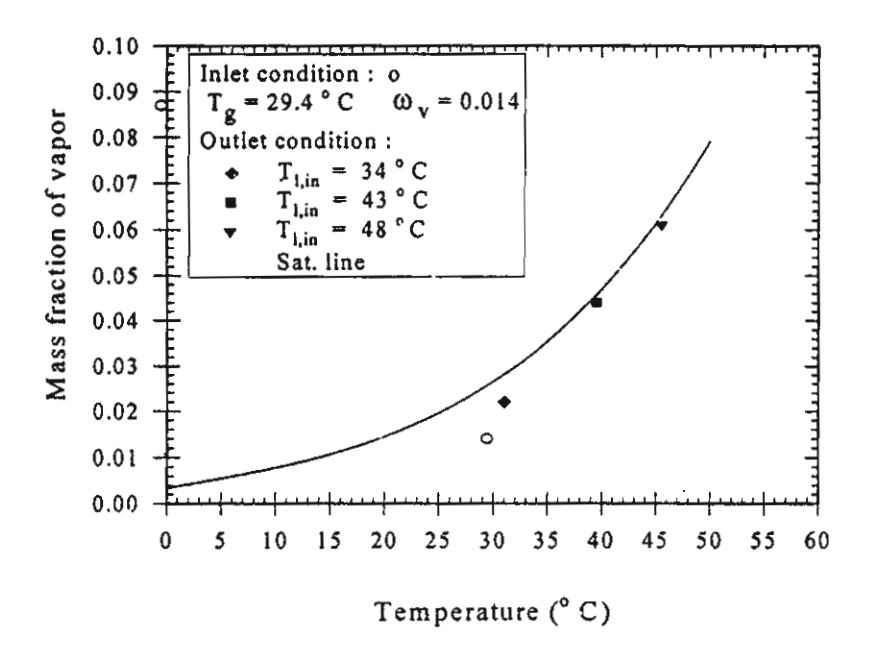


Figure 6. Plot of mass fraction against temperature

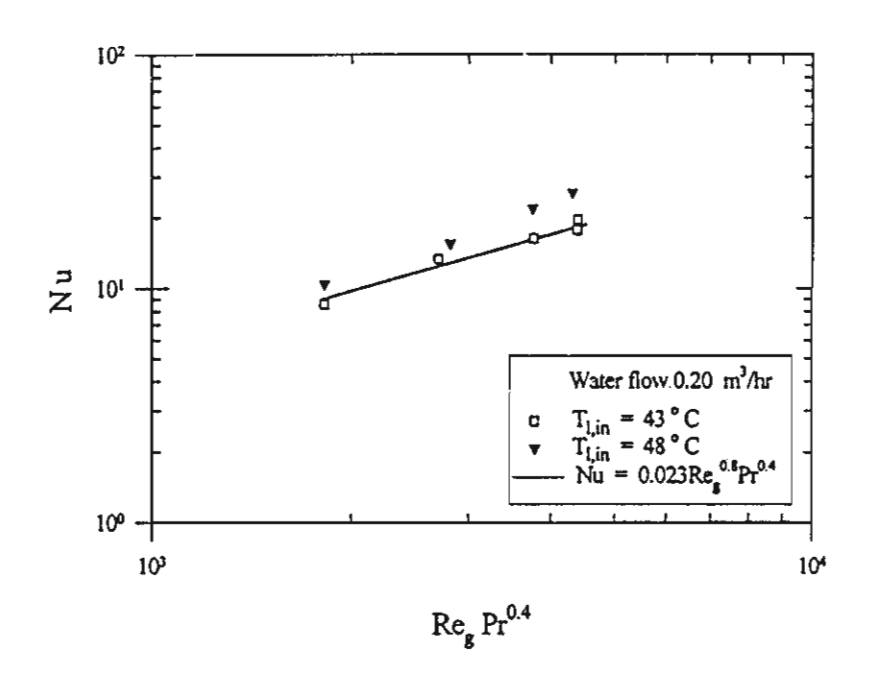


Figure 7. Plot of Nu against Re_gPr^{0.4}

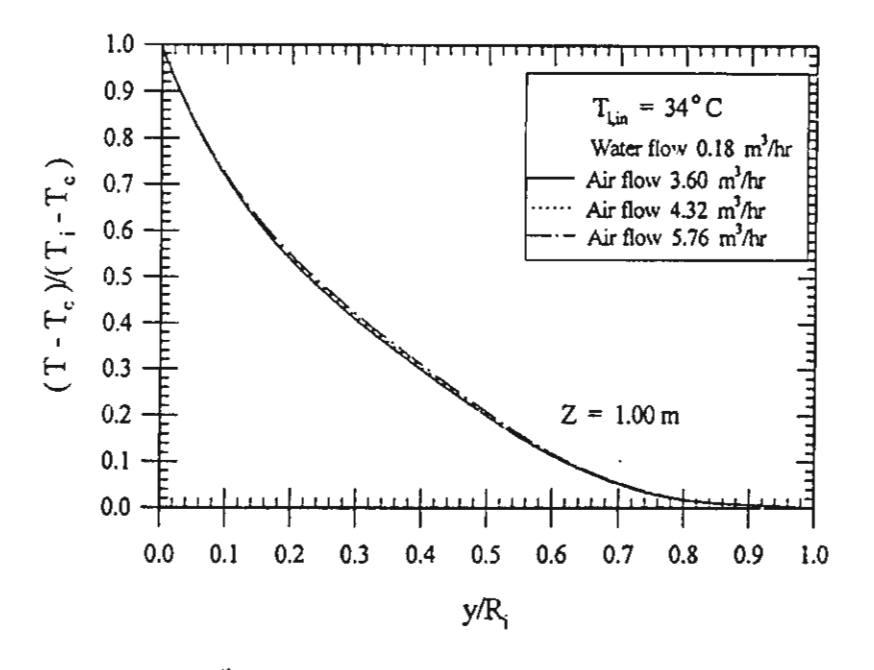


Figure 8. Fully developed temperature profiles

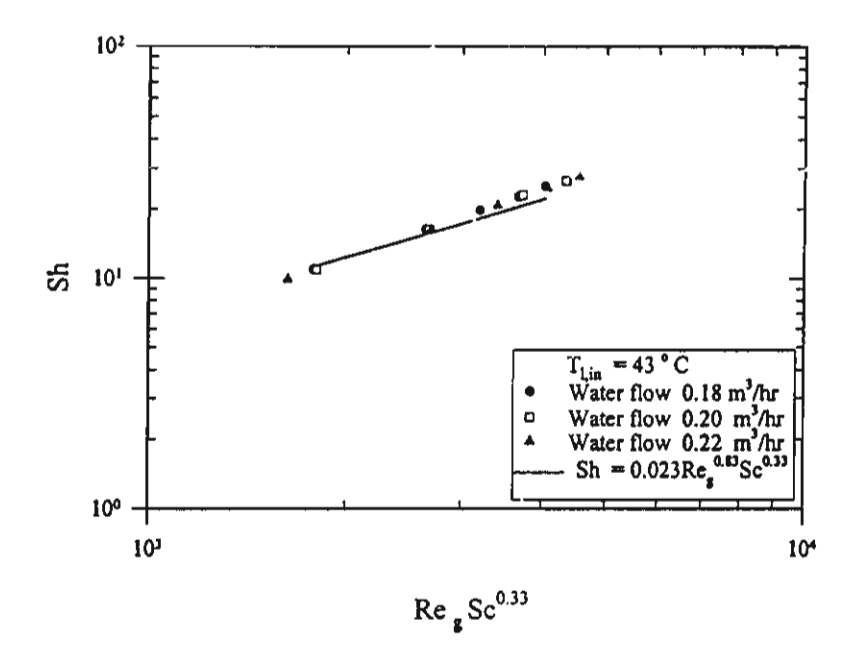


Figure 9. Plot of Sh against RegSc^{0.33}

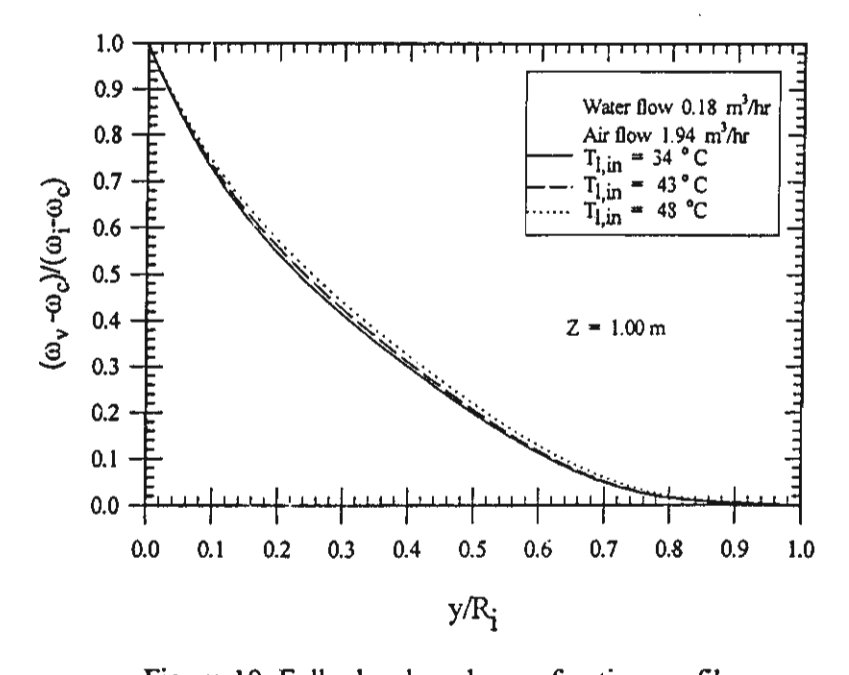


Figure 10. Fully developed mass fraction profiles

Wongwises, S., Chan, P., Luesuwanatat, N., Purattanarak, T., Two-Phase Separated Flow Model of Refrigerants Flowing Through Capillary Tubes, *Int. Com. Heat Mass Transfer*, 2000; 27(3): 343-356.



PH S0735-1933(00)00115-9

TWO-PHASE SEPARATED FLOW MODEL OF REFRIGERANTS FLOWING THROUGH CAPILLARY TUBES

S. Wongwises, P. Chan,
N. Luesuwanatat and T. Purattanarak
Fluid Mechanics and Turbomachinery Research Centre (FUTURE)
Department of Mechanical Engineering,
King Mongkut's University of Technology Thonburi,
Bangmod, Bangkok 10140, Thailand

(Communicated by J.P. Hartnett and W.J. Minkowycz)

ABSTRACT

Capillary tubes are often used as an expansion and controlling device in refrigeration systems. The homogeneous two-phase flow model has been used exclusively in capillary tube flow studies and has not changed appreciably since the 1950's. However, some experimental results show that two-phase flow in small diameter tubes may be not entirely homogeneous due to phase interaction. In this paper, a separated flow model of refrigerants through capillary tubes is derived. The effects of various correlations of relevant parameters; frictional pressure gradient and slip ratio, on the prediction of a separated flow model are investigated. The results calculated by this separated flow model are compared with the measured data reported in the literature. Finally suitable correlations of relevant parameters for a flow model are proposed. © 2000 Elsevier Science Ltd

Introduction

The design and analysis of capillary tubes have received the most attention both analytically and experimentally [1-16]. In two phase flow region, the flow is assumed to be homogeneous in almost all of the analytical studies. Due to the lack of the correlation of the slip-ratio, modeling by separated flow assumption has received comparatively little attention in the literature. Recently Wong et al. [14] have attempted to exploit the possibility of applying a separated flow model to the adiabatic capillary tube flow studies using the Miropolskiy et al.'s slip ratio [19] and Lin et al. 's frictional pressure gradient correlation [7]. In works by Wong et al. [14], comparisons between the predicted results with the experimental data for R-12 from previous workers showed that a separated flow model gave better prediction.

There are, however, various correlations of the relevant parameters that need to be considered such as the slip ratio, the frictional pressure gradient, friction factor and also the type of refrigerant used. The

parameters mentioned above would be expected to affect the predicted results. In the present study, the characteristics of flow within capillary tubes are derived from a separated flow assumption. The model is based on that of Wallis [25] and Wong [14]. The effects of the various relevant parameters on the model prediction are investigated by comparing with the existing measured data.

Mathematical Model

The flow of refrigerant through a capillary tube (Fig. 1) can be divided into two distinct regions; a single-phase subcooled liquid and a two-phase region. In the two-phase region, the model developed is based on separated one-dimensional two-phase flow. In modeling, the basic physical equations governing the capillary tube flow are the continuity and conservations of energy and momentum. The model includes the various relevant parameters and is a tool to determine the size of the capillary tubes used in household refrigerators and freezers, especially to select the capillary tube length for given operating conditions.

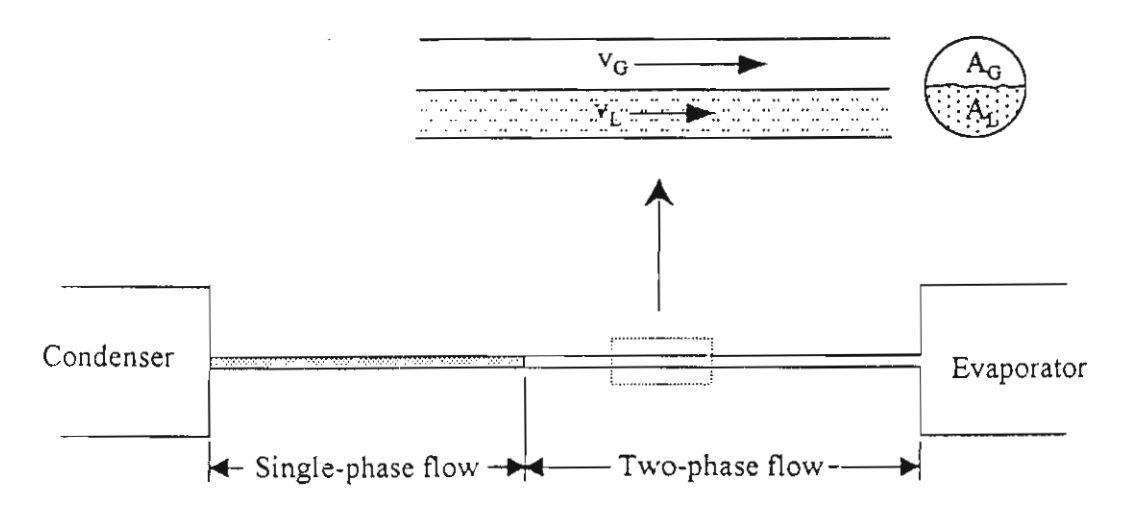


FIG. 1 Schematic diagram of the capillary tube

Subcooled Liquid Region

The subcooled liquid region is the region from the inlet of the capillary tube to the position where the saturation pressure corresponds to the inlet temperature. As the refrigerant flows along the tube in this region, the pressure decreases linearly until the refrigerant becomes a saturated liquid. For steady fully-developed incompressible flow, the integral form of the momentum equation is

$$-A_{o}dp - \tau_{w}(\pi d)dz = 0$$
 (1)

where τ_{W} is the wall shear stress and defined as

$$\tau_{W} = f \frac{(\rho_{L} V_{m}^{2})}{8} \tag{2}$$

where f is the Moody friction factor and can be determined from Colebrook's correlation as follows;

$$\frac{1}{f^{0.5}} = -2 \log \left(\frac{\varepsilon / d}{3.7} + \frac{2.51}{\text{Re } f^{0.5}} \right)$$
 (3)

Substituting Eq. (2) into Eq. (1), the single phase subcooled liquid length (L_{SC}) of the capillary tube can be obtained from

$$p_{inlet} - p_{sat} = \left(f \frac{G^2}{2\rho_L d}\right) L_{SC}$$
 (4)

where the total mass flux (G) is the total mass flow rate of liquid plus vapour divided by total channel cross-sectional area (A_o) .

Two-Phase Region

The specific enthalpy of a substance at a saturation state having a given dryness fraction can be calculated by utilizing the definition of dryness fraction (x).

$$h = x h_{G} + (1 - x) h_{I}$$
 (5)

where the dryness fraction (or mass dryness fraction) is the ratio of the mass of vapour to total mass of liquid plus vapour when a substance is in a saturation state.

Weighting for the mass flow rate of each phase [21], we can write

$$\frac{V^2}{2} = x \frac{V_G^2}{2} + \frac{(1-x)}{2} V_L^2 \tag{6}$$

For adiabatic refrigerant flow in a capillary tube with no externally applied work and neglecting the elevation changes, the following form of energy equation is obtained

$$\frac{d}{dz}\left(xh_G + (1-x)h_L\right) + \frac{d}{dz}\left(x\frac{V_G^2}{2} + (1-x)\frac{V_L^2}{2}\right) = 0$$
 (7)

In the two-phase region for a pure substance in equilibrium, the enthalpies (and also densities) are only functions of pressure. In liquid-vapour flows, void fraction (α) usually represents the time-averaged fraction of the cross-sectional area or of the volume which is occupied by the vapour phase, so

$$\alpha = A_G / A_g \tag{8}$$

¥

Vapour and liquid mass fluxes (G_G and G_L) are the vapour and liquid mass flow rates divided by total channel cross-sectional area, so

$$G_G = \rho_G Q_G / A_o \quad \text{and} \quad G_L = \rho_L Q_L / A_o$$
 (9)

Using above correlations, actual average velocity of vapour and liquid phases (V_G and V_L) can be determined, so

$$V_G = \frac{xG}{\alpha \rho_G}$$
 and $V_L = \frac{(1-x)G}{(1-\alpha)\rho_L}$ (10)

For a liquid-vapour mixture of a given substance, the void fraction correlation is expressed as follows;

$$\alpha = \alpha[p(z), x(z)] \tag{11}$$

Further, from chain rule

$$\frac{d\alpha}{dz} = \left(\frac{\partial \alpha}{\partial p}\right)_{x} \frac{dp}{dz} + \left(\frac{\partial \alpha}{\partial x}\right)_{p} \frac{dx}{dz}$$
(12)

The separated flow model takes into account the fact that the two phases physically flow with different velocities and properties. The correlation of Premoli et al. [20] is a correlation for void fraction (a) in terms of the slip ratio (S). This general equation is then given by

$$\alpha = \frac{1}{1 + S\left(\frac{1 - x \rho_G}{x \rho_L}\right)}$$
 (13)

Eventually, after rearrangement, we obtain an expression for the total pressure gradient

$$\frac{dp}{dz} = -\frac{dx}{dz} \left(\frac{D - E + F}{A - B + C} \right)$$
 (14)

where

$$A = x \frac{dh_G}{dp} + (1-x) \frac{dh_L}{dp} + \left(\frac{x^3 G^2 v_G}{\sigma^2} \right) \frac{dv_G}{dp} + \left(\frac{(1-x)^3 G^2 v_L}{(1-\alpha)^2} \right) \frac{dv_L}{dp}$$

$$B = \left(\frac{x^3 G^2 v_G^2}{\alpha^3}\right) \left(\frac{S(1-x)x v_L \frac{dv_G}{dp} - S(1-x)x v_G \frac{dv_L}{dp}}{(x v_G + S(1-x)v_L)^2}\right)$$

$$C = \left(\frac{(1-x^3)G^2\overline{\upsilon}_L^2}{(1-\alpha^3)}\right) \left(\frac{S(1-x)x\upsilon_L\frac{d\upsilon_G}{dp} - S(1-x)x\upsilon_G\frac{d\upsilon_L}{dp}}{(x\upsilon_G + S(1-x)\upsilon_L)^2}\right)$$

$$D = h_{LG} + \frac{1}{2} \left(V_G^2 - V_L^2 \right) + \frac{x^2 G^2 v_G^2}{\alpha^2} - \frac{(1-x)^2 G^2 v_L^2}{(1-\alpha)^2}$$

$$E = \left(\frac{x^3 G^2 v_G^2}{\alpha^3} \right) \left(\frac{S(1-x) v_G v_L + Sx v_G v_L}{(x v_G + S(1-x) v_L)^2} \right)$$

$$F = \frac{(1-x)^3 G^2 v_L^2}{(1-\alpha)^3} \left(\frac{S(1-x) v_G v_L + Sx v_G v_L}{(x v_G + S(1-x) v_L)^2} \right)$$

The momentum equation is often rewritten as an explicit equation for the pressure gradient. The total pressure gradient $\left(\frac{dp}{dz}\right)$ is, therefore, expressed as the sum of the three different components, so

$$\frac{dp}{dz} = \left(\frac{dp}{dz}\right)_{f} + \left(\frac{dp}{dz}\right)_{g} + \left(\frac{dp}{dz}\right)_{g}$$
 (15)

The three terms on the right hand side are regarded as frictional, accelerational, and gravitational components of the total pressure gradient. Gravitational term in Eq.(15) is negligible because the cross-sectional area of the test section of the capillary is constant. Accelerational pressure gradient can not be measured directly. It can be, however, calculated from measured momentum flux as follows;

$$\left(\frac{dp}{dz}\right)_{R} = -\frac{1}{A_{o}} \frac{d(WV)}{dz} = -\frac{1}{A_{o}} \frac{d}{dz} \left(W_{G}V_{G} + W_{L}V_{L}\right)$$

$$= -G \left(x \frac{dV_{G}}{dz} + V_{G} \frac{dx}{dz} + (1-x) \frac{dV_{L}}{dz} - V_{L} \frac{dx}{dz}\right)$$
(16)

and, so

Expanding the differential term of $\frac{dV_G}{dz}$ and $\frac{dV_L}{dz}$ in Eq. (16) and substituting into Eq. (15) then gives

$$\frac{dp}{dz} = \frac{\left(\frac{dp}{dz}\right)_f - (H - I)\frac{dx}{dz}}{(J - K)}$$
(17)

where

$$H = G^{2} \left(\frac{2xv_{G}}{\alpha} - \frac{2(1-x)v_{L}}{(1-\alpha)} \right)$$

$$I = G^{2} \left(\frac{x^{2} \upsilon_{G}}{\alpha} - \frac{(1-x)^{2} \upsilon_{L}}{(1-\alpha)^{2}} \right) \left(\frac{S(1-x)\upsilon_{G}\upsilon_{L} + Sx\upsilon_{G}\upsilon_{L}}{(x\upsilon_{G} + S(1-x)\upsilon_{L})^{2}} \right)$$

$$J = 1 + G^{2} \left(\frac{x^{2}}{\alpha} \frac{dv_{G}}{dp} + \frac{(1-x)^{2}}{(1-\alpha)} \frac{dv_{L}}{dp} \right)$$

$$K = G^{2} \left(\frac{x^{2} \upsilon_{G}}{\alpha^{2}} - \frac{(1-x)^{2} \upsilon_{L}}{(1-\alpha)^{2}} \right) \left(\frac{S(1-x)x\upsilon_{L} \frac{d\upsilon_{G}}{dp} - S(1-x)x\upsilon_{G} \frac{d\upsilon_{L}}{dp}}{(x\upsilon_{G} + S(1-x)\upsilon_{L})^{2}} \right)$$

It should be noted that, to calculate the total pressure gradient, knowledges of the void fraction (α) ,

slip ratio (S) and the frictional pressure gradient $\left(\frac{dp}{dz}\right)_f$ are required.

Slip Ratio

The slip ratio (S) is the ratio of the velocity of vapour and liquid. Zivi [22] assumed that total kinetic energy flow is a minimum and

$$S = \left(\frac{\rho_L}{\rho_G}\right)^{1/3} \tag{18}$$

That means the slip ratio is assumed to depend only on the phase density ratio. Miropolskiy et al. [19] determined the values of vapour void fraction in steam-fluid mixtures flowing in heated and unheated tubes and proposed the following correlation of slip ratio

$$S = 1 + \frac{135(1 - p/p_C)}{Fr_1^{5/12} Re^{1/6}}$$
 (19)

where

$$F_{\overline{I}_{1}} = \frac{G^{2} \upsilon_{L}^{2}}{g d} \quad \text{and} \quad Re = \frac{G d}{\mu_{L}} \quad .$$

In the correlation of Premoli et al. [20], the slip ratio (S) is given by

$$S = 1 + E_1 \left(\left(\frac{y}{1 + yE_2} \right) - yE_2 \right)^{1/2}$$
 (20)

where

$$y = \frac{\beta}{1-\beta}$$
, $\beta = \frac{\rho_L x}{\rho_L x + \rho_G (1-x)}$, $E_1 = 1.578 \text{ Re}^{-0.19} \left(\frac{\rho_L}{\rho_G}\right)^{0.22}$,

$$E_2 = 0.0273 \text{ We}_1 \text{ Re}^{-0.51} \left(\frac{\rho_L}{\rho_G}\right)^{-0.08}, \quad \text{Re} = \frac{Gd}{\mu_L} \quad \text{and} \quad \text{We}_1 = \frac{G^2d}{\sigma \rho_L}$$

Chisholm [17] proposed a simple correlation;
$$S = \left(1 - x \left(1 - \frac{\rho_L}{\rho_G}\right)\right)^{1/2}$$
 (21)

Frictional Pressure Gradient

The importance of predictions of frictional pressure gradient in the two-phase liquid-gas flow problem is reflected in the large number of models that have been proposed. Because of the space limitation, only correlations used in this work are described briefly. Two-phase frictional pressure gradients are often expressed in terms of the two-phase multipliers defined as follows

$$\phi_{L}^{2} = \frac{(-dp/dz)_{f}}{(-dp/dz)_{L}} \text{ and } \phi_{G}^{2} = \frac{(-dp/dz)_{f}}{(-dp/dz)_{G}} \text{ and } \phi_{LO}^{2} = \frac{(-dp/dz)_{f}}{(-dp/dz)_{LO}}$$
(22)

where $(dp/dz)_L$ and $(dp/dz)_G$ are the single-phase liquid and vapour pressure gradients (N/m^3) calculated using the actual phase flow rates for the two-phase flow, and $(dp/dz)_{LO}$ is the pressure gradient for a flow of the same mass velocity as the two-phase flow, but having the physical properties of the liquid phase.

The classical correlation of frictional pressure gradient for two-phase flow in tubes is that of Lockhart and Martinelli [23] who related ϕ_G^2 and ϕ_L^2 to the parameter X:

$$\phi_L^2 = 1 + \frac{C}{X} + \frac{1}{Y^2}$$
 and $X = \sqrt{\frac{(dp/dz)_L}{(dp/dz)_G}}$ (23)

where C = 20 for turbulent liquid - turbulent gas flow. Equation (23) is equivalent to

$$\phi_G^2 = 1 + CX + X^2 \tag{24}$$

From the research by Friedel [18], the multiplier can be determined from

$$\phi_{LO}^2 = L + \frac{3.24 \text{ M N}}{\text{Fr}_2^{0.045} \text{We}_2^{0.035}}$$
 (25)

where
$$L = (1-x)^2 + x^2 \frac{\rho_L f_{GO}}{\rho_G f_{LO}}$$
, $M = x^{0.78} (1-x)^{0.224}$, $N = \left(\frac{\rho_L}{\rho_G}\right)^{0.91} \left(\frac{\mu_G}{\mu_L}\right)^{0.19} \left(1 - \frac{\mu_G}{\mu_L}\right)^{0.7}$

$$\mathrm{Fr_2} \ = \frac{\mathrm{G}^2}{\mathrm{g} \ \mathrm{d} \rho_\mathrm{H}^2} \,, \qquad \mathrm{We_2} \ = \frac{\mathrm{G}^2 \mathrm{d}}{\mathrm{\sigma} \, \rho_\mathrm{H}} \qquad \mathrm{and} \qquad \rho_\mathrm{H} \ = \left(\frac{\mathrm{x}}{\rho_\mathrm{G}} + \frac{\mathrm{l} - \mathrm{x}}{\rho_\mathrm{L}}\right)^{-1}$$

 f_{GO} and f_{LO} are the friction factors for the total mass flux flowing with the vapour and liquid properties respectively. It should be noted that the definition of the Weber number is not the same as that used to calculate the slip ratio.

From the research by Lin et al. [7], the multiplier can be determined from

$$\phi_{LO}^{2} = \left(\frac{A_{LO} + B_{LO}}{A_{T} + B_{T}}\right)^{1/8} \left(1 + x \left(\frac{v_{G}}{v_{L}} - 1\right)\right)$$
 (26)

where

$$A_{LO} = \left(2.457 \ln \left(\frac{1}{(7/Re_{LO})^{0.9} + 0.27 \epsilon/d}\right)\right)^{16}, \quad B_{LO} = \left(\frac{37530}{Re_{LO}}\right)^{16}$$

$$A_{T} = \left(2.457 \ln \left(\frac{1}{(7/Re_{T})^{0.9} + 0.27 \epsilon/d}\right)\right)^{16}, \quad B_{T} = \left(\frac{37530}{Re_{T}}\right)^{16}$$

$$Re_{LO} = \frac{dG}{\mu_{L}}, \quad Re_{T} = \frac{dG}{\mu_{T}} \quad \text{and} \quad \mu_{T} = \frac{\mu_{L}\mu_{G}}{\mu_{G} + x^{1.4}(\mu_{L} - \mu_{G})}$$

From the research by Chisholm [17], the multiplier can be determined from

$$\phi_{LO}^2 = 1 + (Y^2 - 1) \left(\xi x^{(2-n)/2} (1-x)^{(2-n)/2} + x^{2-n} \right)$$
 (27)

where

$$Y = \sqrt{\frac{(dp/dz)_{GO}}{(dp/dz)_{LO}}}$$
 (28)

where $(dp/dz)_{GO}$ is the pressure gradient for a flow of the same mass velocity as the two-phase flow, but having the physical properties of the vapour phase, and n is the power to which Re is raised in the friction factor/Reynolds number relationship. The parameter ξ is given by

$$\xi = 55/G^{1/2}$$
 (0 < Y < 9.5) (29)

$$= 520/(YG^{1/2}) \qquad (9.5 < Y < 28) \tag{30}$$

$$= 15,000/(Y^2G^{1/2}) \qquad (28 < Y) \tag{31}$$

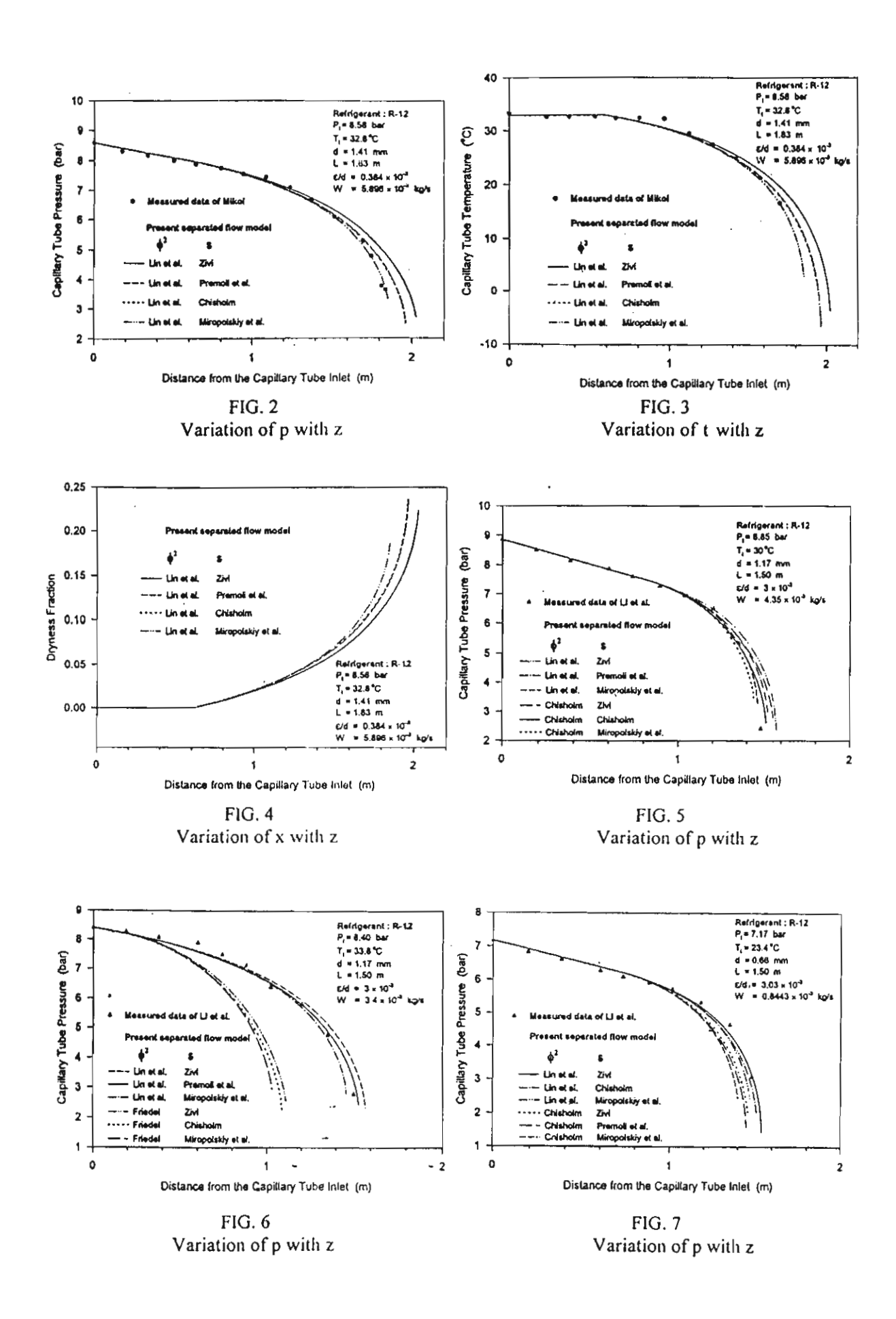
The refrigerants investigated in this study are R-12, R-22 and R-134a. All refrigerant thermodynamic and thermophysical properties (specific volume, dynamic viscosity, specific enthalpy and surface tension) are taken from REFPROP [24] and are developed as a function of pressure. The calculation is divided into two parts; subcooled single-phase region and two-phase vapour liquid region.

Initial conditions required in the calculation are pressure and temperature of refrigerant at capillary tube inlet, mass flow rate of refrigerant, roughness and diameter of pipe. In the single-phase flow region, after calculating the friction factor by Colebrook equation and substituting p_{sat} with the saturation pressure of refrigerant at the inlet temperature, the single-phase region length is determined. In two-phase flow region, a program is written to solve equations (14) and (15) by using the fourth order Runge-Kutta method with a 1 mm length increment. Several key parameter correlations of the frictional pressure gradient and slip ratio are varied in the model. The results from the calculation are pressure, temperature and dryness fraction at each position along capillary tubes. Initial condition of this region is the end condition of the single phase flow region. The calculation in two-phase flow region is terminated when the flow approaches the choked or critical flow condition $(dp/dz \rightarrow \infty)$. Total tube length is the sum of the single-phase region and the two-phase region lengths.

Results and Discussion

Figure 2 and 3 show comparisons between the pressure and temperature distribution along capillary tubes obtained from the model and those obtained from the experiment. The conditions for the numerical calculation to obtain curves in Figs. 2-3 correspond to the experimental condition of Mikol [11] for R-12. As described, the flow of refrigerant through the capillary tube from the outlet of the condenser to the inlet of the evaporator can be divided into two regions; a subcooled liquid and a twophase region. In the subcooled liquid region, due to friction, the pressure of refrigerant drops linearly while temperature remains constant along the tube. After the position of the inception of vaporization, due to friction and acceleration, the pressure of refrigerant drops rapidly and more rapidly as the flow approaches the critical condition. There is good agreement between experimental and numerical results with respect to the shapes of the pressure and temperature distributions. However, due to the delay of vaporization, the actual point of inception of vaporization does not occur at the end of subcooled liquid region (as shown in Fig. 3). Figure 4 shows the variation of the dryness fraction of R-12 along the capillary tube obtained from the model with the same experimental condition as in Figs.2 and 3. In the single phase region, the dryness fraction along the capillary is zero. After the inception of vaporization, due to a large pressure drop, the dryness fraction increases and increases more rapidly as the flow approaches the critical condition.

Figures 5-8 also show the comparisons of the present numerical results with the experimental data obtained by Li et al. [8] for R-12. The results from Figs. 2-3 and 5-8 show that the effect of the frictional pressure gradient on the model results is more than those of slip ratio. Numerical results obtained from using the frictional pressure gradients of Lin et al. [7] or Chisholm [17] combined with various slip ratio correlations agree within the experimental data scatter whereas the Lockhart-Martinelli [23] and Friedel [18] correlations are very different. Numerical results obtained using the slip ratios by



.

Premoli et al.[20] or Chisholm [17] combined with various frictional pressure gradient give almost the same predictions. However Premoli's slip ratio correlation can be used, only if surface tension data are available. Comparisons of five sets of R-12 experimental data with numerical results show that the frictional pressure gradient correlation expressed by Lin et al. [7] combined with the slip ratio correlations expressed by Zivi [22] or Premoli et al.[20] or Chisholm [17] or Miropolskiy et al. [19] give better predictions.

Figures 9 and 10 show comparisons of the output of the program for several frictional pressure gradient and slip ratio correlations with the R-22 test data of Mikol [11] and Koizumi et al. [5] respectively. In Fig. 9, the model predicts well only for the subcooled liquid region, but for the twophase flow region, the predicted values of pressure are found to be higher than the observed values. The difference between the observed and predicted values might be caused by a variation of flow pattern. Recently, the model predicted by Sami et al. [12] assuming small bubble flow pattern agrees well with this same set of R-22 data. It is, however, surprising that the other experimental results obtained by Mikol [11] (but for R-12) is predicted excellently by the present separated flow model (Figs.2 and 3). In Fig. 10, experimental data for R-22 by Koizumi et al [5] is compared with the present simulation results. The position 0.15 m in the work of Koizumi et [5] is the position which z = 0 in Fig. 10. The present simulation results show a very good agreement in the subcooled liquid region and a fair agreement in the two-phase flow region. The present prediction results are, however, better than the results from the prediction by Sami et al. [12]. Due to the lack of the experimental data from R-134a, the simulation results for the new alternative R-134a, proposed as substitute for R-12, are compared with the other simulation results reported in the literature at the same working conditions. Figs. 11 and 12 show comparisons of R-134a simulation results of Wong et al. [13], and Sami et al. [12] and Kim [16] with the present model respectively. In Fig. 11, the present model using the frictional pressure gradient by Friedel [18] and slip ratio by Zivi [22] or Chisholm [17] give nearly the same critical length as given by Wong et al. [13]. However, the present model using the frictional pressure gradient by Lin et al. [7] and slip ratio by Miropolskiy et al. [19] give the pressure distribution corresponding to those from Wong et al. [13]. It should be noted that comparing the pressure drop characteristics of R-12 (Fig. 8) and of R-134a (Fig. 11). the flow through the capillary tube of R-134a gives a higher pressure drop than those of R-12. On the other hand, the subcooled liquid region and the critical tube lengths are shorter for the flow of R-134a. In Fig. 12, recent simulation results published by Sami et al [12] and Kim [16] on R-134a are compared with the present simulation results. Reasonable agreement between the present separated flow model using the frictional pressure gradient of Friedel [18] combined with all slip ratio correlations, and the prediction from Sami [12] is obtained.

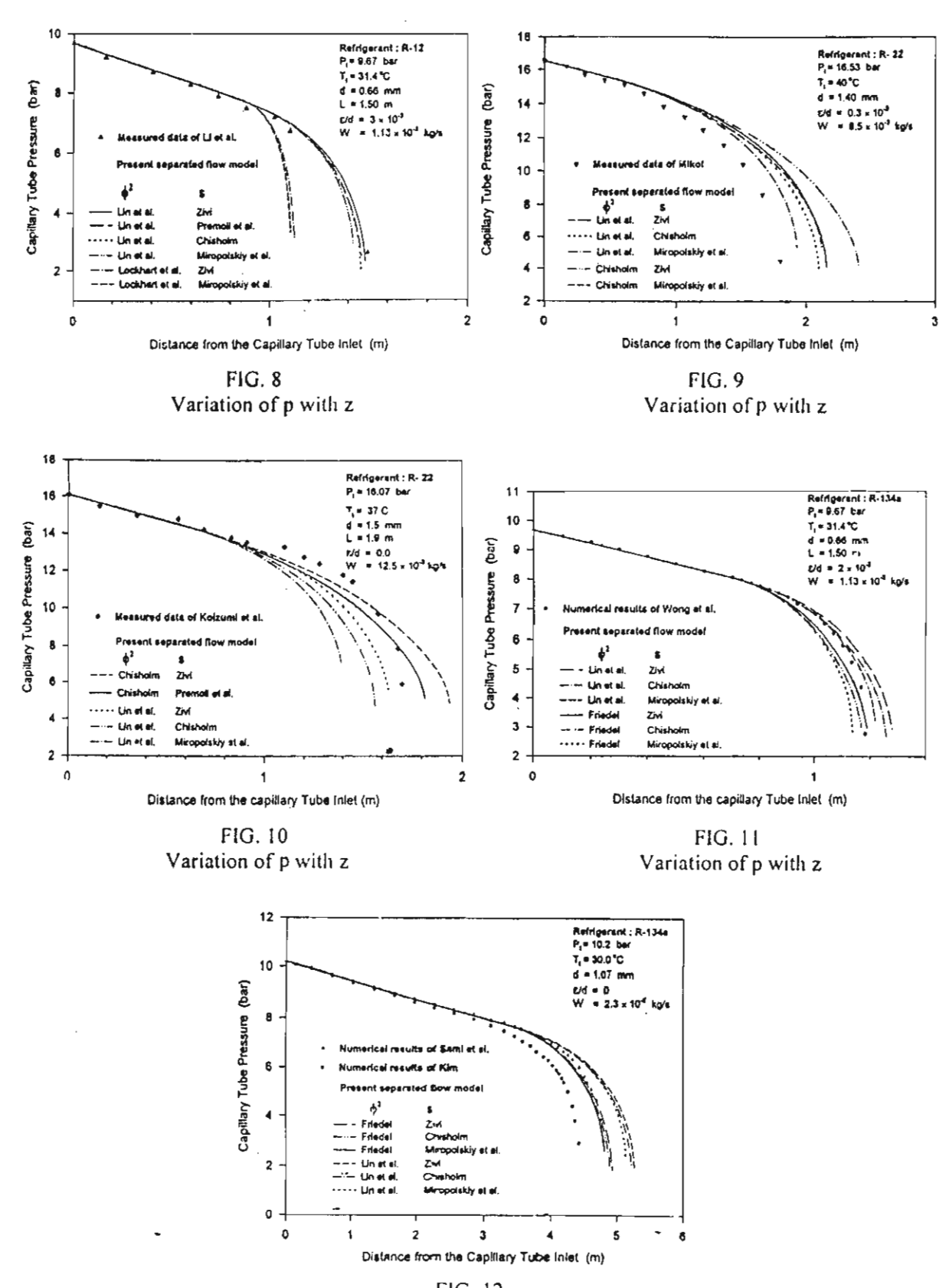


FIG. 12 Variation of p with z

Conclusions

A two-phase separated flow model has been developed to determine the refrigerant flow characteristics in capillary tubes for vapour compression systems. The basic physical equations governing capillary tube flow are established from the conservations of mass, energy and momentum. The partial differential equations derived are solved simultaneously by using the fourth order Runge-Kutta method. Several correlations of the frictional pressure gradient and slip ratio which are the important parameters in the flow model are evaluated and a recommendation of the best one for each refrigerant is given. The agreement between experimental and simulation results obtained from the flow of R-12, R-22 and R-134a through capillary tubes indicates that the separated flow model with appropriate correlations of the frictional pressure gradient and slip ratio can be used to predict the two-phase flow behaviour of refrigerant in capillary tubes used in air conditioning and refrigerating systems.

Acknowledgments

The present study was supported financially by the Thailand Research Fund (TRF) whose guidance and assistance are gratefully acknowledged.

Nomenclature

Α	cross-sectional area, m ²	A_{o}	cross-sectional area of tube, m ²	d	tube diameter, m
f	friction factor	Fr	Froude number	G	mass flux, kg/s m ²
g	gravitational acceleration, m/s ²	h	specific enthalpy, kJ/kg	L	length, m
p	pressure, N/m ²	Re	Reynolds number	S	slip ratio
V	velocity, m/s	W	mass flow rate, kg/s	We	Weber number
x	dryness fraction	z	axial; direction or length, m		
Gı	reek Symbols				
μ	dynamic viscosity, Pa s	υ	specific volume, m ³ /kg	ρ	density, kg/m ³
ε	roughness, m	τ	shear stress, N/m ²	α	void fraction
σ	surface tension, N/m	ϕ_{LO}^2	$, \phi_L^2, \phi_G^2$ frictional pressure gradi	ent m	ultiplier

Subscripts

a	accelerational	С	critical condition	f	frictional component	g	gravitational
G	vapour	inlet	capillary tube inlet	L	liquid	m	mixture
sat	saturation	SC	subcooled	t	temperature	w	wall

References

- 1. P.K. Bansal and A.S. Rupasinghe, Applied Thermal Engineering, 18, 207 (1998).
- 2. R.R. Bittle and M.B. Pate, ASHRAE Transactions, 100, 52 (1994)
- 3. Z.H. Chen, R.Y. Li, S. Lin and Z.Y. Chen, ASHRAE Transactions, 96, 550 (1990).
- 4. L. Cooper, C.K. Chu and W.R. Brisken, Refrigerating Eng., 65, 37 (1957).
- 5. H. Koizumi and K. Yokoyama, ASHRAE Transactions, 86, 19 (1980).
- 6. S.J. Kühl and V.W. Goldschmidt, ASHRAE Transactions, 97, 139 (1991).
- 7. S. Lin, C.C.K. Kwork, R.Y. Li, Z.H. Chen and Z.Y. Chen, Int.J. Multiphase Flow, 17, 95 (1991).
- 8. R.Y. Li, S. Lin and Z.H. Chen, ASHRAE Transactions, 96, 542 (1990).
- 9. C. Melo, R.T.S. Ferreira, C. B. Neto, J.M. Goncalves, R.H. Pereira and M.R. Thiessen, *Proceedings of the IIR Conference*, Hannover, Germany, pp. 621-630 (1994).
- 10. C. Melo, R.T.S. Ferreira, C. B. Neto and J.M. Goncalves, *Proceedings ASME Int. Mech. Engrs. Congress and Exposition*, AES, vol.34, pp. 19-30 (1995).
- 11. E.P. Mikol, ASHRAE Journal, November, 75 (1963).
- 12. S.M. Sami and C. Tribes, Applied Thermal Engineering, 18, 491 (1998)
- 13. T.N. Wong and K.T. Ooi, Int. Comm. Heat Mass Transfer, 22, 595 (1995).
- 14. T.N. Wong and K.T. Ooi, Applied Thermal Eng., 16, 625 (1996).
- 15. T.N. Wong and K.T. Ooi, Int. Comm. Heat Mass Transfer, 23, 993 (1996).
- R.H. Kim, A Numerical Analysis of a Capillary Tube Expansion Valve in a Vapour Compression Refrigeration System with Alternative Refrigerants, ASME, HTD, vol. 243 (1993).
- 17. D. Chisholm, Int. J. Heat Mass Transfer, 16, 347 (1973).
- 18. L. Friedel, Improved Friction Pressure Drop Correlations for Horizontal and Vertical Two-Phase Flow, European Two-Phase Flow Group Meeting, Ispra, Italy (1979).
- 19. Z.L. Miropolskiy, R.I. Shneyerova, A.I. Karamysheva, Vapour Void Fraction in Steam Fluid Mixture Flowing in Heated and Unheated Channels, paper B 4.7, vol. 25, *Int. Heat Trans. Conf.*, Paris (1970).
- A. Premoli, D. Francesco and A. Prina, An empirical correlation for evaluating two-phase mixture density under adiabatic conditions, European Two-Phase Flow Group Meeting, Milan, Italy (1970).
- 21. P.B. Whalley, Boiling, Condensation and Gas-Liquid Flow, p.45-59, Clarendon Press, Oxford (1987).
- 22. S.M. Zivi, Trans. ASME 86, 247 (1964).
- 23. R.W. Lockhart and R.C. Martinelli, Chem. Eng. Prog., 45, 39 (1949).
- 24. REFPROP, Thermodynamic Properties of Refrigerants and Refrigerant Mixtures, version 6.01, Gaithersburg, M.D. National Institute of Standards and Technology (1998).
- 25. G.B. Wallis, One Dimensional Two-Phase Flow, McGraw-Hill, (1969).

Wongwises, S., Disawas, S., Kaeon J., Onurai C., Two-Phase Evaporative Heat Transfer Coefficients of Refrigerant HFC-134a Under Forced Flow Conditions in a Smooth Horizontal Tube, *Int. Com. Heat Mass Transfer*, 2000; 27(1): 35-48.



PH S0735-1933(00)00082-8

TWO-PHASE EVAPORATIVE HEAT TRANSFER COEFFICIENTS OF REFRIGERANT HFC-134a UNDER FORCED FLOW CONDITIONS IN A SMALL HORIZONTAL TUBE

Somchai Wongwises, Somjin Disawas,
Jatuporn Kaewon and Chatchawan Onurai
Fluid Mechanics and Turbomachinery Research Centre (FUTURE)
Department of Mechanical Engineering,
King Mongkut's University of Technology Thonburi,
Bangmod, Bangkok 10140. Thailand

(Communicated by J.P. Hartnett and W.J. Minkowycz)

ABSTRACT

In this study, the two-phase heat transfer coefficient characteristics of HFC-134a evaporating under forced flow conditions inside a smooth horizontal tube are experimentally investigated. Different from most previous studies, the present experiments have been performed with lubricating oil in the refrigerant loop at high flow rate and high heat flux conditions. The test section is a 1.8 m long counterflow double tube heat exchanger with refrigerant flowing in the inner tube and heating water flowing in the annulus. The inner tube is made from smooth horizontal copper tubing of 9.52 mm, outer diameter and 7.2 mm, inner diameter. The test runs were done at average saturated evaporating temperatures ranging between 4 and 25 °C. The inlet dryness fractions were between 0.1 and 0.25. The mass fluxes were between 160 and 470 kg/m²s, and the heat fluxes were between 8 and 55 kW/m². The inlet dryness fraction of the refrigerant in the test section was calculated using the temperature and pressure obtained from the experiment. The exit dryness fraction and heat transfer coefficient of the refrigerant were determined by applying an energy balance based on knowledge of the energy going into the test section. The effects of heat flux, mass flux, evaporation pressure and lubricating oil on the convection heat transfer coefficients are also discussed. The results from the experiment are compared with those calculated from correlations reported in the literature. Moreover, new correlations for the convection heat transfer coefficient are proposed for practical applications. The results of this study are of technological importance for the efficient design of evaporators when systems are assigned to utilize HFC-134a. © 2000 Elsevier Science Ltd

Introduction

Stratospheric ozone absorbs the high energy ultraviolet rays from the sun and protects both humans and other living things from the exposure to ultraviolet radiation. Results from many researches show that this ozone layer is being depleted. The general consensus for the cause of this event is that the free chlorine radicals removes ozone from the atmosphere and later the chlorine atom is continued to

convert more ozone to oxygen. The presence of chlorine in the stratosphere is the result of migration of chlorine-containing chemicals. The chlorofluorocarbons (CFCs) is a large class of chemicals which behaves in this manner. These chemicals have many unusual properties for example, nonflammability, low toxicity, and material compatibility that have led to their common widespread use, both consumers and industries around the word as refrigerants, solvents, and blowing agents for foams.

Since the depletion of the earth's ozone layer has been discovered, many corporations have been forced to find alternative chemicals to CFCs. Because the thermophysical properties of HFC-134a are very similar to those of CFC-12. Refrigerant HFC-134a is receiving the supporting from the refrigerant and airconditioning industry as a potential replacement for CFC-12. However, even the difference in properties between both refrigerants is small but it may result in significant differences in the overall system performance. Therefore, the properties of HFC-134a should be studied in detail before it is applied. Evaporation of refrigerants has been studied by a large number of researchers, both experimentally and analytically, mostly for pure refrigerants [1-16]. However, since the most vapour compression machine require a small amount of oil to be mixed in the refrigerant fluid to lubricate the sliding surfaces, the heat transfer characteristics of HFC-134a containing lubricating oil is one have been studied. Evaporation of refrigerant mixtures containing oil has received comparatively little attention in the literature [17-21]. However, most of the data reported in previous literature has not been obtained from the high flow rate and high heat flux experimental conditions as in modern automotive air-conditioning system [9, 20, 21].

Relatively little information is currently available on the evaporation heat transfer characteristics of the HFC-134a-lubricant mixture under high flow rate and high heat flux conditions. In the present study, the main concern is to obtain and analyze the experimental results of the heat transfer coefficient of the HFC-134a containing lubricating oil during forced convection in a small horizontal tube under high flow rate and high heat flux conditions. The data obtained from the present study are also compared with the correlations reported in the literature. In addition, the large amount of collected data is correlated and used to predict the evaporative heat transfer coefficient of the HFC-134a.

Experimental Apparatus and Method

A diagram of an experimental apparatus is shown schematically in Fig. 1. It consists essentially of a well instrumented vapour compression refrigeration system. The principal modifications to the standard refrigeration system are the addition of two heat exchangers for subcooling the liquid refrigerant and for heating the refrigerant flowing through the test section, by-pass line, and measuring devices. The main components of the system are a test section, a refrigerant loop, a heating water flow loop, a cooling water flow loop and instrumentation. A commercial HFC-134a is used as the working fluid. Polyalkylene glycol

37

(PAG, 180 cSt) is used as lubricating oil. A refrigerant loop capable of investigating HFC-134a flowing in horizontal tubes is the main feature. Two water loops are connected to the refrigerant loop to provide heating and cooling, respectively. The test section and the connections of the piping system are designed such that parts can be changed or repaired very easily. In addition to the loop components, a full set of instruments for measuring and control of temperature and pressure of refrigerant, the temperature of water, compressor speeds and electrical power, is installed at all important points in the circuit.

The refrigeration flow loop is set up with the desired test section and charged with the refrigerantoil mixture. The amount of oil dissolved in the refrigerant is typical for normal use and determined by a technique described in ASHRAE standard [23]. Vapour refrigerant is discharged by a variable-speed refrigerant compressor (Denso, 10PA17C) from a low pressure and temperature to a higher pressure and temperature, and is passed through a condenser in which it is condensed. Subcooled liquid exiting the condenser flows through a receiver, in which the liquid refrigerant under high pressure is stored, a filter/dryer, a sight glass and then a refrigerant flow meter (Bailey F&P, 10A3225). The inside diameter of each piece of additional equipment is adjusted to be equal to the diameter of the refrigerant line, so perturbations in the flow pattern are minimized. Once the refrigerant exits the flow meter, it enters a compact plate heat exchanger (Alonte, CB26-24H). A precise amount of heat is rejected for subcooling the liquid. Once the refrigerant exits the heat exchanger, it is then expanded through a manually controlled expansion valve to nearly its original pressure. Since heat from heating water is added in the test section, the refrigerant then flows and partially evaporates in the test section and then returns to the evaporator. The cycle is then repeated. A bypass line connects the outlet of the sight glass with the entrance of the evaporator. The bypass valve allows isolation of the test section from the outer test loop components to allow for repair or replacement. Instrumentation is located at various positions to give information on the state of the flowing fluid at each respective point. All sensors are wired directly to terminal control panels mounted on the bench.

A compact plate heat exchanger is used to subcool the liquid refrigerant flowing out from the condenser. The heat exchanger is connected to the hydraulic bench which consists of a 0.165 m³ storage tank, a centrifugal pump and a rotameter. With this, more heat is rejected through cooling water and the dryness fraction of the two-phase refrigerant flowing into the test section can be varied. The heating water flow loop also consists of a 0.037 m³ storage tank, an electric heater controlled by adjusting the voltage, a centrifugal pump and rotameters. The purpose of this loop is to add heat to vaporize the refrigerant flowing in the test section. After the water is heated to the required temperature, the hot water is pumped out of the storage tank, delivered to the test section and then returned to the storage tank.

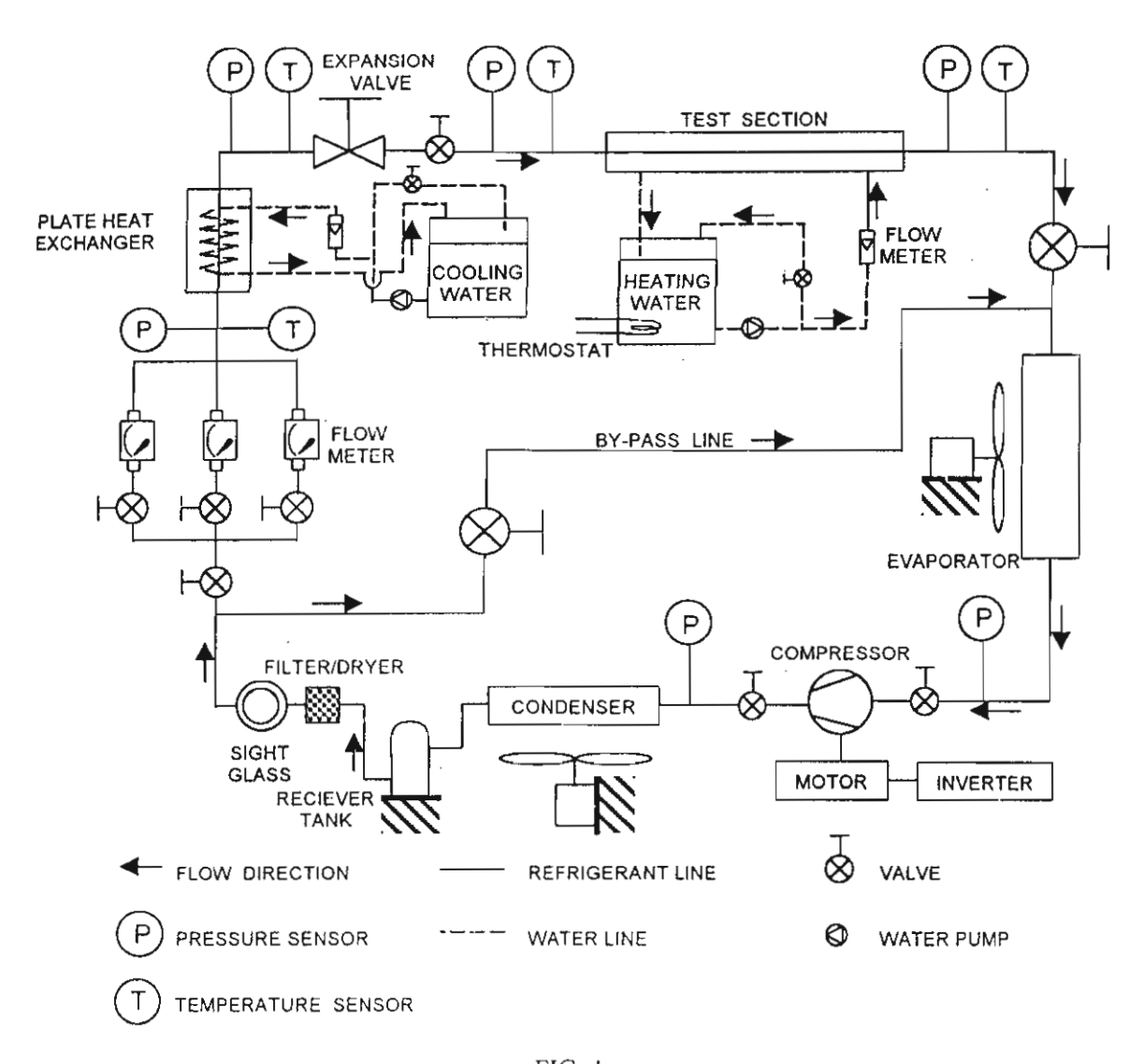


FIG. 1 Schematic diagram of experimental apparatus

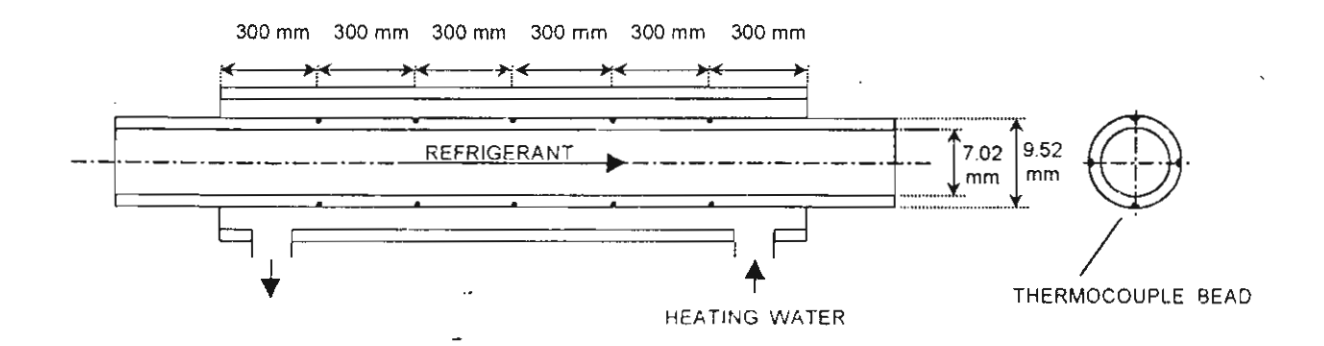


FIG. 2 Evaporation test section

The test section is a 1.8 m long horizontal counterflow heat exchanger. It consists of a tube within a tube as shown in Fig.2. Such an arrangement operates in counterflow with the hot water passing through the annular space and the refrigerant passing through the inside of the inner tube. Both outer and inner tubes are made from smooth copper tubes. The inner and outer diameter of the inner tube is 7.2 mm and 9.52 mm. respectively. This inner tube is located concentrically within an outer tube which serves as a water jacket. The inner and outer diameters of the outer tube are 28 mm and 31.75 mm., respectively. At the ends of the test section, pressure gauges and thermocouples are also installed to measure the refrigerant pressures and temperatures inside the test section. The ends of the inner tube of the test section are connected to the refrigerant loop by special fittings with an inside diameter identical to that of the test section. These fittings allow removal of the test section without disturbing either side of the test section. The experimental set-up is equipped with three basic instrumentation systems; temperature, pressure and flow rate. Refrigerant temperature, cooling and heating water temperatures and inner tube wall temperature in the test section are measured by type-T copper-constantan thermocoupies. A digital indicator (Shimaden, SD 20) and selector (Shimaden, KR15) are used together with thermocouples. All temperature measuring devices are well calibrated in a controlled temperature bath using standard precision mercury glass thermometers. Uncertainty of temperature measurements after considering the data acquisition system is ± 0.1 °C.

Refrigerant bulk temperature is measured in four positions with 1 mm. diameter probes extending inside the tube in which the refrigerant flows. The probes consist of type T copper-constantan thermocouples grounded to a stainless steel outer sheath. The entering and exiting water temperatures of both heat exchangers are also measured by the same type of thermocouple, each with two-thermocouples. A schematic of temperature measurements on the wall surface of the inner tube of the test section is shown in Fig.2. Thermocouples are mounted at five longitudinal positions on the inner tube wall surface, each with four thermocouples equally spaced around the tube circumference. The thermocouples are soldered into a small hole drilled 0.5 mm. deep into the tube wall surface. Refrigerant pressures are measured by precision Bourdon tube pressure gauges in six positions: inlet and exit of the compressor, inlet and exit of the plate heat exchanger and, inlet and exit of the test section. The pressure is measured through a tap with a 1.5 mm hole drilled into the tube in which the refrigerant flows. All static pressure taps are mounted flush in the tube wall. The pressure gauges are calibrated against a primary standard, the dead weight tester.

Three sets of precision flow meters are used to measure the volumetric flow rate of the refrigerant. These flow meters are armored of a variable area type and have a float that moves vertically in a tapered metering tube. All flow meters are specially calibrated for R-134a from the manufacturer. The total capacity of all refrigerant flow meters is 0-2.2 gal/min. The flow rates of cooling and heating water are measured by two sets of rotameters (Dwyer) within the range of 0-20 L/min and 0-40 L/min, respectively.

Experiments were conducted with various flow rates of refrigerants, various dryness fractions of refrigerant entering and exiting the test section and various temperatures and pressures of refrigerant evaporating in the test section. In the experiments, the refrigerant flow rate and pressure in the test section were controlled by adjusting the expansion valve and speed of the compressor, respectively. An inverter (Yaskawa, CIMR-G5A47P5) was used to control the speed of the motor for driving the compressor. To vary the refrigerant dryness fraction at the inlet and exit of the test section, the cooling water flow rates and the heating water flow rates were varied by small increments while the refrigerant flow rate was kept constant. The electric power going into the water heater was measured by Watt transducers and controlled by a thermostat. During each experiment, the heat transferred to the refrigerant in the test section was kept at a desired, preselected value. This might be obtained by simultaneously adjusting and controlling the temperature and flow rate of the heating water entering the test section. The system was allowed to approach the steady state before any data was recorded. The steady state condition was reached when the pressure, temperature and flow rate at the measuring points were not fluctuating. After stabilization, temperatures on the tube wall, temperature and pressure of refrigerant at the locations mentioned above, inlet and outlet temperature of heating water and cooling water and the flow rates of heating water, cooling water, and refrigerant were recorded. The experiments could be done by increasing the refrigerant flow rate while the saturation pressure in the test section was kept constant.

The amount of refrigerant charged in the test loop has a significant effect on the operating characteristics of the test apparatus. If the charge is insufficient, the condition at condenser exit may fall into the two-phase flow region. For a practical refrigeration cycle, the heat transfered from the condenser must be rejected by virtue of an appreciable temperature difference, so that the size of the condenser remains within reasonable limits. The condensed liquid must therefore be subcooled before entering the expansion device. At the beginning of the experiment, during the charge process of the refrigerant into the test loop, conditions of flow must be observed through the sight glass located at the exit of the filter/dryer. The flow phenomena will be gradually changed from two-phase to single-phase flow. To obtain an appropriate amount of refrigerant in the test loop, once the single-phase flow appears, the charge process of the refrigerant can be stopped.

Data Reduction Techniques

The following calculation is employed to determine the dryness fraction of the refrigerant entering and exiting the test section, and the convection heat transfer coefficient, from the data recorded during each test run at steady state conditions. The thermodynamic and transport properties of refrigerant are evaluated by using the REFPROP computer program. Version 6.01 [22].

side

The dryness fraction of refrigerant entering the test section is determined from

$$x_{r,in} = (h_{r,in} - h_{f,in}) / h_{fg,in}$$
 (1)

The heat transfer rate in the test section is obtained from the water flow rate and temperature difference of the water on the annulus according to the following relation;

$$Q_{is} = m_{hw} C_{p,hw} (T_{hw,in} - T_{hw,out})$$
 (2)

The exit enthalpy of the refrigerant is determined by applying an energy balance on the refrigerant

$$h_{r,out} = h_{r,in} + Q_{ts} / m_{r,ts}$$
 (3)

Then, the exit dryness fraction of refrigerant can be determined from

$$x_{r,out} = (h_{r,out} - h_{f,out}) / h_{fg,out}$$
 (4)

An average heat transfer coefficient of refrigerant flowing through the test section can be determined by applying an energy balance knowing the energy going into the test section;

$$\alpha_{tp} = \frac{Q_{ts}}{\pi DL(T_{wall} - T_{r,sat})} = \frac{\phi_{ts}}{(T_{wall} - T_{r,sat})}$$
 (5)

The circumferentially averaged values of wall surface temperatures (Twall) of the test section tube are taken as the arithmetic mean of the 20 measurement positions:

$$T_{\text{wall}} = \frac{\sum_{i=1}^{20} T_i}{20}$$
(6)

Since the flow meters require a density to convert volumetric flow to mass flow, the following density relation of the refrigerant-lubricant mixture at the flow meter is required [20]:

$$\frac{1}{\rho_{\text{mix}}} = \frac{1 - \omega_{0}}{\rho_{r}} + \frac{\omega_{0}}{\rho_{0}} \tag{7}$$

Mass flux (G) is then calculated from the product of volumetric flow rate measured by the flow meter and mixture density calculated from eq.(7), divided by cross-sectional area of the test section.

Results and Discussion

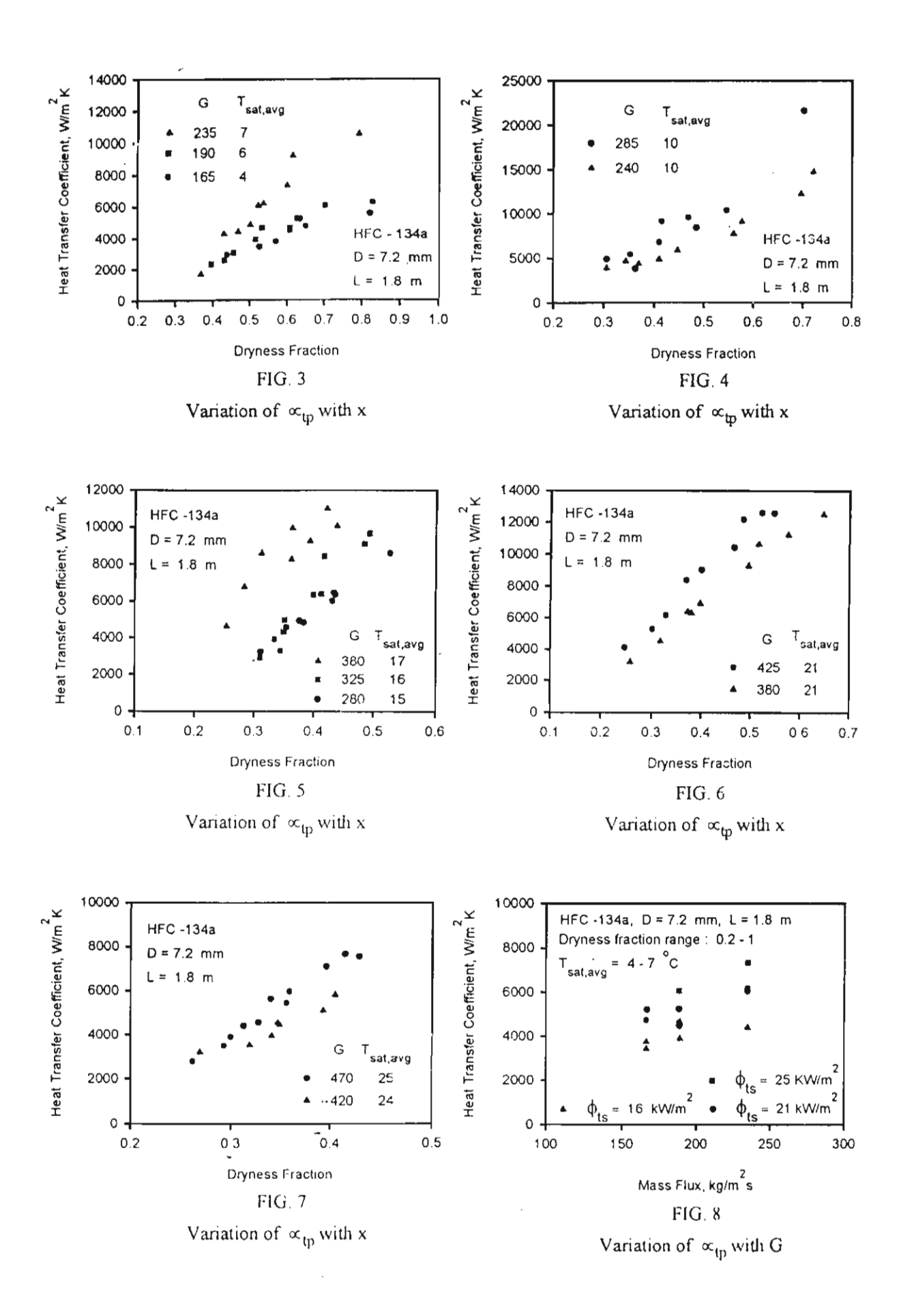
Figures 3 to 7 show the variation of the measured heat transfer coefficient with average dryness fraction in the test section with a fixed mass flux and varying heat flux. In the experiment, it is quite difficult to keep the saturation pressure (or saturation temperature) constant. However, the experimental

results for similar saturation temperature are grouped and shown in Figs 3 to 7. Note that there are, therefore, some small differences of those in each figure. As aspect, the average heat transfer coefficients increase with increasing average dryness fraction. Since the tests run in this research are focused on the high heat fluxes and high mass fluxes, annular flow patterns, therefore, occur in most test runs. With annular flow pattern, a refrigerant film flows adjacent to the tube wall and the vapour flows in the center core. Heat transfer coefficients in annular flow regime are typically much higher than those in the stratified flow regime [20]. During the evaporation of the annular liquid film on the wall, the liquid film thickness gradually decreases. The thermal resistance to the convective boiling is therefore decreased, in the other word, the heat transfer coefficient is increased. Figures 3 to 7 also show the effect of mass flux on the heat transfer coefficient. In Figs. 3 and 4, the results indicate that at low dryness fraction (x < 0.35) and low saturation temperature (T_{sat} < 10 °C), there is almost no effect of mass flux on the average heat transfer coefficient. However, for higher dryness fraction (0.35 < x < 0.6), as mass flux is increased, the heat transfer coefficients are increased in small increment. For high dryness fraction (x > 0.6), the heat transfer coefficient is much higher for a higher mass flux than those for a lower mass flux. In Figs. 5, 6 and 7, note that for high heat flux and high mass flux, the heat transfer coefficient tends to be merged due to the suppression of the nucleate boiling by the thinning of the annular liquid film.

Figure 8 shows the variations of the measured heat transfer coefficients with the mass fluxes at an average evaporating temperature of 4 to 7 °C. The inlet and exit dryness fractions are 0.2 and 1, respectively. For all heat fluxes, the heat transfer coefficients increase with mass flux. At a given mass flux, the heat transfer coefficients for higher heat fluxes are higher than those for lower ones. For lower heat flux, the heat transfer coefficient increases in small increments with mass flux. But for higher heat flux, the more pronounced heat transfer coefficient is increased as mass flux increases. The result shown in Fig. 9 tends to be the same.

Figure 10 shows the variations of the heat transfer coefficient with the mass flux at an average heat flux of 16 kW/m² for two difference average saturation temperatures (5°C and 15°C). The inlet and exit dryness fraction are 0.2 and 0.9 respectively. As mentioned, the heat transfer coefficients increase with mass flux. It should be noted that at higher saturation temperature of 15 °C, the mass flux is much more effective to heat transfer coefficient. However at the higher heat flux (25 kW/m²), the trend of the relationship between heat transfer coefficient with mass flux is the same for two difference saturation temperature (5°C and 15°C) as shown in Fig. 11

The heat transfer coefficient results obtained from this study are compared with two correlations in literature proposed by Chaddock and Noerager [1] and Wattelet et al. [8]. The correlation of Chaddock and



Noerager [1] based on the experimental data for evaporation of pure CFC-12 in a horizontal tube is of the

form.
$$\frac{\alpha_{tp}}{\alpha_{fo}} = \frac{3}{(X_{tt})^{2/3}}$$
 (8)

and
$$\frac{\alpha_{tp}}{\alpha_f} = \frac{3}{(X_{tt})}$$
 (9)

where X_{tt} is the Lockhart-Martinelli parameter and defined by;

$$X_{tt} = \left(\frac{1-x}{x}\right)^{0.9} \left(\frac{\rho_g}{\rho_f}\right)^{0.5} \left(\frac{\mu_f}{\mu_g}\right)^{0.1}$$
 (10)

 α_f is the heat transfer coefficient for the flow of the liquid phase alone in the tube;

$$\alpha_{f} = 0.023 \left(\frac{k_{f}}{D}\right) \left(\frac{G(1-x)D}{\mu_{f}}\right)^{0.8} \left(\frac{C_{p,f} \mu_{f}}{k_{f}}\right)^{0.4}$$
 (11)

 α_{f0} is the heat transfer coefficient for the total mass flux flowing with liquid property;

$$\alpha_{fo} = 0.023 \left(\frac{k_f}{D}\right) \left(\frac{GD}{\mu_f}\right)^{0.8} \left(\frac{C_{p,f} \mu_f}{k_f}\right)^{0.4}$$
 (12)

Wattelet et al. [8] conducted the experiments for pure HFC-134a evaporating in a test section heated by longitudinally wrapped strip heaters. They proposed a correlation which match their experimental data to within \pm 8 %. The correlation is of the form

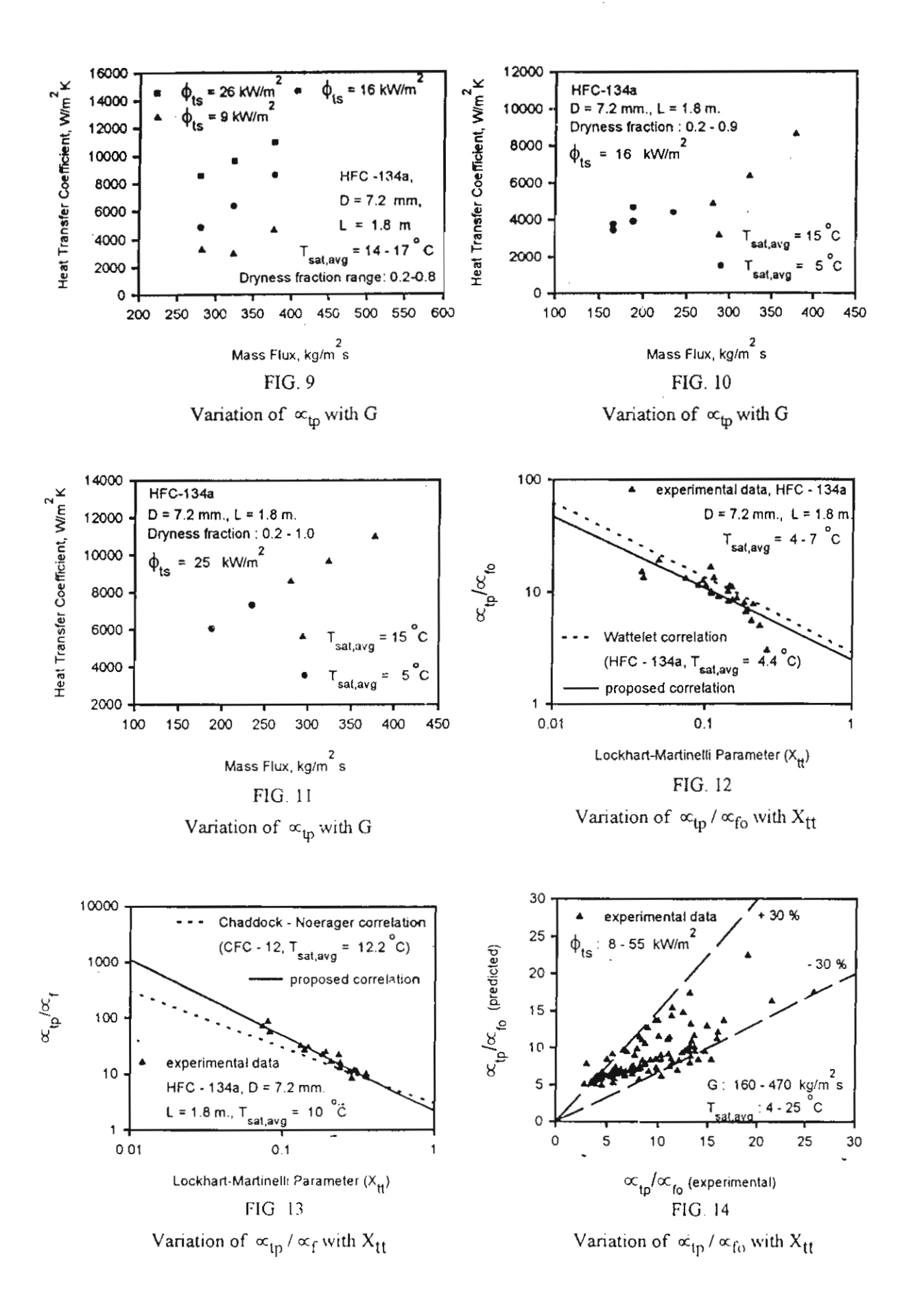
$$\frac{\alpha_{\rm tp}}{\alpha_{\rm fo}} = \frac{2.9}{(X_{\rm ff})^{0.666}}$$
 (13)

Althrough the correlation reported in the literature can predict the heat transfer coefficient of HFC-134a with fair agreement, the more accuracy correlation should be determined. Based on the present data, heat transfer coefficient correlations in the similar form proposed by Chaddock and Noerager [1] are found to be suitable, the correlations are of the form

$$\frac{\alpha_{\text{tp}}}{\alpha_{\text{fo}}} = \frac{a_1}{(X_{\text{tt}})^{b_1}} \tag{14}$$

$$\frac{\alpha_{lp}}{\alpha_f} = \frac{a_2}{(X_{tt})^{b_2}} \tag{15}$$

and



The values of the coefficients a₁ and b₁ in eq.(14), a₂ and b₂ in eq.(15) can be provided by least square method in the sense of least-squares deviation to the interesting group of the data points. Since most of the data reported in the literature cover the experimental conditions that difference from the present study, the comparison is only possible for a few cases. The comparison of the present experimental data at T_{sat,avg} = 4-7 °C with the Wattelet correlation (eq.13) obtained from pure HFC-134a data points (at $T_{\text{sat,avg}} = 4.4$ °C and $x_{\text{in,ts}} = 0.20$) is shown in Fig. 12. The presence of lubricating oil in the refrigerant may affect the thermal and physical properties of the mixture. Therefore the correlation slightly overpredicts the values of the present heat transfer coefficient ratios. With the Wattelet correlation, the calculated mean deviation for α_{tp}/α_{fo} is 21 %. The values of a_1 and b_1 for this data group determined by least square method are 2.4704 and 0.6394, respectively. This correlation is also plotted in Fig. 12 along with the Wattelet correlation. The present experimental data at T_{sat,avg} = 10 °C plotted against the values predicted by the Chaddock and Noerager correlation (eq.9) is shown in Fig.13. Note that the Chaddock and Noerager correlation fitted from pure CFC-12 data points at T_{sat,avg} = 12.2 °C, x_{in,ts} = 0.20, underpredicts the values of the present heat transfer coefficient ratios. This due to the heat transfer coefficient of HFC-134a is higher than CFC-12 at identical evaporation conditions. With the Chaddock-Noerager correlations, the calculated mean deviation for α_{tp}/α_{1} is 37.10 %. The value of a_{2} and b_{2} in eq. (15) are 2.2039 and 1.3514, respectively. This correlation is also plotted in Fig. 13 along with the Chaddock-Noerager correlation

A correlation in the form proposed by Chaddock and Noerager [1] is developed—from all experimental data for predicting the heat transfer coefficients. The values of a_1 and b_1 with minimum squares of errors are 3.3775 and 0.6285 respectively. Comparison of the proposed heat transfer coefficient correlation with all present measured data is shown in Fig.14. The mean deviation is found to be 27 % for α_{tp}/α_{to} . Figure 14 shows also that more than 90 % of the data measured from the present study fall within \pm 30 % of the proposed correlation.

Conclusion

This paper presents new experimental data from the measurement of evaporation heat transfer coefficients of mixture of refrigerant HFC-134a and a polyalkylene glycol lubricant flowing through a small horizontal tube. The lubricant was tested at viscosity of 180 cSt and a lubricant concentration of 5 % A test apparatus which consisted essentially of a well instrumented vapour compression refrigeration system was designed and constructed. This experimental system can control mass flux, heat flux, entering dryness fraction, saturation pressure and temperature of refrigerant flowing through the test section. A 1.8

m long horizontal test section is a double tube heat exchanger. The inner tube is located concentrically within an outer tube with refrigerant flowing in the inner tube and heating water flowing in the annulus. The inner tube and refrigerant loop tube are smooth, commercially available, copper tube of 7.2 mm. inner diameter and 9.52 mm. outer diameter. The test runs were done at average saturated evaporating temperatures ranging between 4 and 25 °C. The inlet dryness fractions to the test section were between 0.1 and 0.25. The mass fluxes were between 160 and 470 kg/m² s and the heat fluxes were between 8 and 55 kW/m². The data obtained from the present study are compared with previous correlations reported in the literature. In addition, new proposed correlations based on the present experimental data are given for practical applications.

Acknowledgments

The present study was supported financially by the Thailand Research Fund (TRF) and the National Energy Policy Office (NEPO) whose guidances and assistances are gratefully acknowledged.

Nomenclature

C_{p}	specific heat, kJ/kg K	D	inner diameter of the test section, m				
G	mass flux, kg/sm ²	h	specific enthalpy,kJ/kg	k	thermal conductivity, W/mK		
L	tube length, m	Q	heat transfer rate, kW	T	temperature, °C		
m	mass flow rate, kg/s	х	dryness fraction	X_{tt}	Lockhart-Martinelli parameter		

Greek Symbols

ω_{o}	lubricating oil concentration, kgo/kgr	ф	heat flux, W/m ²	ρ	density, kg/m ³
α	heat transfer coefficient, W/m ² K	μ	dynamic viscosity, Pa s		

Subscripts

avg	average value	cw	cooling water	fg	vaporization	latent quantity
f	liquid portion	fo	entire mixture flowing as a l	iquid o	nly g	gas
hw	heating water	in	inlet	mix	mixture of re	frigerant and oil
0	oil	out	outlet	r	refrigerant	
sat	saturation condition	tp_	two-phase, vapour and liquid	d mixe	d together	
ts	test section	wall	internal tube wall surface co	ntactin	g the refrigera	nt

References

1. J.B. Chaddock and J.A. Noerager, ASHRAE Transaction 72, 90 (1966).

- 2. K. Stephan and M. Abdelsalam, Int. J. Heat Mass Transfer 23, 73 (1980).
- D.S. Jung, M. McLinden, R. Radermacher and D. Didion, Int. J. Heat Mass Transfer 32, 1751 (1989).
- S.G. Kandlikar, J. of Heat Transfer 112, 219 (1990).
- 5. S.J. Eckels and M.B. Pate, Int. J. Refrigeration 14, 70 (1991).
- 6. S.J. Eckel and M.B. Pate, ASHRAE Transaction 97, 71 (1991).
- 7. S. M. Sami and T.N. Duong, Int. Comm. Heat Mass Transfer 19, 203 (1992).
- J.P. Wattelet, J.M. Saiz Jabardo, J.C. Chato, J.S. Panek and A.L. Souza, Experimental evaluation of convective boiling of refrigerants HFC-134a and CFC-12, ASME HTD-197, 121 (1992)
- 9. J.P. Wattelet, J.C. Chato, A.L. Souza and B.R. Christofferson, ASHRAE Transactions 100, 603 (1994).
- 10. H. Wijaya and M.W. Spatz, ASHRAE Transaction 14, 1020 (1995).
- 11. C.C. Wang, C.S. Kuo, Y.J. Chang and D.C. Lu, ASHRAE Transaction 12, 830 (1996).
- 12. A. Singh, M.M. Ohadi and S. Dessiatoun, J. Heat Transfer 118, 497 (1996).
- 13. L.M. Chamra and R.L. Webb, Int. J. Heat Mass Transfer 39, 1827 (1996)
- 14. X. Liu, J. Heat Transfer 119, 158 (1997).
- 15. C.C. Wang, C.S. Chiang and J.G. Yu, Int. Heat Fluid Flow 19, 259 (1998).
- 16. YY.Yan and T.F. Lin, Int. Heat Mass Transfer 42, 4183 (1998).
- 17. G.H. Green and F.G. Furse, ASHRAE Journal, October, 63 (1963).
- 18. J.A. Tichy, W.M.B. Duval and N.A. Macken, ASHRAE Transactions 92, 450 (1986).
- 19. K. Hambraeus, Int. J. Refrig. 14, 357 (1991).
- 20. J.S. Panek, Evaporation heat transfer and pressure drop in ozone-safe refrigerants and refrigerant-oil mixtures, M.S. Thesis, The University of Illinois at Urbana-Champaign (1992).
- 21. S.J. Eckels, T.M. Doerr and M.B. Pate, ASHRAE Transaction 100, 265 (1994).
- 22. REFPROP, Thermodynamic properties of refrigerants and refrigerant mixtures, Version 6.01, Gaithersburg, MD. National Institute of Standards and Technology (1998).
- 23 ASHRAE, ANSI/ASHRAE Standard 41.4, Standard method for measurement of proportion of oil in liquid refrigerant. Atlanta: American Society of Heating, Refrigerating and Air-Conditioning Engineers, Inc (1984).

Kalinitchenko, V., Sekerj-Zenkovitch, S., Wongwises, S., Mijangos, R., The Generation of Sand Waves by Oscillating Flows, *Proceedings of the International Conference on Modern Approaches to Flows in Porous Media*, Moscow, September 6-8, 1999.



РОССИЙСКАЯ АКАДЕМИЯ НАУК ИНСТИТУТ ПРОБЛЕМ МЕХАНИКИ РОССИЙСКИЙ ФОНД ФУНДАМЕНТАЛЬНЫХ ИССЛЕДОВАНИЙ



RUSSIAN ACADEMY OF SCIENCES INSTITUTE FOR PROBLEMS IN MECHANICS RUSSIAN FOUNDATION FOR BASIC RESEARCH

современная теория фильтрации

МЕЖДУНАРОДНАЯ КОНФЕРЕНЦИЯ ПОСВЯЩАЕТСЯ ПЕЛАГЕЕ ЯКОВЛЕВНЕ ПОЛУБАРИНОВОЙ-КОЧИНОЙ (1899-1999)

Тезисы докладов

MODERN APPROACHES TO FLOWS IN POROUS MEDIA

INTERNATIONAL CONFERENCE
DEDICATED TO
PELAGEYA YAKOVLEVNA POLUBARINOVA-KOCHINA
(1899-1999)

Abstracts

Москва, 6-8 сентября 1999

Moscow, September 6-8, 1999

THE GENERATION OF SAND WAVES BY OSCILLATING FLOWS

Vladimir A. KALINITCHENKO¹, Sergey Ya. SEKERJ-ZENKOVITCH¹, Somehai WONGWISES¹, Ricardo Rodriguez MIJANGOS³

¹ Lab.of Wave Processes, Inst. for Problems in Mechanics, Russian Academy of Sciences, pr. Vernadskogo, 101 Moscow, 117526 RUSSIA, kalin@ipmnet.ru

²Dept. of Mechanical Engineering, King Mongkut's Univ.of Technology Thonburi, Suksawad 48 Rd., Bangkok 10140 THAILAND

³Centro de Investigacion en Fisica, Apdo. Postal 5-88 C.P. 83190, Hermosillo, Sonora MEXICO

Abstract. In this experimental study the onset of the instability at the interface of two-phase fluid system (fluid granular fluid, two immiscible fluids, or two miscible fluids) in relative oscillating shearing motion is examined. A qualitative and quantitative comparison between the prediction of stability theory and experimental observations of sand waves under an oscillating fluid flow, secondary waves in node regions of standing internal waves, and wave-like formations at the interface between two miscible fluids is carried out.

1. Introduction

The dynamics of the water-sediment interface have been received much attention in recent years, especially mechanisms governing the interaction between fluid flow and bottom materials. It is well known that the interfaces of sand beds subjected to shear flows of sufficient intensity to transport the sand are unstable and deform in wavelike forms. Since Bagnold's work [1] that assumed a stress instability between fluid and granular fluid, it has been suggested many models to explain the mechanism of sand waves' development. However, these models are too restrictive, and without the introduction of a phase shift in the fluid velocity field relative the boundary perturbation they lead to the conclusion that a flat sand bed is stable to any shear flow.

Experiments have shown that for steady uniform flows first sand waves occur when sediment is transport as 'bed load' - particles are moved along in thin layer near the bed [2]. According to the observations this layer has a small finite thickness in proportion to a mean size of sediment particles. By assuming that the density of this movable granular fluid is constant, one obtains the two-layer fluid system. The aim of this study is to consider the instability at the interface between oscillating 'pure' fluid and granular fluid. In the present paper, we first present experimental results for the dynamics of the interface between fluid-granular fluid, two immiscible fluids. and two miscible fluids. We next describe the possible method of stability analysis for a viscous oscillating fluid in the quasi-steady approximation and compare experimental and theoretical results.

2. Results and Discussion

2.1. Experiments

In this section the results of three sets of experiments investigating different aspects of the shear instability are discussed. In all experiments the oscillatory motion of one fluid relative to the other was produced by parametrically excited standing waves in the rectangular tank (50x4x40 cm). The experimental set-up has been presented in details in ref. [3,4].

The aim of the first set of experiments was to examine the instability of initially plane sand beds in oscillatory flow produced by surface standing waves. The physical characteristics of the material used in experiments are given below:

•			
	Material	Diameter (mm)	Density (g cm ⁻¹)
	Natural fine quartz		
	sand	i	

With porosity n=0.4, the density of sediment layer was $\rho 2=1.95$ g cm³. Dynamic viscosity of sediment was μ 2=1.8 cP. The orbital motion of fluid particles in the region under nodes of standing waves was uniplanar and horizontal. The development of sand waves was examined over a wide range of experimental parameters: first, second, and third modes of standing surface waves (basic flow) at fluid depth h=10 cm, and sediment layer thickness $h^*=0.2-1.2$ cm.

A common feature we observed in our experiments was that smooth interface became unstable when the fluid velocity just outside oscillatory boundary layer at the bed exceeded some critical value. Before it sand particles oscillated almost in phase with fluid motion. The

instability was accompanied by the formation of a periodic array of vortices - standing sand waves. Their development shown in Fig. 1 is typical of that obtained. These photographs were taken in 167 s. Note that in the case of side views the sand waves could be detected only when their amplitude was approximately 0.5 cm. When the flow is viewed from below, the development of the interface instability becomes more apparent (Fig. 1a). Furthermore, the sand wave length L increases with time - L=1.7 cm in Fig. 1a, and L=3.0 cm in Fig. 1b.

The second set of experiments concerned with the instability of oscillatory flow over thin viscous fluid layer. In our opinion this configuration is capable of simulating the viscous instability of two-phase fluid system considered above - oscillatory flow-sediment bed interface. Aqueous sugar solution ($\rho 2=1.20 \text{ g cm}^3$, μ 2=5.8 cP) was selected as a fluid in the bottom layer ($h^*=1.0$, 1.3, 3.0 mm). Figure 2 shows the wave form of the interface. The lower layer depth was 3.0 mm. Oscillatory flow was generated by first wave mode: T=1.10 s, $\zeta = 4 \text{ cm}$. The length of wave-like formation was about L=1.1 cm.

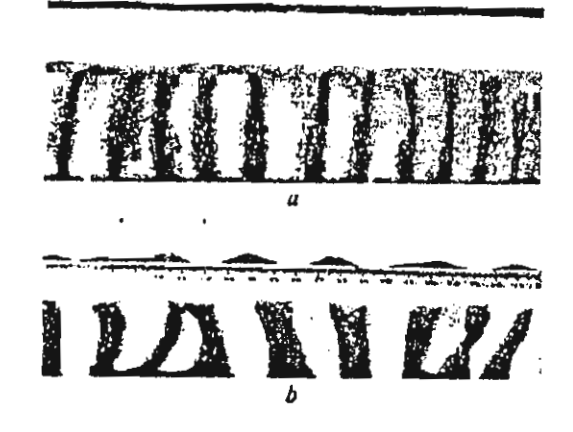


Fig.1. Side and plan views of sand waves. Basic flow was produced by first mode of standing surface wave (h=10 cm), wave period is T=1.09 s, wave amplitude is $\zeta = 4 \text{ cm}$, sediment layer thickness is h=0.2 cm: a - within t=25 s after the establishment of steady fluid motion; b - t=192 s

WIND STATES

Fig. 2. The wave-like formation at the interface water - aqueous sugar solution under oscillatory motion of the upper fluid

Shear instability in internal standing waves was the subject of investigation in third set of experiments. Applying the Faraday resonance as the method of

waves' generation, there is a good chance of observing and studying the development unsteady instabilities in the node's regions from initiation of regular groups of secondary waves to vortex formation. As working fluids we used kerosene-water, kerosene-aqueous thiosulphate solution, and kerosene-aqueous sugar solution.

With increasing the internal wave amplitude, secondary wave formation was observed in the region near the node (See Fig. 3). As the amplitude of the main wave increased still further, the secondary waves became unstable and transformed into the vortex formation. This type of shear instability is very complex to study because the local velocity shears at the interface are periodic in space and time, and the interface itself is not horizontal, but changes its position.

2.1. Stability analysis

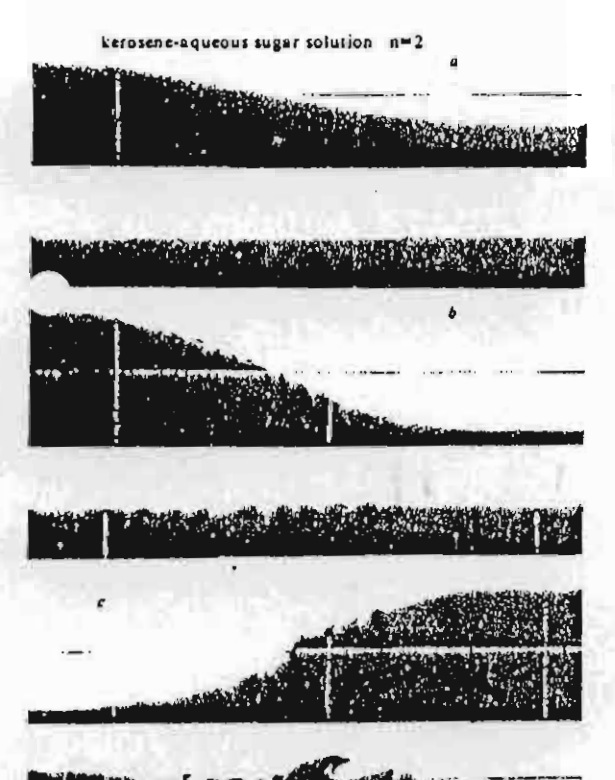
The flow whose stability is studied here is an oscillatory stratified flow of two fluids. The development of a stability theory for viscous oscillating fluids, such as we have in the experiments, has no proved possible by analytical methods. However, the stability analysis of small disturbances to the flow defined by Graebel [5], Drazin [6], and Hayakawa & Unny [7] has been used in quasi-steady approximation. Based on theoretical ground [8], it can be shown that the approach of quasi-steadiness is able to predict stability or instability over the time intervals small compared with period of oscillatory fluid motion.

Graebel [5] considered two laminar streams of viscous fluids of different densities flowing in opposite direction between two parallel inclined planes under the action of gravity. He found the unstable regime of flow and derived the expression for wavelength appropriate to maximal growth of wavy disturbances. We used this model to estimate the length of secondary waves on the time interval near maximal development of standing internal waves (Fig. 3).

To predict the instability in the cases shown in Figs. 1, 2, and 3 (the interface is horizontal) we used the results [6,7], in which the flow of two superposed fluids of nearly equal properties was considered. Note that the shear flow in the lower layer was not negligible.

Below, for sand waves we have tabulated all experimental parameters, observed and calculated wavelengths.

Mode number	h, cm	h*, cm	T, s	ζ, cm	Lexp	Lealc
1	12	1.2	1.04	6.5	3.8 - 5.5	3.6
. 2	12	1.2	0.61	4.3	2.4	2.6
3	12	1.2	0.48	6.5	1.5	1.0
1	10	0.2	1.09	4.0	1.7 - 3.0	1.5



kerosene-water n=2



Fig. 3. The development of secondary instability in the nodes' regions of standing internal waves: $a - \zeta = 1.8 \text{ cm}$; $b - \zeta = 2.9 \text{ cm}$; $c - \zeta = 5.2 \text{ cm}$; $d - \zeta = 4.3 \text{ cm}$

ACKNOWLEDGMENTS

The research reported in this paper was supported by the Russian Foundation for Basic Research (Project No.99-01-01080).

REFERENCES

- Bagnold R.A., Proc. Roy. Soc. London, A249, 235 (1956)
- Kalinitchenko V.A., Wongwises S., Proc. FEDSM ASME, FEDSM97-3042, 6 p. (1997)
- Kalinitchenko V.A., Izv. Acad. Nauk, Atmospheric and Oceanic Physics, 22, 206 (1986)
- Kalinitchenko V.A., Nesterov S.V., Sekerzh-Zen'kovich S.Ya., Chaykovskii A.A., Fluid Dynamics, 30, 101 (1995)
- 5. Graebel W.P., J. Fluid Mech., 8, 321 (1960)
- 6. Drazin P.G., Proc. Camb. Phil. Soc., 58, 646 (1962)
- 7. Hayakawa N., Unny T.E., Phys. Fluids, 17, 679 (1974)
- Kravtsov A.V., Sekerzh-Zen'kovich S.Ya., Comput. Maths. Math. Phys., 3, 533 (1993)

Wongwises, S., Pornsee, A., Siroratsakul, E., Gas-Wall Shear Stress Distribution in Horizontal Stratified Two-Phase Flow, *Int. Com. Heat Mass Transfer*, 1999; 26(6): 849-860.



Int. Comm. Heat Mass Transfer, Vol. 26, No. 6, pp. 849-860, 1999

Copyright © 1999 Elsevier Science Ltd

Printed in the USA. All rights reserved

0735-1933/99/\$-see front matter

PII S0735-1933(99)00073-1

GAS-WALL SHEAR STRESS DISTRIBUTION IN HORIZONTAL STRATIFIED TWO-PHASE FLOW

Somchai Wongwises, Apichart Pornsee and Egarin Siroratsakul Fluid Mechanics and Turbomachinery Research Centre (FUTURE) Department of Mechanical Engineering, King Mongkut's University of Technology Thonburi, Bangmod, Bangkok 10140, Thailand

(Communicated by J.P. Hartnett and W.J. Minkowycz)

ABSTRACT

Gas-wall shear stresses in the stratified gas-liquid flow in pipes are obtained using Preston's method for measuring skin friction in the turbulent boundary layer. The non-dimensional relationship between the Preston tube reading and wall shear stress over a wide range of single-phase gas flow rates is reported. The wall shear stresses up to positions close to the gas-liquid interface, for various interface conditions, are obtained for the two-phase flow experiment. The distribution of the gas-wall shear stress and the effect of diameter on those distributions are investigated. The friction factors obtained from the experiments are also compared with those reported in the literature. © 1999 Elsevier Science Ltd

Introduction

Gas-liquid stratified flow is encountered in several industrial applications including the flow of oil and natural gas in petroleum industries, the flow of refrigerants in air conditioning and refrigeration systems and the flow of steam and water in emergency core cooling (ECC) systems in nuclear reactors during the postulated loss of coolant accidents (LOCA). To understand the flow behavior and transfer mechanisms, the determination of the local structure of stratified gas-liquid flow, is certainly a powerful method. Wall shear stress in two-phase flow is one of the main factors governing transport phenomena and its distribution is required for modeling the flow in these applications. However, the major studies of gas-wall shear stresses in two phase pipe flow has been in rectangular channels [1-8]. Some of the earliest works to measure the gas-wall shear stresses for stratified two-phase flow in circular pipes were performed by Kowalski [9] with the anemometry technique proposed by Shiralkar [10]. Two probes were mounted flush in the pipe, one on the top and one on the bottom of the pipe. Each probe was operated by a linearized, constant-temperature anemometry system. However, the effect of pipe diameter on the distribution of the shear stress was not examined. Later, Newton et al. [11] presented the measurements of

gas-wall shear stress by Preston tubes. However, the calibration technique, the achievement of the correlation between Preston reading and shear stress and also the effect of pipe diameter were not given.

Relatively little information is currently available on the gas-wall shear stress in co-current stratified two-phase flow in circular pipes. The objective of the present study is to measure the gas-wall shear stress using Preston's method of measuring turbulent skin friction, which makes use of a simple Pitot tube resting on the surface (a so-called Preston tube). The measurement technique, the calibration and calculation methods, the distribution of the gas-wall shear stress up to positions close to the gas-liquid interface for various interface conditions and the effect of pipe diameter are shown in detail.

Experimental Apparatus and Method

A schematic diagram of the test facility is shown in Fig 1. Air and water were used as the working fluids. The main components of the system consisted of the test section, an air supply, a water supply and instrumentation. The horizontal test sections, with inside diameters of 29 mm. and 54 mm. and a length of 10 m. were constructed from transparent acrylic glass to permit visual observation of the flow patterns. The connections of the piping system were designed such that the component part can be changed very easily. Water was pumped from the storage tank through a rotameter, to the water inlet section at the bottom of the pipe and hence flowed back to the storage tank. Air was supplied to the test section by a suction-type blower. The air flow could be controlled by a valve at the outlet of the blower. Many small rods were used as guide vanes at the air inlet section to maintain a uniform flow (Fig.2). Both the air and water streams were brought together in a mixer and then passed through the test section concurrently.

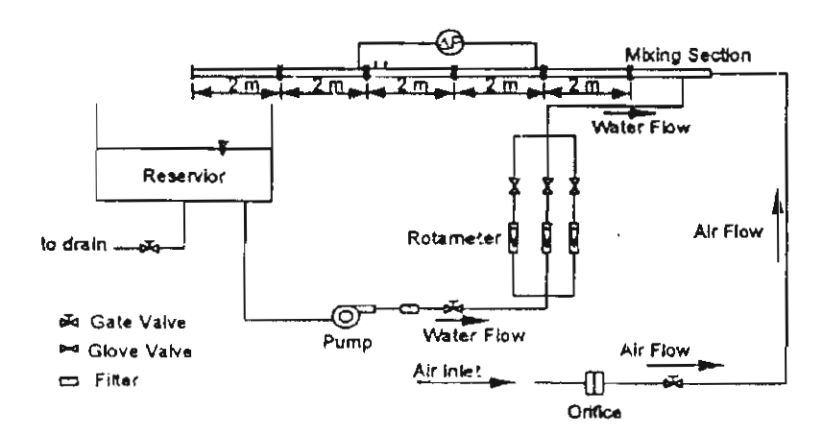


_ FIG. 1
Schematic diagram of experimental apparatus

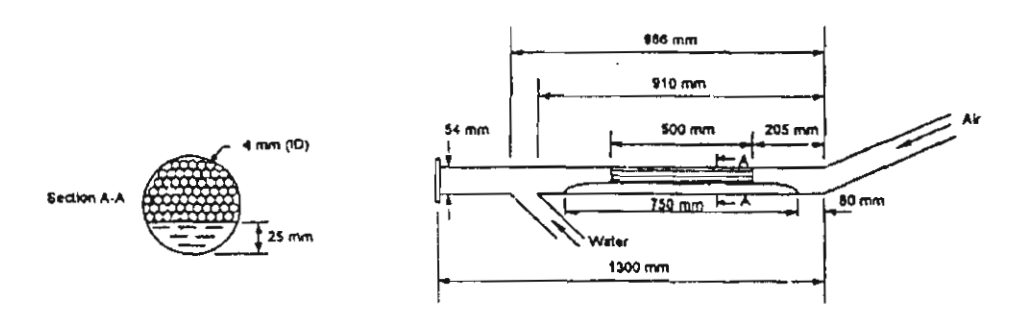


FIG. 2 Mixing section

The inlet flow rate of air was measured by means of a round-type orifice. The inlet flow rate of water was measured by three sets of rotameters. The temperature of the air and water was measured by T type thermocouples. The two phase pressure drop between the test section was measured by a digital micromanometer. Stainless steel ring electrodes were mounted flush in the tube wall for measuring the liquid hold up, which is defined as the ratio of the cross-sectional area filled with liquid to the total cross-sectional area of the pipe. The electrodes operated on the principle of the variation of electrical resistance following changes in the water level between two parallel electrode rings. The same description of the calibration procedures for stratified flow can be found in Andreussi [12] and Wongwises et al. [13]. Due to the variation of conductivity caused by temperature change and coating of the electrodes with impurities, the gauges were calibrated before and after each run. For measuring the wall shear stress, special care was taken in implementing the measuring system. A Preston tube and a static tapping were placed on the inner wall at the upper part of the pipe in the gas flow region. Figure 3 shows the method of installing the Preston and static tubes. The small copper rods with two different external diameters were used as the Preston tubes; 2.0 mm. for 29 mm. pipe diameter and 2.12 mm. for 54 mm. pipe diameter.

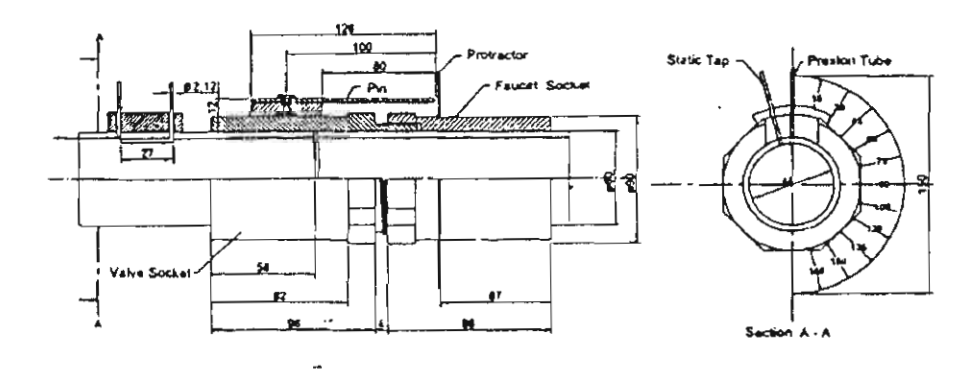


FIG. 3
Details at the measuring station

The ratios of the external Preston tube diameter and the internal pipe diameter used in the experiments were 0.068 and 0.039 for the 29 mm. and 54 mm. pipe diameters, respectively. These diameter ratios were smaller than those which were recommened by Patel [6]. The Preston tube and static tapping were located on the pipe which was connected with the others by a specially constructed pipe connection that could be rotated until the Preston tube was in close proximity to the gas-liquid interface. The various pressure differences from the Preston and static tubes were measured with digital micromanometers. To make sure that the flows were fully developed, all measuring positions were located between 2 m. to 6 m. from the inlet of the test section.

At first, the Preston tubes were calibrated over a wide range of single-phase air flow rates. In the experiments, the air flow rate was increased by small increments. After each change in inlet air flow rate, the flow rates of air and water, the pressure drop in the test section and the pressure differences between Preston and static probes were recorded. To verify that the distribution of measured pressure differences between two probes around the inner wall of pipe was symmetrical, the preston tube was rotated for measuring the pressure differences at various 0 (Fig. 3). In the two-phase flow study, experiments were conducted at various air and water flow rates under ambient conditions. The air flow rate was increased by small increments while the water flow rate was kept constant at a preselected value. After each change in inlet air flow rate, the flow phenomena was detected by visual observation, both the air and water flow rates were recorded. The liquid hold-up was registered through the transducers. The Preston probe was rotated clockwise from the top of the pipe towards the interface for measuring the pressure differences between the Preston and static probes. To confirm that the distribution of measured pressure differences between the Preston and static probes were symmetrical, some pressure readings were also taken in an anticlockwise direction.

Mathematical Model

Consider an equilibrium horizontal stratified co-current pipe flow as shown in Fig. 4.

The momentum equations for liquid and gas phases are

$$A_L dP + \tau_L S_L dx + \tau_i S_i dx - \rho_L A_L g \sin \alpha dx = 0$$

$$A_G dP - \tau_G S_G dx - \tau_i S_i dx - \rho_G A_G g \sin \alpha dx = 0$$
(1)

Solving for the pressure gradient in each equation gives

$$\frac{dP}{dx} = \frac{1}{A_L} \left(-\tau_L S_L - \tau_i S_i \right) + \rho_L g \sin \alpha = \frac{1}{A_G} \left(\tau_G S_G + \tau_i S_i \right) + \rho_G g \sin \alpha \quad (2)$$

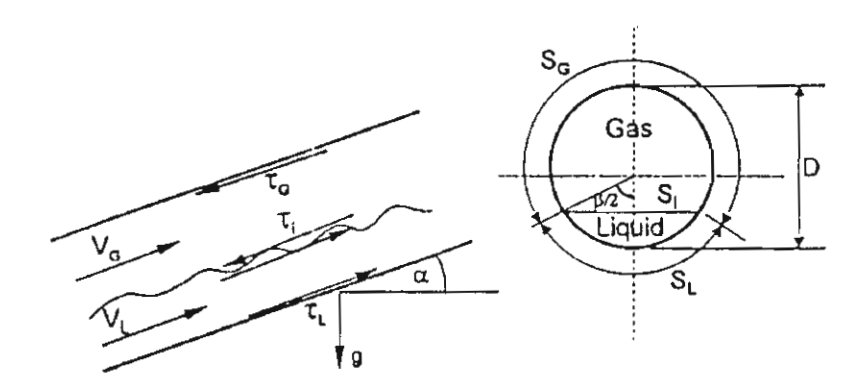


FIG. 4

A model of stratified two-phase pipe flow

Relationships for the fluid-wall shear stresses, τ_{L} and τ_{G} can be determined from

$$\tau_k = f_k \left(\frac{1}{2} \rho_k V_k^2 \right) \quad ; \quad k = G, L \tag{3}$$

The usual empirical result is used,

$$f_k = C_k Re_k^{-n} , \qquad (4)$$

$$Re_{k} = \frac{D_{k} V_{k}}{V} \quad ; \quad k = G, L \qquad (5)$$

The Reynolds number is based on D_k the hydraulic diameter, defined for the purpose of this two-phase flow in the manner used by Agrawal et.al.[14] and later by, for example, Johnston [15] and Espedal [16]. The liquid is visualized as if it is flowing in an open channel. The gas is visualized as flowing in a closed duct,

thus

$$D_{L} = \frac{4A_{L}}{S_{L}}, \qquad D_{G} = \frac{4A_{G}}{S_{G} + S_{i}}$$
 (6)

$$S_G = \left(\pi - \frac{\beta}{2}\right)D$$
, $S_L = \left(\frac{\beta}{2}\right)D$, $S_i = D\sin\left(\frac{\beta}{2}\right)$ (7)

Taitel and Dukler [17] used the following empirical values for the constants in the friction factor equation; in turbulent flow regime: $C_k = 0.046$, n = 0.2; in laminar flow regime: $C_k = 16$, n = 1

The velocity at the interface between the gas and the liquid phases would be expected to vary between 0 and V_L , therefore, it is assumed that $V_i = V_L$ [15]. Under these conditions the interfacial shear stress can be determined from

$$\bar{\tau}_{i} = f_{i} \left(\frac{1}{2} \rho_{G} (V'_{G} + V_{L})^{2} \right)$$
 (8)

Also, in order to calculate the gas-wall shear stress, Agrawal [14] suggested the Blasius equation for smooth pipe flow by substituting $C_k = 0.079$ and n = 0.25 into eq.(4).

Preston [2] proposed a simple method of determining local turbulent skin friction on a smooth surface by means of a round Pitot tube or impact tube resting on the surface. Assuming that the inner law

$$u/u_{\tau} = f(u_{\tau}y/v) \tag{9}$$

is valid in a region close to the surface in both fully developed pipe flow and boundary layer flow, and the functional relationship is the same for both types of flow, the following equation relating the wall shear stress (τ_w) and the pressure difference between the total pressure recorded by the preston tube and static pressure at wall (ΔP_n) is developed:

$$\log_{10} \frac{\tau_{w} d^{2}}{4\rho v^{2}} = A + B \log_{10} \frac{(\Delta P_{p}) d^{2}}{4\rho v^{2}}$$
 (10)

where constants (A = -1.396, B = 0.875) were obtained by calibration. Head and Rechenberg [5] tested and compared the experimental data obtained from Preston and Stanton tubes, both for pipe and boundary layer flows. They confirmed the validity of Preston's method.

Patel [6] suggested that Preston's original calibration was in error. He made a more extensive study of the Preston tube and compared the various proposed correlations. Over a wide range of experimental conditions, Patel's calibration equation is obtained as follows:

$$y^* = 0.8287 - 0.1381x^* + 0.1437x^*^2 - 0.0060x^*^3$$
 (11)

$$x^* = \log_{10} \frac{(\Delta P_P)d^2}{4\rho v^2}$$
 and $y^* = \log_{10} \frac{\tau_w d^2}{4\rho v^2}$ (12)

The simplicity, low cost and sufficient accuracy of the Preston tube makes it useful and suitable for determining the shear stress distribution at the solid boundaries in two-phase stratified flow.

Results and Discussion

The Preston tubes were calibrated over a wide range of single-phase air flow rates by measuring the air flow rate, the pressure drop along the test section (ΔP_L) and the pressure difference between the Preston and static probes (ΔP_P). To examine the symmetry of the shear stress distribution, the preston tube was rotated for measuring the pressure differences at various circumferential locations around the pipe (θ). The experiment was performed for both sizes of pipe diameters (54 mm. and 29 mm.). From the

momentum balance equation (eq.2) for single-phase air flow and substituting the measured pressure drop along the test section (ΔP_L) and α (= 0), the fully developed wall shear stress can be estimated.

Assuming the existence of a region near the surface in which conditions are functions only of the skin friction, the relevant physical constants of the fluid and a suitable length, a universal non-dimensional relationship between the total pressure recorded and the static pressure at the wall in terms of the skin friction proposed by Preston [2], namely

$$\frac{\tau_{w}d^{2}}{4\rho v^{2}} = f\left(\frac{(\Delta P_{p})d^{2}}{4\rho v^{2}}\right) \tag{13}$$

will be used to form the correlation. On this assumption, this relationship is independent of the pressure gradient. Assuming symmetry about the center of the circular pipe, the wall shear stress terms along the horizontal inner surfaces for each run were curve-fitted by the least squares method to a third degree polynomial as follows

$$y^* = 0.5947 + 0.3975 x^* - 0.0168 (x^*)^2 + 0.0071 (x^*)^3$$
 (14)

In the stratified two-phase flow study, the air flow rate was increased by small increments while the water flow rate was kept constant. The smooth and two dimensional wavy flows were obtained in accordance with results obtained from the study. At each flow rate of air and water, the pressure difference between Preston and static probes was recorded at various circumferential location. To do this, the test section which was attached with Preston and static probes was rotated clockwise in small steps towards the interface. Substituting the measured $\Delta P_{\rm p}$ into eq.(14), the gas-wall shear stresses were determined. The measured wall shear stress distributions were found to be strongly influenced by the flow pattern which exists. A number of graphs can be drawn from the experimental results but because of space limitation, only typical results are shown. Figures 5 to 7 show typical wall shear stress distributions encountered in two-phase smooth stratified flow. The measured wall shear stress decreases slightly with circumference distance to a minimum point. As a result of a small wavy interface, it then increases sharply to a specific shear stress value at the interface. Typical gas-wall shear stress distributions encountered in two dimensional wavy flow are shown in Figures. 8 to 10. As a result of wavy interface, the gas-wall shear stress increases slightly and approaches a specific value at the interface. Because the amplitude of the water layer fluctuation increases slightly with the air flow rate, the gas-wall shear stress for higher air flow rate is higher than for lower flow rate. The wall shear stress distributions obtained are the same for both pipe sizes. The literature contains considerable data on wall shear in horizontal two-phase flow, but only the works of Kowalski [9] and Newton et al. [11] were performed in circular pipes. The present experimental results are also compared with those and some qualitative agreement is noted. Kowalski did

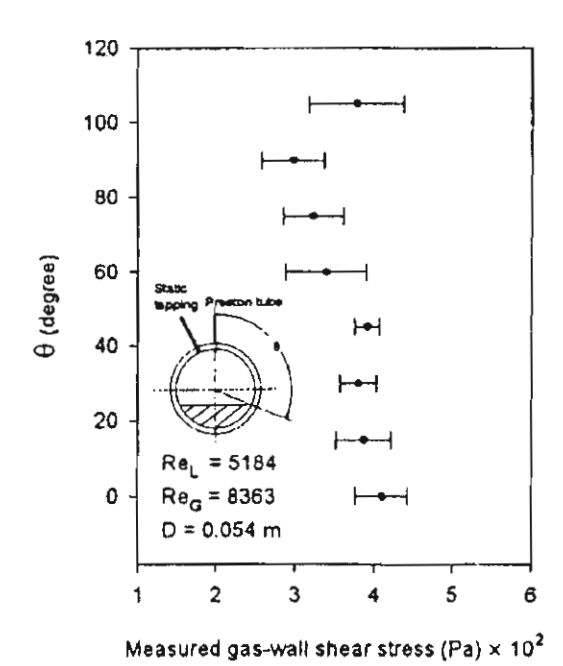
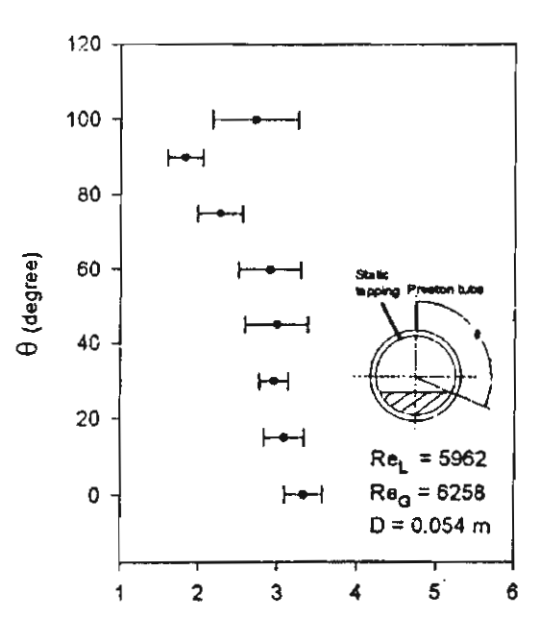


FIG. 5
Gas-wall shear stress distribution around circumference of pipe for stratified smooth flow



Measured gas-wall shear stress (Pa) × 10²

FIG. 6
Gas-wall shear stress distribution around circumference of pipe for stratified smooth flow

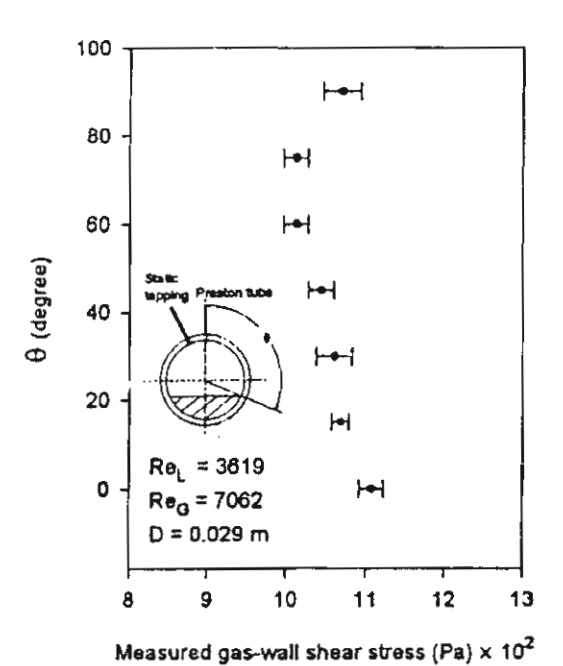


FIG. 7 Gas-wall shear stress distribution around circumference of pipe for stratified smooth flow

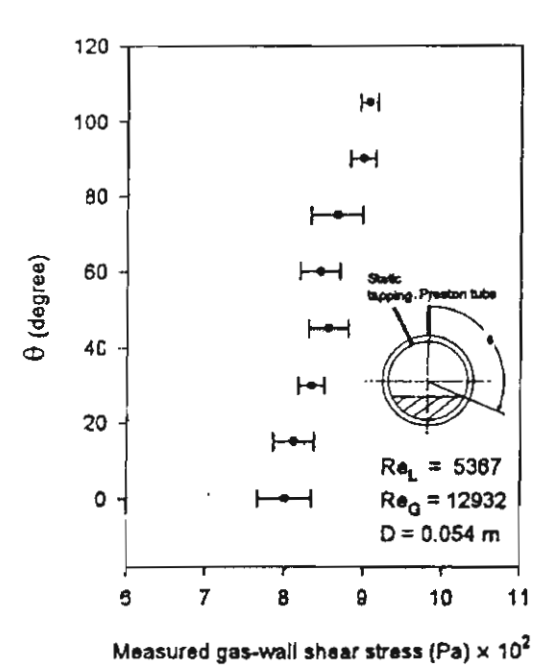


FIG. 8
Gas-wall shear stress distribution around circumference of pipe for stratified wavy flow

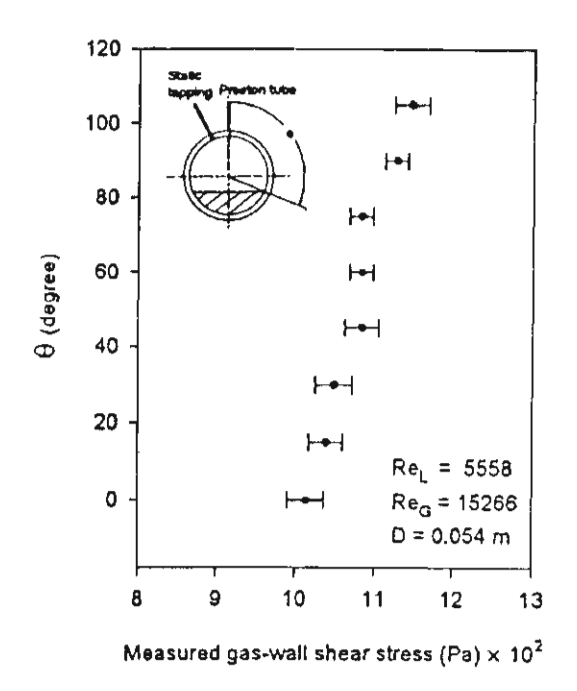
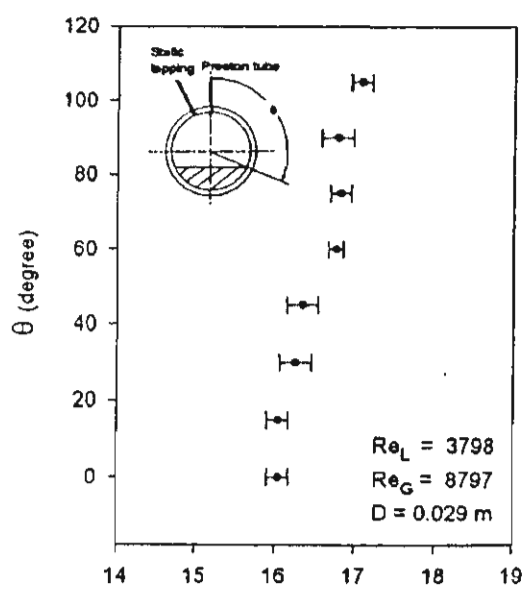


FIG. 9
Cas-wall shear stress distribution around circumference of pipe for stratified wavy flow



Measured gas-wall shear stress (Pa) × 10²

FIG. 10
Gas-wall shear stress distribution around circumference of pipe for stratified wavy flow

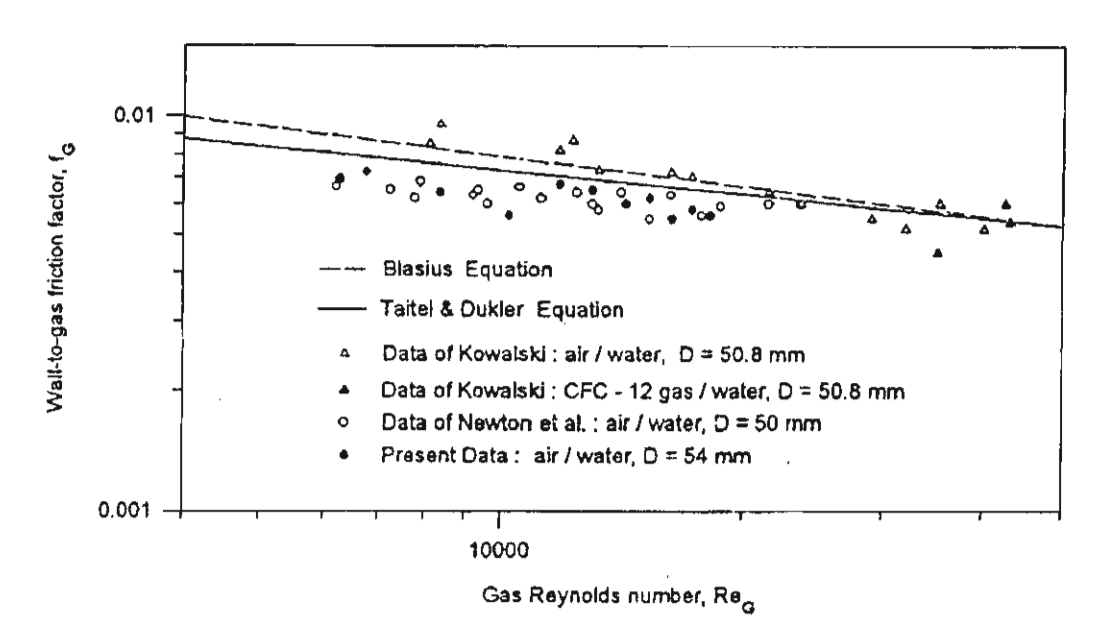


FIG. 11
Comparison of present measured gas-wall friction factor with results reported in the literature

not measure the shear stress at the region very close to the liquid-gas interface. However his existing data show that some major variations occured close to the interface. The measured wall shear stress distribution is different from those that were obtained by Davis [7] because of the difference in pipe configuration. The average gas-wall friction factors were calculated from eq. (3) and were plotted against the gas Reynolds number (Re_G) obtained from eq. (5). It can be observed that the friction factor decreases slightly with increasing Re_G. Figure 11 compares the experimental values of the gas-wall friction factor with theoretical values for smooth pipe flow given by the Blasius and Taitel & Dukler equations. Concerning the gas flow rates, the Blasius and Taitel et al. relationships overpredict the friction factor for Re_G by less than 20,000. The friction factor data obtained by Kowalski [9] and Newton et al. [11] are also compared with the present results. Kowalski's data points were taken from a log scale, thus were a cause of some uncertainties. The present measurements agree well with those from Newton et al. for D = 50 mm.

Conclusion

This paper presents the results of the experimental work on the gas-wall shear stress for the cocurrent air-water stratified flow in pipes. The measurement of wall shear stress by a calibrated Preston tube appears to be accurate and convenient. Preston and static probes are installed on the dry walls of the circular pipe and are calibrated by measuring the pressure drops along the test section and pressure differences between the Preston and static probes for single-phase air flow over a wide range of flow rates. The non-dimensional relationship between the Preston probe reading and wall shear stress is reported in a practically more convenient form. The probes are used to measure the gas-wall shear stress distribution up to positions close to the air-water interface. The gas-wall friction factor is determined and compared with other reported models.

Acknowledgments

The present study was supported financially by the Thailand Research Fund (TRF) whose guidance and assistance are gratefully acknowledged.

Nomenclature

A_G, A_L	crossectional area of gas and liquid phase, m ²	C	constant
d	external diameter of Preston tube, m	D	pipe diameter, m
D_G, D_L	hydraulic diameter of gas and liquid phase, m	$\mathbf{f}_{G},\mathbf{f}_{L}$	gas-wall and liquid-wall friction factor
\mathbf{f}_{i}	interfacial friction factor	g	gravitational acceleration, m/s2
n	constant	P	pressure, N/m ²
ΔP_L	pressure drop along the test section, Pa	S	perimeter, m

ΔP_P pressure difference between Preston and static tubes reading, Pa

Re Reynolds number ut friction velocity, m/s

velocity, m/s V₀ average velocity of gas, m/s

V_L average velocity of liquid, m/s x* group of variables in eq.(12)

y vertical position measured from bottom, m y* group of variables in eq.(12)

Greek Symbols

 β angle in eq. (7), radian α inclination angle from the horizontal, deg.

θ circumferential location, degree ρ density, kg/m³

kinematic viscosity, m²/s t shear stress, N/m²

Subscripts

k gas or liquid G gas phase L liquid phase

interface w wall

References

- 1. F.H. Clauser, J. Aero. Sci. 21, 91(1954).
- 2. J.H. Preston, Journal of the Royal Aeronautical Society 58, 109 (1954).
- 3. D. W. Smith and J.H. Walker, Skin Friction Measurements in Incompressible Flow, NACA Report TN 4231 (1958).
- 4. S.R.M. Ellis and B. Gay, Trans. Inst. Chem. Eng. 37, 206 (1959).
- 5. R.M. Head and I. Rechenberg, J. Fluid Mech. 14,1 (1962).
- 6. V.C. Patel, J. Fluid Mech. 23, 185 (1965).
- 7. E.J. Davis, Ind. Eng. Chem. Fundam. 8, 153 (1969).
- 8. L. Fabre, L. Masbernat and C. Suzanne, Some Remark on the Constitutive Equations of Stratified Gas-Liquid Flow, T.N. Veziroglu and A.E. Bergles, (eds.), Multiphase and Heat Transfer III. Part A: Fundamentals, elsevier, Amsterdam, 41 (1984).
- J.E. Kowalski, AIChE Journal 33, 274 (1987).
- B.S. Shiralkar, A Study of the Liquid Film in Adiabatic Air-Water Flow with and without Obstacles, General Electric Rept., GEAP-10248 (1970).
- 11. C.H. Newton and M. Behnia, AIChE Journal 42, 8 (1996).
- 12. P. Andreussi, D. Donfrancesco and M. Messia, Int. J. Multiphase Flow 14, 6 (1988).

- 13. S. Wongwises and P. Naphon, Int. Comm. Heat Mass Transfer 25, 819 (1998).
- 14. S.S. Agrawal, G.A. Gregory and G.W. Govier, Can. J. Chem. Eng. 51, 280 (1973).
- 15. A.J. Johnston, Int.J. Multiphase Flow 10, 371 (1984).
- 16. M. Espedal, Influence of the Interfacial Waves on the Pressure Drop in Stratified Pipe Flow at Small Inclinations, *Proc. 3 rd Int. Conf. on Multiphase Flow*, Lyon, France (1998).
- 17. Y. Taitel and A.E. Dukler, AIChE Journal 22, 47 (1976).

Received March 22, 1999

Wongwises, S., Kritsadathikarn, P., Songnetichavarit, T., Lokathada, N., Pressure Distribution of Refrigerant Flow in an Adiabatic Capillary Tube, *Science Asia*, (in press)



April 26, 2001

Dr. Somchai Wongwises, Department of Mechanical Engineering, KMUTT. Bangkok 10140.

Dear Dr. Somchai,

Thank you very much for submitting the manuscript entitled: Pressure Distribution of Refrigerant Capillary Tubes (Code 0012-152, received 7 December 2000) for consideration for publication in Science Asia.

The manuscript has been read by two independent referees, whose reports are enclosed for your information. Although the referees have found the work to be of interest, there are a number of cueries and comments which require clarification from you. In addition, the manuscript needs to be revised in light of their comments. Please reply to every point of the referees' comments or queries, and send 3 copies of the revised manuscript, together with the diskette, back to me as soon as possible.

Looking forward to receiving the revised manuscript and your reply to the referees from you soon. Thank you again for your interest in contributing to our journal.

Yours sincerely,

Prof. Dr. MR. Jisnuson Svasti

Editor ScienceAsia

J. Shurz.



July 4, 2001

Dr. Somchai Wongwises, Department of Mechanical Engineering, KMUTT. Bangkok 10140.

Dear Dr. Somchai.

Thank you very much for submitting the manuscript entitled: Pressure Distribution of Refrigerant Capillary Tubes (Code 0012-152, received 7 December 2000, 1st revision received 24 May 2001) for consideration for publication in ScienceAsia.

The revised manuscript has been read by one of the two referees, whose report is enclosed for your information. Please reply to every point of the referees' comments or queries, and send 3 copies of the revised manuscript with the attached sheet(s) indicating responses or changes in the manuscript against the referees' amendments, together with the diskette, back to me as soon as possible.

Looking forward to receiving the revised manuscript and your reply to the referee from you soon. Thank you again for your interest in contributing to our journal.

Yours sincerely.

Prof. Dr. MR. Jisnuson Svasti

Editor ScienceAsia



August 20, 2001

Dr. Somchai Wongwises, Department of Mechanical Engineering, KMUTT. Bangkok 10140.

Dear Dr. Somchai,

Thank you very much for submitting the manuscript entitled: Pressure Distribution of Refrigerant Capillary Tubes (Code 0012-152, received 7 December 2000) for consideration for publication in Science Asia.

The manuscript has been read by two independent referees, who have recommended acceptance of the manuscript for publication in ScienceAsia. Would you please ensure that your final manuscript follows the style of the journal, especially references, and send to us together with a diskette of the final manuscript. Your paper is expected to be published in ScienceAsia Vol. 28 No. 1. You will receive further information later.

Thank you for your interest in contributing to our journal.

Yours sincerely,

Prof. Dr. MR. Jisnuson Svasti

Editor ScienceAsia

Pressure Distribution of Refrigerant Flow in an Adiabatic Capillary Tube

Somchai Wongwises*, Pakawat Kritsadathikarn, Tirawat Songnetichaovalit and Noppadon Lokathada

Fluid Mechanics, Thermal Engineering and Multiphase Flow Research Laboratory (FUTURE)

Department of Mechanical Engineering,

King Mongkut's University of Technology Thonburi,

Bangmod, Bangkok 10140, Thailand

* Corresponding author, E-mail: somchai.won@kmutt.ac.th

ABSTRACT

This paper presents the results from a numerical study on the local pressure distribution of some common traditional and alternative refrigerants flowing in adiabatic capillary tubes. The present model developed from the basic conservation law of mass, energy and momentum includes various relevant parameters. A homogeneous flow model is used in the two-phase flow region. Numerical results show that the alternative refrigerants used as examples in the present study consistently give higher pressure gradients than the traditional refrigerants. The present model can be used to simulate and compare the flow characteristics of the other refrigerants. It may be also an important tool for selecting the length of the capillary tube used in household refrigerators and freezers for given operating conditions.

Keywords: Two-phase flow, Local pressure distribution, Pressure gradient, Refrigerant, Capillary tube

INTRODUCTION

The small bore capillary tube is the most widely used as expansion device in small domestic vapor compression air conditioners and refrigerators. The main concern in practical consideration is to determine the appropriate tube diameter and length at a given operating condition. The investigation on the flow characteristics in the capillary tubes has received the most attention ¹⁻⁹. Bansal et al. ¹ developed a homogeneous two-phase flow model, CAPIL, to study the performance of adiabatic capillary tubes. They used the REFPROP data base to calculate the refrigerants' thermodynamic and thermophysical properties.

Sami et al. ⁷ proposed a numerical model for predicting the capillary tube performance of pure refrigerants (R12, R22, R134a) and binary mixtures (R410A, R410B, R507, R32/R134a). Wong et al. ⁹ developed a homogeneous two-phase flow model to simulate the flow characteristics of R12 and R134a. The results showed that the differences in flow characteristics are due to minor differences in refrigerant properties. Wongwises ¹⁰ provided the results of simulations using an adiabatic capillary tube model. The investigation was concerned about making comparisons of the pressure distributions between various alternative mixtures of refrigerant. Jung et al. ³ modified the Stoecker's model ¹¹ to provide simple correlations for sizing the capillary tubes used with R22, R134a, R407C and R410A. Effects of the sudden contraction at capillary tube inlet, degree of subcooling, friction factors and various viscosity models were discussed. Melo ⁵ investigated experimentally the effects of the condensing pressure, size of adiabatic capillary tube, subcooling and the types of the refrigerant (R12, R134a and R600A) on the mass flow rates.

There is relatively little information in the open literature on comparisons of flow characteristics for traditional and alternative refrigerants flowing in a capillary tube. To be a guide-line in the future for selecting the appropriate refrigerants, in the present study, the main concern is to study on the pressure distribution of various refrigerants along the capillary tube and to compare the flow characteristics between some pairs of refrigerants.

MATHEMATICAL MODEL

The flow of refrigerant in a capillary tube used as an expansion device in the refrigerating system is divided into two regions; a single-phase sub-cooled liquid region and a two-phase vapour-liquid flow region.

SINGLE- PHASE SUB-COOLED LIQUID REGION

The single-phase sub-cooled liquid region is the region from the capillary tube inlet to the position where the saturation pressure corresponds to the temperature at the capillary inlet. For steady and fully-developed incompressible flow, the integral form of the momentum equation at distance dz in a capillary tube is

$$A_0 dP + \tau_W(\pi d) dz = 0$$
 (1)

where τ_W is the wall shear stress and defined as

$$\tau_{\rm W} = f \frac{(\rho_{\rm L} V_{\rm L}^2)}{8} \tag{2}$$

where f is the Moody friction factor and can be determined from Colebrook's correlation as follows;

$$\frac{1}{f^{0.5}} = -2 \log \left(\frac{e/d}{3.7} + \frac{2.51}{Re_L f^{0.5}} \right)$$
 (3)

Substituting Eq. (2) into Eq. (1), the single phase length (L_{SC}) of the capillary tube is obtained:

$$L_{sc} = \left(p_i - p_{sat} \right) / \left(f \frac{G^2}{2\rho_L d} \right)$$
 (4)

where the total mass flux (G) is the total mass flow rate of fluid divided by total cross-sectional area of the tube (A_o) .

TWO-PHASE FLOW REGION

In the present study, the model used in the two-phase region is derived from the one dimensional homogeneous two-phase flow assumption. The model is based on that of Wong et al. ⁹ and Wallis ¹³. The basic physical equations governing the capillary tube flow are the conservations of mass, energy and momentum.

First, the specific enthalpy at a saturation state of a pure substance having a specific quality can be determined by using the definition of quality (x) as follows;

$$h = h_1 (1 - x) + h_G x$$
 (5)

With no applied works and neglecting the elevation changes, the following form of energy equation for refrigerant flow in a capillary tube is obtained:

$$\frac{d}{dz}\left(xh_G + (1-x)h_L + \frac{V^2}{2}\right) = 0$$
 (6)

where the quality of the mixture in a saturated condition (x) is the ratio of the vapour mass flow rate to total mass flow rate and the velocity of each phase is equal ($V = V_G = V_L$).

For a pure substance in the equilibrium homogeneous two-phase region, the enthalpies and densities are functions of pressure (h = h(p), $\rho = \rho(p)$).

Mass fluxes of vapour and liquid phase (G_G and G_L) are the mass flow rates of the vapour and liquid divided by the cross-sectional area of the capillary tube, so

$$G_G = G_L = \rho V \tag{7}$$

Void fraction (α) is a terminology in the two-phase flow study, it represents the time-averaged fraction of the cross-sectional area or of the volume which is occupied by the vapour phase. The general equation for determining the void fraction in the homogeneous flow is

$$\alpha = \frac{1}{1 + \left(\frac{1 - x}{x} \frac{\rho_G}{\rho_L}\right)}$$
 (8)

Actual average velocity of vapour and liquid phases (V_G and V_L) can be obtained from

$$V = Gv = G(xv_G + (1-x)v_L)$$
(9)

After all above equations are rearranged, the following form of the total pressure gradient is obtained:

$$\frac{dP}{dz} = -\frac{dx}{dz} \left(\frac{A}{B} \right) \tag{10}$$

where

$$A = h_{LG} + G^2 v v_{LG}$$

$$B = x \frac{dh_G}{dP} + (1-x) \frac{dh_L}{dP} + G^2 v \left[x \frac{dv_G}{dP} + (1-x) \frac{dv_L}{dP} \right]$$

The total pressure gradient $\left(\frac{dP}{dz}\right)$ is often expressed as the sum of the three distinct components, so

$$\frac{dP}{dz} = \left(\frac{dP}{dz}\right)_{f} + \left(\frac{dP}{dz}\right)_{a} + \left(\frac{dP}{dz}\right)_{g}$$
 (11)

Three terms on the right hand side are represented the frictional, accelerational, and gravitational components of the total pressure gradient, respectively.

Frictional term in Eq.(11) can be obtained from

$$\left(\frac{dP}{dz}\right)_{f} = \frac{-f_{tp} G^{2}(xv_{G} + (1-x)v_{L})}{2d}$$
(12)

Accelerational term in Eq.(11) can not be measured directly. However, it can be calculated from the momentum flux as follows;

$$\left(\frac{dP}{dz}\right)_{a} = -G^{2}\left(\frac{dP}{dz}\right)\left(x\frac{d\upsilon_{G}}{dP} + (1-x)\frac{d\upsilon_{L}}{dP}\right) - G^{2}\upsilon_{LG}\frac{dx}{dz}$$
(13)

Gravitational term in Eq.(11) can be negligible because the flow is horizontal.

Substituting Eqs. (12) and (13) into Eq. (11), gives

$$\frac{dx}{dz} = \frac{\left(\frac{dP}{dz}\right)_{f} - C\frac{dP}{dz}}{D} \tag{14}$$

where

$$C = 1 + G^{2} \left(\frac{x dv_{G}}{dP} + \frac{(1 - x)}{dP} \frac{dv_{L}}{dP} \right)$$

$$D = G^{2} v_{LG}$$

The two-phase friction factor (f_{tp}) can be calculated from Colebrook's equation with the Reynolds number being defined as:

$$Re = \frac{Gd}{\mu_{tp}}$$
 (15)

The following Dukler 's equation 14 is used to determine μ_{tp} :

$$\mu_{\text{tp}} = \frac{x v_{\text{G}} \mu_{\text{G}} + (1 - x) v_{\text{L}} \mu_{\text{L}}}{x v_{\text{G}} + (1 - x) v_{\text{L}}}$$
(16)

where μ_L and μ_G are absolute viscosity of liquid and gas, respectively.

SOLUTION METHODOLOGY

In the present study, the following pairs of refrigerants whose properties are very similar are chosen as examples and used in the present simulation;

- R12 vs R134a,
- R12 vs R409A (R22/124/142b; 60/25/15)
- R12 vs R409B (R22/124/142b; 65/25/10)
- R501 (R22/12; 75/25) vs R402A (R125/290/22; 60/2/38)
- R501 (R22/12; 75/25) vs R402B (R125/290/22; 38/2/60)

All thermodynamic and transport properties of refrigerants are taken from REFPROP ¹² and are developed as a function of pressure. The calculation is divided into two steps; sub-cooled single-phase region and two-phase vapour liquid region. Initial conditions required in the calculation are temperature and pressure of refrigerant at capillary tube inlet, roughness and diameter of the capillary tube and mass flow rate of refrigerant. In the single-phase flow region, after substituting the friction factor calculated from Colebrook equation and the saturation pressure at the capillary inlet temperature into Eq.(4), the single-phase region length is obtained. The end condition of the single phase flow region is used to be an inlet condition of the two-phase flow region. The Runge-Kutta method is used to solve Eqs. (10) and (14) in the two-phase flow region. The calculation in two-phase flow region is terminated when the flow is at the critical flow condition. Total capillary tube length is the sum of the single and two-phase length.

RESULTS AND DISCUSSION

The refrigerant mass flow rate, temperature and pressure at the inlet of the capillary tube, diameter and relative roughness of the tube were each varied in turn to investigate the effect on the total length of capillary tube. The results from the simulation are properties at each position along the capillary tubes. Figures 1,2,3 and 6 show the variation of the local pressure of all refrigerants with position along the capillary tube. In the sub-cooled liquid region, due to friction, the pressure of refrigerant drops linearly. After the position of the inception of vaporization due to both friction and acceleration, the pressure of refrigerant drops rapidly and more rapidly as flow approaches the critical flow condition. However, in real situation, the actual point of inception of vaporization may not occur at the end of the sub-cooled liquid region because of the delay of vaporization. In order to validate the present model, comparisons are made with limited available measured data of Li et al. ⁴ which were obtained from 10 pressure transducers installed along the capillary tube. Figures 1 and 2 also compare the simulation results obtained from the present model with the R12 data measured by Li et al. ⁴ The model is shown to fit the data quite well.

Comparison on the pressure distributions of R12 and R134a (Figures 1 and 2), in general, the flow of R12 in the capillary tube gives a lower pressure gradient than that of R134a. In the other word, the total tube length for R134a is shorter. Comparisons on the pressure drop characteristics for the rest of each pair of refrigerant (R12 vs R409A and R409B; R501 vs R402A and R402B) show that for all cases in the single-phase region, the traditional refrigerant gives a slightly lower pressure gradient than the alternative refrigerants. In the two-phase flow region, the traditional refrigerant gives a momentous lower pressure gradient than the alternative refrigerant.

Figures 4 and 7 show the quality distributions along the capillary tube. For all cases, the quality in the single phase region is zero till the flash point at which the two-phase region begins and then increases more rapidly in a non-linear fashion as the critical flow condition is approached. It is also shown that in general, traditional refrigerants vaporize later than their corresponding alternative refrigerants. Figures 5 and 8 show the distributions of temperature along the capillary tube for each pair of refrigerant type. In all cases, in the single phase region, because the flow is incompressible, the refrigerant temperature along the capillary tube remains constant. After the position of the inception of vaporization, the temperature drops rapidly as the flow approaches the critial flow condition. In general, the traditional refrigerants give longer total capillary tube length.

CONCLUSIONS

A homogeneous two-phase flow model is modified to study the flow characteristics of some refrigerants flowing in adiabatic capillary tubes. The basic governing equations are based on the conservations of mass, energy and momentum. The differential equations obtained are solved simultaneously by the Runge-Kutta method. It is found that even the differences in properties of each pairs of the refrigerants is small, the differences on the overall system performance may be meaningful. By varying various input parameters, it is found that the traditional refrigerants consistently give lower pressure gradients and give longer total length of the capillary tube.

ACKNOWLEDGMENTS

This work was given financial supported by the Thailand Research Fund whose guidance is gratefully acknowledged. The first author wish to acknowledge his lovely undergraduate students; Mr. Pakawat Kritsadathikarn, Mr. Tirawat Songnetichaovalit and Mr. Noppadon Lokathada for their generous assistance.

NOMENCLATURE

A_o cross-sectional area of tube, m² d diameter of the capillary tube, m

e roughness, m f friction factor

G mass flux, kg/s m² h specific enthalpy, kJ/kg

m mass flow rate, kg/s P pressure, MPa

Re Reynolds number T Temperature, °C

V velocity, m/s x quality

z axial; direction or length, m α void fraction

μ absolute viscosity, Pa s υ specific volume, m³/kg

o density, kg/m³ τ shear stress, N/m²

Subscripts

a accelerational " f frictional g gravitational " G vapour i capillary tube inlet L liquid

sat saturation SC single-phase sub-cooled

tp two-phase w wall

REFERENCES

- Bansal, P.K. and Rupasinghe, A.S., An homogeneous model for adiabatic capillary tubes, Applied Thermal Eng., 18 (1998) 207-219.
- 2. Bittle, R.R. and Pate, M.B., A theoretical model for predicting adiabatic capillary tube performance with alternative refrigerants, ASHRAE Transactions, 100 (1994) 52-64.
- 3. Jung, D., Park, C. and Park, B., Capillary tube selection for HCFC22 alternatives, *Int. J. Refrigeration*, 22 (1999) 604-614.
- Li, R.Y., Lin, S. and Chen, Z.H., Numerical modeling of thermodynamics nonequilibrium flow of refrigerant through capillary tubes, ASHRAE Transactions, 96 (1990) 542-549.
- 5. Melo, C., Ferreira, R.T.S., Neto, C.B., Goncalves, J.M. and Mezavila, M.M., An experimental analysis of adiabatic capillary tubes, *Applied Thermal Engineering*, 19 (1999) 669-684.
- 6. Mikol, E.P., Adiabatic single and two phase flow in small bore tube, ASHRAE J., 5 (1963) 75-86.
- 7. Sami, S.M. and Tribes, C., Numerical prediction of capillary tube behaviour with pure and binary alternative refrigerants, *Applied Thermal Engineering*, 18 (1998) 491-502.
- Wong, T.N. and Ooi, K.T., Adiabatic capillary tube expansion device: A Comparison of the Homogeneous Flow and the Separated Flow Models, *Applied Thermal Engineering*, 16 (1996) 625-634.
- 9. Wong, T.N. and Ooi, K.T., Evaluation of capillary tube performance for CFC12 and HFC134a, *Int. Com. Heat Mass Transfer*, **23** (1996) 993-1001.
- Wongwises, S. and Pirompak, W., Flow Characteristics of Pure Refrigerants and Refrigerant Mixtures
 in Adiabatic Capillary Tubes, Applied Thermal Engineering, 21 (2001) 845-861.
- 11. Stoecker, W.F. and Jones, J.W., Refrigeration and air conditioning, McGraw-Hill (1982).
- 12. REFPROP, Thermodynamic properties of refrigerants and refrigerant Mixtures, version 6.01, Gaithersburg, M.D. National Institute of Standards and Technology (1998).
- 13. Wallis, G.B., One dimensional two-phase flow, McGraw-Hill (1969).
- Dukler, A.E., Wicks, M. and Cleveland, R.G., Frictional pressure drops in two-phase flow, AIChE Journal, 10 (1964) 38-51.

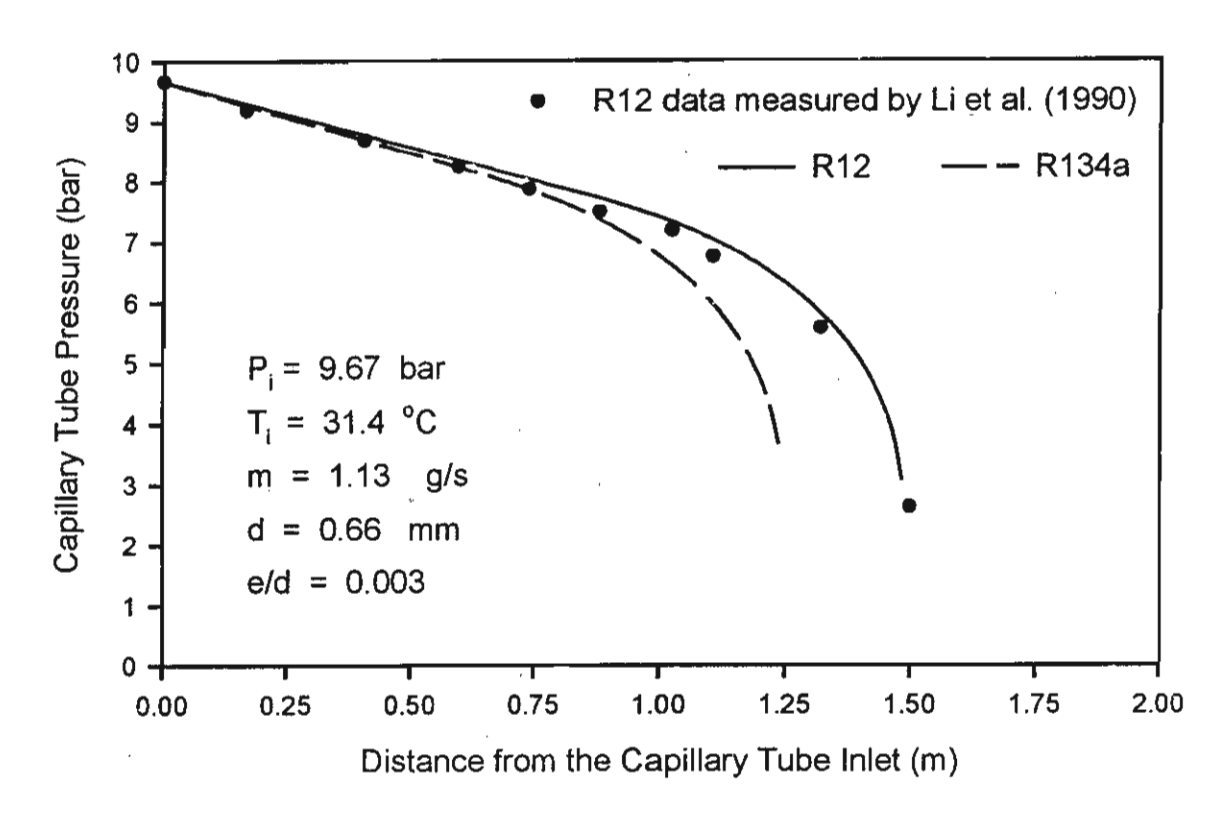


Fig.1 Comparison of pressure distributions along the capillary tube for R12 and R134a

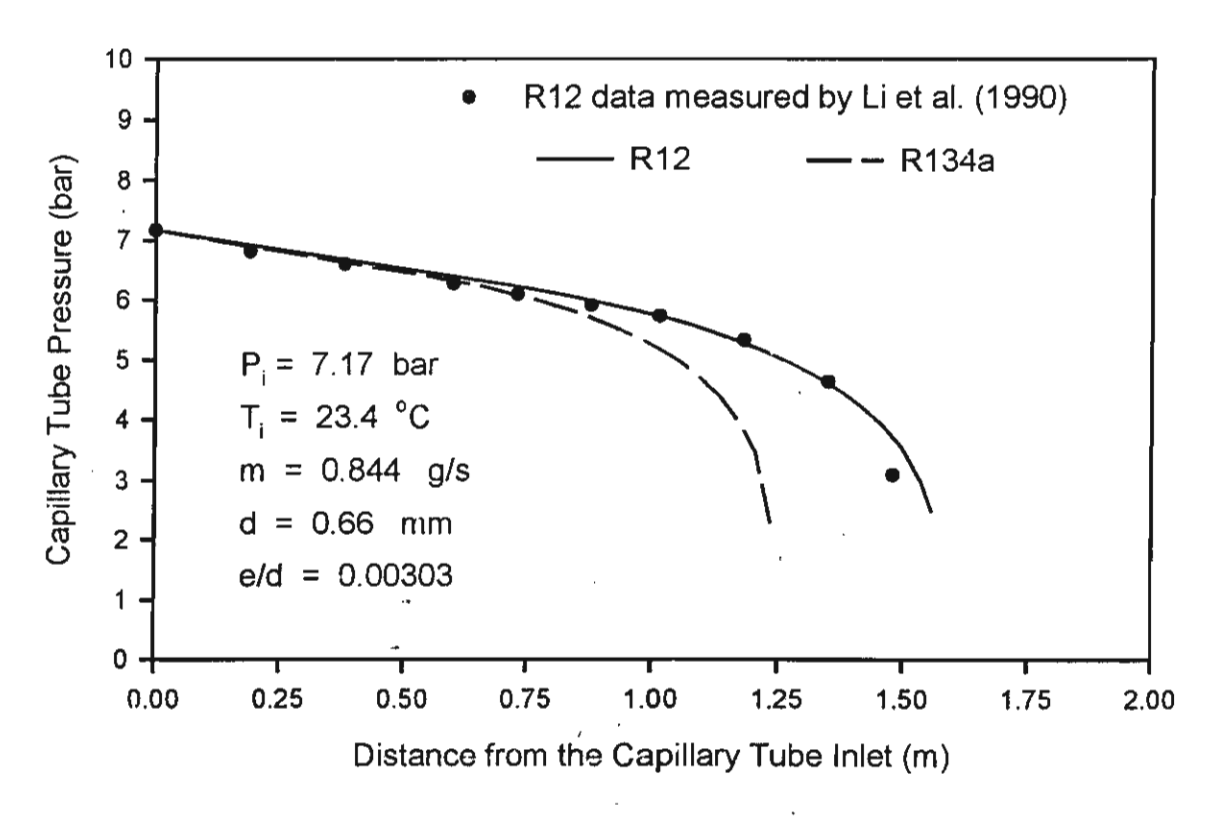


Fig.2 Comparison of pressure distributions along the capillary tube for R12 and R134a

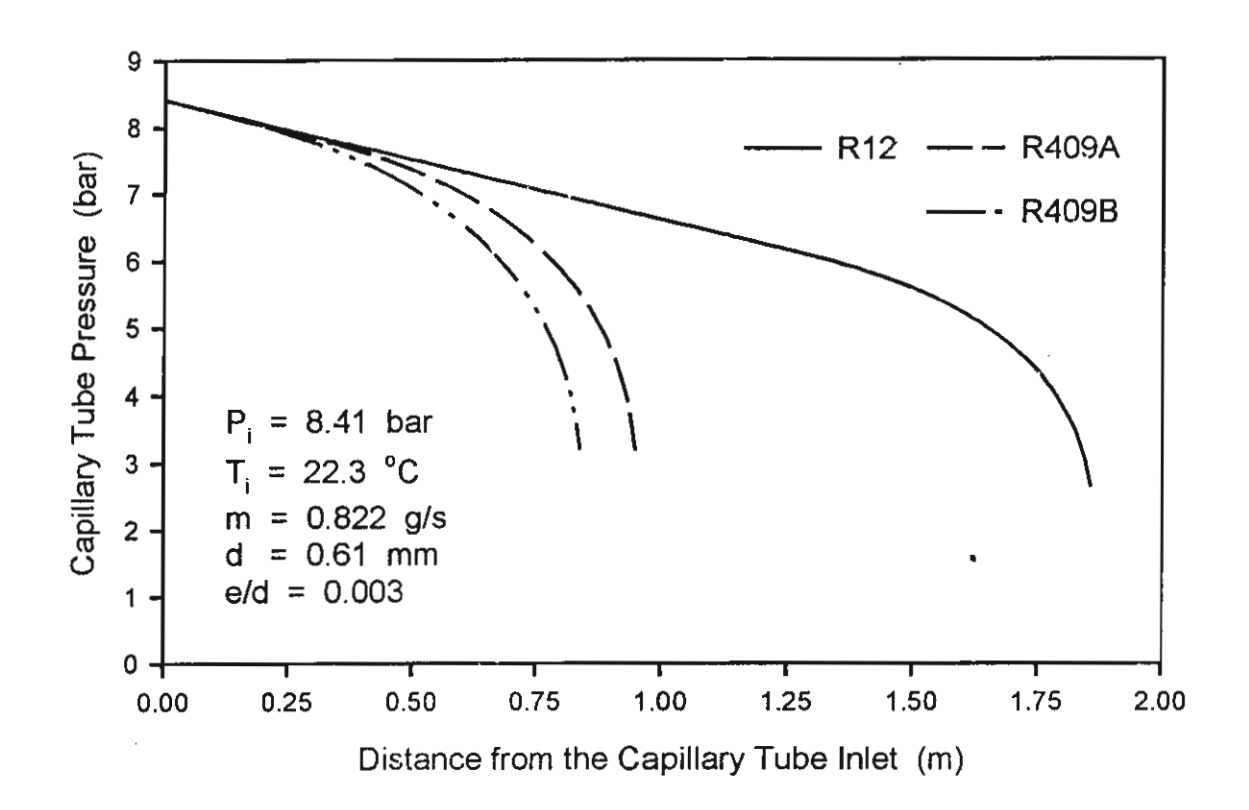


Fig. 3 Comparison of pressure distributions along the capillary tube for R12, R409A and R409B

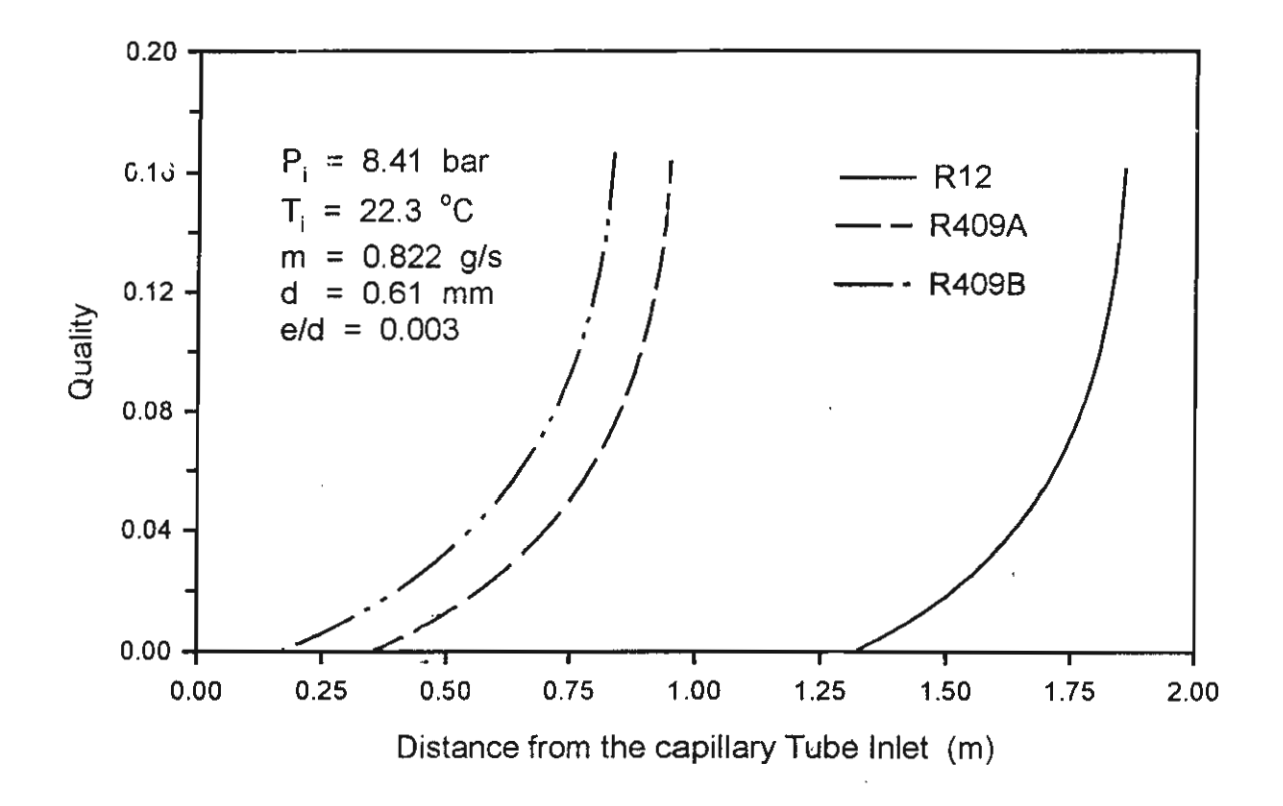


Fig. 4 Comparison of quality distributions along the capillary tube for R12, R409A and R409B

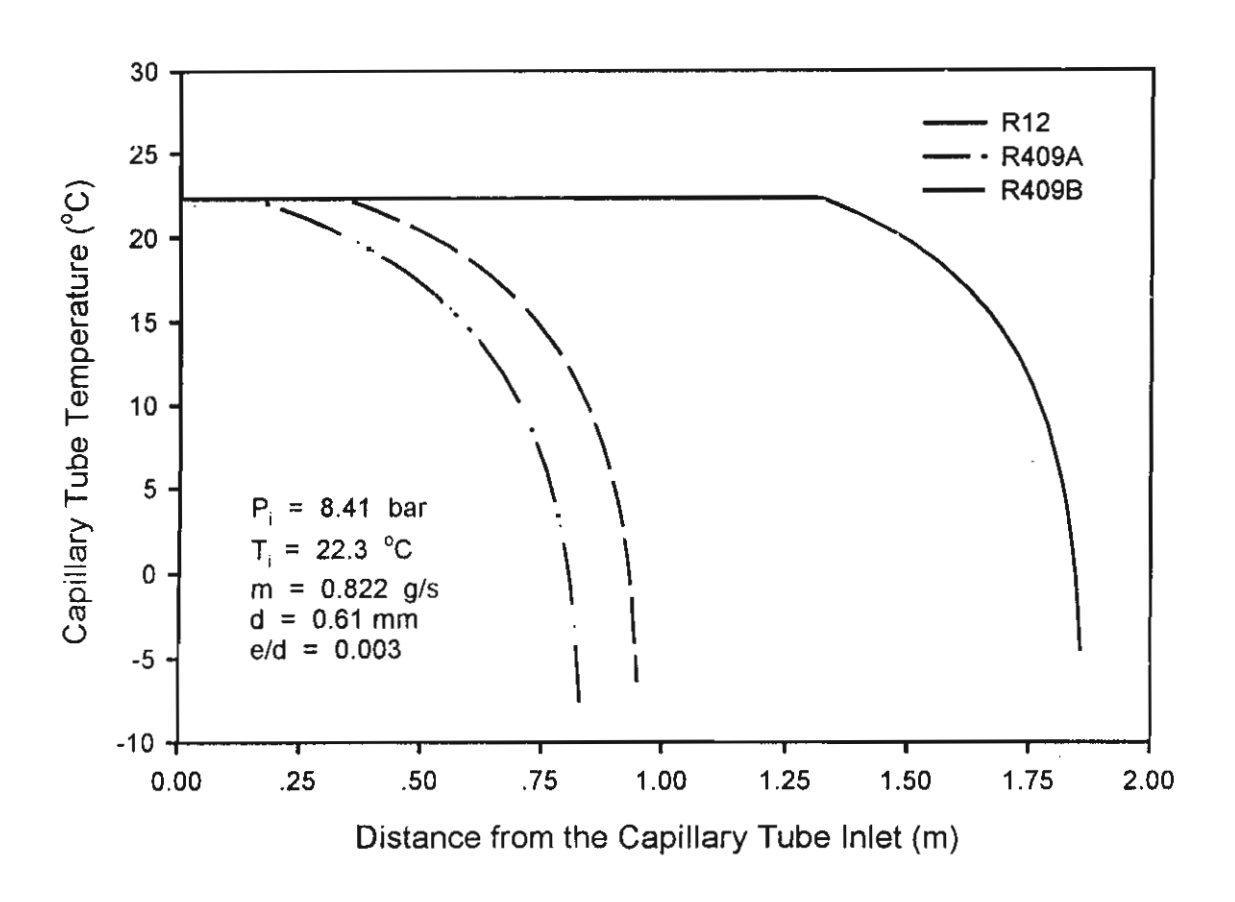


Fig. 5 Comparison of temperature distributions along the capillary tube for R12, R409A and R409B

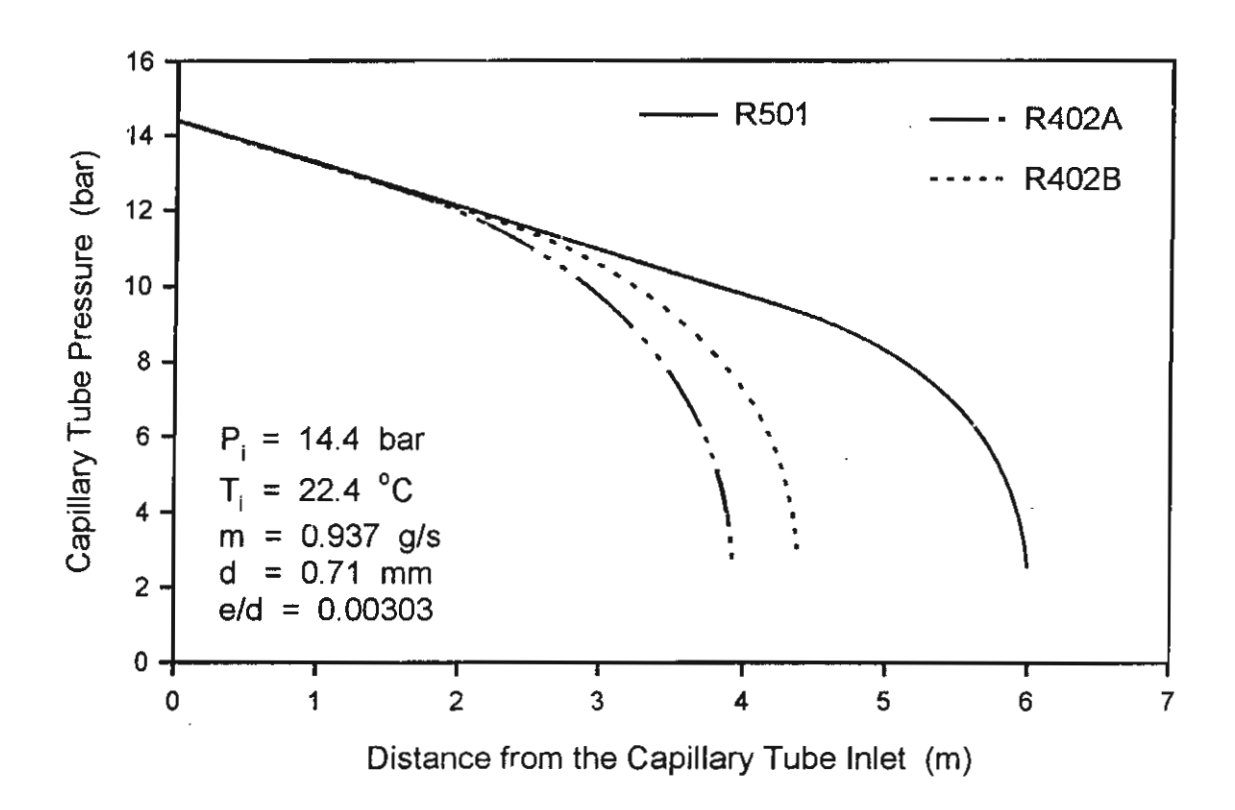


Fig. 6 Comparison of pressure distributions along the capillary tube for R501, R402A and R402B

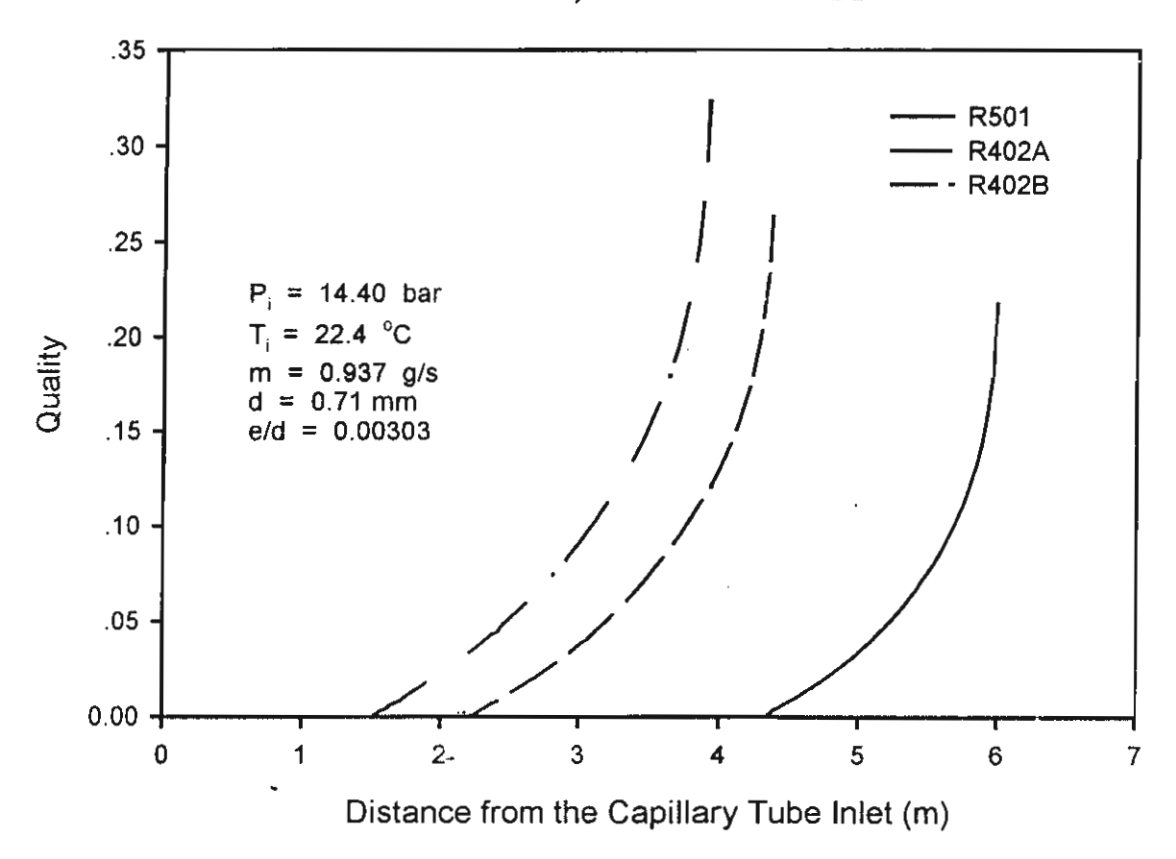


Fig. 7 Comparison of quality distributions along the capillary tube for R501, R402A and R402B

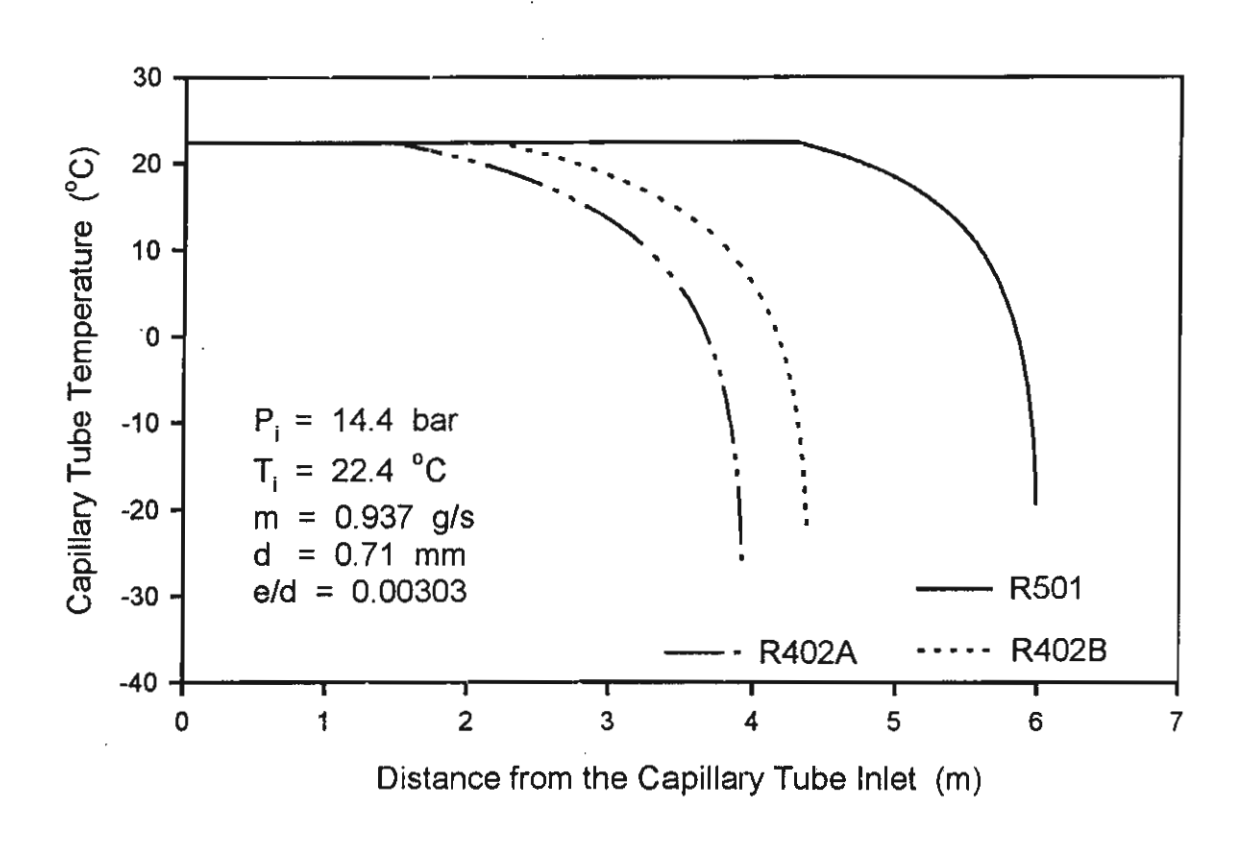


Fig. 8 Comparison of temperature distributions along the capillary tube for R501, R402A and R402B

Wongwises, S., Songnetichavarit, T., Lokathada, N., Kritsadathikarn, P., Investigation on Adiabatic Flows of Traditional and Alternative Refrigerants Through Capillary Tubes, *J.of Energy Heat and Mass Transfer* (in press).

JOURNAL OF ENERGY HEAT AND MASS TRANSFER

I.I.T. Madras Campus Chennai - 600 036, INDIA.

÷ +91 (44) 445 - 9359

+91 (44) 445 - 8209 -ax : +91 (44) 235 - 3094

+91 (44) 235 - 0509

E-mail: arbala@iitm.ac.in



Editors:

A.R. Balakrishnan, Ph.D. (Waterloo) N.K. Anand, Ph.D. (Purdue)

Editor Emeritus :

V.M.K. Sastri, Ph.D. (Dalaware)

May 11, 2001

Dr. Somchai Wongwises
Department of Mechanical Engineering
King Mongkut University of Technology Thonburi
Suksawas 48
Radburana, Bangkok 10140
Thailand

Re: Manuscript Number JEHMT/25 entitled "Investigation on Adiabatic Flows of Alternative Refrigerants Through Capillary Tubes" by S. Wongwises, P. Kritsadatlıkarn, T. Songnetichaovalit and N. Lokathada.

Dear Dr. Wongwises:

Please find enclosed the review received on your paper cited above. The reviewer has a few comments which I would like you to incorporate in the text. The revised manuscript may be sent to me in duplicate.

It is generally presumed by this Journal that if the revised version is not received by the editorial office within four months, the authors are no longer interested in publishing with us. I, therefore, request you to kindly send your revised paper well before this deadline.

A copy of the guidelines to authors is enclosed for your reference.

Thanking you,

Yours sincerely,

Prof. A. R. Balakrishnan

R. A. 3-1-1-

Editor

Encl: 1. Review Comments
2. Authors' guidelines

Somchai Wongwises

From: <arb_ijhmt@che.iitm.ac.in>
To: <somchai.won@kmutt.ac.th>
Sent: Thursday, July 19, 2001 1:31 PM

Dr. Somchai Wongwises
Department of Mechanical Engineering
King Mongkut University of Technology Thonburi
Suksawas 48
Radburana, Bangkok 10140
Thailand

Re: Manuscript Number JEHMT/25 entitled "Investigation on Adiabatic Flows of Alternative Refrigerants Through Capillary Tubes" by S. Wongwises, P. Kritsadathikarn, T. Songnetichaovalit and N. Lokathada.

Dear Dr. Wongwises:

Thank you for your revised version of the above paper. I am pleased to inform you that it has been accepted for publication in the Journal of Energy Heat and Mass Transfer.

You will receive the proofs shortly.

With regards,

Yours sincerely,

Prof. A. R. Balakrishnan Editor, JEHMT

Investigation on Adiabatic Flows of Traditional and Alternative Refrigerants Through Capillary Tubes

Somchai Wongwises, Tirawat Songnetichaovalit, Noppadon Lokathada and Pakawat Kritsadathikarn

Fluid Mechanics, Thermal Engineering and Multiphase Flow Research Laboratory (FUTURE)

Department of Mechanical Engineering,

King Mongkut's University of Technology Thonburi,

Bangmod, Bangkok 10140, Thailand

ABSTRACT

In this paper, the local pressure, temperature and quality of some common traditional and environmentally acceptable alternative refrigerants flowing through adiabatic capillary tubes are numerically determined. The mathematical model is developed from the basic law of mass, energy and momentum conservations. Homogeneous flow is assumed for the two-phase liquid-vapor flow region. Numerical results reveal that, in general for both single-and two-phase regions, the alternative refrigerants used in this study consistently give higher pressure drops per unit length than the traditional refrigerants.

INTRODUCTION

The capillary tube is a kind of expansion devices used in small vapour-compression refrigerating and air conditioning systems. In practical consideration, the main concern is to determine the appropriate length and diameter of the tube at a given refrigeration capacity. The design and analysis of capillary tubes have been received the most attention, both analytically and experimentally [1-12]. Bansal et al.[1] presented a homogeneous two-phase flow model to study the performance of adiabatic capillary tubes. The REFPROP data base [14] which is based on the Carnahan-Starling-DeSantis equation of state was used to determine the refrigerant's properties. Sami et al.[10] presented a numerical model for predicting capillary tube performance using new alternative refrigerants, both pure and binary mixtures. Wong et al.[11] developed a homogeneous two-phase flow model to simulate and compare the flow characteristics of CFC12 and HFC134a. The results showed that even with minor differences in thermophysical properties of both refrigerants, the difference in pressure, temperature, mixture velocity and quality distributions in capillary tube may be significant. More recently, Jung et al.[4] modified the Stoecker's basic model [13] and provided simple correlations for sizing the capillary tubes for practicing engineers. Various effects due to subcooling, area contraction, different equations for viscosity and friction factor were considered. Melo [8] studied the effects of diameter and length of capillary tube, refrigerant subcooling, condensing pressure and

type of the refrigerant on the mass flow rates in adiabatic capillary tubes. The experiments were performed with R12, R134a and R600a. Wongwises et al. [12] provided the results of simulation using a developed adiabatic capillary tube model. The investigation was concerned about making comparisons between various alternative mixtures of refrigerant. Although some information is currently available on flow characteristics in adiabatic capillary tubes, there still remains room to discuss. The present study is concerned with making comparisons between some pairs of traditional refrigerants with alternative ternary refrigerant mixtures.

MATHEMATICAL MODEL

The flow of refrigerant through a capillary tube can be divided into two distinct regions as shown in Fig.1; a single-phase sub-cooled liquid region and a two-phase liquid-vapor region. In Fig.1, point 1 represents the capillary tube inlet at the conderser side, point 2 represents the capillary tube inlet at the capillary tube side, point 3 is the end of the single- phase subcooled liquid (saturation point) or the beginning of the two-phase region, point 4 is the capillary tube exit at the capillary tube side and point 5 represents the capillary tube exit at the evaporator side. The typical pressure-enthalpy relationship from point 1-5 is shown in Fig.2

The mathematical model developed is based on the assumptions as follows;

- one-dimensional flow,
- adiabatic and homogeneous two-phase flow,
- straight horizontal and constant inner diameter and roughness capillary tube,
- thermodynamic equilibrium through the capillary tube
- no metastable liquid region

SUB-COOLED LIQUID REGION

The sub-cooled liquid region is the region from the inlet of the capillary tube to the position where the saturation pressure corresponds to the inlet temperature. For steady fully-developed incompressible flow, the integral form of the momentum equation at distance dz in a capillary tube is

$$_{..}A_{o}dP + \tau_{W}(\pi d)dz = 0$$
 (1)

where τ_W is the wall shear stress and defined as

$$\tau_{W} = f \frac{(\rho_{L} V_{L}^{2})}{8} \tag{2}$$

where f is the Moody friction factor and can be determined from Colebrook's correlation as follows;

$$\frac{1}{f^{0.5}} = -2\log\left(\frac{e/d}{3.7} + \frac{2.51}{Re_L f^{0.5}}\right)$$
(3)

Substituting Eq. (2) into Eq. (1), the single phase subcooled liquid length, L_{SC}, of the capillary tube can be obtained

$$L_{sc} = \frac{\left(p_i - p_{sat}\right)}{\left(f \frac{G^2}{2\rho_L d}\right)} \tag{4}$$

where the total mass flux, G, is the total mass flow rate divided by total cross-sectional area of channel, Ao.

TWO-PHASE FLOW REGION

In the two-phase flow region, the model is derived from the one dimensional homogeneous two-phase flow assumption. The model is based on that of Wong et al.[11] and Wallis [15]. In the modeling, the basic physical equations governing the capillary tube flow are the continuity and conservations of energy and momentum.

The specific enthalpy of a substance at a saturation state having a given quality can be calculated by utilizing the definition of quality, x,

$$h = x h_G + (1 - x) h_L (5)$$

where the quality is the ratio of the mass flow rate of vapour to total mass flow rate when a substance is in a saturation state.

For homogeneous flow, the velocity of each phase can be expressed as

$$V = V_G = V_L \tag{6}$$

Also, for refrigerant flow in a capillary tube with no externally applied works and neglecting the elevation changes, the following form of energy equation is obtained

$$\frac{d}{dz} \left(x h_G + (1 - x) h_L + \frac{V^2}{2} \right) = 0$$
 (7)

In the homogeneous two-phase region for a pure substance in equilibrium, the enthalpies (and also densities) may be arranged in the function of pressure,

$$h = h(p), \quad \rho = \rho(p) \tag{8}$$

Vapour mass flux, G_G , and liquid mass flux, G_L , are the vapour and liquid mass flow rates divided by total cross-sectional area of channel, so

$$G_G = G_L = \rho V \tag{9}$$

In liquid-vapour flows, void fraction, a, usually represents the time-averaged fraction of the cross-sectional area (or the volume) which is occupied by the vapour phase. The homogeneous flow model takes into account the fact that the two phases physically flow with same velocities. This general correlation is then

$$\alpha = \frac{1}{1 + \left(\frac{1 - \mathbf{x}}{\mathbf{x}} \frac{\rho_{G}}{\rho_{I}}\right)} \tag{10}$$

$$= \alpha(x,p) \tag{11}$$

Actual average velocity of vapour and liquid can be determined from

$$V = G \upsilon = G(x \upsilon_G + (1-x)\upsilon_L)$$
 (12)

Eventually, after rearrangement using above correlations, an expression for the total pressure gradient is obtained as follows;

$$\frac{dP}{dz} = -\frac{dx}{dz} \left(\frac{A}{B} \right) \tag{13}$$

where

$$A = h_{LG} + G^2 v v_{LG}$$

$$B = x \frac{dh_G}{dP} + (1-x) \frac{dh_L}{dP} + G^2 \upsilon \left[x \frac{d\upsilon_G}{dP} + (1-x) \frac{d\upsilon_L}{dP} \right]$$

The momentum equation is often rewritten as an explicit equation for the pressure gradient. The total pressure gradient $\left(\frac{dP}{dz}\right)$ is, therefore, expressed as the sum of the three different components, so

$$\frac{dP}{dz} = \left(\frac{dP}{dz}\right)_{f} + \left(\frac{dP}{dz}\right)_{a} + \left(\frac{dP}{dz}\right)_{g}$$
(14)

The three terms on the right hand side are regarded as frictional, accelerational, and gravitational components of the total pressure gradient. Gravitational term in Eq.(14) is negligible because the flow is horizontal. Accelerational pressure gradient can not be measured directly. However, it can be calculated from momentum flux as follows;

$$\left(\frac{dP}{dz}\right)_{a} = -\frac{m}{A_{o}} \frac{d(V)}{dz} \tag{15}$$

and, so

$$- = -G^2 \left(\frac{dP}{dz}\right) \left(x \frac{dv_G}{dP} + (1-x) \frac{dv_L}{dP}\right) - G^2 v_{LG} \frac{dx}{dz}$$

Frictional pressure gradient can be obtained from

$$\left(\frac{dP}{dz}\right)_{f} = \frac{-f_{tp} G^{2}(x \upsilon_{G} + (1-x)\upsilon_{L})}{2d}$$
(16)

Substituting Eqs. (15) and (16) into Eq. (14), gives

$$\frac{dx}{dz} = \frac{\left(\frac{dP}{dz}\right)_{f} - C\frac{dP}{dz}}{D}$$
(17)

where

$$C = 1 + G^{2} \left(\frac{x dv_{G}}{dP} + \frac{(1 - x)}{dP} \frac{dv_{L}}{dP} \right)$$

$$D = G^{2} v_{LG}$$

The friction factor for the homogeneous two-phase flow, f_{tp} , can be determined from Colebrook's equation with the Reynolds number being defined as:

$$Re = \frac{Gd}{\mu_{tp}}$$
 (18)

Dukler's equation [16] is used to calculate μ_{tp} as follows:

$$\mu_{tp} = \frac{x v_G \mu_G + (1-x) v_L \mu_L}{x v_G + (1-x) v_L}$$
 (19)

where μ_L and μ_G are dynamic viscosity of liquid and gas, respectively.

RESULTS AND DISCUSSION

The calculation is divided into two parts; sub-cooled single-phase region and two-phase vapour-liquid region. The thermodynamic and transport properties of all refrigerants are taken from REFPROP [14]. All properties are developed as a function of pressure. Initial conditions required in the calculation are pressure and temperature of refrigerant at capillary tube inlet (or condition at outlet of condenser), mass flow rate of refrigerant, roughness and diameter of the capillary tube. In the single-phase flow region, after substituting the friction factor calculated from Colebrook equation (eq.(3)) and the saturation pressure of refrigerant at the temperature at the capillary tube inlet, P_{sat} , into eq.(4), the single-phase region length is obtained. The exit condition of the single phase flow region is used to be an initial condition of the two-phase flow region. In the two-phase flow region, the Runge-Kutta method is used to solve equations (13) and (17). The calculation in two-phase flow region is terminated when the flow is at the choked flow condition (dP/dz $\rightarrow \infty$).

In the present study, the comparisons are concerned between the following pairs of refrigerants;

- R12 vs R134a,
- R12 vs R414B (R22/R124/R600a/R142b; 50/39/1.5/9.5)
- R12 vs R411A (R1270/R22/R152a; 1.5/87.5/11.0)
- R12 vs R411B (R1270/R22/R152a; 3/94/3)
- R22 vs R407A (R32/R125/R134a; 20/40/40)
- R22 vs R407B (R32/R125/R134a; 10/70/20)
- R22 vs R407D (R32/R125/R134a; 15/15/70)
- R500 (R12/R152a; 73.8/26.2) vs R401A (R22/R152a/R124; 53/13/34)
- R500 (R12/R152a; 73.8/26.2) vs R401B (R22/R152a/R124; 61/11/28)
- R500 (R12/R152a; 73.8/26.2) vs R401C (R22/R152a/R124; 33/15/52)

Figures 3-5 show the relationship between the pressure and temperature at the saturated conditions for each group of the refrigerant. As shown in the figures, the saturated conditions of refrigerant in each group are similar. However even with the small differences in property in each group, it is not necessary that performances of the system are similar and this issue will be investigated in the present study. The mass flow rate, pressure and temperature at the capillary tube inlet, diameter and relative roughness of tube were each varied in turn to investigate their effect on the total length of capillary tube. The results from the calculation by the present model developed are pressure, temperature and quality at each position along the capillary tubes. In order to validate the present model, comparisons are made with limited available measured data of Li et al. [7].

Figures 6-8 compare the simulation results of the present model with the R12 measured data obtained by Li et al.[7]. The experimental conditions used by Li et al. [7] are given in Table 1. The present model is shown to agree with the measured data.

Table 1 Experimental conditions of Li et al. [7]

Case	T _i (°C)	P _i (bar)	m (g/s)	d (mm)	e/d
1	30.00	8.85	4.35	1.17	0.003
2	31.40	9.67	1.13	0.66	0.003
3	23.40	7.17	0.844	0.66	0.003

Figures 6-8, 9, 11, 13 and 15 show variation of local pressure of all refrigerants with position along the capillary tube. In the subcooled liquid region, due to frictional effects in fully developed flow in a constant-area tube, the pressure of refrigerant drops linearly along the capillary tube. After the position of the inception of vaporization, due to frictional and accelerational effects, the pressure of refrigerant decreases relatively fast and, more and more rapidly as the flow approaches the critical flow condition. But in fact, due to the delay of vaporization, from a single-phase subcooled liquid to a two-phase mixture, the actual starting point of vaporization may not occur at the end of the single-phase liquid region or at the saturated liquid condition.

It should be noted that comparing the local pressure distribution of R12 and of R134a as shown in Figure 9, the flow of R12 through the capillary tube gives a lower pressure drop per unit length than that of R134a. In the other word, at the same total pressure drop, the total tube length by using R134a is shorter. Except Figs. 15-16, comparisons of the pressure drop characteristics for the rest of each pair of refrigerant type show that for all cases in the single-phase region, the elder traditional refrigerants flowing through the capillary tube give longer single-phase region and give a slightly lower pressure drop per unit length than the newer alternative refrigerants. In the two-phase flow region, the traditional refrigerants give a meaningfully lower pressure drop than the alternative refrigerant which results in a longer total tube length. In Fig.15, R500 gives lower pressure drop than R401A and R401B but gives higher pressure drop than R401C. This may be due to the difference in the composition of each refrigerant. R401A and R401B is quite difference from those in R401C. It is also interesting to note that the comparison between the pressure drop characteristics for R22 and R407D in Fig.13, R407D gives a little bit longer single phase region and slightly shorter two-phase flow region. The result shows that although both refrigerants have a difference in composition, the pressure distributions along the capillary tube are almost the same.

Figures 10, 12 and 14 show the distributions of the temperature along the capillary tube for each pair of refrigerant type. In all cases, in the single phase region, the refrigerant temperature remains constant along the capillary tube. After the position of the inception of vaporization, the temperature drops rapidly as the flow approaches the critial condition. In general, the traditional refrigerants show a slightly lower temperature drop along the capillary tube, which corresponds to the lower pressure drop. Figure 16 shows the quality distribution along the capillary tube. In the single phase region, the quality is zero til the flash point which the two-phase region begins and then increases more rapidly as the choked flow condition is approached. It is also shown that, in general, traditional refrigerants vaporize later than their corresponding alternative refrigerants.

CONCLUSIONS

A homogeneous flow model has been applied to determine the characteristics of refrigerants flowing through adiabatic capillary tubes. The basic physical governing equations are established from the conservations of mass, energy and momentum. The differential equations derived are solved by using the Runge-Kutta method. By varying the model input parameters, in general, it has been found that the traditional refrigerants consistently give lower pressure drops per unit length for both single-phase and two-phase regions. The present model includes the various relevant parameters and is a tool for sizing the capillary tubes used in household refrigerators and freezers, especially to select the capillary tube length for given operating conditions.

ACKNOWLEDGMENTS

The present study was supported financially by the Thailand Research Fund (TRF) and National Energy Policy Office (NEPO) whose guidance and assistance are gratefully acknowledged.

NOMENCLATURE

A_o cross-sectional area of tube, m² d tube diameter, m e roughness, m f friction factor

G mass flux, kg/s m² lı specific enthalpy, kJ/kg

m mass flow rate, kg/s P pressure, MPa

Re Reynolds number T Temperature, °C

re regions number 1 Temperature

V velocity, m/s x quality

z axial; direction or length, m α void fraction

μ dynamic viscosity, Pa s υ specific volume, m³/kg

 ρ density, kg/m³ τ shear stress, N/m²

Subscripts

tp two-phase w wall

REFERENCES

- 1. Bansal, P.K. and Rupasinghe, A.S., An homogeneous model for adiabatic capillary tubes, *Applied Thermal Eng.*, 18, 207-219 (1998).
- Bittle, R.R. and Pate, M.B., A theoretical model for predicting adiabatic capillary tube performance with alternative refrigerants, ASHRAE Transactions, 100, 52-64 (1994).
- 3. Chen, Z.H., Li, R.Y., Lin, S. and Chen, Z.Y., A correlation for metastable flow of refrigerant 12 through capillary tubes, *ASHRAE Transactions*, **96**, 550-554 (1990).
- Jung, D., Park, C. and Park, B., Capillary tube selection for HCFC22 alternatives, Int. J. Refrigeration, 22,604-614 (1999).
- Koizumi, H. and Yokoyama, K., Characteristics of refrigerant flow in a capillary tube, ASHRAE Transactions, 86, 19-27 (1980).
- Kuehl, S.J. and Goldschmidt, V.W., Modeling of steady flows of R-22 through capillary tubes, ASHRAE Transactions, 97, 139-148 (1991).
- 7. Li, R.Y., Lin, S. and Chen, Z.H., Numerical modeling of thermodynamics nonequilibrium flow of refrigerant through capillary tubes, ASHRAE Transactions, 96, 542-549 (1990).
- 8. Melo, C., Ferreira, R.T.S., Neto, C.B., Goncalves, J.M. and Mezavila, M.M., An experimental analysis of adiabatic capillary tubes, *Applied Thermal Eng.*, 19, 669-684 (1999).
- 9. Mikol, E.P., Adiabatic single and two phase flow in small bore tube, ASHRAE J., 5, 75-86 (1963).
- Sami, S.M. and Tribes, C., Numerical prediction of capillary tube behaviour with pure and binary alternative refrigerants, *Applied Thermal Eng.*, 18, 491-502 (1998).
- 11. Wong, T.N. and Ooi, K.T., Evaluation of capillary tube performance for CFC12 and HFC134a, *Int. Com. Heat Mass Transfer*, 23, 993-1001 (1996).
- 12. Wongwises, S., Flow characteristics of pure refrigerants and refrigerant mixtures in adiabatic capillary tubes, *Applied Thaermal Engineering*, 21, 845-861 (2001).
- 13. Stoecker, W.F. and Jones, J.W., Refrigeration and air conditioning, McGraw-Hill (1982).
- 14. REFPROP, Thermodynamic properties of refrigerants and refrigerant Mixtures, version 6.01, Gaithersburg, M.D. National Institute of Standards and Technology (1998).
- 15. Wallis, G.B., One dimensional two-phase flow, McGraw-Hill (1969).
- 16. Dukler, A.E., Wicks, M. and Cleveland, R.G., Frictional pressure drops in two-phase flow, AIChE Journal, 10, 38-51 (1964).

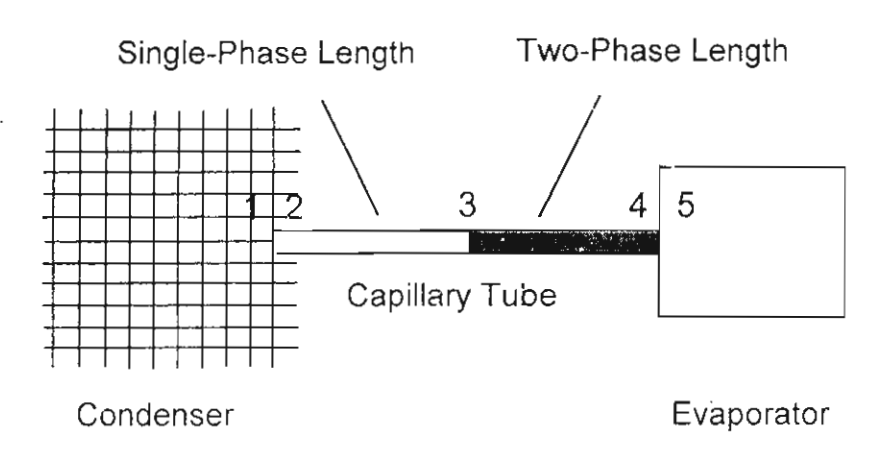


Fig. 1 Schematic diagram of an adiabatic capillary tube

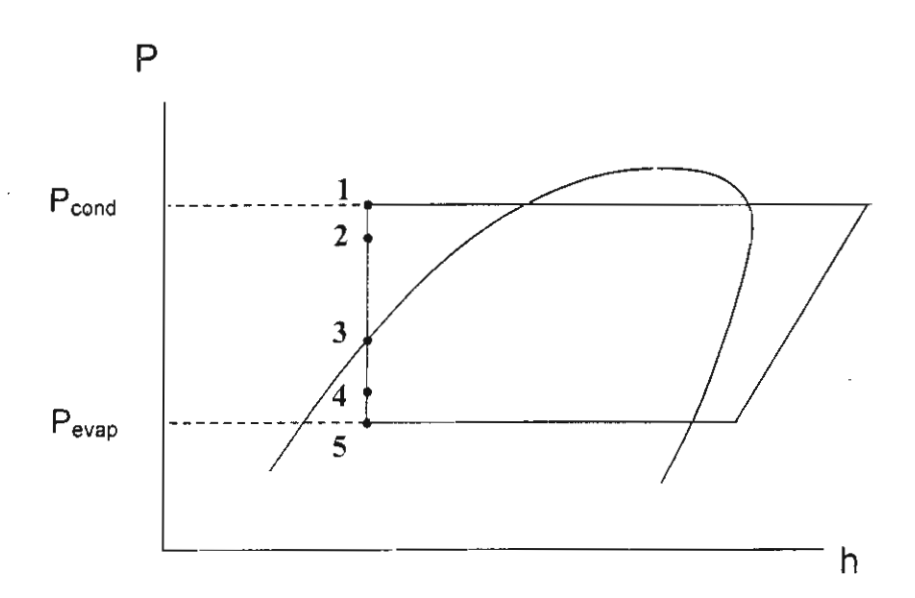


Fig. 2 Pressure – Enthalpy diagram for the vapor – compression cycle

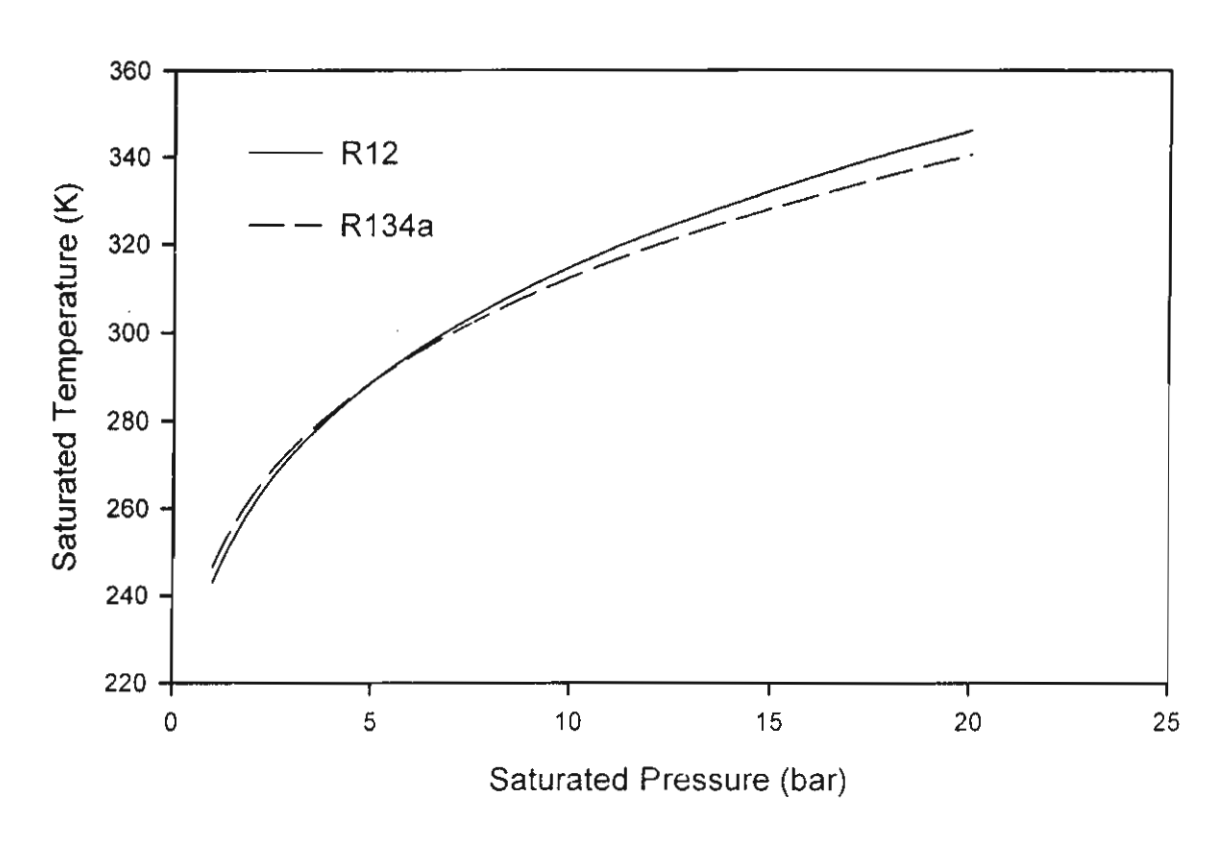


Fig. 3 Comparison of saturated pressure and temperature for R12 and R134a

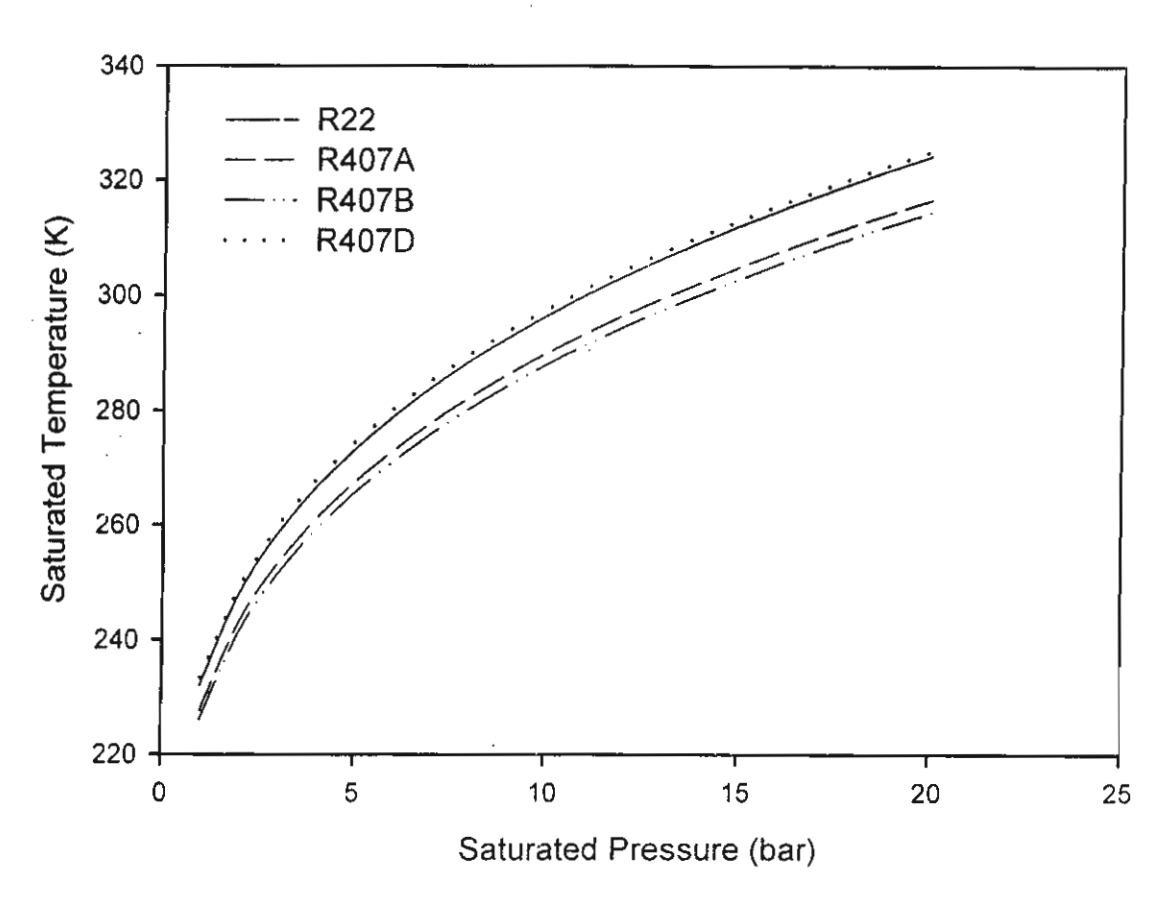


Fig. 4 Comparison of saturated pressure and temperature for R22, R407A, R407B and R407D

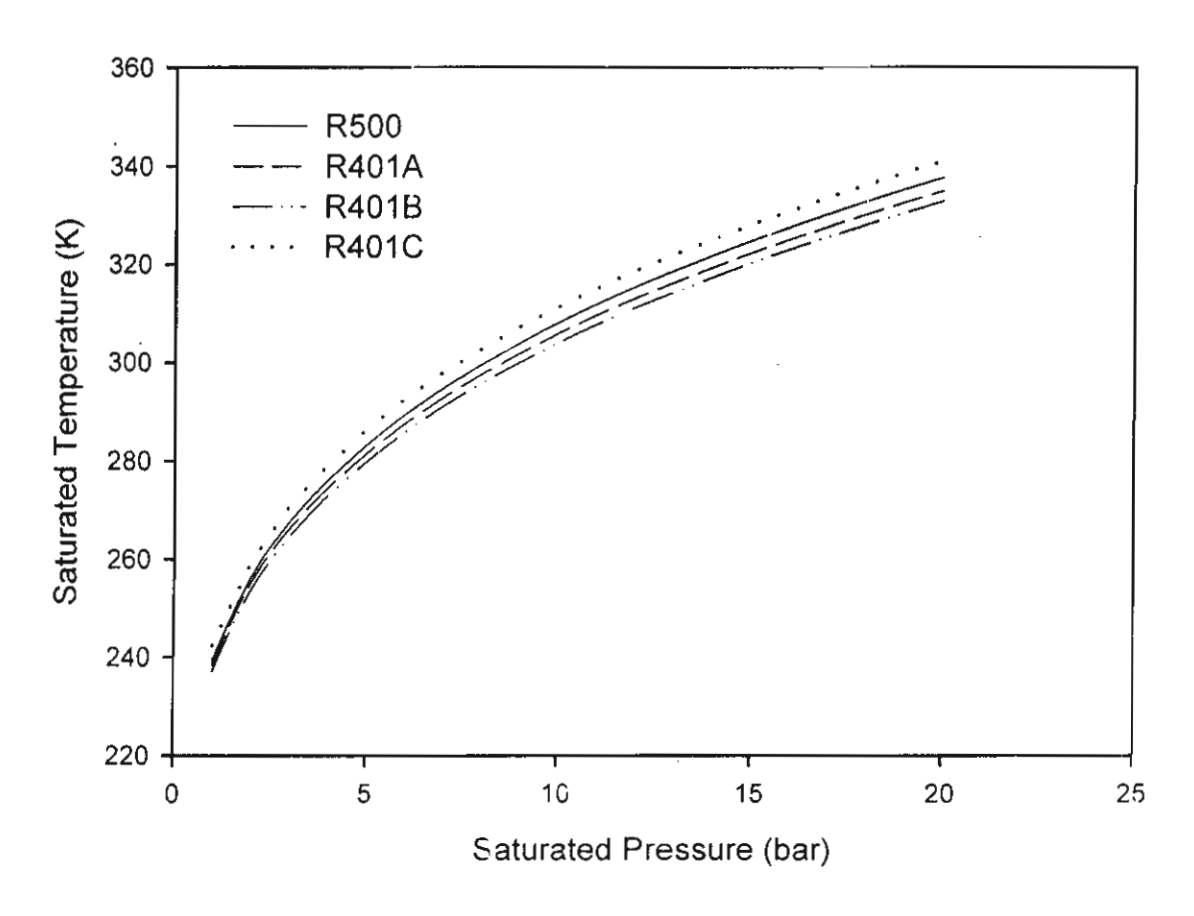


Fig. 5 Comparison of saturated pressure and temperature for R500, R401A, R401B and R401C

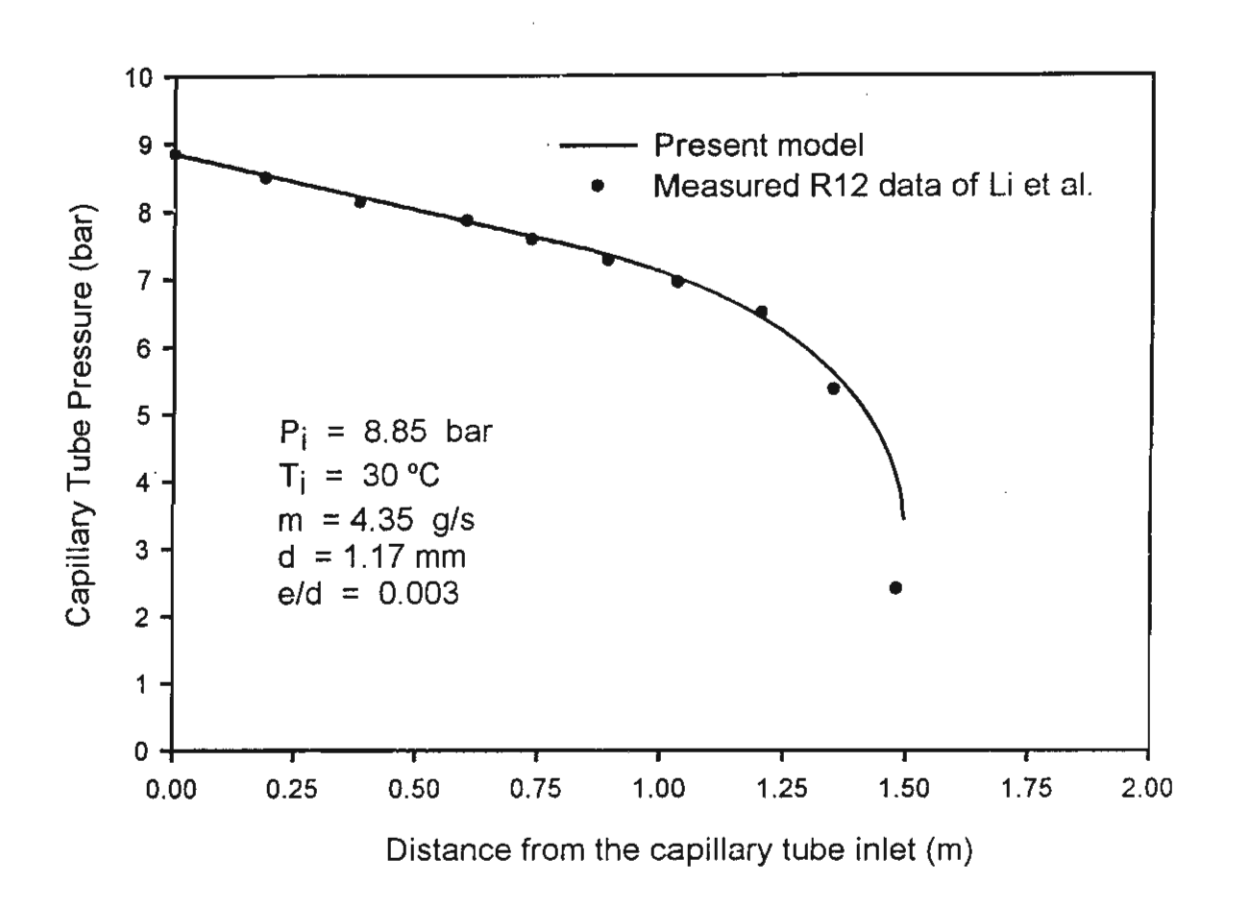


Fig. 6 Comparison of measured pressure distributions with present numerical results

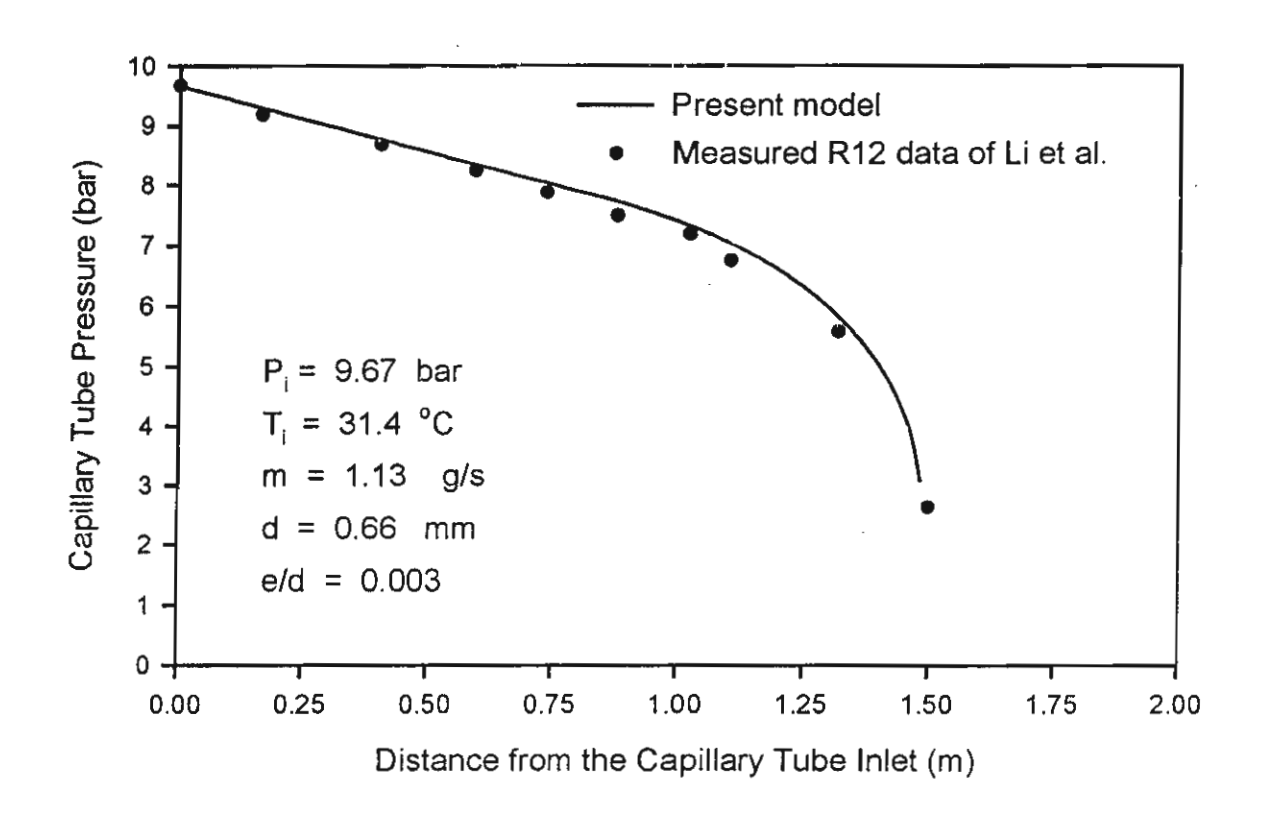


Fig. 7 Comparison of measured pressure distributions with present numerical results

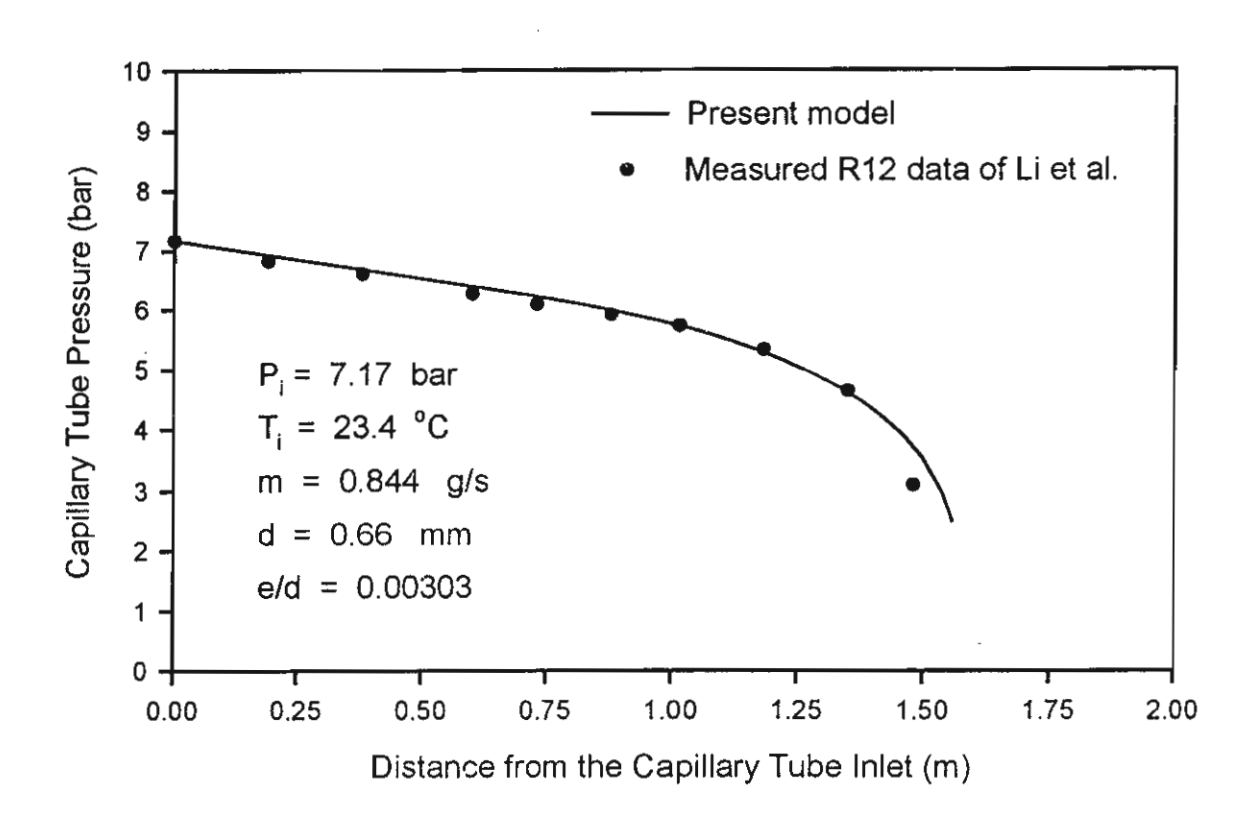


Fig. 8 Comparison of measured pressure distributions with present numerical results

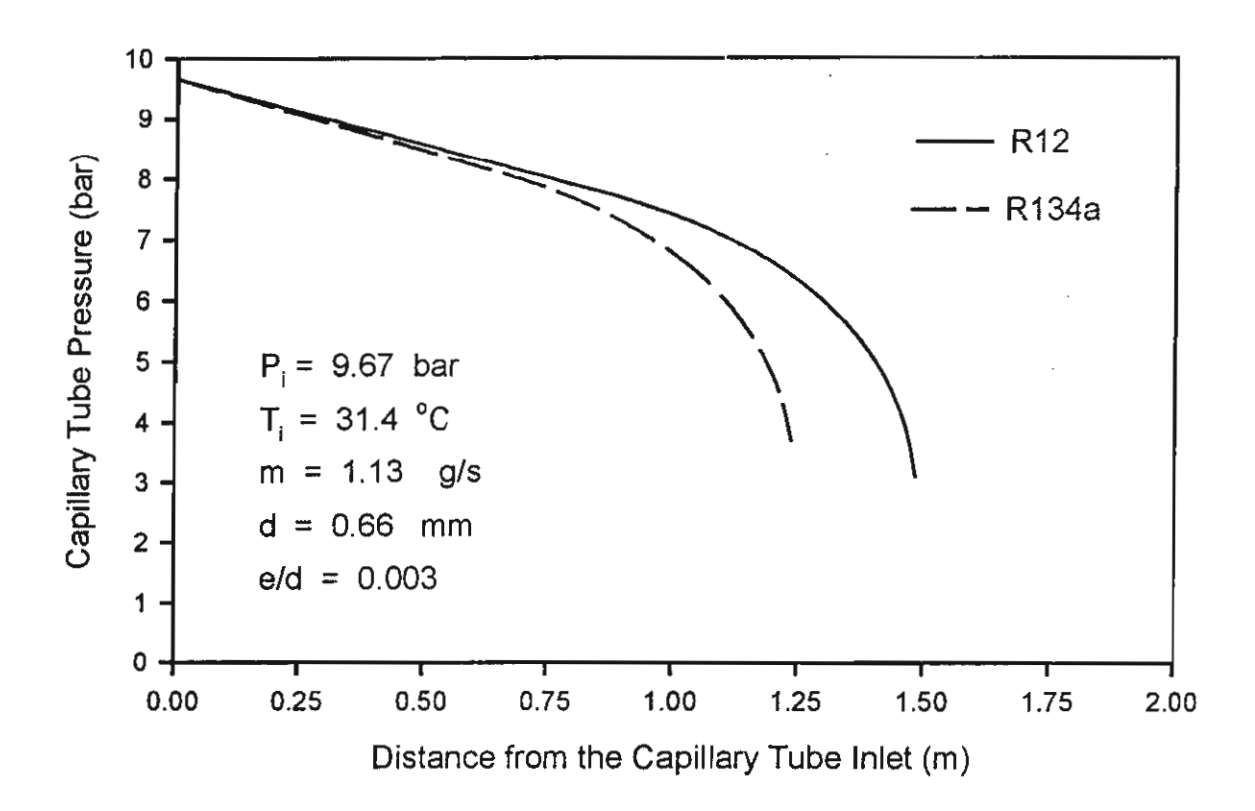


Fig. 9 Comparison of pressure distributions along the capillary tube for R12 and R134a

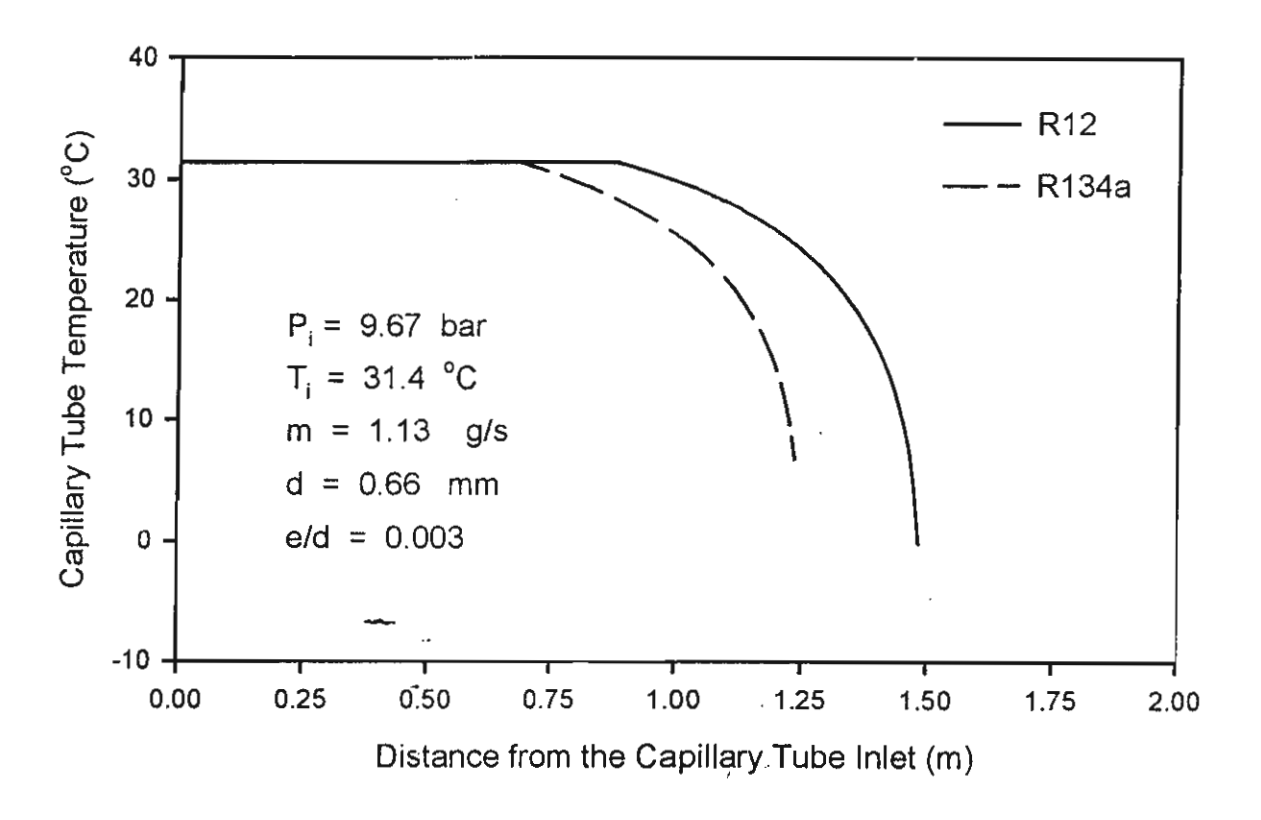


Fig. 10 Comparison of temperature distributions along the capillary tube for R12 and R134a

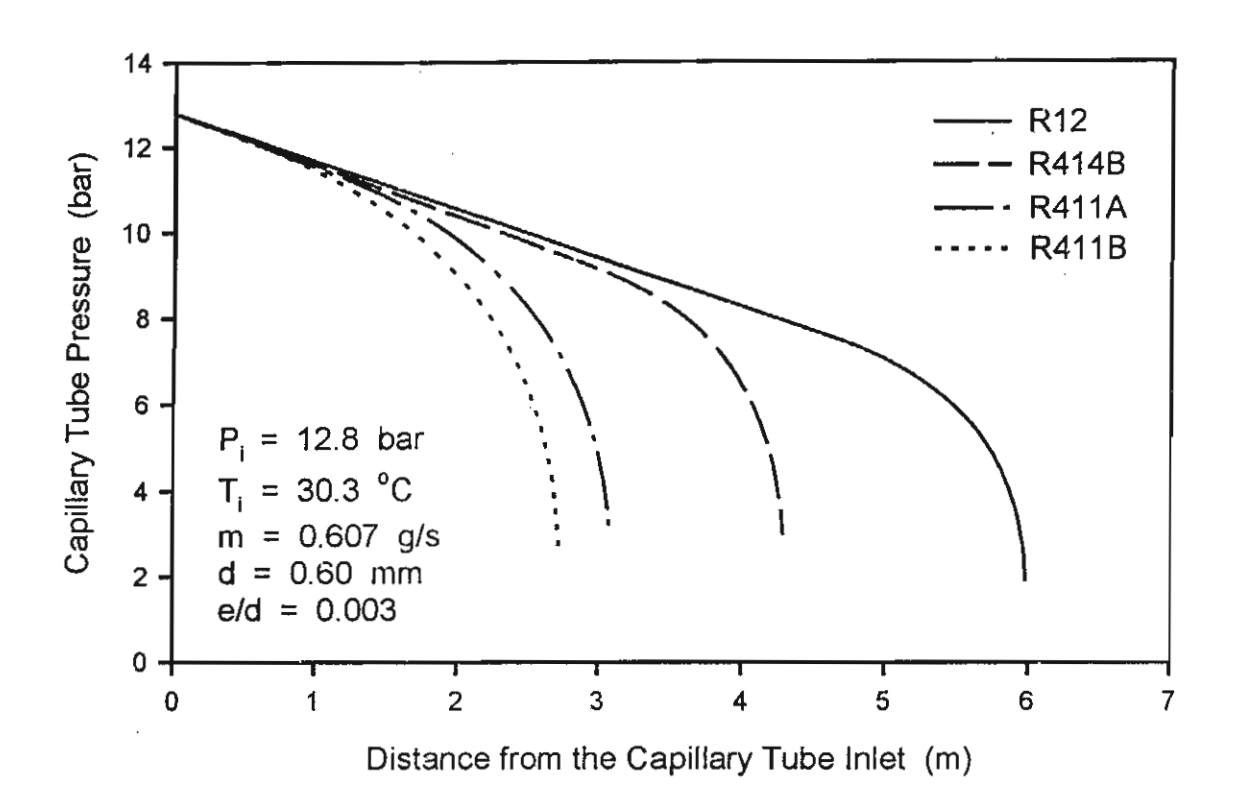


Fig. 11 Comparison of pressure distributions along the capillary tube for R12, R414B, R411A and R411B

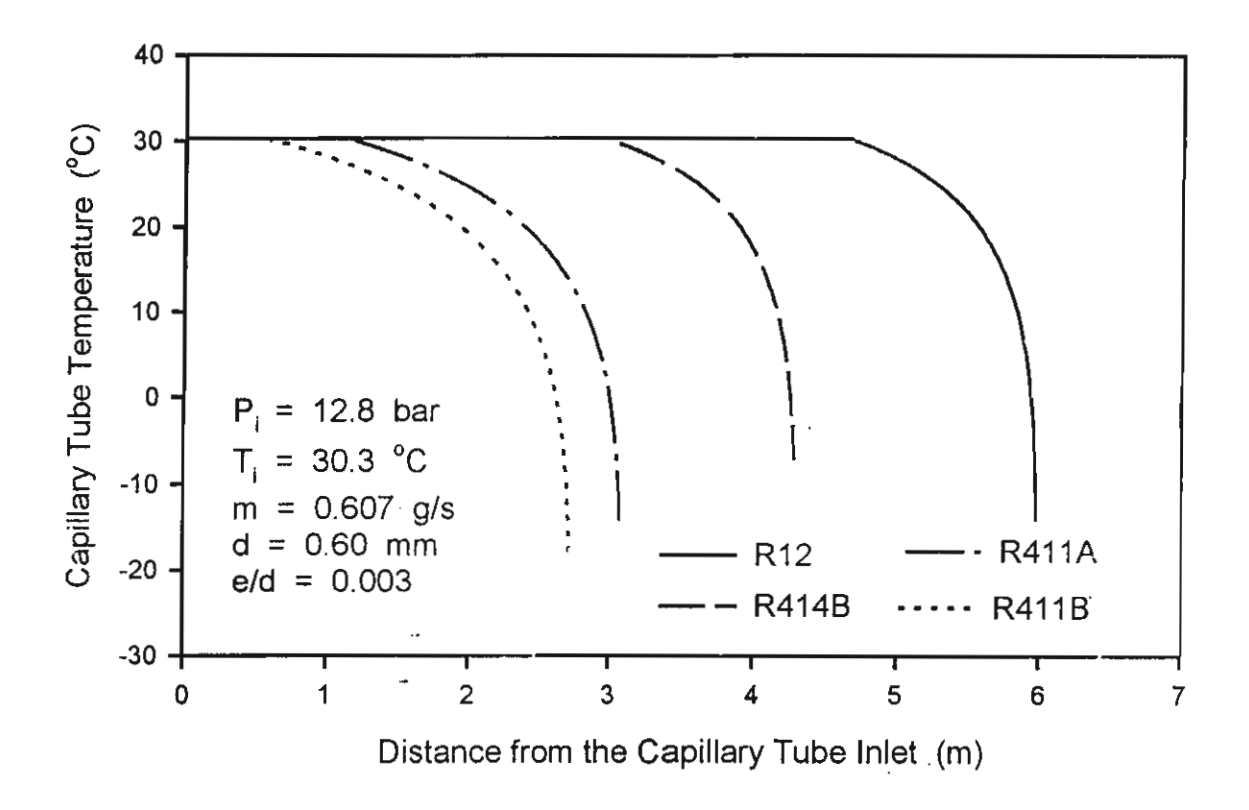


Fig. 12 Comparison of temperature distributions along the capillary tube for R12, R414B, R411A and R411B

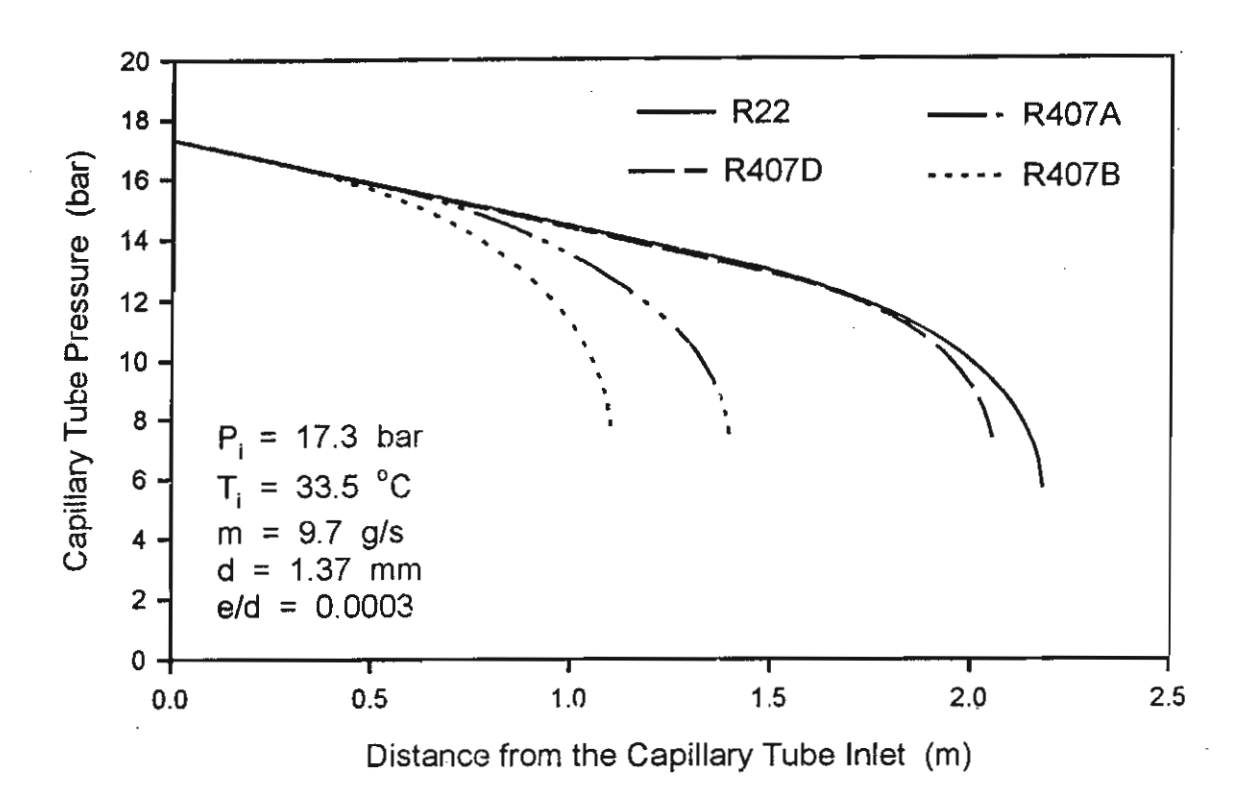


Fig. 13 Comparison of pressure distributions along the capillary tube for R22, R407A, R407B and R407D

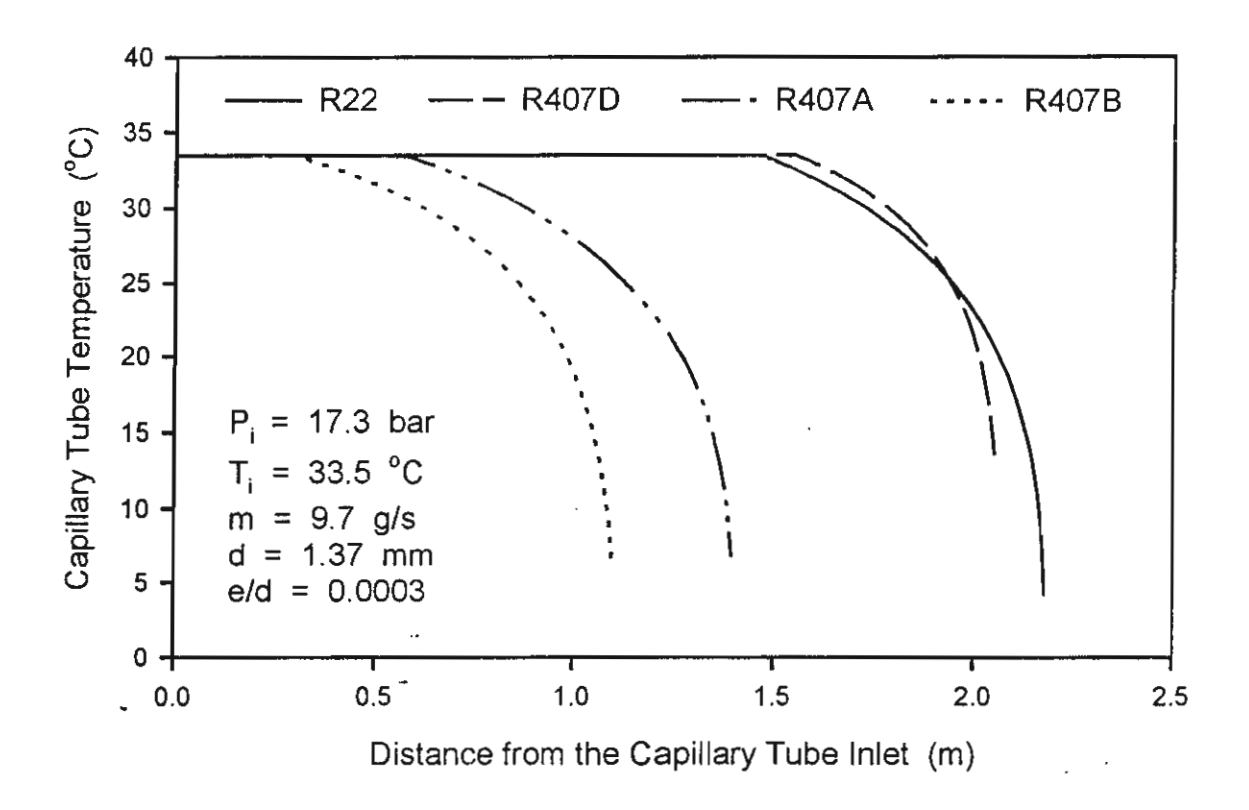


Fig. 14 Comparison of temperature distributions along the capillary tube for R22, R407A, R407B and R407D

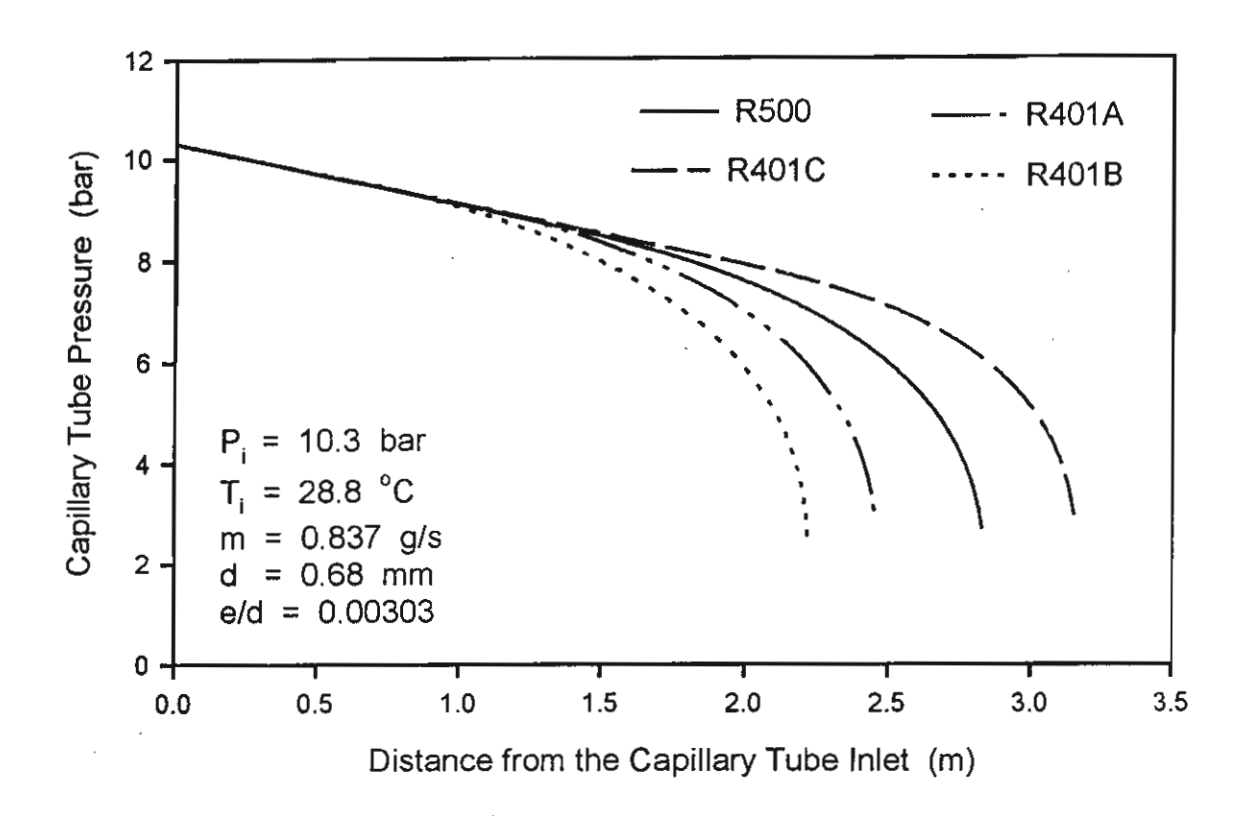


Fig. 15 Comparison of pressure distributions along the capillary tube for R500, R401A, R401B and R401C

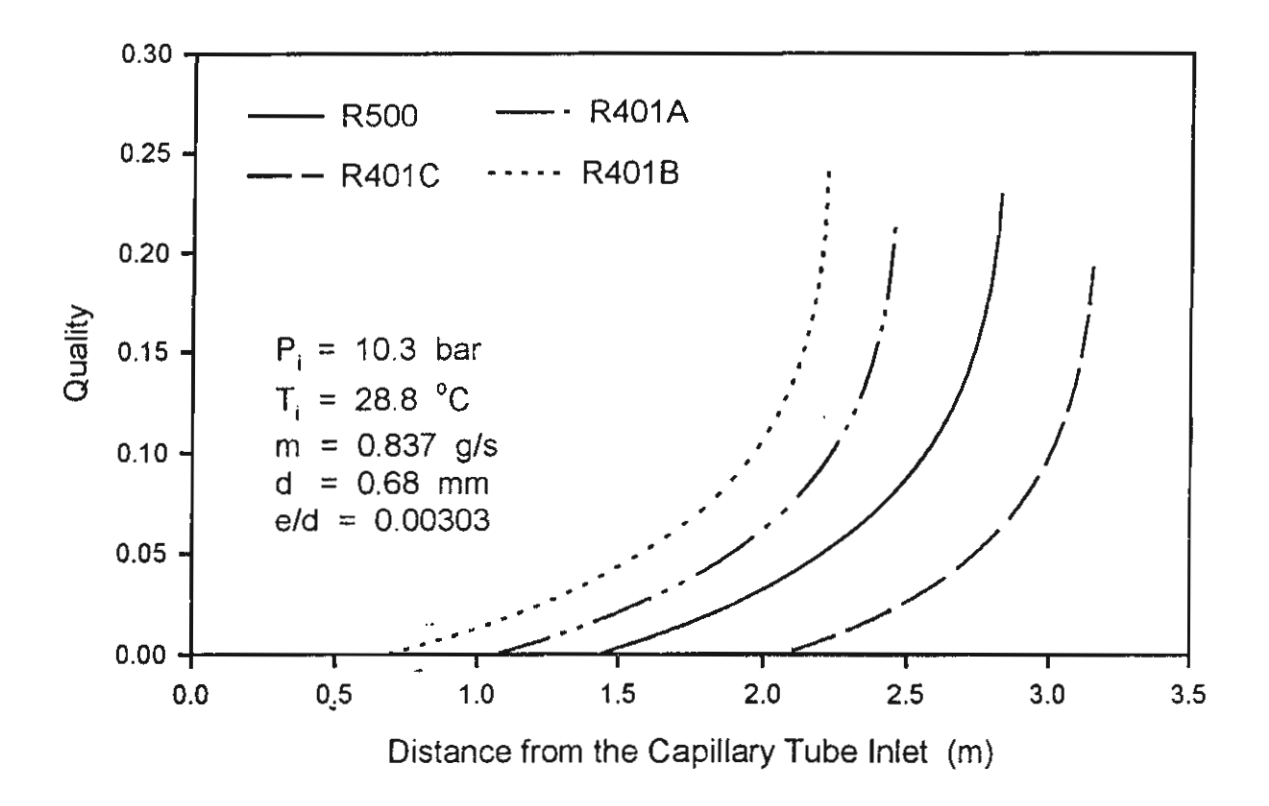


Fig. 16 Comparison of quality distributions along the capillary tube for R500, R401A, R401B and R401C

Wongwises, S., Lokathada, N., Kritsadathikarn, P., Songnetichavarit, T., A Simulation of Refrigerant Flow Through Capillary Tube Expansion Device, *Asian J. of Energy and Environment*, 2001; 2(1):69-88.

ASIAN JOURNAL OF

ENERGY & ENVIRONMENT

The Joint Graduate School of Energy and Environment (JGSEE) King Mongkut's University of Technology Thonburi (KMUTT) 91 Prachauthit Road, Bangmod, Tungkru, Bangkok 10140 Thailand Tel: (662) 4708309-10, 8729014-15

Fax: (662) 4279634, 8726736 E-mail: ajee@jgsee.kmutt.ac.th

Ref.: AJEE/046/2001

Dr. Somehai Wongwises
Faculty of Engineering
King Mongkut's University of
Technology Thonburi (KMUTT)
91 Prachauthit Road, Bangmod,
Tungkru, Bangkok 10140 Thailand

18 April 2001

Dear Dr. Somchai Wongwises,

Your paper "A Simulation of Refrigerant Flow Through Capillary Tube Expansion Device" (our ref.: AJEE290101) has been read by two reviewers. They both recommended acceptance subject to revisions in accordance with the details given on the attached sheets.

We, therefore, hope that you will resubmit the paper after making revisions based on these recommendations. We suggest that if you disagree with any of recommendations, you may wish to rewrite the relevant passages to clarify why you present the information in the way you do.

Yours sincerely,

MICH

(R.H.B. Exell) Editor-in-Chief

ASIAN JOURNAL OF

ENERGY & ENVIRONMENT

The Joint Graduate School of Energy and Environment (JGSEE) King Mongkut's University of Technology Thonburi (KMUTT) 91 Prachauthit Road, Bangmod, Tungkru, Bangkok 10140 Thailand Tel: (662) 4708309-10, 8729014-15

> Fax: (662) 4279634, 8726736 E-mail: ajee@jgsee.kmutt.ac.th

Prof. Dr. Somchai Wongwises
Department of Mechanical Engineering,
King Mongkut's University of Technology Thonburi,
91 Prachauthit Rd., Bangmod, Tungkru, Bangkok 10140 Thailand

Ref.: AJEE/012/2001

16 August, 2001

Dear Prof. Dr. Somchai Wongwises,

AJEE290101: "A Simulation of Refrigerant Flow Through Capillary Tube Expansion Device"

From your submission of the revised above paper, for publication in the Asian Journal of Energy & Environment (AJEE), we are please to inform you that your revised paper has been accepted for publication in the next issue (Volume 2 Issue 1).

In order for publication of your paper to proceed, your manuscript is being sent to the copy editor and then to the publisher for typesetting. Due to a large backlog of accepted manuscripts with the copy editors, there will be a delay in your receipt of your galley proofs. However, please be assured that you will receive "master proofs" for your approval from the typesetters via e-mail prior to publication.

Thank you very much for your cooperation.

Yours sincerely,

(R. H. B. Exell) Editor-in-Chief

ASIAN JOURNAL OF

ENERGY & ENVIRONMENT

The Joint Graduate School of Energy and Environment (JGSEE) King Mongkut's University of Technology Thonburi (KMUTT) 91 Prachauthit Road, Bangmod, Tungkru, Bangkok 10140 Thailand Tel: (66) 02-4708309-10, 02-8729014-15 Fax: (66) 02-4279634, 02-8726736

E-mail: ajee@jgsee.kmutt.ac.th

Dr. Somchai Wongwises Faculty of Engineering King Mongkut's University of Technology Thonburi (KMUTT) 91 Pracnauthit Road, Bangmod, Tungkru, Bangkok 10140 Thailand

November 20, 2001

Ref.: AJEE/159/2001

Dear Dr. Somchai Wongwises,

AJEE290101 -- A Simulation of Refrigerant Flow Through Capillary **Tube Expansion Device**

From your accepted paper to be published the Asian Journal of Energy & Environment (AJEE) Volume 2 Issue 1/2001, enclosed here are master proof for your approval from the typesetters prior to publication.

Please be informed that galley proofs will be sent to the corresponding author for minor corrections. The corrections are restricted to printer's error or misprints only. Major alterations are not accepted and should be returned to the Production Manager within one week. If the master proof is not be returned within the specific time, we will regard that the draft is all correct.

In case you encounter any technical difficulties or require other assistance, please feel free to contact us. We will be happy to help you.

Thank you for submitting your manuscript to AJEE for publication.

Yours sincerely,

(Prathumthip Sawangamporn)

- Prathumtlip Sawangampon

Production Manager

A Simulation of Refrigerant Flow Through Capillary Tube Expansion Device

S. Wongwises, N. Lokathada, P. Kritsadathikarn and T. Songnetichaovalit

Fluid Mechanics, Thermal Engineering and Multiphase Flow Research Laboratory (FUTURE) Department of Mechanical Engineering, King Mongkut's University of Technology Thonburi, Bangmod, Bangkok 10140, Thailand

(Received: 29 January 2001)

Abstract: A homogeneous flow model is applied to study the flow characteristics of refrigerants in adiabatic capillary tubes. The basic physical equations governing the flow are established from the conservation of mass, energy and momentum. The obtained differential equations are solved simultaneously by the Runge-Kutta method. The model input parameters are pressure and temperature at capillary tube inlet, mass flow rate of refrigerant, roughness and diameter of the capillary. The simulation can be used to determine the appropriate size of the capillary tubes used in household air conditioners and refrigerators, especially to select the capillary tube length for given operating conditions.

Keywords: two-phase flow, homogeneous flow, capillary tube, adiabatic flow, alternative refrigerant

Introduction

The capillary tube is the most widely used as expansion device in small domestic vapor compression air conditioners and refrigerators. It is made from a small-bore hollow copper tube (in the order of $0.5 \times$ 10^{-3} to 1.5×10^{-3} m. diameter) of about 2 to 5 m. in length [1]. It is used as an automatic flow rate controller for the refrigerant when varying load conditions and varying condenser and evaporator temperatures are to be encountered. Its simplicity, low initial cost and low starting torque of compressors are compelling reasons for its use. The capillary tube's physical configuration is very simple, the design and analysis of flow and heat transfer characteristics inside the tube are however complex ones. The design of capillary tubes has been studied both analytically and experimentally, mostly for pure refrigerants. Bansal et al. [1] presented a homogeneous two-phase flow model, CAPIL to study the performance and design aspects of adiabatic capillary tubes. The REFPROP data base which is based on the Carnahan-Starling-DeSantis equation of state was used to determine the thermodynamics and transport properties of the refrigerants. Melo [5] investigated experimentally the effects of diameter and length of adiabatic capillary tube, refrigerant subcooling, condensing pressure and the type of the refrigerant (R12, R134a, R600A) on the mass flow rates. Sami et al. [7] presented a numerical model for predicting capillary tube performance using new alternative refrigerants, both pure refrigerants (R12, R22, R134a) and binary mixtures (R410A, R410B, R507, R32/ R134a). Numerical results revealed that the proposed model fairly

simulated their experimental data and those of other researchers. Wong et al. [8] used a homogeneous two-phase flow model to simulate and compare the flow characteristics of R12 with those obtained from the separated flow model. The results showed that the separated flow model using Lin's pressure gradient correlations [4] and the Miropolskiy's slip ratio [6], gave better prediction. Jung et al. [2] modified the Stoecker's model [10] to provide simple correlations for sizing the capillary tubes used with R22, R134a, R407C and R410A. Various effects due to the degree of subcooling, sudden contraction at capillary tube inlet, various viscosity models and friction factors were considered. Wongwises et al. [9] provided the results of numerical simulation for R12, R22, R134a, R502, R404A, R407B, R407C, R410A, R410B, R507A. An example of capillary tube selection chart developed from the simulation is shown.

Although some information is currently available on flow characteristics of refrigerant in a capillary tube, there still remains room to discuss. In the present study, the main concern is to develop the flow model and study the flow characteristics of some pure refrigerants (R12, R22, R134a) and refrigerant mixtures (R407E (R32/R125/R134a; 25/15/60%), R410B (R32/R125; 45/55%), R502 (R22/R115; 48.8/51.2), R408A (R125/R143a/R22; 7/46/47%)).

Mathematical Modelling

As shown in Fig. 1, the flow of refrigerant through a capillary tube can be divided into two different regions; a sub-cooled liquid region (the region from the inlet of the capillary tube to the position where the saturation pressure corresponds to the capillary inlet temperature) and a liquid-vapor two-phase region.

The following assumptions are used to formulate the model:

- · adiabatic flow
- · one-dimensional flow
- homogeneous two-phase flow
- · thermodynamic equilibrium
- straight horizontal, constant inner diameter and roughness capillary tube
 - no metastable effects

Sub-cooled Liquid Region

For steady fully-developed incompressible flow in a capillary tube, the integral form of the momentum equation at differential distance dz is

$$\tau_W(\pi d)dz + A_o dP = 0 \qquad (1)$$

where the shear stress at wall, τ_w , can be determined from

$$\tau_W = f \frac{(\rho_L V_L^2)}{8}$$
(2)

where f is the friction factor determined from Colebrook's equation as follows;

$$\frac{1}{f^{0.5}} = -2 \log \left(\frac{e/d}{3.7} + \frac{2.51}{\text{Re}_L f^{0.5}} \right) -----(3)$$

Substituting Eq. (2) into Eq. (1) and rearranging, the sub-cooled liquid length, L_{sc} , is obtained as follows;

$$L_{SC} = \left(p_i - p_{sat} \right) / \left(f \frac{G^2}{2\rho_L d} \right) \quad ---- (4)$$

where the mass flux, G, is the total mass flow rate divided by cross-sectional area of tube.

Two-phase Flow Region

The one dimensional homogeneous two-phase flow model based on that of Wong et al. [8] and Wallis [12] is used in the present study. In the model, the basic physical equations governing the flow are the continuity and conservations of energy and momentum.

As the refrigerant flows along the capillary tube, its pressure gradually drops and the liquid flashes into vapour arising purely from the reduced pressure. So at any point

$$h = x h_G + (1-x)h_L$$
 ----(5)

where the quality, x, is the ratio of the mass flow rate of vapour to total mass flow rate when a substance is in a saturation state.

For homogeneous flow, the velocity of each phase is equal, so

$$V = V_G = V_L \qquad (6)$$

For flow in a capillary tube with no applied works and neglecting the elevation changes, the following form of energy equation is obtained

$$\frac{d}{dz} \left(x h_G + (1 - x) h_L + \frac{V^2}{2} \right) = 0$$
 (7)

or
$$\left(x\frac{dh_G}{dz} + h_G\frac{dx}{dz}\right) + \left((1-x)\frac{dh_L}{dz} - h_L\frac{dx}{dz}\right) + \left(V\frac{dV}{dz}\right) = 0$$
 ----(8)

For a pure substance in equilibrium, the enthalpies and densities at saturation state can be arranged in the function of pressure.

From elementary calculas we know that if h is a differentiable function of P, and P is a differentiable function of z, then

$$\frac{dh}{dz} = \frac{dh}{dP} \frac{dP}{dz} \tag{9}$$

On rearranging, we get

$$\left(\frac{dP}{dz}\right)\left(x\frac{dh_G}{dP} + (1-x)\frac{dh_L}{dP}\right) + \left(h_{LG}\frac{dx}{dz}\right) + \left(V\frac{dV}{dz}\right) = 0 - - - (10)$$

Average velocity of refrigerant flowing along the capillary tube

$$V_G = V_L = V = Gv \qquad -----(11)$$

where mass flux, G, is the mass flow rate of mixture divided by the cross-sectional area of tube and specific volume of the mixture, v, is determined from

$$v = xv_G + (1-x)v_L \qquad (12)$$

Determining the differential term of Eq.(11), we get

Substituting Eq. (13) into Eq.(10) and rearranging gives

is

where $A = h_{LG} + G^2 v v_{LG}$

$$B = x \frac{dh_G}{dP} + (1-x)\frac{dh_L}{dP} + G^2 v \left[x \frac{dv_G}{dP} + (1-x)\frac{dv_L}{dP} \right]$$

The momentum equation is often rewritten as an explicit equation for the pressure gradient. The total pressure gradient $\left(\frac{dP}{dz}\right)$ can be expressed as follows

$$\frac{dP}{dz} = \left(\frac{dP}{dz}\right)_a + \left(\frac{dP}{dz}\right)_g + \left(\frac{dP}{dz}\right)_f -----(15)$$

The different three components are regarded as accelerational, gravitational and frictional terms of the total pressure gradient.

Accelerational pressure gradient cannot be measured directly. It can be, however, obtained from the momentum flux as follows

$$\left(\frac{dP}{dz}\right)_{a} = -\frac{m}{A_{o}} \frac{d(V)}{dz} - \dots (16)$$

and, so =
$$-G^2 \left(v_{LG} \frac{dx}{dz} + \left((1-x) \frac{dv_L}{dP} + x \frac{dv_G}{dP} \right) \frac{dP}{dz} \right)$$

Gravitational pressure gradient is negligible in this case because the flow is horizontal.

Frictional pressure gradient can be calculated from

$$\left(\frac{dP}{dz}\right)_f = \frac{-f_{tp} G^2((1-x)v_L + xv_G)}{2d} - \dots (17)$$

Substituting Eqs. (16) and (17) into Eq. (15), gives

$$\frac{dx}{dz} = \frac{\left(\frac{dP}{dz}\right)_f - C\frac{dP}{dz}}{D} - C\frac{dP}{dz}$$

where

$$C = 1 + (1-x)G^2 \frac{dv_L}{dP} + xG^2 \frac{dv_G}{dP}$$
$$D = G^2 v_{LG}$$

Eq. (3) used for the single-phase will be modified to calculate the twophase friction factor, f_{tp} , with the Reynolds number being defined as:

$$Re = \frac{Gd}{\mu_{tp}} \qquad ----(19)$$

The two-phase viscosity, μ_{tp} , is calculated from Dukler's equation [13] as follows:

$$\mu_{tp} = \frac{x v_G \mu_G + (1 - x) v_L \mu_L}{x v_G + (1 - x) v_L} \qquad (20)$$

where μ_G and μ_L are dynamic viscosity of gas and liquid, respectively.

Solution Method

The properties of refrigerent are taken from REFPROP [11] and are developed as a function of pressure. The calculating the friction factor by Eq.(3) and substituting P_{sat} into Eq.(4) with the saturation pressure of refrigerant at the inlet temperature of the capillary tube, the length of the single-phase region is obtained. The exit condition of the single phase flow region is used to be an inception of vaporization of the two-phase flow region. In the two-phase flow region, the Runge-Kutta method is used to solve Eqs. (14) and (18) and the calculation is terminated when the flow is at the choked flow condition.

Results and Discussion

Figures 2 and 3 show the relation between saturation pressure and saturation temperature for each pairs of the refrigerants. It can be seen that the differences of the pressure-temperature profiles for each pairs are small. The results from the simulation obtained by using the mathematical model are properties along the capillary tubes. The effect of mass flow rate, pressure and temperature at the capillary tube inlet, diameter and relative roughness, on the total length of capillary tube were investigated. The present model is validated by comparing with the R12 data measured by Li et al. [3]. Figures 4 and 5 show the comparison of the simulation results with the R12 data of Li et al for inlet temperatures of 23.4 °C and 31.4 °C respectively. The experimental data agree quite well with the model.

Figures 4 and 5 also show how pressure varies with position along the capillary tube. In the single-phase region, due to frictional effects in fully developed flow in a constant-area tube, the pressure of refrigerant decreases linearly along the capillary tube. After the position of the inception of vaporization, due to frictional and accelerational effects, the pressure of refrigerant drops relatively fast and more rapidly as the flow approaches the choked flow condition. However, in real situation, due to the delay of vaporization, the onset of vaporization may not occur at the end of the single-phase region.

The comparison of the local pressure distribution of R12 and of R134a is shown in Figure 6, the flow of R12 through the capillary tube gives a lower pressure drop per unit length (dP/dz) than that of R134a. In the other word, at the same pressure drop, R134a needs shorter capillary tube length. Figures 7 and 11 show the temperature distributions along the capillary tube for R12, R134a and R502, R408A

respectively. In the single phase region, the temperature of refrigerant along the capillary tube remains constant as expected. Once the inception of vaporization has taken place, the temperature drop will be accelerated as the flow approaches the choked condition.

Comparisons on the pressure drop characteristics for the rest of each pair of refrigerant (R22 vs R407E and R410B; R502 vs R408A) show that for all cases the traditional refrigerant flowing through a capillary tube gives a slightly lower pressure drop per unit length in the single-phase region and gives a sinificantly lower pressure drop per unit length in the two-phase region than the alternative refrigerants. The traditional refrigerants also give longer single-phase region which resulted in a longer total tube length. Figure 9 shows the distribution of quality along the capillary tube. For all cases, the quality in the single phase region is zero up to the flash point and then increases in a non-linear fashion, rising more rapidly as the choked flow condition is approached. It is also shown that in general, traditional refrigerants vaporize later than their corresponding alternative refrigerants.

Conclusions

The distributions of local pressure, temperature and quality of some common traditional and alternative refrigerants flowing through adiabatic capillary tubes are numerically investigated. The mathematical model is developed from the basic law of mass, energy and momentum conservations. Homogeneous flow is assumed for the two-phase liquid-vapor flow region. Numerical results reveal that, it is possible to use the present calculation to predict the flow characteristics in capillary tubes. The model includes various relevant parameters and can be used

to determine the size of the capillary tubes used in household refrigerators and freezers.

Acknowledgement

The present study has been supported financially by the Thailand Research Fund (TRF) whose guidance and assistance are gratefully acknowledged. The first author wish to acknowledge his lovely undergraduate students; Mr. Noppadon Lokathada, Mr. Pakawat Kritsadathikarn and Mr. Tirawat Songnetichaovalit, for their assistance during this work.

Nomenclature

		,	4.1.19
A	cross-sectional area of tube, m ²	d	tube diameter, m
e	roughness, m	f	friction factor
G	mass flux, kg/s m ²	h	specific enthalpy, kJ/kg
m	mass flow rate, kg/s	P	pressure, MPa
Re	Reynolds number	T	Temperature, °C
V	velocity, m/s	\mathbf{x}	quality
Z	axial; direction or length, m	CY.	void fraction
μ	dynamic viscosity, Pa s	υ	specific volume, m³/kg
ρ	density, kg/ni ³	τ	shear stress, N/m ²
Subscripts			
a	accelerational	ť	frictional
g	gravitational	G	vapour
i	capillary tube inlet	L	liquid
sat	saturation	SC	sub-cooled
tp	two-phase	w	wall

References

- Bansal, P.K. and Rupasinghe, A.S., An homogeneous model for adiabatic capillary tubes, *Applied Thermal Engineering*, 18 (1998) 207-219.
- [2] Jung, D., Park, C. and Park, B., Capillary tube selection for HCFC22 alternatives, *International Journal of Refrigeration*, 22 (1999) 604-614.
- [3] Li, R.Y., Lin, S. and Chen, Z.H., Numerical modeling of thermodynamics nonequilibriumflow of refrigerant through capillary tubes, ASHRAE Transactions, 96 (1990) 542-549.
- [4] Lin, S., Kwork, C.C.K., Li, R.Y., Chen, Z.H. and Chen, Z.Y., Local frictional pressure drop during vaporisation of R12 through capillary tubes, *International Journal of Multiphase* Flow, 17 (1991) 95-102.
- [5] Melo, C., Ferreira, R.T.S., Neto, C.B., Goncalves, J.M. and Mezavila, M.M., An experimental analysis of adiabatic capillary tubes, *Applied Thermal Engineering*, 19 (1999) 669-684.
- [6] Miropolskiy, Z.L., Shneyerova, R.I., Karamysheva, A.I., Vapour void fraction in steam fluid mixture flowing in heated and unheated channels, paper B 4.7, vol. 25, Int. Heat Trans. Conf., Paris (1970).
- [7] Sami, S.M. and Tribes, C., Numerical prediction of capillary tube behaviour with pure and binary alternative refrigerants, *Applied Thermal Engineering.* 18 (1998) 491-502.
- [8] Wong, T.N. and Ooi, K.T., Adiabatic capillary tube expansion device: A Comparison of the Homogeneous Flow and the Separated Flow Models, Applied Thermal Engineering, 16 (1996) 625- 634.

- [9] Wongwises, S. and Pirompak, W., Flow Characteristics of Pure Refrigerants and Refrigerant Mixtures in Adiabatic Capillary Tubes, *Applied Thermal Engineering*, **21** (2001) 845-861.
- [10] Stoecker, W.F. and Jones, J.W., Refrigeration and air conditioning, McGraw-Hill (1982).
- [11] REFPROP, Thermodynamic properties of refrigerants and refrigerant Mixtures, version 6.01, Gaithersburg, M.D. National Institute of Standards and Technology (1998).
- [12] Wallis, G.B., One dimensional two-phase flow, McGraw-Hill (1969).
- [13] Dukler, A.E., Wicks, M. and Cleveland, R.G., Frictional pressure drops in two-phase flow, *AIChE Journal*, **10** (1964) 38-51.

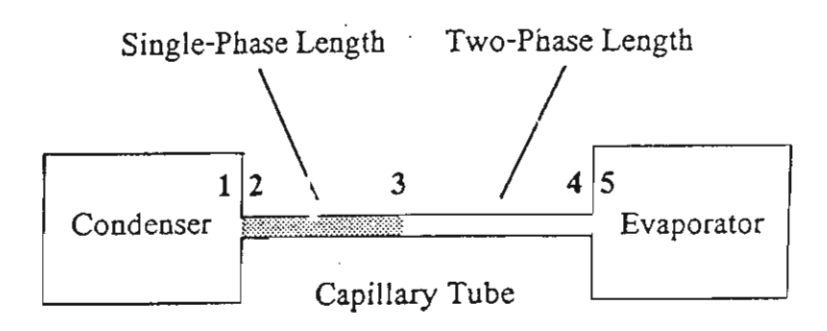


Figure 1. Schematic diagram of an adiabatic capillary tube.

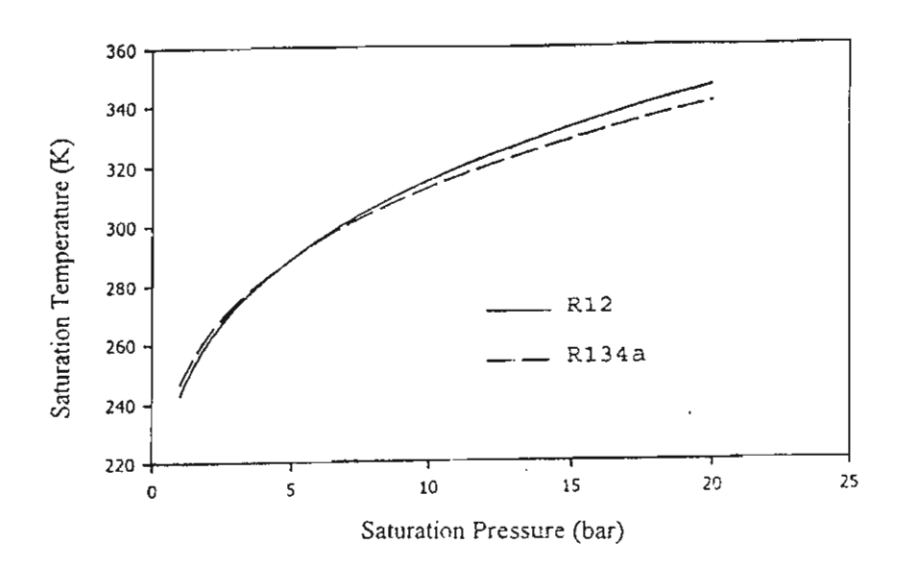


Figure 2. Saturation pressure and temperature for R12 and R134a.

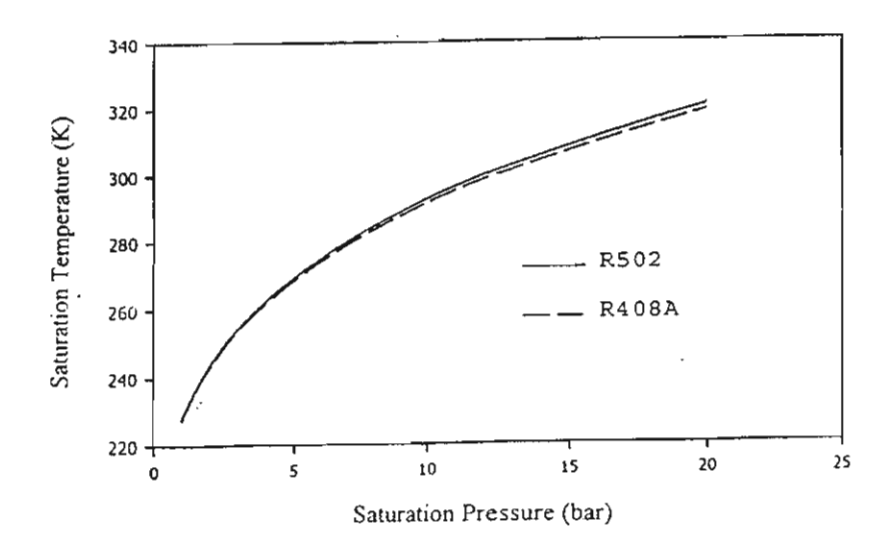


Figure 3. Saturation pressure and temperature for R502 and R408A.

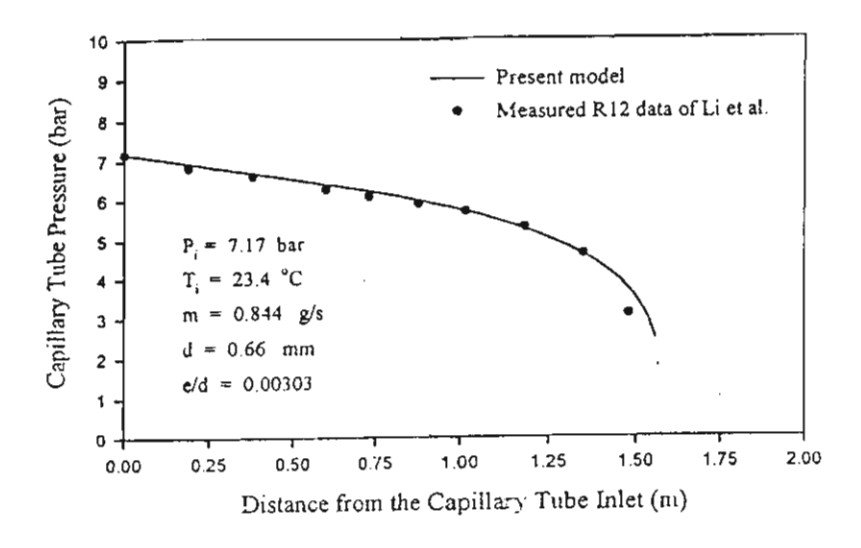


Figure 4. Comparison of pressure distributions along the capillary tube.

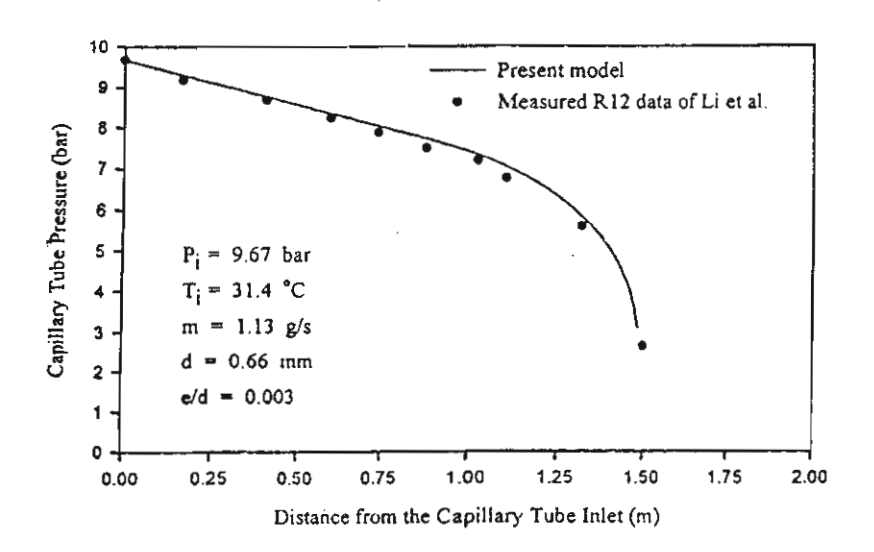


Figure 5. Pressure distributions along the capillary tube.

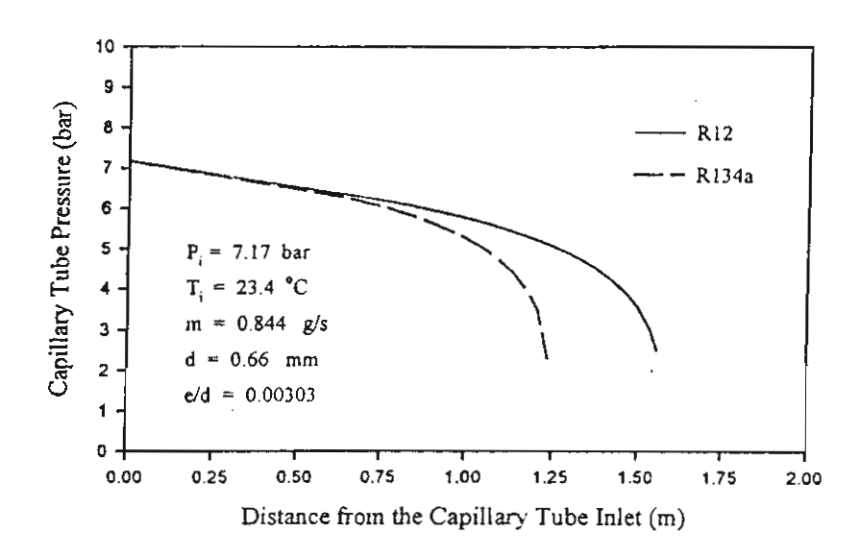


Figure 6. Comparison of pressure distributions along the capillary tube for R12 and R134a.

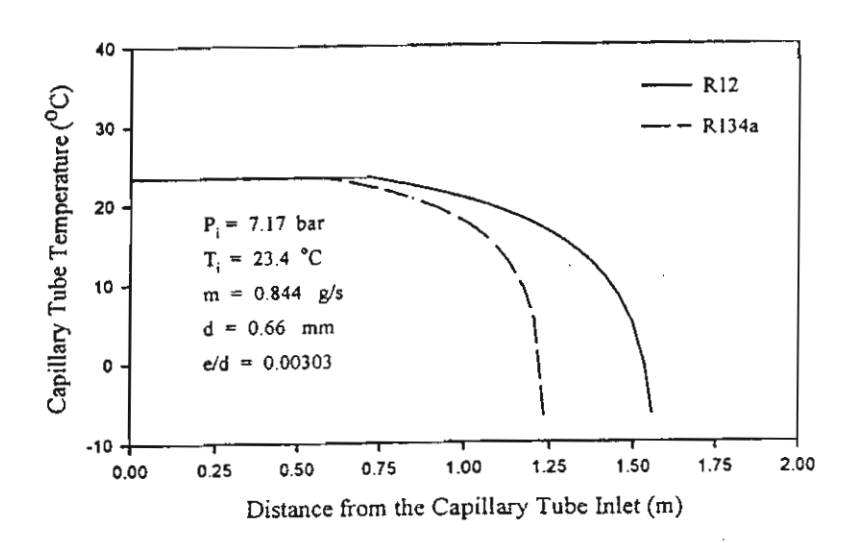


Figure 7. Comparison of temperature distributions along the capillary tube for R12 and R134a.

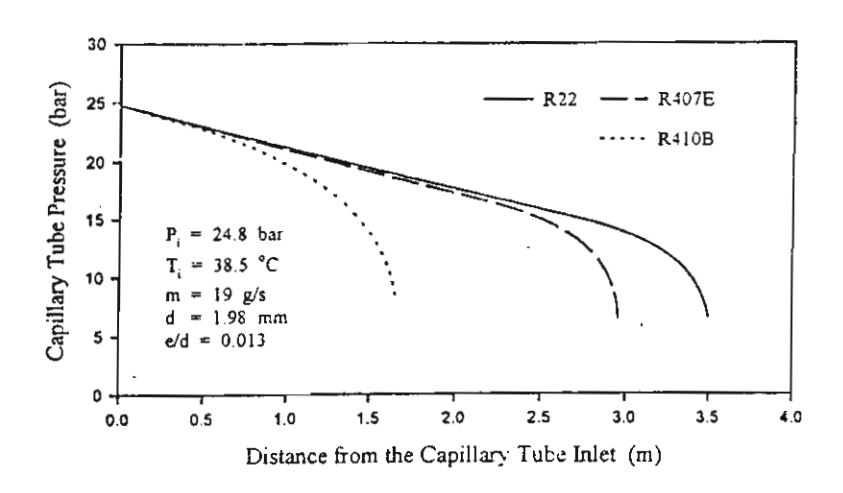


Figure 8. Comparison of pressure distributions along the capillary tube for R22, R407E and R410B.

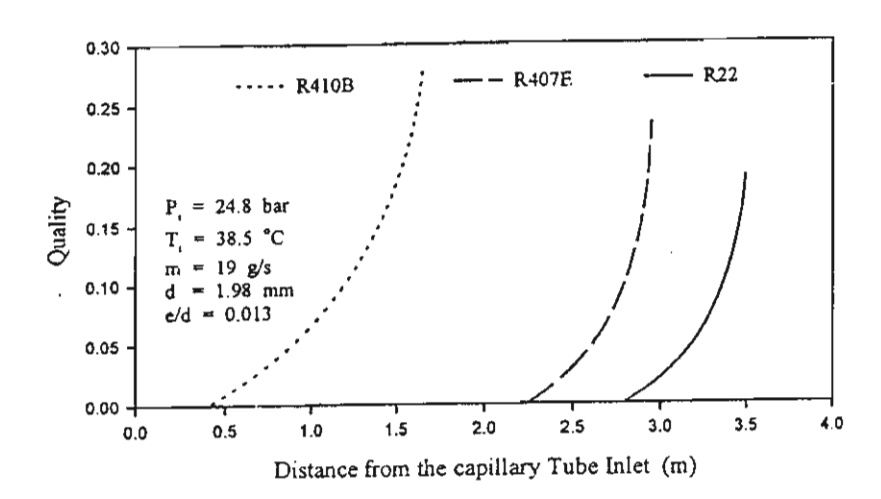


Figure 9. Comparison of quality distributions along the capillary tube for R22, R407E and R410B.

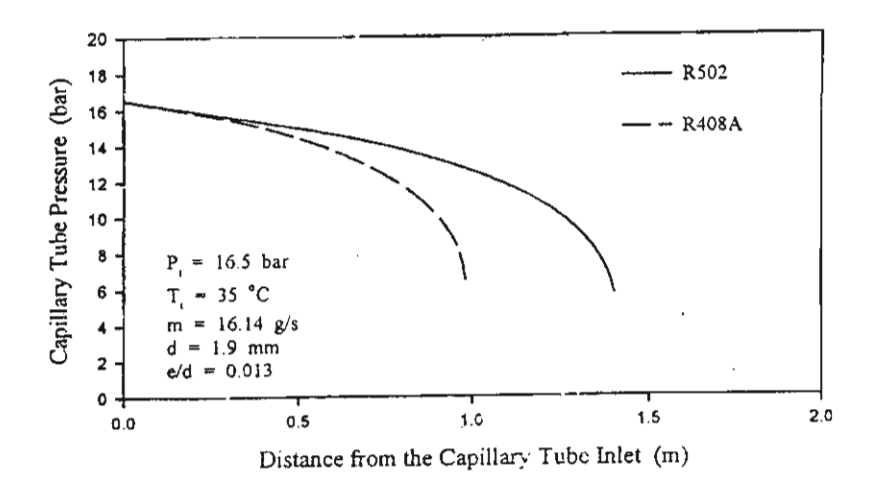


Figure 10. Comparison of pressure distributions along the capillary tube for R502 and R408A.

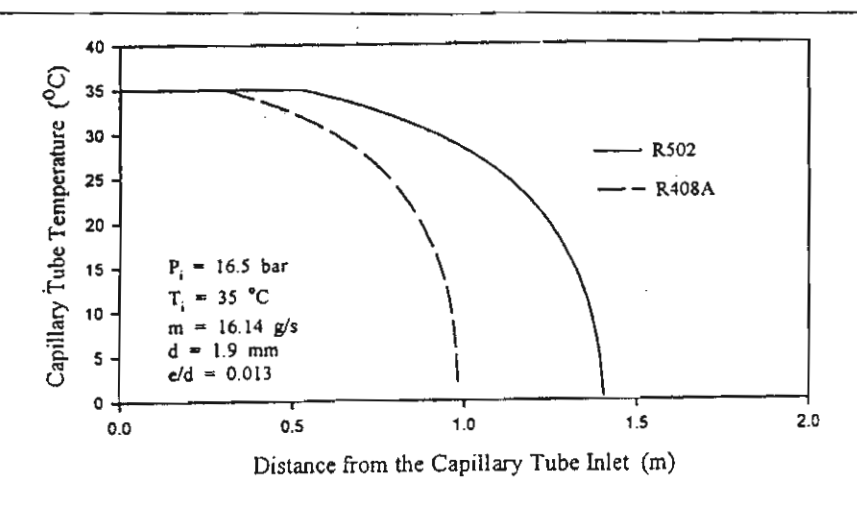


Figure 11. Comparison of temperature distributions along the capillary tube for R502 and R408A.